TURBULENCE STRUCTURE IN AXISYMMETRIC WALL-BOUNDED SHEAR FLOW

by

SADEK ZAKARIA KASSAB

A thesis
presented to the University of Manitoba
in partial fulfillment of the
requirements for the degree of
DOCTOR OF PHILOSOPHY
in
DEPARTMENT OF MECHANICAL ENGINEERING

Winnipeg, Manitoba

(c) SADEK ZAKARIA KASSAB, 1986

Permission has been granted to the National Library of Canada to microfilm this thesis and to lend or sell copies of the film.

The author (copyright owner) has reserved other publication rights, and neither the thesis nor extensive extracts from it may be printed or otherwise reproduced without his/her written permission.

L'autorisation a été accordée à la Bibliothèque nationale du Canada de microfilmer cette thèse et de prêter ou de vendre des exemplaires du film.

L'auteur (titulaire du droit d'auteur) se réserve les autres droits de publication; ni la thèse ni de longs extraits de celle-ci ne doivent être imprimés ou autrement reproduits sans son autorisation écrite.

ISBN 0-315-33563-7

TURBULENCE STRUCTURE IN AXISYMMETRIC WALL-BOUNDED SHEAR FLOW

BY

SADEK ZAKARIA KASSAB

A thesis submitted to the Faculty of Graduate Studies of
the University of Manitoba in partial fulfillment of the requirements
of the degree of

DOCTOR OF PHILOSOPHY

© 1986

Permission has been granted to the LIBRARY OF THE UNIVERSITY OF MANITOBA to lend or sell copies of this thesis, to the NATIONAL LIBRARY OF CANADA to microfilm this thesis and to lend or sell copies of the film, and UNIVERSITY MICROFILMS to publish an abstract of this thesis.

The author reserves other publication rights, and neither the thesis nor extensive extracts from it may be printed or otherwise reproduced without the author's written permission.

I hereby declare that I am the sole author of this thesis.

I authorize the University of Manitoba to lend this thesis to other institutions or individuals for the purpose of scholarly research.

SADEK ZAKARIA KASSAB

I further authorize the University of Manitoba to reproduce this thesis by photocopying or by other means, in total or in part, at the request of other institutions or individuals for the purpose of scholarly research.

SADEK ZAKARIA KASSAB

The University of Manitoba requires the signatures of all persons using or photocopying this thesis. Please sign below, and give address and date.

ABSTRACT

Turbulent structure in three shear flows— low Reynolds number turbulent boundary layer, fully developed pipe flow and conical diffuser flow have been examined through determination of the mean velocities, mean strain-rates, energy, shear stress, triple products, length scales and balances of energy and shear stress.

In the low Reynolds number turbulent boundary layer, the results corroborate other published works. For fully developed pipe flow, all the published results agree with the present one within experimental error. For the flow in the conical diffuser, the sudden application of extra strain-rate at the inlet seems to affect conditions so drastically that final picture of the flow in terms of mean and turbulent fields becomes unrecognizable from the initial condition.

This investigation deals also with the study of turbulent energy dissipation. Different results have been reviewed and compared. First of all, methods are tested and compared in two well-known flows : boundary layer and fully developed pipe flow, and then applied to diffuser flow. A new method of measuring dissipation that is proved to be most successful is one where the dissipation obtained from

integration of spectra from different lengths of the hot wire are extrapolated to zero length. High intensity of turbulence up to 60% is present in a large portion of the wall layer of a diffuser. The correction for dissipation due to high intensity of turbulence, introduced by Lumley (1965) and followed by Champagne (1978) in specific form, has been adopted to correct the dissipation in diffuser flow. Thus the corrected dissipation compares quite well with the dissipation obtained from the kinetic energy equation as a closing term after taking into consideration the large residual error involved in the closing term.

ACKNOWLEDGEMENTS

The author would like to express his deepest gratitude to Dr. R.S. Azad for his guidance, help and advice during the course of this work. The encouragement and contribution (Appendix D) provided by Dr. A.C. Trupp are also acknowledged.

Thanks are due to K. Tarte for his valuable assistance in the preparation of the figures. The assistance of R.W. Derksen at the begining of this study is also acknowledged. The author would like to thank Ö. Turan for the computer programmes for differentiation and linear regression.

The financial support provided by The University of Manitoba in the form of graduate fellowship to the author is gratefully acknowledged. In addition, financial support from NSERC CANADA through the grant of Professor R.S. Azad is gratefully acknowledged.

TABLE OF CONTENTS

page

ABSTRACT iv

ACKNOWLEDGEMENTS vi

LIST OF TABLES x

LIST OF FIGURES xi

NOMENCLATURE xviii

1. INTRODUCTION 1

2. EXPERIMENTAL FACILITIES AND PROCEDURE 5

2.1 Boundary layer facilities 5

2.2 Fully developed pipe flow and diffuser flow facilities 7

2.3 Instrumentation 9

2.3.1 Pressure measurements 9

2.3.2 Hot wire probes 10

2.3.3 Single wire measurements 11

2.3.3.1 Set-up(a) 13

2.3.3.2 Set-up(b) 14

2.3.4 X-wire measurements 14

2.3.5 Spectra measurements 16

2.4 General Procedure 18

PART I

3. SPECTRAL DATA IN AXISYMMETRIC WALL-BOUNDED SHEAR FLOW 21

3.1 Introduction 21

3.2 Results and discussion 22

4. EXPERIMENTAL ASSESSMENT OF k_1^{-1} SPECTRAL LAW 28

4.1 Introduction 28

4.2 Results and discussion 32

5. DISSIPATION OF ENERGY IN TURBULENT FLOW 36

5.1 Introduction 36

5.2 Measurements of dissipation rate 37

5.2.1 Measurement of $\overline{(\partial u/\partial t)^2}$ 37

5.2.2 Measurement of spectra 38

5.2.3 Dissipation measurements by different length of the wire 39

5.2.4 Dissipation obtained from kinetic energy equation as a closing term 40

5.3 Results 41

5.4 Discussion 44

5.5 Concluding remarks 52

PART II

6. LOW REYNOLDS NUMBER TURBULENT BOUNDARY LAYER 54

6.1 Introduction 54

6.2 Results and discussion 57

6.2.1 Mean velocity field 57

6.2.2 Turbulence field 59

6.2.2.1 Reynolds stresses 59

6.2.2.2 Higher moments 60

6.2.2.3 Length scales 63

6.2.2.4 Energy and shear stress balances 64

6.3 Concluding remarks 67

7. TURBULENT FLOW IN A CONICAL DIFFUSER 69

7.1 Introduction 69

7.2 Results 70

7.3 Discussion 76

7.4 Concluding remarks 92

REFERENCES 94

APPENDIX A. REMARKS ON STEM CONFIGURATION OF X-ARRAY HOT WIRE PROBES 106

APPENDIX B. EXPERIMENTAL EVALUATION OF APPROXIMATIONS FOR $\overline{w^2}$ AND $\overline{vw^2}$ 109

APPENDIX C. FULLY DEVELOPED PIPE FLOW 114

APPENDIX D. NEAR-WALL VELOCITY DISTRIBUTION WITHIN A STRAIGHT CONICAL DIFFUSER 120

TABLES 125

FIGURES 130

LIST OF TABLES

Table 2.1 Preston tubes dimensions.

Table 2.2 Dimensions of four of the standard DISA 55P05 boundary layer probes used in the present study.

Table 2.3 Dimensions of the wires used to examine the spatial resolution of a hot wire.

Table 6.1 Mean quantities of the low-Reynolds number turbulent boundary layer.

Table 6.2 Friction velocity, u*.

Table C.1 Fully developed pipe flow mean velocity data.

Table D.1 u* values and y^+ ranges at different stations.

LIST OF FIGURES

Figure 2.1 Plan view of wind tunnel for turbulent boundary layer on a pipe wall.

Figure 2.2 Tunnel for the studies of fully developed pipe flow and diffuser flow.

Figure 2.3 Block diagram for a single wire measurements
(a) Set-up(a).
(b) Set-up(b).

Figure 2.4 Block diagram for X-wire measurements.

Figure 2.5 Block diagram for spectra measurements.

Figure 3.1 $\overline{u^2}$-spectra in the boundary layer, $R_\theta = 2756$.

Figure 3.2 $\overline{u^2}$-spectra in a turbulent boundary layer. $y/\delta = 0.011, 0.022, 0.043$ & 0.109.

Figure 3.3 Symmetrical $\overline{u^2}$-spectra to test the symmetry of the flow and the noise correction.

Figure 3.4 $\overline{u^2}$-spectra for different l/d ratios in the boundary layer, $R_\theta = 2756$.

Figure 3.5 $\overline{u^2}$-spectra in fully developed pipe flow, $Re = 1.15*10^5$.

Figure 3.6 $\overline{u^2}$-spectra in fully developed pipe flow. $y/R = 0.010, 0.020, 0.039, 0.069$ & 0.108.

Figure 3.7 $\overline{u^2}$-spectra in diffuser flow at three different locations.

Figure 3.8 $\overline{u^2}$-spectra at three different locations for different l/d ratios.

Figure 3.9 $\overline{u^2}$-spectra measured on line perpendicular to the wall of the diffuser for two different locations

Figure 3.10 $\overline{u^2}$-spectra to emphasize the initial spectral laws in diffuser flow.
(a) $x_w/D = 0.59$.
(b) $x_w/D = 4.13$.

Figure 3.11 Fourth-order non-dimensional spectra to show the accuracy of spectra measurements at high

wavenumber.

Figure 4.1 The non-dimensional mean velocity profile and fluctuating velocity distribution in the boundary layer flow.

Figure 4.2 Normalized values of longitudinal spectrum $E_1(k_1)$ in the boundary layer.

Figure 4.3 The non-dimensional mean velocity profile and fluctuating velocity distribution in the fully developed pipe flow.

Figure 4.4 Normalized values of longitudinal spectrum $E_1(k_1)$ in the fully developed pipe flow.

Figure 4.5 The non-dimensional mean velocity profile and fluctuating velocity distribution in the diffuser at $x_w/D = 0.59$

Figure 4.6 The non-dimensional mean velocity profile and fluctuating velocity distribution in the diffuser at $x_w/D = 4.13$

Figure 4.7 Normalized values of longitudinal spectrum $E_1(k_1)$ in the present diffuser flow at $x_w/D = 0.59$ & 4.13.

Figure 5.1 Dissipation obtained from spectra and from $\partial u/\partial t$ for different lengths of the hot wire in boundary layer flow.

Figure 5.2 Dissipations obtained from spectra and from $\partial u/\partial t$ for different lengths of the hot wire in diffuser flow at $x = 42$ cm, $r/R_{LOC} = 0.85$ and $R_{LOC} = 8$ cm.

Figure 5.3 Dissipations from $\partial u/\partial t$ across the boundary layer with different hot wires.

Figure 5.4 Different methods of obtaining dissipation rate in turbulent boundary layer.

Figure 5.5 Dissipation from $\partial u/\partial t$ with different hot wires in a fully developed pipe flow.

Figure 5.6 Different methods of obtaining dissipation rate in a fully developed pipe flow.

Figure 5.7 Assessment of dissipation rate by comparing three promising methods in a fully developed pipe flow.

Figure 5.8 Dissipation from $\partial u/\partial t$ with different hot wires in a diffuser flow at $x = 6$ cm.

Figure 5.9 Dissipation from ∂u/∂t with different hot wires in a diffuser flow at x = 42 cm.

Figure 5.10 Dissipation from ∂u/∂t with different hot wires in a diffuser flow at x = 66 cm.

Figure 5.11a Different methods of obtaining dissipation rate in a diffuser flow at x = 6 cm.

Figure 5.11b Assessment of dissipation rate by comparing present methods with the dissipation rate obtained from the closing term of the turbulent energy equation in a diffuser flow at x = 6 cm.

Figure 5.12a Different methods of obtaining dissipation rate in a diffuser flow at x = 18 cm.

Figure 5.12b Assessment of dissipation rate by comparing present methods with the dissipation rate obtained from the closing term of the turbulent energy equation in a diffuser flow at x = 18 cm

Figure 5.13a Different methods of obtaining dissipation rate in a diffuser flow at x = 30 cm.

Figure 5.13b Assessment of dissipation rate by comparing present methods with the dissipation rate obtained from the closing term of the turbulent energy equation in a diffuser flow at x = 30 cm

Figure 5.14a Different methods of obtaining dissipation rate in a diffuser flow at x = 42 cm.

Figure 5.14b Assessment of dissipation rate by comparing present methods with the dissipation rate obtained from the closing term of the turbulent energy equation in a diffuser flow at x = 42 cm

Figure 5.15a Different methods of obtaining dissipation rate in a diffuser flow at x = 54 cm.

Figure 5.15b Assessment of dissipation rate by comparing present methods with the dissipation rate obtained from the closing term of the turbulent energy equation in a diffuser flow at x = 54 cm

Figure 5.16a Different methods of obtaining dissipation rate in a diffuser flow at x = 66 cm.

Figure 5.16b Assessment of dissipation rate by comparing present methods with the dissipation rate obtained from the closing term of the turbulent energy equation in a diffuser flow at x = 66 cm

Figure 5.17 Ratio of dissipation obtained between the

different lengths of wire and standard wire plotted against non-dimensional radial distance.

Figure 5.18 Dissipation rate obtained from the measurements of $\partial u/\partial t$ with standard boundary layer probe in a diffuser flow
(a) x = 6 cm.
(b) x = 42 cm.
(c) x = 66 cm.

Figure 5.19 Area integrated value of dissipation rate obtained by extrapolation to zero length and then corrected for high intensity turbulence compared with the one obtained from the closing term of the turbulent energy equation.

Figure 6.1 Mean velocity profiles for different free-stream velocities.

Figure 6.2 Skin friction coefficient variation with Reynolds number.

Figure 6.3 Distribution of U^+ versus y^+ in the boundary layer.

Figure 6.4 Distribution of the u, v, w fluctuations normalized by the free stream velocity.
(a) Results away from the wall.
(b) Results in the vicinity of the wall.

Figure 6.5 Distribution of stress-energy ratio across the boundary layer.

Figure 6.6 Skewness of u, $S(u) = \overline{u^3}/\overline{(u^2)^{3/2}}$.

Figure 6.7 Flatness factor of u, $F(u) = \overline{u^4}/\overline{(u^2)^2}$.

Figure 6.8 Higher-order moments of the normal fluctuating velocity component in the boundary layer.
(a) Third order.
(b) Fourth order.

Figure 6.9 Flatness factor of w, $F(w) = \overline{w^4}/\overline{(w^2)^2}$,

Figure 6.10 Profiles of turbulent transport velocity of $\overline{q^2}$, $V_q = \overline{vq^2}/\overline{q^2}$ and of uv, $V_\zeta = \overline{uv^2}/\overline{uv}$, expressed nondimensionally in relation to U.

Figure 6.11 The integral scale of the longitudinal turbulent component velocity.

Figure 6.12 Dissipation length parameter, $L = \overline{(-uv)^{3/2}}/\epsilon$, expressed nondimensionally in relation to δ.

Figure 6.13 Turbulent energy balance across the boundary

layer, all terms made dimensionless by U_∞^3/δ.

Figure 6.14 Shear stress balance across the boundary layer, all terms made dimensionless by U_∞^3/δ.

Figure 7.1 Surface pressure and its gradient in fully developed pipe flow and in diffuser flow.

Figure 7.2 Friction velocity in fully developed pipe flow and in conical diffuser flow.

Figure 7.3a Area weighted mean values of twice the mean and turbulent kinetic energies per unit mass along the axial distance of the diffuser.

Figure 7.3b Variation of $\langle\overline{q^2}\rangle_{AM}$ and $\overline{q^2}_{max}$ along the axial length of the diffuser.

Figure 7.4 Rate of normal strain, $\partial U/\partial x$.

Figure 7.5 Basic rate of shear strain, $\partial U/\partial r$.

Figure 7.6a Transverse mean velocity V across different locations in the diffuser.

Figure 7.6b Extra strain-rate $\partial V/\partial x$ in the diffuser.

Figure 7.6c Extra strain-rate non-dimensionalized by main strain-rate in a diffuser flow.

Figure 7.7 Ratio of transverse to longitudinal mean-square turbulent intensity in diffuser and pipe flow.

Figure 7.8 Profiles of turbulent energy $\overline{q^2} = 0.5(\overline{u^2}+\overline{v^2}+\overline{w^2})$.

Figure 7.9 Shear-stress profiles.

Figure 7.10 Stress-energy ratio $a_1 = \overline{uv}/\overline{q^2}$.

Figure 7.11a Profiles of turbulent transport velocity of $\overline{q^2}$, $V_q/U_b = \overline{vq^2}/(\overline{q^2}U_b)$.

Figure 7.11b Relative strength of large eddies, $[(\overline{vq^2})_{max} - (\overline{vq^2})_{min}]/(\overline{q^2})^{3/2}_{max}$.

Figure 7.12a Profiles of turbulent transport velocity of $\overline{uv}$, $V_\tau/U_b = \overline{uv^2}/(\overline{uv}U_b)$.

Figure 7.12b Ratio of triple products, $\overline{uv^2}/\overline{vq^2}$.

Figure 7.13 The time scale $\tau = \overline{q^2}/(2\epsilon)$.

Figure 7.14 Dissipation length scale.
(a) $L_\epsilon = (\overline{q^2})^{3/2}/\epsilon$.
(b) $L^\epsilon = (\overline{uv})^{3/2}/\epsilon$.

Figure 7.15 Profiles of the difference of production, P and dissipation, ϵ. P and ϵ are nondimensionalized by R/U_b^3. R = 0.0508 m and U_b = 18.06 ms^{-1}.

Figure 7.16 Turbulent energy balance.
(a) Fully developed pipe flow.
(b) Diffuser flow: x/D = 0.59.
(c) Diffuser flow: x/D = 1.77.
(d) Diffuser flow: x/D = 4.13.
(e) Diffuser flow: x/D = 6.50.
All terms made dimensionless by R/U_b^3.

Figure 7.17 Shear stress balance.
(a) Fully developed pipe flow.
(b) Diffuser flow: x/D = 0.59.
(c) Diffuser flow: x/D = 1.77.
(d) Diffuser flow: x/D = 4.13.
(e) Diffuser flow: x/D = 6.50.
All terms made dimensionless by R/U_b^3.

Figure 7.18 strain parameter, β, and relaxation length scale, L_R.

Figure 7.19 Area integrated values of terms of turbulent energy equation along the diffuser.
All terms made dimensionless by R/U_b^3.

Figure 7.20 The ratio of advection to production.

Figure A.1 Geometries of X-array hot-wire probe set-ups used in measurements.

Figure A.2 Mean velocity profile in a boundary layer obtained by three different X-array hot-wire probes.

Figure A.3 Distribution of Reynolds stress coefficient, $R_{12} = -\overline{uv}/(\overline{u^2}\overline{v^2})^{1/2}$, in a boundary layer.

Figure B.1 Moments of turbulent fluctuating velocity in boundary layer
(a) $\overline{w^2}/(\overline{u^2} + \overline{v^2})$
(b) $\overline{vw^2}/(\overline{u^2}\overline{v} + \overline{v^3})$

Figure B.2 Moments of turbulent fluctuating velocity in fully developed pipe flow
(a) $\overline{w^2}/(\overline{u^2} + \overline{v^2})$
(b) $\overline{vw^2}/(\overline{u^2}\overline{v} + \overline{v^3})$

Figure B.3 Moments of turbulent fluctuating velocity in diffuser flow: x= 42 cm from the inlet.
(a) $\overline{w^2}/(\overline{u^2} + \overline{v^2})$
(b) O $\overline{vw^2}$, Δ $0.5(\overline{u^2}\overline{v} + \overline{v^3})$

Figure C.1 Skin friction coefficient versus Reynolds number.

Figure C.2 Distribution of U^+ versus y^+ for different Reynolds numbers.

Figure C.3 Wall static pressure measurements.
(a) Circumferential measurements.
(b) longitudinal measurements.

Figure C.4 Distribution of the skewness of u at different stations.

Figure C.5 Longitudinal turbulence intensity across the pipe.

Figure D.1 Dimensionless mean velocity profiles.
(a) Pipe flow and stations 1-5.
(b) Stations 5-9.
(c) Stations 9-13.
(d) Stations 13-17.

NOMENCLATURE

A, B	Coefficients in logarithmic law velocity distribution.
C_f	Skin friction coefficient [$= 2(u^*/U_\infty)^2$].
D	Pipe inside diameter (= 10.16 cm).
d	Diameter of the hot wire.
d_p	Outer diameter of Preston tube.
d_i	Inner diameter of Preston tube.
$E_1(k_1)$	One dimensional u^2-spectra.
f	Midband frequency.
f_k	Kolmogoroff frequency [$= U/(2\pi\eta)$].
k_1	One dimensional wavenumber ($= 2\pi f/U$).
L	Dissipation length scale ($= \overline{(uv)^{3/2}}/\epsilon$).
L_ϵ	Dissipation length scale ($= \overline{(q^2)^{3/2}}/\epsilon$).
L_R	Relaxation length scale.
L_f	Eulerian longitudinal integeral length scale.
l	Sensitive length of the hot wire.
P_s	local static pressure.
p	Fluctuating component of the pressure field.
$\overline{q^2}$	Twice the turbulent kinetic energy, ($= \overline{u^2} + \overline{v^2} + \overline{w^2}$).
R	Pipe radius.
R_{LOC}	local radius of the diffuser.
Re	Reynolds number ($= U_b D/\nu$).
R_λ	Turbulent Reynolds number [$= \overline{(u^2)^{1/2}}\lambda/\nu$].
R_θ	Reynolds number based on the momentum thickenss ($U_\infty\theta/\nu$).

r	radial distance from the axis.
U	Local mean velocity in x-direction.
U_b	Cross-sectional average mean velocity (x-direction) in pipe.
U_c	Centreline velocity.
U^+	Dimensionless local mean velocity (= U/u^*).
u	Fluctuating velocity in x direction.
u^*	Friction velocity.
V	Mean radial velocity.
v	Fluctuating velocity in transverse direction.
w	Fluctuating circumferential velocity component.
x	Axial distance in the streamwise direction.
x_w	Distance along diffuser wall (measured from the inlet).
y	Radial distance from the wall and perpendicular to the axis.
y_w	Distance from the diffuser wall in direction orthogonal to wall.
y^+	Dimensionless position (= yu^*/ν).
δ	Boundary layer thickness.
δ^*	Displacement thickness.
Δ	Dimensionless pressure gradient parameter, [= $\{\nu/(\rho u^{*3})\}dP_s/dx$].
Δ'	Dimensionless pressure gradient parameter [= $(\delta^*/\tau_w)dP_s/dx$].
ϵ	Turbulent energy dissipation per unit mass.
η	Kolmogoroff length scale [= $(\nu^3/\epsilon)^{1/4}$].
κ	Von Karman constant (= 0.41).
λ	Taylor's microscale (dissipation length scale).
ν	Kinematic viscosity.
θ	Momentum thickness.

ρ Density.

τ_w Wall shear stress.

CHAPTER 1

INTRODUCTION

Turbulence is neither a completely random, nor well ordered phenomenon. Therefore, it has structure which has been the subject of many theoretical and experimental investigation. By structure of turbulence is meant the organization of turbulence phenomenon, the source of its energy supply and the mechanism by which this energy is extracted from the mean flow, and distributed to the whole flow field and finally how it is converted to the internal (heat) energy by the action of viscosity. The theoretical investigation has not been successful, so the experimental as well as modelling of the flow have been attempted and borne some fruit. To achieve this, it is necessary to do experiments on turbulence in order to expand our understanding and to provide empirical data for calculation methods. Towards this end, the present study in axisymmetric wall bounded flow was chosen in the hope that the turbulent flows in this geometry would reveal physical features of turbulence.

A completely axisymmetric bounded flow can have three basic geometrical configurations, namely, pipe-like flow, contraction-like flow and diffuser-like flow. The most complicated of these flows is the flow in a diffuser.

Further, an axisymmetric flow has characteristics intermediate between those of two and three dimensional flows. In addition, such a flow has identical points at a fixed radius at a given location on the axis of symmetry where any physical parameters can be verified one against the other experimentally in the long time mean. Furthermore, any parameter can be averaged at such corresponding spatial locations to give reliable experimental results. To accommodate these advantages in the present investigation, the turbulence structure has been experimentally studied in three different shear flows, namely, low Reynolds number turbulent boundary layer growing inside a pipe wall, fully developed pipe flow and conical diffuser flow. The first two flows are simple flows but they have great importance for many engineering problems. The conical diffuser has a simple geometry, but its flow is considered to be a complex one.

Boundary layer and fully developed pipe flows were first investigated to prove the instrumentations and the known physics of turbulence available in the open literature. Another reason for studying fully developed pipe flow was because it was the inlet flow to the diffuser flow that was investigated in the present study.

A diffuser research program has been underway in the Department of Mechanical Engineering of the University of Manitoba for two decades. This experimental work has

concentrated on examining the flow structure within a straight conical diffuser having a total divergence angle of 8^0 and an area ratio of 4:1 with fully developed pipe flow at entry. The choice of the diffuser geometry was guided by the work of Sprenger (1959) and Sovran and Klomp (1967), whose results show that such a diffuser possesses optimum pressure recovery characteristics. The results of this program have been published periodically, e.g. Okwuobi and Azad (1973), Arora and Azad (1980a; b), Azad and Hummel (1971, 1979; 1981) and Singh and Azad (1981). The present study is a continuation of this program. In particular attempts have been made to improve the accuracy of the turbulent energy balances.

The turbulent energy balance provides insight into the relative importance of each physical mechanism in the turbulent flow field. Further, knowledge of the energy balance is also important from the point of view of developing and testing mathematical models for turbulence. For example, as suggested by Townsend (1980, p. 205), the choice of model of flow can be decided on after examining the terms of the kinetic energy equation. One of the physical quantity, the so-called dissipation, has been obtained from spectra of wires of different lengths to improve the accuracy of dissipation and to assess the error involved in the closing term of the turbulent energy equation. Spectral analysis provides the description of the

structure of turbulence which shows how the eddies of different sizes are dynamically related in exchange of energy. Most of the spectral ideas are present for isotropy in general or for local isotropy. These ideas are used in shear flows in the hope of obtaining some physical picture of the flow in the present case.

Experimental set-up and procedure are described in chapter 2. The main part of the thesis is divided into two parts. Part one starts with chapter 3 which contains the spectral data which form the basis for chapters 4 and 5. In chapter 4, k_1^{-1} spectral law is discussed for the three different flows under investigation. The dissipation of turbulent energy in boundary layer, fully developed pipe flow and in diffuser flow, are presented and thoroughly discussed in chapter 5. Part two contains chapters 6 and 7. Chapter 6 contains the results of low Reynolds number turbulent boundary layer flow. Finally, the general picture of the flow in the fully developed pipe flow and the diffuser flow are presented and thoroughly discussed in chapter 7.

CHAPTER 2

EXPERIMENTAL FACILITIES AND PROCEDURE

The study of turbulence in axisymmetric flows was selected because of its simplicity as well as its position being half way between two and three dimensional flows. Internal axisymmetric flow may be described by the flows in a pipe, a contraction cone and a diffuser. In the present study, the flow structures in the pipe and the diffuser have been examined. For this, separate experimental set-ups are described for three shear flows. Because the instruments and the procedures for the measurements have common features, they are outlined collectively.

2.1 BOUNDARY LAYER FACILITIES

The boundary layer developed on the wall of a pipe was studied in an open-return type low speed wind tunnel. A plan view of the wind tunnel which uses air as a fluid medium is shown in figure 2.1. The aerofoil-bladed 30.5 cm diameter Woods four-stage fans of the wind tunnel are driven by two-speed four-pole ball bearing motors. Different flow velocities in the tunnel are obtained with the combination of two fan speeds, different blade angles and damper settings. A detailed description of most of the parts of the wind tunnel is available in Appendix A of Trupp (1973).

A gunmetal pipe of mirror-finish smooth surface of nominal diameter 27.0 cm and 2.67 m length was attached to the circular contraction cone of area ratio 16:1. Boundary layer tripping and its thickening were obtained by pasting No. 16 floor-sanding paper [recommended by Klebanoff and Diehl (1952)] to the first 27 cm length of the pipe.

The measuring stations were located at 2.25 to 2.29 m from the end of the trip and all the X-wire data are presented for the middle of the region. These locations were well inside the pipe (11 to 15 cm from the exit) to be free from end effects.

Also, intermittency is known to exist up to 1.2δ, where δ is the boundary layer thickness at which the mean velocity is 0.99 of free stream velocity, U_∞. The non-turbulent central region was almost three times of 1.2δ to avoid boundary layer interaction from opposite sides of the tunnel.

The tunnel can generate free stream velocities from 2 ms^{-1} to 14 ms^{-1} on the centreline at the measuring stations. Required free stream velocities were obtained by adjusting the fan power and measuring the pressure drop across the contraction cone which was calibrated with a Pitot-tube in terms of free stream velocity on the centreline at the measuring station. The pressure across the contraction cone was measured with a 0-0.5 inch water gauge inclined

manometer (Airflow Developments). Probes were brought into the pipe from its open end and manipulated using the traversing mechanism described in details by Burhanuddin (1980).

2.2 FULLY DEVELOPED PIPE FLOW AND DIFFUSER FLOW FACILITIES

Figure 2.2 shows the layout of the open circuit air tunnel used for the studies of fully developed pipe flow and diffuser flow. A fan driven by a 25 h.p. D.C. motor blows air into a rectangular-to-circular duct followed by a flexible coupling. The settling chamber, 91.4 cm in diameter and 2.20 m long, was provided with three sets of fine mesh screens with each set consisting of two screens. The circular contraction cone with an area ratio of 89:1 was fabricated from plywood. Boundary layer tripping was obtained by pasting the first 8 cm length of the pipe with No. 16 floor-sanding paper.

For the fully developed pipe flow, the total length of the pipe attached to the contraction cone exit was 8.2 m. The pipe inside diameter was D = 0.1016 m. Following Preston's (1950) recommendation, the position of the measurements reported here is 0.5D from the pipe exit. This gives a pipe length L = 78D from the end of the trip to the measurements location. Four sets of static pressure holes of 1 mm diameter and spaced 90^0 apart were drilled at intervals of 1 m along the pipe wall. The last set was located at the measurement position.

For the diffuser flow, a seventy-four diameter long steel pipe of inside diameter, D = 10.16 cm was used to feed fully developed flow into the diffuser. The conical diffuser, which discharged to the atmosphere, was machined from cast aluminum and had 8^0 solid angle and an area ratio of 4:1 over its length of 72 cm. Static pressure holes of 0.6 mm diameter and spaced 90^0 apart were drilled at intervals of 6 cm along the wall of the diffuser.

The Reynolds number of the flow was varied by changing the fan speed and observing the pressure drop across the contraction cone which was calibrated in terms of centreline mean velocity.

Probes were brought into the pipe as well as the diffuser from their open end. The traversing mechanism for this wind tunnel consists of a coordinate table (Model FB102, M.S. Tool Supplies) having a longitudinal feed of 37 cm, a cross feed of 15 cm, attached to a circular milling table for angle setting and a micro-stage which could slide on the coordinate table. A digit micrometer head (dual directional counter type, Mitutoyo Mtg.) having 0.01 mm graduation and 0-25 mm range was used to slide the micro-stage on the table along the horizontal diameter of the pipe and the diffuser. A vertical slide attached to the micro-stage was used to hold the DISA 55E40 traversing mechanism. The coordinate table was kept in a horizontal position by using balancing weights and a spirit level. Initial

positioning of the probes involved using a sensitive resistance meter (Honar KRT 101 or ELCO 68), connected between the probe and the conducting wall, to indicate contact when the probe touched the wall.

2.3 INSTRUMENTATION

Electronic and mechanical instruments were used for this research. Because the instruments are the same for the measurements in the three flows, they will be mentioned collectively.

2.3.1 PRESSURE MEASUREMENTS

Velocity measurements were made using both Pitot-tube and linearized hot wire anemometry. The Pitot-tube (United Sensor, USC-E-120-03) was of 1.2 mm outer diameter with a flattened tip. Measurements of local static pressure were made using a static pressure tube of 1.2 mm outer diameter (United Sensor, USC-E-120-04). Measurements of local wall shear stress were obtained (beside other methods) using five locally made Preston tubes (see Table 2.1). Pressure differences were measured using a Betz projection manometer (graduations of 0.1 mm water and range from -17 to 400 mm water) and a Combustion Instruments Ltd. micromanometer design by Bradshaw (1965) (graduation of 0.01 mm water and range from 0 to 30 mm water). A MKS Baratron Type 223B pressure transducer became available near the end of this

study. Tested with the same pressure, the Baratron and the manometers gave nearly identical results.

2.3.2 HOT WIRE PROBES

Nearly all measurements of single wire were made by standard hot wire probe DISA 55P05 used for boundary layer, since this probe could approach closest to the wall. The hot wire had nominal length of 1.25 mm and of diameter 5 μm. True dissipation by invoking isotropy to the dissipating eddies can be obtained by extrapolating the results of dissipation calculated from the measured spectra for different lengths of the hot wire. Hence it was decided to select five hot wire probes of the same diameter but different lengths for measurements of $\partial u/\partial t$ as well as of spectra. In addition to this another probe of different diameter and the length equal to one of the above was chosen because the value of dissipation obtained from the previous group was lower than its position on the extrapolated line due to lower l/d ratio than 200. All these probes were specially made by DISA based on the DISA 55P05 boundary layer probe. The individual wires were photographed with ISI min-sem scanning electron microscope for obtaining a precise estimate of the wire dimensions. Table 2.2 gives the dimensions of four standard wires used and Table 2.3 gives the dimensions of the special wires and the mean dimensions of standard wires obtained from Table 2.2.

Most of the X-wire measurements were made with the standard DISA 55P51 gold plated X-probe. To study the aerodynamic interference of the probe stem, two right angled X-probes DISA 55P53 and DISA 55P54 were used beside the in-line probe DISA 55P51. The sensing wire of these probes was platinum plated tungsten of nominal length of 1.25 mm and nominal diameter of 5 μm and its supports were gold plated.

2.3.3 SINGLE WIRE MEASUREMENTS

Two different set-ups for a single hot wire were used during the measurements of quantities necessary for this study. These set-ups (a) and (b) are shown in block diagrams in figure 2.3. The common part of the diagram for both the set-ups will described first and then the remainder in each diagram is followed. Signal from the single hot wire was led to the Constant Temperature Anemometer (CTA) DISA 55M01 and one output from it went to Channel Selector DISA 52A35, and other went to a Linearizer DISA 55M25 or DISA 55D10. The linearizer output connecting channel selector and CTA formed a group to produce linearized turbulence signal after the procedures were followed as outlined in DISA instruction manuals. The Digital Voltmeter (DVM) DISA 55D31 gave the mean voltage corresponding to the mean velocity, U, in the streamwise direction. The channel selector was also connected to the oscilloscope to display a.c. signal corresponding to the fluctuating velocity, u, in the streamwise direction.

Differentiation of the a.c. signal is used for the calculation of the dissipation in the isotropic turbulence. Consequently the equipment used, procedures and the methods adopted for obtaining the differentiation of a.c. signal are described below. The second output from the linearizer went to Low-Pass (LP) filter (Krohn-Hite 3550) to eliminate high frequency electronic noise from the circuits of anemometer, linearizer etc before differentiation and afterwards the clean signal went to the differentiator, called Spectral Processor, which was based on the circuit used by Wyngaard and Lumley (1967). In order to improve signal-to-noise ratio and to minimize aliasing, the output of the differentiator was again low passed through a filter (Krohn-Hite 3550). The above procedure was also followed by Champagne (1978).

Both low-pass filters were set at the Kolmogoroff frequency $f_k = U/(2\pi\eta)$, where the Kolmogoroff length scale, $\eta = (\nu^3/\epsilon)^{1/4}$, the mean dissipation rate, ϵ, and the kinematic viscosity of the fluid, ν, for consistency of different Reynolds numbers [in this regard see Kuo and Corrsin (1971) and also Frenkiel and Klebanoff (1975)]. At the start of an experiment the f_k was not known and so its value was assumed to be 20 KHz. After these settings the measurement of $\overline{(\partial u/\partial t)^2}$ was made and its value was used to calculate ϵ. Once ϵ and η were known the new value of f_k was calculated. This process was repeated twice to obtain the repeatable value for f_k [see Hummel (1978, p. 68)].

Now, the separate parts of set-ups (a) and (b) can be described on their own.

2.3.3.1 SET-UP(a)

In this case another Channel Selector was used and its function was to receive a.c. signal from the linearizer and also to receive signal corresponding to $\partial u/\partial t$ after the second low-pass filter which was located after the differentiator. Root mean square, mean square and instantaneous mean square values were obtained from RMS meter DISA 55D35. The inputs A and B of Turbulence Processor DISA 52B25 were fed by instantaneous square signal and just instantaneous signal from RMS meter and channel selector respectively. Different combinations of these signals, the mean cube and fourth power of a signal were obtained. This set-up(a) enabled us to measure the following quantities in the shear flow that was under investigation :

$$U,\ \overline{(u^2)^{1/2}},\ \overline{u^2},\ \overline{u^3},\ \overline{u^4}$$

$$\overline{[(\partial u/\partial t)^2]^{1/2}},\ \overline{(\partial u/\partial t)^2},\ \overline{(\partial u/\partial t)^3},\ \overline{(\partial u/\partial t)^4}$$

The drawback of this set-up(a) was that two signals were not from the same time domain of the flow but at different time domain and the difference in time could have been as much as ten minutes.

2.3.3.2 SET-UP(b)

In this case a.c. signal from the linearizer and the differentiated signal from the output of the second low-pass filter went respectively to inputs B and A of the Multi-function Turbulence Processor TM377. The details of this instrument is not given here, since it is described adequately by Arora and Azad (1978). This set-up interchanged the Channel Selector and Turbulence Processor of set-up(a). In addition it processed both the primary data, i.e., a.c. and its differential signals, in the frozen time domain. In other words, the processed data can be thought of as coming from the same sample so that reliable physical picture can be built due to these data being timewise related to each other. The set-up(b) also reduced the time required for measurements since simultaneous measurements were obtained. Only part of the measurements in the boundary layer were made by set-up(a) and the other measurements in the boundary layer and other flows were obtained with set-up(b)

2.3.4 X-WIRE MEASUREMENTS

Moments other than the longitudinal velocity fluctuating ones can only be measured by using X-wire. For energy budgets and shear stress equations moments of pure and mixed types of order three are required to assess them. The block diagram for these configurations are shown in figure 2.4.

The signals from each X-wire first go to CTA (DISA 55M01) and then from each anemometer one signal goes to channel selector (DISA 52A35) and the other to the linearizer (DISA 55M25). Each linearizer is connected to channel selector and to input A or B of the Multi-function Turbulence Processor (TM 377). The channel selector hereafter is connected to Digital Voltmeter (DISA 55D31) and also to the Tektronix 466 storage oscilloscope. DISA technical manuals were followed to obtain linearized hot-wire signals. The outputs of the Multi-function turbulence processor are first integrated and then fed to digital voltmeter to register the voltages corresponding to the moments. Three settings, namely, 5, 20 and 100 seconds are available on the Multi-Integraters. In the present experiment the suggestion of Johnson and Eckelmann (1984) regarding longer time for averaging higher moments has been adopted and in turn an averaging time of 100 seconds is used for all the moments. To avoid phase difference, which is necessary in adding and subtracting two signals to obtain instantaneous values of the signals, the time constant for both wires of the X-probe have been matched according to method suggested by Schubauer and Klebanoff (1946). When the X-wire is lying in x-r plane, the following outputs are obtained:

$\overline{u^2}/10$, $\overline{u^3}/100$, $\overline{u^4}/1000$, $\overline{uv}/10$, $\overline{v^2}/10$, $\overline{v^3}/100$,

$\overline{v^4}/1000$, $\overline{uv^2}/100$, $\overline{uv^3}/1000$, $\overline{u^3v}/1000$,

$\overline{u^2v^2}/1000$, $\overline{u^2v}/100$, U and V.

These quantities are also given in figure 2.4. The signals corresponding to instantaneous velocities u and v also obtained from this location of X-probe and are displayed on storage oscilloscope for the purpose of constant observation and adjusting the signal for clipping and also under amplification. The root mean square (RMS) values of u and v are obtained from two RMS meters (DISA 55D35) which are fed from Multi-function Turbulence Processor. If the X-wire is placed in x-θ plane, all the quantities similar to the ones that obtained in x-r plane are obtained but the difference in the quantities would be the replacement of v by w. Reader interested in the circuit of the Multi-function Turbulence Processor are directed to consult Arora and Azad (1978).

2.3.5 SPECTRA MEASUREMENTS

To measure spectra, the low-pass cut-off frequency is generally set at the Kolmogoroff frequency, f_k, since no practicable measured energy in turbulence is available after this frequency due to predominance of noise. Kuo and Corrsin (1971) have also used low-pass filter to cut-off the highest frequencies at f_k. Another reason for choosing Kolmogoroff frequency is to be consistent with different Reynolds number flows. Frenkiel and Klebanoff (1975) have also followed the above procedure. To obtain f_k, it is necessary to measure mean dissipation, ϵ, which is used to calculate $\eta = (\nu^3/\epsilon)^{1/4}$. Now the dissipation may be calculated using isotropic relationship :

$$\epsilon = 15\nu\overline{(\partial u/\partial t)^2}/U^2$$

In the above expression, the $\overline{(\partial u/\partial t)^2}$ and mean velocity U have to be measured by hot wire anemometer preferably by a single hot wire. For these measurements, the details of the circuit and the procedure are given in subsection 2.3.3. Once the heightest Kolmogoroff frequency, f_k, at any cross-section of the flow was determined, then thirty midband frequencies were chosen between 2 Hz and $2f_k$ for measurement of spectra. The minimum value of frequency i.e., 2 Hz was dictated by the available band-pass filter. These frequency positions were chosen to be logarithmically distributed so that Simpson's rule of integration can be easily adopted and furthermore this choice gave equal distribution of data points on the spectral curve.

The block diagram for measurement of spectra is shown in figure 2.5. In the figure shown, a signal corresponding to instantaneous longitudinal component of velocity from a single hot wire was fed to a Constant Temperature Anemometer (CTA) DISA 55M01 and the signal from CTA went to a Linearizer DISA 55M25 to linearize the signal and to a Channel Selector DISA 55A35 so that the signal was displayed on Tektronix 466 Storage Oscilloscope. The average of the linearized signal gave the mean velocity which was read by Digital Voltmeter DISA 55D31. The fluctuating part of the signal was squared and averaged by Root Mean Square (RMS) meter DISA 55D35. The a.c. signal from the linearizer first

went to Low-Pass (LP) filter Krohn-Hite 3550 set at f_k and then went to Band-Pass (BP) filter Krohn-Hite 3550 for measurement of energy in each frequency. The output from each band was measured by RMS meter DISA 55D35. Any output signal was displayed on the Oscilloscope shown in the figure.

Noise from electronic circuits were thought to mask the lower values of the signals at higher frequencies available for spectra. Hence it was necessary to investigate the noise and the results of this investigation are reported in next chapter.

2.4 GENERAL PROCEDURE

The standard procedure recommended in the DISA technical literature for the hot wire operation was followed to obtain the linearized turbulence signal from the single and X-wire probes. The circumferential velocity component, w, was obtained by rotating the X-probe on its axis by 90^0 from the u-v plane. The vw component was obtained by aligning the X-probe at 45^0 to both x-y and x-z planes.

In view of the significant change in probe calibration due to change in ambient temperature and dust deposition, it is considered that the safest procedure is to calibrate the probe in situ against a Pitot, during the course of the turbulence measurements.

The linearized outputs from the X-probe wires were matched to within 1.5% over the required operation range. The probes were calibrated for measurements at each station. The thermal stability of the electronic equipment was maintained by allowing the units to remain powered during the course of the experimental work even when the instruments were not in use. The single and X-wire probes were operated at an overheat ratio of 0.8.

The experimental values obtained via X-probe for v and w fluctuating velocities have been corrected for yaw using the yaw factor, $k = 0.23$. This value has been obtained after comparing the theoretical with the measured Reynolds shear stress, $\overline{uv}$, in the fully developed pipe flow.

Previous works on conical diffuser were analyzed to see whether it was possible to obtain axial derivatives of mean and turbulence quantities that had been measured radially. It was concluded that the axial derivatives cannot be obtained from radial measurements of turbulent flows in conical diffuser at different days. The reason for this is two fold, one being its smaller values and the other is that the values varies slowly with x-direction. In addition turbulent flow cannot be repeated exactly in its entirely from day to day. These facts have also been observed by many researchers, just to name a few, Comte-Bellot and Corrsin (1966) and Simpson et al. (1981). Based on this study all the quantities in the turbulent kinetic energy equation

(TKEE) and shear stress equation (SSE) whose axial derivatives are needed, are measured axially to improve the derivative of these quantities. Thus measurements are made axially as well as radially, because radial derivatives are also needed for both equations, TKEE and SSE.

CHAPTER 3

SPECTRAL DATA IN AXISYMMETRIC WALL-BOUNDED SHEAR FLOW

3.1 INTRODUCTION

There is a possibility of analyzing the kinetic energy of turbulence fluctuations according to its distribution over the various frequencies which are prevalent in these fluctuations.[1] This type of analysis is referred to as spectral analysis of turbulence. Spectral analysis provides the description of the structure of turbulence which shows how the eddies of different sizes are dynamically related in exchange of energy. While the largest eddies cause fluctuations of low frequencies, the smallest eddies cause fluctuations of high frequencies. When the turbulence is dominated by large eddies, the spectrum function exists mainly in the region of low frequencies. On the other hand if the turbulence contains only small eddies, the spectrum function only exists in the higher frequency range. The eddies that lie between these two regions are not affected by viscosity; this region is called the inertial subrange about which Kolmogoroff (1941) has formulated -5/3 spectral law. Most of the spectral ideas are present for isotropy in general or for local isotropy. These ideas are used in shear

[1] This chapter is based on the report by Azad and Kassab (1985a).

flows in attempting to get some physical picture of the flow. For this reason the measurements of spectra have been made in a boundary layer, fully developed pipe flow and in a conical diffuser.

Tabulated results are given in a report by Azad and Kassab (1985a) for its ease and convenience to use in testing spectral models in shear flows. To illustrate the importance of these data the mechanism of turbulence in these different shear flows are discussed and illustrated by figures. For example dissipation in these flows can be obtained from the energy spectra.

3.2 RESULTS AND DISCUSSION

At each position of measurements, the local mean velocity, U, the mean square of the longitudinal velocity fluctuation, $\overline{u^2}$, and the mean square of the filtered signal u^2 for each midband frequency setting were obtained. These results are changed into the wavenumber space by using Taylor hypothesis as $k_1 = 2\pi f/U$, where k_1 is the one dimensional wavenumber and f is the midband frequency. The details of the calculation starting from the measured values to the final products in the wavenumber space is given in Appendix C of Azad and Kassab (1985a). Now we have one dimensional energy spectrum denoted by $E_1(k_1)$ and the one dimensional wavenumber k_1.

Figures are drawn of $E_1(k_1)$ versus k_1. They are presented in two forms. Firstly, all the spectra at any cross-section, whether it is in a boundary layer or in a pipe or in a diffuser, are plotted together so that they can be compared with each other. For each flow they are separately plotted. In the case of diffuser flow there are three set of spectra for cross-section perpendicular to the axis of the diffuser. Beside these, there are two other figures for diffuser flow in which one figure shows measurement of spectra normal to the wall whereas the second shows spectra at three different locations measured with different diameters and lengths of the hot wire.

The second form of presentation of results are given where some of the spectra previously plotted are again plotted in enlarged form from lowest wavenumber of measurement to past the wavenumber of the inertial subrange. The reason for doing this is three fold : one to find the integral length scale defined by

$$\lim_{k_1 \to 0} E_1(k_1)/\overline{u^2} = 2L_f/\pi$$

where L_f is the Eulerian longitudinal length scale, the second is to examine k_1^{-1} spectral law introduced by Tchen (1953) and the third is to investigate the spectra for the inertial subrange. The inertial subrange spectral law is defined by

$$E_1(k_1) = C_2 \epsilon^{2/3} k_1^{-5/3}$$

from which the dissipation rate ϵ can be calculated.

Results for three flows are given separately. First there are twelve positions between 0.5 mm and the boundary layer thickness, δ, where spectra were measured. The first closest point to the wall i.e., 0.5 mm was chosen because the hot wire signal was not affected by the wall [see Azad and Kassab (1986a) and see also Azad (1983) for comprehensive review on the subject]. The spectra results for twelve positions are given in figures 3.1 and 3.2. Ozimek (1986, pp. 112-123) has made comparison of digital and analog processing of $\overline{u^2}$-spectra and has found no difference between them. The present results for $\overline{u^2}$-spectra in boundary layer are also given in the comparison. Because the boundary layer was grown on a pipe-wall, the axisymmetry of the flow in the pipe was checked by measurements of spectra and their results are given in figure 3.3. Spectra for different wire lengths and diameters are given in figure 3.4.

Fifteen results of one dimensional spectra were obtained in the pipe. These are presented in figures 3.5 and 3.6.

The locations of measurements in the diffuser were first chosen at 6, 18, 30, 42, 54 and 66 cm from the inlet of the diffuser. First, the measurements were made at 42, 54 and 66 cm. Two of the objectives, namely, finding the integral length scale and investigating the k_1^{-1} spectral law, looked bleak after the spectral functions at 42, 54 and 66cm. In addition to this, large amounts of time were required to finish all the spectra at three cross-sections. Hence, it

was decided to abandon the measurement of spectra at other locations. Thirteen spectra results perpendicular to the axis of the diffuser are presented for each locations chosen in the diffuser in figure 3.7. The first position closest to the wall chosen for measurement was again located at 0.5 mm from the wall, where the wall effect was not felt.

Results of spectra obtained with five different probes are presented in figure 3.8. These spectra were measured at r/R_{LOC}= 0.85 , where r is the distance from the axis of the diffuser and R_{LOC} is the local radius of the diffuser, for three axial locations, namely, 6 , 42 and 66 cms from the inlet of the diffuser.

The last set of the results of spectra are presented to examine the k_1^{-1} spectral law introduced by Tchen (1953) in figures 3.9 and 3.10. These results were obtained by traversing the probe normal to the wall within y_w/R_{LOC} = 0.1, where y_w is the distance from the wall. The distance y_w/R_{LOC}= 0.1 was chosen according to the findings of Perry and Abell (1977) who found the k_1^{-1} spectral law to be valid only within this distance in the fully developed pipe flow. Discussion of these results is given in the next chapter. Next, the noise in the spectrum is examined.

Since the free stream turbulence would be present in almost all the flow, so the flow in the core region of the pipe, where boundary layer was grown on its wall, also

contained free stream turbulent. However the magnitude of the turbulence was very low. The signal at the centreline in core region of the pipe was assumed, according to Gibson (1963) and later on followed by Champagne (1978), to consist of entirely electronic noise. Under this assumption, spectra of the noise were obtained at the centreline which had mean velocities the same as the points where the spectra were corrected. Spectra at two locations, namely, 1 and 30 mm from the wall were corrected by subtracting the noise from them for each band. The values of noise spectra corresponding to the lower velocity at 1 mm from the wall were lower than the one corresponding to that of 30 mm from the wall [see Tables 99 and 100 of Azad and Kassab (1985a)]. This reason was partially due to higher turbulence for higher mean velocity. The corrected and uncorrected values of spectra for y = 30 mm are shown in figure 3.3. The hot wire produced higher noise level with increasing frequencies or wavenumbers [see for example Rasmussen (1966)]. Pao (1965) noted this fact in his investigation too. Large wavenumber were more pronounced if the spectra corresponding to dissipation of vorticity were plotted, i.e.,

$$(k_1\eta)^4\Phi(k_1\eta) \quad \text{vs.} \quad (k_1\eta)$$

where,

$$\Phi(k_1\eta) = E_1(k_1)/(\eta v^2) = E_1(k_1)/(\epsilon\nu^5)^{1/4} ,$$

$$\eta = (\nu^3/\epsilon)^{1/4} \quad \text{and} \quad v = (\epsilon\nu)^{1/4}$$

This type of presentation is shown in figure 3.11. In this figure we compare the noise corrected and uncorrected spectra which has been outlined previously but multiplied by the fourth power of the wavenumber and nondimensionalized. From the figure one can see that noise effect is accentuated around $k_1\eta = 1$ and this may be due to cut-off frequency set at this value. Considering all these, one can conclude that the noise did not affect the results of spectra which was used for measurement of dissipation. From here onwards no noise correction of hot wire signals in any form was made during whole of this investigation.

CHAPTER 4

EXPERIMENTAL ASSESSMENT OF K_1^{-1} SPECTRAL LAW.

4.1 INTRODUCTION

Tchen (1953) formulated the spectral analog of the turbulent energy equation for shear flow.[2] He considered the strong interaction between the turbulent and mean fields where the mean vorticity is large, along with sufficiently small wavenumber, the production is more dominant than other terms. The solution of the resulting equation gives

$$E(k) \propto k^{-1} \tag{4.1}$$

where k is the wavenumber. Under these conditions the solution to the spectral energy equation as formulated by Tchen (1953) is operative, i.e. the spectral law is k^{-1}. This region of the spectral law is considered to be representative of energy containing eddies. Hinze (1975, p. 349) has also obtained the solution of the approximate spectral equation like Tchen by dimensional reasonings:

$$E(k) = \text{const.}[\epsilon/(dU/dy)]k^{-1} \tag{4.2}$$

where dU/dy is the mean shear and ϵ is the rate of dissipation. Panchev (1969) has extend the work of Tchen (1953) and obtained a parametric solution for E(k). He has

[2] This chapter is based on the paper by Azad and Kassab (1984).

presented his results in the form of curves of E(k) for various values of the shear parameter

$$m = (dU/dy)/(\epsilon/\nu)^{1/2} \qquad (4.3)$$

The curves of E(k) predict conclusively that an increasing (lower) wavenumber range with a slope (-1) results in increasing values of m.

Rotta (1962, pp. 51-52) has expressed the degree of anisotropy of the flow locally by the ratio,

$$(dU/dy)/\overline{[(\partial u/\partial x)^2]}^{1/2}$$

He uses the relationship for the turbulent energy dissipation to replace this ratio by

$$(dU/dy)/(\epsilon/\nu)^{1/2}$$

which is the shear parameter m. Hence the higher values of m may indicate higher degree of anisotropy and in turn larger range of k_1^{-1} spectral law is evidence in $\overline{u^2}$-spectra.

Through dimensional argument and from an examinations of many experimental data, Kader and Yaglom (1984) concluded that the following equations should constitute the spectral laws:

$$E_1(k_1)/(yu^{*2}) = 0.8(k_1y)^{-1},$$

and

$$E_1(k_1)/(yu^{*2}) = 0.9(k_1y)^{-5/3} \qquad (4.4)$$

Following Millikan (1939) for the derivation of a logarithmic distribution of mean velocity from the overlap of the 'inner law' and the 'defect law' Perry and Abell (1977) proposed a region of overlap between inner and outer laws in which $\overline{u^2}/u^{*2}$ equal a universal constant. Their measurements in fully developed pipe flow confirm the preceding assertions. Perry and Abell found that the region of validity as $y^+ > 100$ and $y/R < 0.1$. This region of validity closely corresponds to the logarithmic region of the mean flow. In the domain of constant $\overline{u^2}/u^{*2}$, i.e., in the wall layer, they hypothesized a universal wall similarity for the energy containing motions expressed by

$$E_1(k_1)/(yu^{*2}) = f(k_1y) \tag{4.5}$$

They argued that Eq.(4.5) must break down at very low wavenumber where the large-scale geometry of the flow had an influence, so that Eq.(4.5) must be reformulated to include the pipe radius, R, i.e.,

$$E_1(k_1)/(yu^{*2}) = f_2(y/R, k_1y) \tag{4.6}$$

Abell (1974) set the requirement on the Eq.(4.6) that $E_1(k_1)$ must be independent of the wall distance y. As a result Eq.(4.6) becomes

$$E_1(k_1)/(yu^{*2}) = f_3\{1/(k_1R)\} \tag{4.7}$$

Now considering the overlap between Eq.(4.5) and Eq.(4.7) Perry and Abell (1977) obtained a particular form for the spectrum function:

$$E_1(k_1)/(yu^{*2}) = A''/(k_1 y) \qquad (4.8a)$$

$$E_1(k_1)/(Ru^{*2}) = A''/(k_1 R) \qquad (4.8b)$$

where A" is a universal constant.

A recent study by Lagrini and Moffat (1986) in rough boundary layer is also in agreement with Perry and Abell (1977) regarding the validity of k_1^{-1} spectral law in the inner region. In addition, Lagrini and Moffat (1986) concluded that the similarity of smooth and fully rough spectra in their figure 16 for $k_1 y > 0.1$-0.2 is a result of 'active' motions and universal wall structure in the inner boundary layer regions.

In the present study the spectral law k_1^{-1} pertaining to energy-containing eddies has been examined experimentally for one to one mapping from the scaling laws needed to give the logarithmic law for the mean velocity and constant streamwise Reynolds stress. In addition the k_1^{-1} spectral law has also been examined in the light of shear parameter m. For this, altogether three flows, namely, boundary layer, fully developed pipe flow and diffuser flow have been investigated for log-law, for constant $\overline{u^2}/u^{*2}$, for different values of m and for k_1^{-1} spectral law in the wall layer.

4.2 RESULTS AND DISCUSSION

Mean velocity, U, profiles were measured for the boundary layer of free stream velocity, U_∞ = 8 ms^{-1}. The r.m.s. values of streamwise fluctuating turbulent velocity, $\overline{(u^2)^{1/2}}$, were also obtained for the same condition. The mean velocity, U, and the r.m.s. turbulent fluctuating velocity, $\overline{(u^2)^{1/2}}$, are normalized by the friction velocity, u*, and their profiles are presented in figure 4.1. Figure 4.1a represents the Reynolds normal stress whereas figure 4.1b represents mean velocity in the form $U^+ = U/u^*$. Mean and turbulent quantities i.e., U/u^* and $\overline{(u^2)^{1/2}}/u^*$, are plotted on top of each other against one abscissa, y^+. The purpose of this plot is to see whether a region of constant value of $\overline{(u^2)^{1/2}}/u^*$ corresponds to the logarithmic region in mean velocity. Very small region of constant $\overline{(u^2)^{1/2}}/u^*$ in the neighbourhood of $y^+ = 100$ does seem to correspond to the logarithmic region for the mean velocity. This may be due to low Reynolds number of the boundary layer because similar results of smaller extend of constant $\overline{(u^2)^{1/2}}/u^*$ for low Reynolds number, $R_c = 78*10^3$, in fully developed pipe flow are shown in figure 8 of Perry and Abell (1975).

According to Perry and Abell (1977), the upper and lower limits of k_1^{-1} spectral law in the present boundary layer, i.e. $y^+ > 100$ and $y/R < 0.1$ appear to overlap. However, as seen in figure 4.2, there is a definite region of k_1^{-1} spectral law at y = 5.0 mm ($y^+ = 102.5$, $y/\delta = 0.109$). At

this position, the corresponding value of the constant of proportionality A" in Eq.(4.8a) is in close agreement with Kader and Yaglom prediction [Eq.(4.4)].

For the fully developed pipe flow, mean velocity and turbulent fluctuating velocities are normalized by friction velocity and are plotted in figure 4.3. Figure 4.3a contains the $\overline{(u^2)^{1/2}}/u^*$ against y^+ and figure 4.3b shows the U^+ versus y^+. Here the constant region in $\overline{(u^2)^{1/2}}/u^*$ extends from $y^+ = 100$ to about 300 and logarithmic law for mean velocity is approximately valid within the following limits $30 < y^+ < 500$. These regions cover the one defined by Perry and Abell (1977), i.e., $y > 100$ and $y/R < 0.1$. The pipe Reynolds number for the present case (based on the centreline mean velocity) is $140*10^3$ compared with $260*10^3$ the largest Reynolds number of Perry and Abell (1975, 1977). The present results in fully developed pipe flow agree with Perry and Abell.

Figure 4.4 shows the fully developed pipe flow spectra results in the inner region, i.e. $y/R < 0.1$. The spectra data presented in figure 4.4 within the range $y^+ > 100$ and $y/R < 0.1$ are in agreement with Perry and Abell (1977) with respect to the validity of k_1^{-1} spectral law. Also, these results are in agreement with Kader and Yaglom (1984) predictions and the numerical coefficient is sufficiently close to their value.

According to Bradshaw (1967c) the outer boundary of logarithmic region decreases to $y^+ = 30$ at about $\Delta = (\nu/\rho u^{*3})dP_s/dx = 0.01$ and thus logarithmic region vanishes. In addition, Bradshaw and Galea (1967) stated that the logarithmic region vanishes for $\Delta = 0.01$ to 0.04. One position in the diffuser where the value of $\Delta = 0.03$ was chosen for the presentation of the result. The second location where logarithmic region exists and which has a value of $\Delta = 0.12$ was selected for illustrating the present experimental study. The mean velocity and Reynolds normal stress normalized by u* are shown in figures 4.5 and 4.6 at locations $x_w/D = 0.59$ and 4.13 respectively. In figure 4.5, there is no logarithmic region for mean velocity, since $\Delta = 0.03$, so it corroborates the empirical findings of Bradshaw and Galea (1967). However, there is nearly one cycle of y^+ of constant value of $\overline{(u^2)^{1/2}}/u^*$. Therefore, there is no region of correspondence between the log-law and constant $\overline{(u^2)^{1/2}}/u^*$ in this location. For $x_w/D = 4.13$, figure 4.6 shows that there is a logarithmic region for mean velocity but there is no region of constant $\overline{(u^2)^{1/2}}/u^*$. This result points out that there is no necessary condition for the logarithmic region of mean velocity to have a corresponding region of constant $\overline{(u^2)^{1/2}}/u^*$ in the wall region of a complex flow like the conical diffuser flow.

Figure 4.7 shows the spectra results from the inner region of two positions in the diffuser, namely, $x_w/D = 0.59$

and 4.13. As shown in this figure, k_1^{-1} spectral law is not valid in the diffuser. This may be due to the strong adverse pressure gradient. It is natural to expect that k_1^{-2} spectral law will be valid within the layer of adverse pressure gradient flow where the mean velocity gradient is proportional to $y^{-1/2}$. A recent study by Kader (1984) using the experimental data of Okwuobi and Azad (1973) and Azad and Hummel (1979) shows that this is true for the present diffuser flow.

The failure of k_1^{-1} spectral law illustrated by figure 4.7 may be due to production being not equal to dissipation in the region (see chapter 7) since the production and dissipation of turbulence kinetic energy balance each other in fully developed pipe flow at the locations where k_1^{-1} spectral law is present. Also, the theoretical formulation of the shear parameter, m, is not justified in the diffuser because the representation of dissipation as inversely proportional to distance from the wall is not valid in the diffuser. More discussion about the shear parameter, m, is given in Azad and Kassab (1984).

The results of k_1^{-1} spectral law in boundary layer and fully developed pipe flows agree well with Kader and Yaglom (1984) predictions and the numerical coefficient is sufficiently close to their value. However, this law is not valid in diffuser flow with strong adverse pressure gradient.

CHAPTER 5

DISSIPATION OF ENERGY IN TURBULENT FLOW

5.1 INTRODUCTION

To understand turbulence from a physical as well as a practical point of view, it is imperative to know how the turbulent energy is created, transported and finally dissipated.[3] The above physical processes are described by the turbulent kinetic energy equation. Two terms, namely, the pressure transport and the dissipation cannot yet be measured in a strict sense. The former has not yet been successfully measured by any means but the latter can be measured by invoking local isotropy for most of the fine scales of dissipating eddies. This chapter deals with the study of dissipation of turbulent energy in turbulent flow.

It is well known that all terms of the dissipation rate, ϵ, cannot be measured experimentally in turbulent shear flows. Hence, other methods of measurement must be developed and justified on sound physical grounds. One physical fact regarding dissipation is that practically all the turbulent energy is dissipated at high wavenumbers or on fine scales of turbulence. Hence we can invoke local isotropy for the dissipating eddies and consequently we are

[3] This chapter is based on the report by Azad and Kassab (1985b) and the paper by Azad and Kassab (1986b).

at liberty to use isotropic theory. In shear flows, local isotropic theories are used to express ϵ either in terms of the mean square of the spatial derivatives or the spectral representations. These two methods also require Taylor's hypothesis. The report of the Working Group on Hot-wire Anemometry at Low Mach Number will be mentioned in this connection. The working group was the AD-HOC Committee No. 1 of 1980-81 AFOSR-HTTM-STANFORD CONFERENCE ON COMPLEX TURBULENT FLOW (1981, p. 583), and consisted of prominent international experimentalists in turbulence exclusively using the hot wire anemometer. Hereafter this reference will be denoted by AD-1. These experimentalist considered dissipation measurement in three different ways, first through measuring $\partial u/\partial t$, second through measuring the spectrum and third also through spectrum measurement, but close to the wall. However, the last method gave doubtful results, and will not be discussed further. The methods based on $\partial u/\partial t$ and on the spectrum for measurement of dissipation will be briefly outlined before discussing any other methods.

5.2 MEASUREMENTS OF DISSIPATION RATE

5.2.1 MEASUREMENT OF $\overline{(\partial u/\partial t)^2}$

The signal representing $\overline{u^2}$-fluctuation was electronically differentiated to obtain $\overline{(\partial u/\partial t)^2}$ as outlined in chapter 2. After the measurement of mean velocity, U, and $\overline{(\partial u/\partial t)^2}$ at

the point in the flow field were obtained, it was a simple matter to calculate the dissipation using the following equation

$$\epsilon = 15\nu\overline{(\partial u/\partial t)^2}/U^2$$

5.2.2 MEASUREMENT OF SPECTRA

The spectrum of $\overline{u^2}$-fluctuation is measured for all the frequency range in which the energy of $\overline{u^2}$-fluctuation is distributed (see chapter 2). Then the isotropic theory was used to obtain the dissipation,

$$\epsilon = 15\nu \int_0^\infty k_1^2 E_1(k_1)dk_1$$

Another method of obtaining dissipation from measured spectra would be to use the inertial theory of Kolmogoroff, i.e.,

$$E_1(k_1) = C_2\epsilon^{2/3}k_1^{-5/3}$$

The third way to obtain dissipation from experimental spectra is to use the expression

$$\epsilon = G(u'^3/L_f)$$

where G is a known constant as given by Driscoll (1982, p. 31), after examining many experimental data, as

$$G = 0.617 - 0.617R_\lambda^{-1/2} + 18.8R_\lambda^{-1}$$

and

$$L_f = \pi E_1(0)/(2\overline{u^2}) \quad ,$$

which is obtained by extrapolating spectral results at low wavenumber. Extrapolation of spectra at low wavenumbers in all cases is not possible, since the behaviour of spectra are not constant at low wavenumbers (see chapter 3).

5.2.3 DISSIPATION MEASUREMENTS BY DIFFERENT LENGTH OF THE WIRE

The results of dissipation of Derksen and Azad (1983) were obtained using fourteen different wire lengths whose diameters were nominally either 2.5 μm or 5 μm. The dissipation was either measured by $\overline{(\partial u/\partial t)^2}$ or spectra. When these results of dissipation are plotted against lengths of the wire, they result into two straight lines—one for spectra and the other for $\partial u/\partial t$ (see figure 5.1). The scatter of points in the figure is due to experimental errors, probe geometry and defects in their manufacturing [see Derksen (1981)]. The spectra give higher values of dissipation than the one obtained from $\partial u/\partial t$. This is an experimental fact, since Arora and Azad (1978) also obtained similar results. The values of dissipation obtained by the spectra and by $\partial u/\partial t$ have a constant ratio between them. It seems at present they depend on the nature of the flow.

The idea of extrapolation to zero length of the hot wire assumes that the dissipation occurs at fine scale structures and these structures obey local isotropy. If the extrapolation is linear, all experimental defects are taken

into consideration including the filtering effect of the finite length of the hot wire. As far as presently known the dissipation is linear with the length of the wires.

The above findings have some restrictions. One of them is length to diameter ratio shown in figure 5.2. In this figure dissipations obtained from wires having lengths 0.30 and 0.60 mm and their respective l/d ratios of 53 and 109 have lower values than their corresponding values on the line. When another wire of 0.62 mm in length and l/d ratio of 243 was used to obtain dissipation, the correct value on the line was obtained as shown by solid symboles in figure 5.2. From this it can be concluded that l/d should be about 200 as suggested by Gessner and Moller (1971), Hinze (1975, pp. 119-120) and recently by Blackwelder and Haritonidis (1983).

5.2.4 DISSIPATION OBTAINED FROM KINETIC ENERGY EQUATION AS A CLOSING TERM

The dissipation in the turbulent kinetic energy equation has been obtained as a closing term by measuring terms represented by mean flow convection, diffusion, and production of turbulent energy and neglecting terms of pressure transport and viscous diffusion. Pressure transport presently cannot be measured and viscous diffusion has been found to be negligible in comparison to other terms of the equation. Details about the turbulent kinetic energy equation are given in chapter 7.

5.3 RESULTS

The measurement of dissipation by all possible methods described previously are presented separately for each flow field, i.e., boundary layer, fully developed pipe flow and diffuser flow at six different axial locations. These locations in the diffuser were at 6, 18, 30, 42, 54 and 66 cm from the inlet of the diffuser. The dissipation measurement in the boundary layer flow is presented first, second the fully developed pipe flow results are presented and finally the measurements of dissipation in the diffuser flow are described. The spectra that are used for calculating dissipation are given in chapter 3.

For the boundary layer, five different single hot-wires were used for measuring dissipation so that their results could be extrapolated to zero length to obtain the experimentally correct values. These results are shown in figure 5.3. This dissipation is compared with the dissipations obtained by other methods as shown in figure 5.4.

Figure 5.5 shows the dissipations obtained from all six different lengths of the wire in the fully developed pipe flow for Re = $1.15*10^5$. The extrapolated values of the dissipation for zero length are compared with the dissipation obtained by closing terms of the energy budget, dissipation calculated from the integration of the spectra,

and dissipation measured from $\partial u/\partial t$ as illustrated in figure 5.6. Figure 5.7 also shows dissipation results from three best known methods for clarity.

Six different wire length probes similar to those that were used in the boundary layer and the fully developed pipe flow were also used for measurement of dissipation at 6, 42 and 66 cm from the inlet of the diffuser. The results of dissipation obtained from these probes are presented in figures 5.8, 5.9 and 5.10. Apart from these results, the dissipation obtained from $\partial u/\partial t$, from spectra, by extrapolating to zero length with and without correction for high intensity of turbulence, are presented one for each station in figures 5.11a, 5.12a, 5.13a, 5.14a, 5.15a and 5.16a. The measurements of dissipation were made with a standard wire of 1.25 mm length and 5 μm diameter at three stations, namely at 18, 30, and 54 cm from the inlet of the diffuser. First the ratio of values of dissipation from $\partial u/\partial t$ obtained by extrapolating to zero length to the values obtained from standard wire was calculated for each position of measurement at an axial location and the values of this ratio were plotted against non-dimensional radial location. Let this ratio be R_1. Thus we have functional relationship between the ratio R_1 and the non-dimensional distance r/R_{LOC}.

For example, this ratio is available for pipe flow and at 6 cm in the diffuser for different wire lengths as shown in figure 5.17 to illustrate the principle of the correlation

that is explained later. Another ratio of dissipation, say, R_2 between the one obtained by $\partial u/\partial t$ and the other obtained by spectra after extrapolating to zero length in both cases at each position of measurement was calculated across any section and plotted against the non-dimensional radial distance r/R_{LOC} to obtain a second function relation between the second ratio, R_2, and r/R_{LOC}. If one has measurement of dissipation from $\partial u/\partial t$ measured by standard hot wire, ϵ, it is easy to obtain the dissipation from spectra corresponding to extrapolation to zero length, $\epsilon_{s,\ell\to 0}$ by

$$\epsilon_{s,\ell\to 0} = R_1 R_2 \epsilon \ .$$

In the diffuser at 6 cm, $\epsilon_{s,\ell\to 0}$ was obtained by using R_2 in the pipe since the ratio R_1 was found to be the same as the pipe. At 18 cm in the diffuser both ratio, R_1 and R_2, were taken from 6 cm and pipe respectively. Location 30 was closeby 42 cm in the diffuser, so both ratios R_1 and R_2 at 42 cm were used to obtain $\epsilon_{s,\ell\to 0}$ at 30 cm from ϵ measured by standard wire. For 54 cm, the ratio R_1 was taken as the average of the values at 42 and 66 cm. The other ratio R_2 was known at 54 cm, since the dissipation-ratio obtained from spectra and $\partial u/\partial t$ by standard wire was the same as R_2 due to constant relation between these two measurements as shown in figures 5.1 and 5.2. The new method of measuring dissipation by extrapolating to zero length without and with a correction for high intensity of turbulence is compared with the dissipation obtained as a closing term of the

kinetic energy equation as illustrated in figures 5.11b, 5.12b, 5.13b, 5.14b, 5.15b and 5.16b.

5.4 DISCUSSION

Dissipation is the important phase in the state of energy and the dissipation of turbulent energy cannot escape that fate. So its realization in practice is essential to understand turbulence itself. This study is directed towards this objective. In order to do this effectively all the methods of measurement of dissipation have been assessed or adopted where possible in three different flows, namely, in boundary layer, fully developed pipe flow and in a complex flow such as the flow in a conical diffuser where severe adverse pressure gradient exists.

Most of the methods of measurement of dissipation depend on the assumption of local isotropy of fine scale structure at which stage the energy of turbulence finally dissipates into heat. This assumption provides us with a simple equation for dissipation in terms of velocity derivatives or spectral equations. The measurement of $\partial u/\partial t$ and using the Taylor hypothesis give us the dissipation most expediently. However this method generally yields a lower value of dissipation. In the boundary layer, Klebanoff (1955) quotes a value of dissipation being too low by a factor of 2.1. Irwin (1973), in his study of a self-preserving wall jet with an adverse pressure gradient, found that a correction

of order 100% was required for the effect of finite length. The possible inaccuracy of Taylor's hypothesis together with the above filtering defect made Irwin's measurement doubtful and in turn he did not present them. In reference AD-1 the consensus of opinion of the members of the committee in favour of the errors in measurement of dissipation by using $\partial u/\partial t$ after assuming local isotropy and Taylor's hypothesis were ±25 to ±50%. Lawn (1971) quotes error of -29% for his own dissipation measurement in fully developed pipe flow in comparison with -50% error in Laufer's (1954) dissipation measurement also in fully developed pipe flow. These two errors lie in the range quoted in reference AD-1.

Wygnanski and Fiedler (1970) have claimed to have measured five out of the nine derivatives composing the dissipation term in the two-dimensional mixing layer. They state that all terms have the same distribution across the flow and are equal in magnitude. Thus their dissipation term equal $9\nu\overline{(\partial u/\partial x)^2}$, which is different from the isotropic case of $15\nu\overline{(\partial u/\partial x)^2}$. This way of manipulating dissipation indicates that the isotropic relation is not valid for the fine scale of dissipating eddies. Since dissipation measurements have possibilities of error in the range ±25 to ±50%, there is no scientific ground for assessing pressure transport as a closing term of the energy equation. In this respect readers are referred to figure 14b of Bradshaw (1967a) and the associated discussion.

Shishov et al. (1978) found practically no difference between the value of dissipation obtained by using the isotropic relation and Taylor's hypothesis and dissipation obtained by measuring five of the derivatives. This result confirms the statement made in reference AD-1 that accuracies are usually similar.

The present results of dissipation through local isotropy and Taylor's hypothesis obtained by measuring the time differential signal of longitudinal fluctuating velocity in boundary layer, fully developed pipe flow and in diffuser flow as illustrated in figures 5.4, 5.6 and 5.11-5.16, also give lower values in agreement with other published results. Before we proceed to discuss the present results, some results are presented in figure 5.18 to show the reproduciblity of the results in the most complex flow presently investigated, i.e., diffuser flow. Three locations that illustrate three different flow structures in the diffuser are chosen to hopefully represent turbulent shear flow in general. The worst case in repeating dissipation from one day to another away from the wall shows about ±10% variation from the mean. This error also includes the aging of the wire, i.e., the behaviour of the wire varies with its time of use. The error in dissipation measurement is aggravated due to the presence of the wall; this may be due to aerodynamic interference as well as heat loss to the wall.

The dissipation obtained from the integration of spectra, i.e.,

$$\epsilon = 15\nu \int_0^\infty k_1^2 E_1(k_1) dk_1$$

where $$\overline{u^2} = \int_0^\infty E_1(k_1) dk_1$$

gives a higher value than that obtained from $\partial u/\partial t$ as shown in figures 5.1 and 5.2. This is corroborated by the measurement of dissipation made by Arora and Azad (1978). This is more precise since it is normalized by $\overline{u^2}$. In addition $\overline{u^2}$ can be measured more accurately than any other quantity in turbulence and this is borne out by the error of ±5 to ±8% incurred by a single wire in comparison to an X-wire of ±15% as quoted in reference AD-1. The results of dissipation obtained from spectra are illustrated in figures 5.4, 5.6 and 5.11-5.16. However, Hanjalic and Launder (1972) found measurement of dissipation through spectra to have a lower value than by other methods they have quoted in their figure 30. They have used a single and an X-wire to measure spectra. They have referred a suggestion of a referee of J. Fluid Mechanics that the length correction should have been used to correct for the lower value. This may be so, but the error of X-wire measurement together with other measurement errors probably gave the dissipation value lowest in their flow. The magnitude of this dissipation value according to them is about one half that of the dissipation obtained as a closing term of the kinetic energy equation.

The dissipation method based on dimensional reasoning is given by

$$\epsilon = G(u'^3/L_f)$$

This method presents two practical difficulties: one to realize G and the other to obtain L_f . Both of these problems cannot be solved with any confidence. Hence the dissipation can be obtained realistically in only a few flows. Townsend (1980, p. 61) gives the value of G = 0.8 as a constant, where Driscoll's (1982, pp. 25-31) analysis gives us an expression for G, but when it is used in our boundary layer where L_f from spectra can easily be obtained, it gives a value of dissipation equal to $\partial u/\partial t$ as shown in figure 5.4. This method will not be discussed further.

In ref. AD-1 the committee suggests one of the methods of obtaining dissipation from the spectra of the inertial subrange that has been pioneered by Bradshaw (1967b). According to Bradshaw a universal inertial range of the spectrum may exist if the turbulence Reynolds number ($R_\lambda = u'\lambda/\nu$) exceeds 100. This method gives good results of dissipation provided an inertial subrange exists. Strictly the method is not applicable near the wall as pointed out by Gibson et al. (1984). Lawn (1971) uses this method to obtain dissipation, but he chooses a different constant in the wall region to agree with the dissipation obtained as a closing term of the energy equation. Logically, different constants in different regions do not seem correct, so the

method is not working in the wall region. The constant was adjusted by Irwin (1973) to be 0.45 so that the diffusion term integrated across the flow to zero. This view was also presented in ref. AD-1. However the procedure seems to be a kind of manipulation and in no way a verification of the truth, since the closing term contains a very high magnitude of error. The present results obtained by using this method are shown in figure 5.4 and 5.7 in which the results in the wall regions are lower than the dissipations calculated from the energy budget as a closing term after neglecting the pressure transport term. These two flows, namely, the boundary layer flow shown in figure 5.4 and the fully developed pipe flow shown in figure 5.7 are the two standard flows where the methods which are previously unknown, should be proved as suggested in ref. AD-1.

We have noticed a method credited to Klebanoff in ref. AD-1 similar to our own[4] in which different wire lengths are used to measure dissipation either by $\partial u/\partial t$ or by spectra, and these values are extrapolated to zero length of the wire to obtain dissipation which is free from the spatial filtering as well as calibrations for all sorts of experimental defect. The method has been verified in fully developed pipe flow. $\overline{uv}/u^{*2}$ can be obtained exactly if u^{*2} is correctly measured from pressure drop. To obtain the mean strain term, the velocity profile was fitted with the

---

[4] But verbally denied by Klebanoff to Dr. R.S. Azad.

log law and wake function. Using this technique, the production of turbulent energy can be obtained very accurately. The diffusion term integrated across the shear layer to zero to show that the measurements were made correctly. The dissipation was obtained as a closing term of the energy equation and was of high accuracy since the other terms that were used to obtain this closing term were of high accuracy. The closing term in fully developed pipe flow gave us the true dissipation. The extrapolated value of dissipation from spectra to zero length was obtained in each position in the flow, and completely agreed with the values obtained from the closing term as shown in figure 5.7. This method was clearly verified in one of the standard flows, i.e., fully developed pipe flow. Hence the method would be justified to be used in an unknown flow field such as the flow in a conical diffuser.

The boundary layer and fully developed pipe flow have a low intensity of turbulence i.e. $\overline{(u^2)^{1/2}}/U < 10\%$ in most of the shear layer. In a very thin shear layer, in order of 2 mm, the intensity might reach 20%. The measurements in this region are not reliable. However, the region in the beginning of the diffuser has similar situations but as one proceeds downstream in the diffuser the high intensity defined by $\overline{(u^2)^{1/2}}/U > 20\%$ increases in magnitude and in radial extent from the wall of the diffuser. This necessitates correction of the measured dissipation. The

correction of dissipation for high intensity turbulence due to Lumley (1965) is given by Eq.(36) of Champagne (1978), i.e.,

$$\epsilon_m = \epsilon[1 + (\overline{u^2}/U^2) + 2(\overline{v^2} + \overline{w^2})/U^2]$$

where ϵ_m is the measured dissipation and ϵ is the true dissipation. The above equation is used to correct the dissipation obtained by extrapolation at all stations in the diffuser. In figure 5.11a the uncorrected and corrected dissipation do not differ from each other. This may be because there is no high intensity at this station. Figures 5.12a, 5.13a, 5.14a, 5.15a and 5.16a show the corrected dissipation to have a lower value than the uncorrected values of dissipation near the wall obtained by extrapolating to zero length. This is directly attributable to the high intensity of turbulence and this radial region from the wall increases nearly linearly as one goes downstream of the diffuser.

Finally, the corrected dissipation, i.e., extrapolating the results of dissipation from spectra obtained by different lengths of the wire to zero length and then correcting the dissipation value corresponding to zero length for high intensity turbulence as suggested by Champagne (1978), is compared with the dissipation obtained as a closing term of the energy equation (see chapter 7). Differences between these two results become more and more pronounced as one goes downstream. In addition the wall

layer shows difference of one kind whereas the core region shows the opposite trend. The discrepancies are largely due to cumulative error in the closing term as discussed in Azad and Kassab (1985c). In spite of this there is no claim made for absolute accuracy of the measurement of dissipation as shown in figure 5.18. However, the two methods have been assessed by area integration at each station and are illustrated in figure 5.19. The results show maximum deviation of ±7 from the mean value of these two results. These results seem to justify the method of obtaining dissipation by extrapolation of results of different lengths of wire to zero and also correcting the results for higher intensity where necessary.

5.5 CONCLUDING REMARKS

The dissipation of kinetic energy of turbulence fluctuation was thoroughly investigated for three different shear flows namely, boundary layer, fully developed pipe and diffuser flows. Different methods of measurement of dissipation were tested and verified in two well-known shear flows mentioned previously, i.e., boundary layer and fully developed pipe flow. The proved method of dissipation measurement was applied to a complex flow such as diffuser flow which was fed by fully developed pipe flow.

The dissipation obtained by (a) the inertial method and (b) extrapolation to zero length agreed with the dissipation

obtained from the kinetic energy equation as a closing term in boundary layer and fully developed pipe flow. However, the agreement between the dissipation method by extrapolation to zero length and the closing term is better, since these two have been more accurately assessed in fully developed pipe flow.

The correction of dissipation proposed by Lumley (1965) and given in specific form by Champagne (1978) has been used for high intensity turbulence up to 60% occuring in the wall region of the diffuser and the resulting dissipation after correction agrees within errors due to experiment and data processing with the dissipation calculated from the kinetic energy equation as a closing term.

The new method of obtaining dissipation by extrapolating the dissipations from different lengths to zero length is found to have ±10% uncertainty as illustrated in figure 5.18.

CHAPTER 6

LOW REYNOLDS NUMBER TURBULENT BOUNDARY LAYER

6.1 INTRODUCTION

The objective of the present study is to demonstrate the basic simple physics of turbulence in boundary layer growing on the inside region of pipe.[5] In other words, this is the axisymmetric boundary layer that can be approximated to two-dimensional boundary layer. Therefore, a low cost and easily constructed developing pipe flow facility has been built to grow the boundary layer on the inside pipe wall. Head and Rechenberg (1962) have demonstrated that their two values of concave transverse curvature do not show any different effect whatsoever on the inner boundary layer. Thus, they infer that the universality of the inner law is substantially unaffected by the transverse curvature of the surface for their flow, and consequently the flat plate boundary layer and the growing boundary layer on the pipe wall are substantially identical. Furthermore, Patel and Head (1969), Huffman and Bradshaw (1972), and Patel (1973) corroborate the above findings. In the present flow, there was a small positive velocity gradient, and in turn the nondimensional pressure gradient, $\Delta = (\nu/\rho u^{*3}) dP_s/dx$, at the

---

[5] This chapter is based on the report by Azad, Derksen and Kassab (1984).

measuring stations were slightly favourable (see Table 6.1). According to Patel (1973), the present boundary layer flow should be nearly identical to flow with a zero pressure gradient. Extensive work on turbulent boundary layers on flat plates has been recently carried out and, in turn, better physical insight is available for the turbulent boundary layer with zero pressure gradient. This wealth of knowledge can be utilized for the boundary layer growing on the pipe wall.

The turbulent boundary layer is one topic of study of turbulent flow. Most of the researchers in the field have reported turbulent boundary layers on a flat plate with zero or near-zero pressure gradient. The law of the wall is a pertinent characteristics of this flow. Simpson (1970, 1976) asserts that the von Karman constant, κ, varies with Reynolds number, and Landweber (1953), Preston (1958) and Granville (1977) state that the logarithmic region disappears below some Reynolds number. Coles (1956, 1962) shows that any variation of the turbulent boundary layer is primarily reflected in the outer region of the flow and the law of the wall is completely independent of the Reynolds numbers. An analysis of duct flow by Huffman and Bradshaw (1972) concurs with the Coles findings. Some data of Murlis (1975) and the exhaustive data of Purtell (1978) tend to support the conclusion that a truly constant value of the von Karman constant, κ, exists for all Reynolds numbers. A

theoretical study of Gol'dshtik and Kutateladze (1969) also indicates a constant value for κ = 0.40. Purtell et al. (1981) experimentally found that the extent of the logarithmic region remained nearly a constant fraction of the boundary layer thickness.

In the present study, a turbulent boundary layer was grown on the inside pipe wall. Distributed roughness, recommended by Klebanoff and Diehl (1952), was used to trip and thicken the boundary layer. The mean velocity field was examined from the point of view of inner law similarity and related attributes. The results obtained from measurements of the turbulence field by a single normal hot wire and X-wire probes are presented and compared, where possible, with similar available data. The measurable terms of the kinetic energy and shear stress equations have been obtained and examined to reveal the physics of turbulence in this particular boundary layer. It is hoped that the present study will provide a more complete picture of the boundary layer through achievement of the objectives outlined above, and furthermore it may lay a solid foundation for future research.

6.2 RESULTS AND DISCUSSION

6.2.1 MEAN VELOCITY FIELD

Mean velocity profiles were measured for the growing boundary layer for three free stream velocities. The results are shown in figure 6.1 and denote a boundary layer thickness of nearly 4.6 cm. Since the velocity, U, approaches the free-stream velocity, U_∞, more or less asymptotically with increasing y it is difficult to determine the value of δ accurately. In this respect the momentum thickness, θ, is a much more useful parameter, since its value can be obtained exactly. The constancy of δ in the present study is not surprising because Klebanoff and Diehl (1952) , using the same type of boundary layer trip as the one used in this study, reported that, δ = 3.1 inch for U_0 = 55 and 108 fps (see their figure 28). Antonia and Luxton (1972) obtained δ = 2.8 inch at Reynolds numbers $R_\delta = U_\infty\delta/\nu = 2.6*10^4$ and $4.8*10^4$. Recently, Badri Narayanan et al. (1984) found that δ was about 25 mm and it remained nearly constant in the free stream range of 5-30 ms^{-1}. The boundary layer parameters are given in Table 6.1 for the present study. Accurate measurements of the friction velocity, $u^* = (\tau_w/\rho)^{1/2}$, where ρ is the air density and τ_w is the wall shear stress, is necessary for application of the scaling laws of the boundary layer.

The mean velocity data were used in a cross-log plot to obtain the friction velocity. Secondly the linear velocity

profile next to the wall was obtained, by using the method outlined by Burhanuddin (1980), and also by Azad and Burhanuddin (1983), for friction velocity, $u^* = (\nu dU/dy)^{1/2}$. This method, entailing hot-wire correction procedure in proximity of a wall, has been evaluated in an exhaustive report by Azad (1983). The third method for friction velocity was to use five different diameter Preston tubes to measure dynamic pressure and use Patel's (1965) calibration. Results from these methods are given in Table 6.2. The result for the smallest tube from the Preston tube method for 4 ms^{-1} is missing from the Table, because the dynamic pressure was too low ($\cong$ 0.01 mm water) to measure correctly. The values of friction velocity obtained from the Preston tube method is nearly the same as those given by the cross-plot method, since both methods are based on the log law. The present results obtained from the cross-plot method in terms of the skin friction coefficient, $C_f = 2(u^*/U_\infty)^2$ are presented in figure 6.2 together with other published results. The value of friction velocity obtained from the cross-plot method is about 13.7% higher than obtained from the velocity gradient at the wall for U_∞ = 8 ms^{-1}. Mathieu in the discussion section of Clark (1968) states that the u^* values deduced from the slope of the mean velocity profile are about 10% less than the values deduced from other ways. Chevray and Kovasznay (1969) also found a 19.6% difference in these two methods of obtaining friction velocity. Recently, Blackwelder and Haritonidis (1983) found 15%

difference. Our finding concurs with the above. The friction velocity obtained from a log-cross-plot method for U_∞ = 8 ms^{-1} has been used to calculate the logarithmic distribution of the mean velocity and is shown in figure 6.3. The semi-logarithmic plot of the mean velocity distribution shows different behavior if the friction velocity is calculated from the mean velocity gradient at the wall [see figure 9 of Kline et al. (1967), White (1981) and figure 2 of Blackwelder and Haritonidis (1983)].

6.2.2 TURBULENCE FIELD

6.2.2.1 REYNOLDS STRESSES

Results presented in this section are for second, third and fourth moments of longitudinal, normal and transverse components of turbulent fluctuating velocities. The values of second moments: $\overline{(u^2)^{1/2}}/U_\infty$, $\overline{(v^2)^{1/2}}/U_\infty$ and $\overline{(w^2)^{1/2}}/U_\infty$, across the boundary layer are shown in figure 6.4. The boundary layer probe can approach the wall as close as 0.15 mm from the wall. Hence the moments of u can be obtained very close to the wall. But the X-array probe, DISA 55P51 can only traverse up to 3 mm away from the wall due to the size of the probe holder. So to get closer to the wall, probes DISA 55P53 and DISA 55P54 were used to obtain moments of v and w. In figure 6.4b we have followed Klebanoff (1955) in extrapolating the values of $\overline{(v^2)^{1/2}}/U_\infty$ and $\overline{(w^2)^{1/2}}/U_\infty$ to zero. Hinze (1975, p. 640) also supports this

on the grounds of v being quadratic in nature very close to the wall. The percentages shown in figure 6.4b denote the difference in values obtained from single normal and X-array probes. The results of Murlis (1975) shown in his figures 5.2.5a and b from y/δ = 0.2 to 1.2 compare quite well in trend and magnitude with the present results.

Physically the Reynolds shear stress coefficients are the most revealing turbulence parameters. One in particular, usually occurring in two-dimensional or axisymmetric flow, is $R_{12} = -\overline{uv}/(\overline{u^2}\overline{v^2})^{1/2}$. Detail discussion about this parameter is given in Appendix A.

If the turbulent energy and shear stress are examined not too close to the wall, then the ratio of the shear stress to the turbulent intensity, i.e. $-\overline{uv}/\overline{q^2}$, where $\overline{q^2} = \overline{u^2} + \overline{v^2} + \overline{w^2}$, has a constant value. The ratio, $-\overline{uv}/\overline{q^2}$, is shown in figure 6.5. Similar results can also be found in figure 7.22 of Hinze (1975). The continuous curve in figure 6.5 is from the boundary layer of Klebanoff (1955) taken from figure 9 of Bradshaw (1967a) and it agrees closely with the present results. The dashed line for $-\overline{uv}/\overline{q^2}$ = 0.15 agrees with the present data in the central region of the boundary layer.

6.2.2.2 HIGHER MOMENTS

The skewness of u, $S(u) = \overline{u^3}/(\overline{u^2})^{3/2}$, is presented in figure 6.6 together with other published results. The instantaneous value of odd moments can have either positive or negative sign and very slight off-sets can adversely affect the accuracy of their measurement. Another difficulty with the measurements of both skewness and flatness is that the nondimensionalizing parameter in the case of u is $(\overline{u^2})^{1/2}$, which amplifies the error if it is small. The signals corresponding to skewness and flatness also saturate so the instruments do not register their true values. Recently Johansson and Alfredsson (1983) have concluded that the reported discrepancies for turbulence measurements in proximity to the wall can be due to effects of imperfect spatial resolution of the hot wire and due to small effects of Reynolds number. The large rise and fall in the value of skewness for $y/\delta > 0.4$ in figure 6.6 indicates the effect of the intermittent region of the boundary layer.

The X-wire was used in the x-y and x-z planes to obtain the skewness and flatness of u for $U_\infty = 8$ ms^{-1}. These two data for the skewness and flatness respectively of u were identical to each other but similar to the skewness and flatness of u obtained by a single wire. Only one of these results is given in the figures to avoid confusion. The flatness factor of u, $F(u) = \overline{u^4}/(\overline{u^2})^2$, is shown in figure 6.7 together with the other published results. Figure 6.7

clearly defines the beginning of the intermittent nature of the outer region of the boundary layer at about $y/\delta = 0.4$, where the value of F(u) starts deviating from the nearly constant value of 2.8. Ozimek (1986, figures 5.5 and 5.6) has made comparison of digital and analog processing of the skewness and the flatness factors and has found no difference between them. The present results for skewness and flatness factors in the boundary layer are also given in the comparison.

The skewness of v, $S(v) = \overline{v^3}/\overline{(v^2)^{3/2}}$, and the flatness factor of v, $F(v) = v^4/(v^2)^2$, are shown in figure 6.8. These results concur with the results presented in figures 5-5.1 and 5-5.12 of Murlis (1975) and extend his results to the wall. To complete the picture of higher moments of basic components of velocity, the flatness factor of w, $F(w) = \overline{w^4}/\overline{(w^2)^2}$, is shown in figure 6.9. The skewness factor of w, $S(w) = \overline{w^3}/\overline{(w^2)^{3/2}}$, should be zero due to the axisymmetry of the flow, but because of the difficulties explained before S(w) has a value less than 0.1 for $y/\delta < 0.7$, and increases after that in the rest of the intermittency region [see figure 14 of Azad et al. (1984)].

Other triple products are presented in the form of y component turbulent transport velocities for turbulent energy and shear stress. Experiments in the boundary layer show that the energy balance reduces to 'advection = diffusion' at the outer edge of the boundary layer, then the

rate of propagation of turbulent energy in the y direction is $(\overline{pv} + \overline{vq^2}/2)$ and consequently a velocity of propagation V_q' may be defined as

$$V_q' = (\overline{pv} + \overline{vq^2}/2)/(\overline{q^2}/2) \cong \overline{vq^2}/\overline{q^2} \cong V_q.$$

The transport equation for shear stress is defined as

$$V_\tau' = (\overline{pu} + \overline{uv^2})/\overline{uv} \cong \overline{uv^2}/\overline{uv} \cong V_\tau$$

The values of V_q/U_∞, V_τ/U_∞ are shown in figure 6.10. Figure 6.10 indicates that V_q and V_τ first have a minimum value and then rise linearly from the surface to maximum values at the edge of the flow. The trend of V_q and V_τ are similar across the boundary layer. Their ratios show a constant value in the central region and higher values near the surface.

6.2.2.3 LENGTH SCALES

To describe the structure of a turbulent field it is necessary to know the length scales. One of the length scales, the so called Eulerian longitudinal integral scale, L_f, is considered to represent the average size of large eddy present in the flow. The length scale L_f is determined from the correlation curve and from the one-dimensional energy spectrum. The latter method was used in the present study. In addition the following formula was also used to obtain L_f

$$\lim_{k_1 \to o} E_1(k_1)/\overline{u^2} = 2L_f/\pi$$

where $E_1(k_1)$ is the one-dimensional energy spectrum and k_1 is the wavenumber. In the present boundary layer $E_1(k_1)$ is practically constant for lower wavenumbers (see figures 3.1 and 3.2), so it is possible to determine L accuratly. The variation of the integral scale, L_f, across the boundary layer is shown in figure 6.11. The results of Builtjes (1975) are also given in this figure for comparison. The trend of L_f, obtained by Antonia and Luxton (1971) in a turbulent boundary layer, indicates similar behaviour but their L_f—values have lower magnitude than the present results.

Bradshaw (1967a) introduced the dissipation length parameter, L, defined by $\overline{(-uv)^{3/2}}/\epsilon$, where $\overline{-uv}$ is the shear stress and ϵ is the dissipation rate. The length, L, characterizes the energy containing eddies and it is identical to mixing length near the surface. It has a more physical basis than the mixing length, since the energy balance reduces to "production = dissipation" near the surface. Bradshaw conjectures that L/δ is a universal function of y/δ throughout the boundary layer. Our results together with his results are presented in figure 6.12 and support his conjecture.

6.2.2.4 ENERGY AND SHEAR STRESS BALANCES

The turbulent energy equation that is used for the balance of the energies corresponding to different terms is given by

$$(U \frac{\partial}{\partial x} + V \frac{\partial}{\partial y}) \frac{1}{2} \overline{q^2} + \overline{uv} \frac{\partial U}{\partial y} + \frac{\partial}{\partial y} (\overline{pv} + \frac{1}{2} \overline{q^2 v}) + \epsilon = 0 \qquad (6.1)$$

that is

ADVECTION + PRODUCTION + DIFFUSION + DISSIPATION = 0,

where p is the fluctuating static pressure. All numerical values presented in figure 6.13 for a free stream velocity of 8 ms^{-1} are made dimensionless by multiplying the above equation by δ/U_∞^3. The term pv was ignored and ϵ was found by closing balance of the energy equation. Another estimate of dissipation was obtained from the inertial subrange of u^2-spectra,

$$E_1(k_1) = 0.55\ k_1^{-5/3} \epsilon^{2/3}$$

These values indicate good agreement with the previous values obtained by difference of the energy as shown in figure 6.13. This figure shows also that over most of the flow, energy transferred to turbulence from the mean flow at a rate $\overline{uv}\partial U/\partial y$ (production) is approximately equal to the rate of dissipation locally. A large amount of energy is transferred in the inner layer where large shear is continuously created. Production and dissipation are quite large near the wall. Advection is negligible except near the edge of the boundary layer. This term is on the positive side, which means that there is a loss of energy. At the outer edge the dissipation is greater than the production. So this difference, together with the loss by advection, is balanced by a gain due to turbulence diffusion. In the present flow, turbulence diffusion is

apparently transferring energy from the wall to the outer region of the boundary layer. This energy balance is similar to that given in other published works on the boundary layer with zero pressure gradient. The above description of energy transfer is diagrammatically shown in figure 7.11 of Townsend (1980).

The equation for the Reynolds shear stress, $\overline{uv}$, in a two-dimensional incompressible boundary layer flow, is given by:

$$(U\frac{\partial}{\partial x} + V\frac{\partial}{\partial y})(-\overline{uv}) - \overline{v^2}\frac{\partial U}{\partial y} + \overline{\frac{p}{\rho}(\frac{\partial u}{\partial y} + \frac{\partial v}{\partial x})} - \frac{\partial}{\partial y}(\overline{uv^2} + \overline{\frac{pv}{\rho}}) + \nu(\overline{u\nabla^2 v} + \overline{v\nabla^2 u}) = 0 \quad (6.2)$$

that is

$$\underset{\text{Transport}}{\text{Mean}} + \text{Generation} + \underset{\text{Strain}}{\text{Pressure}} + \underset{\text{Transport}}{\text{Turbulent}} + \underset{\text{Term}}{\text{Viscous}} = 0$$

Following Bradshaw and Ferriss (1972), the differential equation for $\overline{uv}$ is discussed to point out its importance. The Eq.(6.2) for $\overline{uv}$ has been approximated in the past by the mixing length and the eddy viscosity formulas. This was done because all the terms of the shear stress transport equation cannot be measured. In the present experiment the viscous term has been ignored and the pressure velocity correlation of the turbulent transport presently can not be measured. The pressure-strain term is obtained as a balance of the equation. All the terms of the Reynolds shear stress equation have been made dimensionless by δ/U_∞^3. The resulting shear stress balance is shown in figure 6.14. The generation term roughly balance the pressure-strain term

throughout the boundary layer; these two quantities are very large near the wall. At the outer edge of the boundary layer, the destruction by pressure forces is greater than the generation term, so their difference plus the transport by the mean flow is balanced by the turbulent transport. The behaviour of turbulent transport is similar to the turbulent diffusion term of the turbulent energy equation. Rough similarity also exists between the mean transport term of the shear stress equation and the advection term of the turbulent energy equation. This is inevitable because the ratio of shear stress to turbulent energy is constant over most of the boundary layer. The above view is corroborated by Bradshaw et al. (1981, p. 65) by using Castro's (1973) data.

6.3 CONCLUDING REMARKS

The concluding remarks follow from the investigation of turbulent boundary layers growing inside a pipe-wall at low Reynolds number. In general the results may be grouped into two parts-mean and turbulence fields. The present results for the mean field concur with the conclusion of Head and Rechenberg (1962), in which the existence of a universal region of wall similarity is substantially unaffected by the concave transverse curvature of a surface. The characteristics of both mean and turbulence fields as determined by the present investigations, confirm the

respective characteristics of turbulent boundary layers with zero pressure gradient at low Reynolds number reported by Purtell et al. (1981), White (1981) and Murlis et al. (1982). In addition, the present results complement the recently acquired results, e.g., higher moments of w are presented. The parameters of Bradshaw et al. (1967) calculation method are used to compare the results of others and the results of this comparison are found to be in excellent agreement. Other higher moments of the turbulence field are in good agreement as well.

The similarity between the energy and the shear stress equation has been revealed; this fact is supported by the nearly constant ratio of the Reynolds shear stress, $-\overline{uv}$, to the turbulent kinetic energy, $\overline{q^2}$.

Finally, the present study of low-Reynolds number turbulent boundary layers growing on a concave surface of a pipe confirms all the parameters to be similar to those of the flat plate turbulent boundary layer without any pressure gradient.

CHAPTER 7

TURBULENT FLOW IN A CONICAL DIFFUSER.

7.1 INTRODUCTION

A bounded flow can have three basic geometrical configurations, namely, pipe-like flow, contraction-like flow and diffuser-like flow. The most complicated of these flows is the flow in a diffuser.[6] The choice of flow in a conical diffuser was made for its axisymmetry.

Initial conditions of a flow are important for prediction of its subsequent development and in turn they should be precisely defined and verified experimentally. As an illustration, boundary layer flow on a flat plate is generally considered to be simple. On the contrary it is complex since it contains an intermittent surface from y/δ = 0.4 to y/δ = 1.2, and the physics of the intermittent surface is still unknown. Hence it was decided to feed a diffuser with a fully developed flow (see Appendix C) which is in equilibrium state at the inlet of the diffuser. It is important to investigate diffuser flow with fully developed flow in the pipe at the inlet of the diffuser— in other words, the initial conditions of the flow are physically precisely defined. The flow can be studied especially near

[6] This chapter is based on the paper by Azad and Kassab (1986c) and the report by Azad and Kassab (1985c).

the wall, without the complication of an intermittent surface in the outer part of the flow.

Some of the complex turbulent flows have been reviewed by Bradshaw (1975, 1976 and 1978) and also investigated by Bradshaw and his co-workers as referred to elsewhere in this chapter. The flow in the conical diffuser has extra strain rates, $\partial V/\partial r$ and V/r that are respectively identified as streamline curvature and divergence. These strain rates have a step-function like increase at the inlet of the diffuser. The effect of this sudden increase of strain rate is reported in terms of the evolution of mean and turbulent fields. All the mean strain rates have been examined and reported. Turbulent kinetic energy and shear stress are investigated. Triple products have been thoroughly examined for their capability for transporting turbulent energy. Lastly, the balances of kinetic energy and shear stress are reported.

7.2 RESULTS

The polar cylinderical coordinate system in terms of axial distance represented by x, radial distance by r and azimuthal direction by θ, has been used. The origin of the system is at the inlet of the diffuser and this is also the position in the pipe where the flow is fully developed.

Pressure and pressure gradient are shown in figure 7.1 whereas friction velocity is plotted in figure 7.2. Mean and turbulent energy weighted by area at each axial location are plotted in figure 7.3a. Area weighted turbulent energy, maximum value of turbulent energy and their ratio at each axial location are also presented in figure 7.3b. All these curves show very rapid change in the first two diameter of the pipe whereas the change is slow or none at all in the remainder of the diffuser.

In this flow we have three rates of normal strain, namely, $\partial U/\partial x$, $\partial V/\partial r$ and V/r; $\partial V/\partial r$ and V/r are nearly equal and their sum is obviously equal to $\partial U/\partial x$, which is shown in figure 7.4. The rates of shear strain present in this flow are the basic rate of shear strain, shown in figure 7.5, and the extra rate of strain $\partial V/\partial x$ coined by Bradshaw in his numerous publications on complex flows. Numerous profiles of mean velocity V and $\partial V/\partial x$ are presented respectively in figures 7.6a and 7.6b to show the evolution of the extra strain-rate more precisely. Finally the nondimensionalized version of the strain-rate is shown in figure 7.6c. This figure shows that the value of strain-rate has relatively very high value at the inlet, zero value in the neighborhood of $x/D = 0.9$, maximum negative value at $x/D = 1.4$ and finally it attains a zero value at $x/D = 4.2$.

To see whether the flow is approaching isotropy, $\overline{v^2}/\overline{u^2}$ has been plotted in figure 7.7. Turbulent energy and shear-

stress are shown respectively in figures 7.8 and 7.9. The initial conditions at entry to the diffuser, i.e., fully developed pipe flow, are given in these figures to show the evolution of this complex flow in the diffuser. The peaks of these quantities move out away from the wall as we proceed towards the exit of the diffuser. Ratios of these quantities are shown in figure 7.10. Results at the first station stands out on its own but the other results are different than the results of the pipe flow in the wall region.

Turbulent transport velocity of $\overline{q^2}$ is shown in figure 7.11a. and it grows gradually to final form from its initial structure in pipe flow. Figure 7.11b shows the relative size of the triple product term that appears in the turbulent transport of turbulent energy. Here $\overline{vq^2} = \overline{u^2v} + \overline{v^3} + \overline{vw^2}$. The value for fully developed pipe flow is also obtained in the present study and is plotted at the inlet of the diffuser, i.e., $x/D = 0.0$. The data from Azad (1982) are also plotted in this figure. Lawn's (1970b) data for pipe flow is also given and his result agrees with the present result in fully developed pipe flow.

The results of turbulent transport velocity of uv are presented in figure 7.12a. This figure shows continuous evolution of the parameter from its initial stage in the fully developed pipe flow to its final structure in the outlet region of the diffuser. The ratio of triple products

of $\overline{uv^2}/\overline{vq^2}$ is shown in figure 7.12b. A nearly constant value of about 0.5 for this ratio is obtained as illustrated in this figure. Some of the points tend to go either $+\infty$ or $-\infty$ due to singularity in the ratios at the data points.

The time scale $\tau = \overline{q^2}/(2\epsilon)$ is presented in figure 7.13 for modelling the flow. This is because the time scales appear in the derivation of Eqs.(8.6) and (8.7) of Lumley (1981). Lumley states that these time scales are proportional to the ratio of turbulent energy to dissipation rate. Dissipation can display its behaviour through the dissipation length scales $L_\epsilon = \overline{(q^2)^{3/2}}/\epsilon$ and $L = \overline{(uv)^{3/2}}/\epsilon$ which are shown in figures 7.14a and 7.14b respectively. Both of these figures show similar behaviour in general except at the axis of symmetry where L_ϵ has a finite value and L has a zero value. These behaviours of L_ϵ and L are due to $\overline{q^2}$ being finite, $\overline{uv}$ being zero and ϵ being finite at the axis of symmetry. The profiles of the difference of production and dissipation ($P - \epsilon$) are illustrated in figure 7.15 and the maximum of this curve also moves away from the wall. This quantity is used in algebraic modelling [see Eq.(14) of Leslie (1980)].

The balance of the turbulent kinetic energy in fully developed pipe and in diffuser flow at x/D = 0.59, 1.77, 4.13 and 6.50 are presented respectively in figures 7.16a, 7.16b, 7.16c, 7.16d and 7.16e. The shear-stress balance is given in figure 5.17 for the same locations. For further

details of these two parameters— the turbulent kinetic energy and shear stress, the readers are directed to Azad and Kassab (1985c). The terms of the turbulent kinetic energy and shear stress are respectively evaluated from the following equations:

$$\frac{D}{Dt}\left(\frac{1}{2}\overline{q^2}\right) \equiv \left[U\frac{\partial}{\partial x} + V\frac{\partial}{\partial r}\right]\left(\frac{1}{2}\overline{q^2}\right)$$

$$= -\overline{uv}\left(\frac{\partial U}{\partial r} + \frac{\partial V}{\partial x}\right) - \left(\overline{u^2} - \overline{v^2}\right)\frac{\partial U}{\partial x} - \frac{V}{r}\left(\overline{w^2} - \overline{v^2}\right)$$

$$- \frac{\partial}{\partial x}\left(\frac{1}{2}\overline{uq^2}\right) - \frac{1}{r}\frac{\partial}{\partial r}\left(r\,\frac{1}{2}\overline{vq^2}\right)$$

$$- \varepsilon. \qquad (7.1)$$

$$\frac{D}{Dt}\left(-\overline{uv}\right) \equiv \left[U\frac{\partial}{\partial x} + V\frac{\partial}{\partial r}\right]\left(-\overline{uv}\right)$$

$$= \overline{v^2}\frac{\partial U}{\partial r} + \overline{u^2}\frac{\partial V}{\partial x} - \frac{V}{r}\overline{uv}$$

$$- \overline{\frac{p}{\rho}\left(\frac{\partial u}{\partial r} + \frac{\partial v}{\partial x}\right)}$$

$$+ \frac{\partial}{\partial x}\left(\overline{u^2 v}\right) + \frac{1}{r}\frac{\partial}{\partial r}\left(r\overline{uv^2}\right). \qquad (7.2)$$

Eq.(7.1) is obtained after neglecting the terms due to pressure transport and viscous diffusion in complete turbulent kinetic energy equation (TKEE) given in Eq.(1) of Azad and Kassab (1985c). The latter term is neglected owing to its value being too low. One reason for neglecting the pressure transport term is that it cannot be obtained as the closing term of turbulent energy equation because its magnitude is of the same order as that of cumulative errors in the remainder term. In addition its behaviour may be nonlinear and complex like the different errors in various terms. Therefore it is not possible despite all efforts [see Azad & Kassab (1985c)] to separate pressure transport term in diffuser flow and consequently this term is neglected.

Dissipation measurement has been exhaustively reviewed in a report by Azad and Kassab (1985b) and so the methods adopted finally to obtain dissipation are only briefly described here (see also chapter 5). The first method consists of obtaining dissipation by integrating spectra from different lengths of the hot wire and these results are extrapolated to zero length for the final value of dissipation. High intensity of turbulence of up to 60% is present in the wall-layer of the diffuser. The previously obtained value of dissipation was corrected for high intensity of turbulence that was first introduced by Lumley (1965) and later given by Champagne (1978) in specific form.

The second method of obtaining dissipation was by the closing term of the turbulent kinetic energy after neglecting the pressure transport term. The values of dissipation obtained by these methods are given in figure 7.16.

In shear-stress equation, Eq.(7.2), the viscous term is neglected due to flow belonging to high Reynolds numbers and the transport terms due to pressure fluctuations are also neglected, because they can not be measured presently and further their magnitudes are considered to be small. The pressure-strain term can be obtained as a closing term from Eq.(7.2).

7.3 DISCUSSION OF RESULTS

Most of the figures presented by Azad (1982) are complimentary to the present figures, since they present results at different stations. However both results show similar trend. Comparison of the present figures with Azad's (1982) will not usually be mentioned in discussion.

Figure 7.1 shows pressure and pressure gradient in the fully developed pipe flow as well as in diffuser flow. Pressure is nondimensionalized by the average velocity head of the pipe flow, since it renders the distribution independent of Reynolds number [see Okwuobi and Azad (1973) and Azad and Burhanuddin (1983)]. Pozzorini (1976) has

obtained similar results for pressure and its gradient in a conical diffuser like the present one. The pressure-gradient curve shows initially a rapid increase in negative value, then sharp rise in positive value and finally it decreases rapidly before monotonically decreasing to the final stage of its development. In other word, the negative pressure gradient first increases in 0.1D, then positive pressure gradient increases in 0.3D and it decreases first very fast in about 1.6D and gradually in the remainder of the diffuser. Thus the flow based on initial complex behaviour of pressure gradients may produce indeed a truly complex flow.

The distribution of local friction velocity obtained from different Preston tubes are shown in figure 7.2. Methods due to Brown and Joubert (1969) and Frei and Thomann (1980) are also given in this figure and their methods compare favourably with the present results within the bounds of experimental errors. Pozzorini's (1976) results of friction velocity corroborate the present behaviour of the friction velocity shown in figure 7.2. Readers should consult Trupp et al. (1986) for the detail discussion of this parameter (see also Appendix D).

Figure 7.3a illustrates the area mean values of turbulent kinetic energy of mean and fluctuating velocities per unit mass in the pipe and throughout the diffuser. The trends of these two parameters go hand in hand with the friction

velocity in figure 7.2. The maximum value and the area mean of the turbulent kinetic energy of fluctuating velocity and their ratios are shown in figure 7.3b. Rapid changes in first two diameters are indicated in these three parameters and afterwards the quantities attain a constant value in each case. The former trend depicts disturbance of the flow, whereas the latter points towards equilibrium of the flow dynamics. Scrutinizing figures 7.3a and 7.3b one may conclude that some of the mean energies of the flow is converted to pressure (see figure 7.1) and the remainder is supplied to the turbulent field. The latter conversion of energy is evidenced in the rise of the turbulent kinetic energy to about two times its original value.

Mean strain-rates in the diffuser flow consist of $\partial U/\partial x$, $\partial U/\partial r$, $\partial V/\partial x$, $\partial V/\partial r$ and V/r. Three of the above, namely, $\partial U/\partial x$, $\partial V/\partial r$ and V/r together form the divergence and the other two are the mean shear strain-rate present in this axisymmetric flow. Figure 7.4 gives $\partial U/\partial x$ and the latter shear-strain-rates, $\partial U/\partial r$ and $\partial V/\partial x$ are respectively shown in figures 7.5 and 7.6. The reason for showing the behaviour of $\partial U/\partial x$ in figure 7.4 is to obtain V by using the continuity equation, since it is needed to calculate the extra strain rate $\partial V/\partial x$. Initially the values of $\partial U/\partial x$ are high but finally there is a gradual deceleration of the flow. It is worthy to note that high positive values of $\partial U/\partial x$ near the wall is due to the coordinate being along the

axis of the diffuser and not along the wall of the diffuser. This peculiar behaviour is present in all quantities whose derivative with respect to x have been taken. The basic rate of shear strain, $\partial U/\partial r$, is the main link between the mean and turbulence field through the production of kinetic energy. Initially this strain-rate looks similar to the strain-rate in a fully developed pipe flow but the curves representing the latter part of the diffuser flow have different curvatures, reach a maximum and minimum and then finally increases near the wall like the other curves. The present behaviour may be due to the flow being subjected to an adverse pressure gradient. The shape of the mean velocity gradually changes along the axial distance like the one in the flat plate boundary layer under the influence of adverse pressure gradient [see for example the results of Schubauer and Klebanoff (1950), given in figure 22 of Coles (1956) and figure 15.1 of Rotta (1962)].

Bradshaw (1973, 1975 and 1976) has reviewed complex turbulent flows defined as shear layers that result either due to complicating influences like one in particular the extra strain-rates effecting the present flow in the diffuser or due to interaction with other shear layers. A series of complex flows have been studied by Castro and Bradshaw (1976), Smits et al. (1979a and b), Chandrsuda and Bradshaw (1981), Weir et al. (1981), Wood and Bradshaw (1982 and 1984), Shabaka et al. (1985) and Bradshaw and Pontikos

(1985) and the comparison of their works will be made wherever possible with the present study. The extra strain-rate, $\partial V/\partial x$, is presented here in the hope that some of the calculation methods which have proved satisfactory in simple shear layers may be extended with some confidence to complex flows. Before presenting the ratio of extra strain-rate to main shear strain rate in figure 7.6c the mean velocity, V, and $\partial V/\partial x$ are given respectively in figures 7.6a and 7.6b in order to follow the evolution of extra strain-rate since it rises suddenly, passes through zero, becomes negative and finally settles to zero value as illustrated in figure 7.6b. Figure 7.6c does not show different trend than figure 7.6b, but it gives the magnitude that can be compared with the results given in Table 1 of Bradshaw (1973); this Table gives the classification of shear layers by ratio of extra strain rate to mean shear. According to this Table the present results at about 0.1D and 0.6D can be considered as fairly thin shear layer, since

$$10^{-2} < (\partial V/\partial x)/(\partial U/\partial r) < 10^{-1}.$$

These results indicate aprobable large effect of extra strain rate on turbulence structure as pointed out by Castro and Bradshaw (1976) and the present results concerning turbulence validate this finding. Large values of $(\partial V/\partial x)/(\partial U/\partial r)$ usually result from large adverse pressure gradients as corroborated by the figures 7.6c and 7.1. This fact has also been observed by Bradshaw (1975).

The anisotropy parameter in terms of the ratio $\overline{v^2}/\overline{u^2}$ is presented to illustrate the intensity profile in figure 7.7. The values from the present results compare favourably well with the figure 16 of Smits et al. (1979b).[7] The parameter goes to zero in the wall region. The energy in figure 7.8 shows a very rapid increase initially and then attains a nearly asymptotic value. In contrast the shear stress in figure 7.9 shows a gradual increase to its final value. The positions of maximum value of these quantities move away from the surface of the diffuser. The result in diffuser flow is similar to what Bradshaw (1976) described about cylinder-fare. However, the fully developed pipe flow has usual characteristics regarding kinetic energy and shear stress. The values of stress-energy ratio represented by $\overline{uv}/\overline{q^2}$, where $\overline{q^2} = \overline{u^2} + \overline{v^2} + \overline{w^2}$, are shown in figure 7.10. The maximum constant value achieved in fully developed pipe flow is about 0.13. In diffuser-flow, initial region attains a high value of about 0.17, which is probably due to high value of extra strain-rate, but the rest of the results show similarity to pipe flow in the transverse direction defined by $0.3 < y/R_{LOC} < 0.7$. This ratio exhibits a similar behaviour to the data in Smits et al. (1979b) and the dissimilarity shown at the two boundaries of the present results is due to the geometry of the flow.

---

[7] After this figure ordinate scale is corrected by multiplication with 2 as communicated by a referee on previous occasion.

Some of the triple products in boundary layer were introduced on physical grounds and their extensions were made in complex flows. Following this basic trend a velocity of propagation V_q' and a transport velocity for shear stress, V_τ' may by defined respectively as

$$V_q' = (\overline{pv} + \overline{vq^2}/2)/(\overline{q^2}/2) \cong \overline{vq^2}/\overline{q^2} \cong V_q \qquad (7.3)$$

$$V_\tau' = (\overline{pv} + \overline{uv^2})/\overline{uv} \cong \overline{uv^2}/\overline{uv} \cong V_\tau \qquad (7.4)$$

In the final forms of Eqs.(7.3) and (7.4), pressure-velocity correlation has been neglected due to its value being of the same order of magnitude as the error as discussed in detail before. In general the transport velocity displays characteristics that are expected of large eddies that contain and transfer turbulent energy. The results for transport velocities of turbulent energy, V_q/U_b and shear stress, V_τ/U_b are illustrated in figures 7.11a and 7.12a respectively. These two parameters have negative value in the fully developed pipe flow, but have positive values near the wall and negative values in the neighborhood of the axis of the diffuser. The exception for one station at $x/D = 0.6$ in diffuser exists where V_τ/U_b has negative values across the section. Both quantities behave similarly in the region $0 < y/R_{LOC} < 0.7$ but due to geometry the core region has contrasting characters. In figure 7.11a, the maximum for turbulent transport velocity of energy moves away from the wall whereas minimum moves towards the axis as one goes to

the outlet of the diffuser. Transport velocity for shear stress shows an increasing maximum but no minimum. V_q/V_τ may be written as

$$V_q/V_\tau = (\overline{vq^2}/\overline{uv^2})(\overline{uv}/\overline{q^2}) = (\overline{vq^2}/\overline{uv^2})\ a_1$$

The average value for a_1 is about 0.125, obtained from figure 7.10, and the inverse of the right-hand quantity in parenthesis has a constant mean value of 0.5 (see figure 7.12b). Substituting these values, the above expression yields

$$V_q/V_\tau = 0.25$$

The value of Smits et al. (1979b) lie between 0.5 and 0.7. This might be due to their assumption of $\overline{vw^2} = 0.5(\overline{u^2v} + \overline{v^3})$,(see Appendix B). The ratio of V_q to V_τ may be due to higher value of $\overline{uv^2}/\overline{vq^2}$ of 0.5 than Smits et al.'s (1979b) value of 0.3. In the present results the ratio in figure 7.12b tend to go to positive and negative infinity due to division of positive and negative values by zero values. Castro and Bradshaw (1976) have presented the relative strength of large eddies for highly curved mixing layers in their figure 14. The value of $(\overline{vq^2_{max}} - \overline{vq^2_{min}})/(\overline{q^2_{max}})^{3/2}$ increases to about 2.5 times its minimum value along the overall length of the mixing layer. The present results as well as Arora's (1978) results (see figure 7.11b) in diffuser flow also have similar trends but the increase is about 3.8 times its minimum values. In the final region of

the diffuser, a long asymptotic value persists in contrast to a very short region in the case of the mixing layer. This finding also proves that equilibrium large scale structure exists in the final period of the diffuser flow.

The behaviour of the time scale shown in figure 7.13 becomes more linear towards the exit of the diffuser.

The dissipation length scale $L_\epsilon = \overline{(q^2)^{3/2}}/\epsilon$ is a genuine length scale of the energy containing eddies, and is the usual length scale for modelling the flow. Hence this length scale is plotted in figure 7.14a, which shows a linear relationship initially and then flares up into different curves at specific locations to reflect the physical character existing at the place. However its initial evolution may be approximated by

$$L_\epsilon/R = 9.2y/R_{LOC}$$

Lawn (1970b) results, in pipe flow, of dissipation length scale also show similar behaviour except his results have slightly lower values. This is the initial condition at the inlet of the diffuser. The gradual evolution of this scale along the axial length of the diffuser can be evidently traced to the dissipation length scale in the fully developed pipe flow. Liepmann and laufer (1947) reported that L_ϵ is very nearly constant across a plane mixing layer. Furthermore, Castro and Bradshaw (1976) also reported that ϵ was proportional to $\overline{(q^2)^{3/2}}$ in their own plane layer. In

conclusion L_ϵ does not have a constant value in the diffuser flow (see figure 7.14a). Bradshaw (1967a) introduced the dissipation length parameter, L, defined by $\overline{(-uv)^{3/2}}/\epsilon$, where $\overline{-uv}$ is the shear stress and ϵ is the dissipation rate. The length, L, characterizes the energy containing eddies and it is identical to mixing length near the surface. It has more physical basis than the mixing length, since the energy balance reduces to "production = dissipation" near the surface. In the present study, the behaviour of L is similar to L_ϵ (see figure 7.14b); first it increases linearly and then branches away from this line to become another linear line before it reaches the axis of symmetry of the diffuser where its value is zero. The initial linear line may be approximated by

$$L/R = 0.4y/R_{LOC}$$

This expression in fully developed pipe flow gives L = 0.4y which is the mixing length formula with Von Karman constant having a value of 0.4. The final linear line varies from the least steep gradient in the pipe to the steepest gradient at the exit of the diffuser.

Sreenivasan (1985) has introduced the total strain parameter

$$\beta' = \int_0^{T'} (\partial U/\partial r)\, dt \ ;$$

T', typically the lifetime of the large eddy, is the order of $\overline{q^2}/(3\epsilon)$ in equilibrium, so that $\beta' = (1/3)(\overline{q^2}/\epsilon)(\partial U/\partial r)$

and implies that the turbulence structure at any given stage is completely determined by β'. All the quantities defined in the above expression, i.e., $\beta' = (1/3)(\overline{q^2}/\epsilon)(\partial U/\partial r)$, have been area-wise integrated at each cross-section and finally the definition in the present case results in

$$\beta = \frac{\int_0^1 (\overline{q^2}/3)\, d(r/R_{LOC})^2 \int_0^1 \left|\frac{\partial U}{\partial r}\right| d(r/R_{LOC})^2}{\int_0^1 \epsilon\, d(r/R_{LOC})^2}$$

The values of β are plotted in figure 7.17. The value of β first increases and then monotonically decreases nearly to the value it started from. The behaviour of this parameter in the initial region is similar to the extra strain-rate. The relaxation length of 0.16 m obtained in the present case coincides with the distance where total strain parameter attains the maximum value.

Following Bradshaw (1973, pp. 18-20) and Smits and Wood (1985) a relaxation length scale may be defined at each cross-section of the diffuser by

$$L_R = \frac{\int_0^1 (\overline{q^2}/2)\, d(r/R_{LOC})^2 \int_0^1 U\, d(r/R_{LOC})^2}{\int_0^1 \text{Production}\ (r/R_{LOC})^2}$$

where

$$\text{Production} = -\overline{uv}\left(\frac{\partial U}{\partial r} + \frac{\partial V}{\partial x}\right) - (\overline{u^2} - \overline{v^2})\frac{\partial U}{\partial x} - \frac{V}{r}(\overline{w^2} - \overline{v^2})$$

and its values have been plotted in figure 7.17. This figure shows that the L_R has a constant value of about 0.16 m. In other word the relaxation length due to initial perturbation is about 0.16 m and this length in which the extra strain-rate tends to decrease towards zero value. It can be noted that $L_R = 3R$, where R is the radius of the pipe. If time scale is obtained by dividing L_R by the mean velocity at each cross-section of the diffuser, the resulting time scale would increase towards the exit of the diffuser. This observation is qualitatively corroborated by the behaviour of time scale shown in figure 7.13.

Leslie (1980) gives the assumption of the algebraic modelling by the expression

$$T_{ij} = \frac{\langle u_i u_j \rangle}{K} T_K = \frac{\langle u_i u_j \rangle}{K} (P'-\epsilon')$$

where $(P' - \epsilon')$ is the difference of production P' and dissipation ϵ'. It is called algebraic modelling because it gets rid of the differentials implicit in T_{ij} leaving a set of algebraic expressions. The present production P and dissipation ϵ are normalized by R/U_b^3, i.e. $P = P'R/U_b^3$ and $\epsilon = \epsilon'R/U_b^3$. $(P - \epsilon)$ profiles are illustrated in figure 7.15 and show that the peaks have moved away from the wall of the diffuser. According to figure 7.15, the transport of the turbulent energy at x/D = 1.77 has the maximum value and its maximum value is nearly the same at other downstream station. The latter indication shows some sort of equilibrium in the physics of flow.

In axisymmetric flow there are four stresses present, out of which three constitute the normal stress and together they represent twice turbulent kinetic energy per unit mass. It is invariant because of its being a scalar quantity and in turn should be discussed first. Further, the shear stress equation should also be discussed in order to have a complete grasp of Reynolds stresses in an axisymmetric flow. Previous works of Okwuobi and Azad (1973) and Arora and Azad (1980a) regarding turbulent kinetic energy in diffuser flow have been thoroughly reviewed by Singh and Azad (1981). Details regarding this can also be found in Azad and Kassab (1985c).

Figures 7.16a-e show that the maximum in production is located at a distance from the axis of the diffuser equal to the pipe radius throughout this flow field. In other words this point is maintained without any distortion. Singh and Azad (1981) have also made a similar observation about production of turbulent energy. The dissipation rate in wall-bounded shear flow is reviewed in chapter 5. Only part of the results of dissipation are presented in figure 7.16. The behaviour of diffuser flow especially from $x/D = 1.77$ onward to the outlet (figures 7.16c, d and e) is not similar to simple flows like the input flow to the diffuser, i.e., fully developed pipe flow. In other words, the production is not equal to dissipation near the wall of the diffuser (see figure 7.15). Like production the peak value of

dissipation tends to move away from the wall in the downstream direction. Since the production and dissipation do not balance each other at each location in the diffuser, so the transport terms, mean and turbulent, come to play to bring the physical system into equilibrium provided the flow can be approximated to be nearly stationary. Advection partially balances dissipation in the wall layer and partially balances the turbulent diffusion in the core region. The pressure part is neglected from the total transport term for the previously given reasons in the present chapter [see also Azad & Kassab (1985c)]. The remainder term denoted by diffusion partially balances advection in the core region of the diffuser and joins with advection to balance dissipation in the wall region.

All relevant terms of turbulent kinetic energy equation (TKEE) have already been presented and partially discussed. Each and every term contain experimental as well as computational errors of varying degree, but their integrated value across a diffuser section would have the least amount of errors. In addition this scheme represents each physical quantity by a single value at a section and consequently gives a clear transparent picture of turbulent energy mechanism in fully developed pipe flow and along the whole length of diffuser. Integrated values of all terms of TKEE are shown in figure 7.19.

This figure contains two results for dissipation one obtained from TKEE as a closing term after neglecting pressure transport and viscous diffusion terms and the other obtained by extrapolating the dissipation measured by four different wire lengths to zero length (see chapter 5). The latter method is based on isotropic theory. Furthermore, the dissipation has been corrected for high intensity turbulence which is present in the wall region of the diffuser. The difference between these two values of dissipation is called remainder and it is also shown in the figure 7.19. The magnitude of the remainder term is relatively low and it has positive and negative sign. Thus it is random in nature like random errors in measurement and computation.

The integrated value of diffusion is nearly zero within the limits of possible errors from all sources at each location of measurement as it is expected of the diffusion.

The advection that has a zero magnitude in pipe rises sharply at the first station in diffuser, stays nearly at the same value and then finally decreases approximately to zero value by the third location of measurement in the diffuser. Generally, the ratio of advection to production is taken as a measure of perturbation of the flow (see figure 7.20). This ratio is very large at the beginning of the diffuser where pressure gradient is suddenly applied to the flow. Mixing length methods cannot be used in this

region of the diffuser flow because there is inaccuracy of universal mixing length distribution, since advection cannot be neglected. The above observation is also corroborated by Bradshaw (1967c). At first two stations in diffuser, production balances dissipation plus advection. In complex flow, like the present flow in diffuser, mean transport (advection) does not balance turbulent diffusion as shown in figure 7.19.

Apart from the fully disturbed region of the turbulent flow, production is basically balancing the dissipation like any simple flow as shown in the fully developed pipe flow at the inlet of the diffuser. Production and dissipation first increase to a high value and then slowly decrease to some sort of equilibrium values of their own.

The shear-stress balances are presented in figure 7.17 for the sake of completeness and also because some terms in shear stress equation are analogous to terms in turbulent kinetic energy equation, e.g. transport by mean flow analogous to advection. In the present study the pressure-strain term is deduced by measuring all the other terms in Eq.(7.2), since this term has a large magnitude. From magnitude point of view this equation has basically two terms of importance, namely, generation and pressure-strain-rate. The mean and turbulent transport gain importance near the outlet of the diffuser. More details are given in Azad and Kassab (1985c).

7.4 CONCLUDING REMARKS

The diffuser flow has a distinct initial region as well as a distinct final region. The former is characterized by the extra-strain-rate. In addition all parameters, whether they belong to the mean or turbulence fields, increase rapidly in the initial region. However the final region is characterized by the different level and different extend of the equilibrium state. For instance the outlet region of the diffuser flow shows larger equilibrium for $\overline{q^2}$ but shorter one for triple correlations. Near the wall of the diffuser a retarded flow, first thin at the inlet region, starts to grow in a fairly thick layer by the outlet of the diffuser. The outer radial boundary of the layer typifies by the maximum of turbulent energy production and symmetric u-velocity distributions amongst few of its attributes. Furthermore, it contains low mean velocity and high intensity of turbulence. Core region in the final outlet region of the diffuser has higher turbulence activity due to focusing of high turbulence ejecting fluid crossing over the axis; higher turbulence activity is illustrated by higher values of skewness and flatness of u-velocity [see Sabot and Comte-Bellot (1976) and Hummel (1978, Fig. 4.12)].

Some of the results of length scales point towards the growth of large scale structure in the wall region of the diffuser and eventually its growth is finalized in the outlet region. It may also be conjectured that a new growth

of a layer in the diffuser wall underneath the retarded fully developed flow coming from the pipe into the diffuser.

REFERENCES

Abell, C.J. 1974 scaling laws for pipe flow turbulence. Ph.D. Thesis, University of Melbourne.

Andreopoulos, J. and Wood, D.H. 1982 The response of a turbulent boundary layer to a short length of surface roughness. J. Fluid Mech. 118, 143-164.

Antonia, R.A. and Luxton, R.E. 1971 The response of a turbulent boundary layer to a step change in surface roughness. Part 1. Smooth to rough. J. Fluid Mech. 48, 721-761.

Antonia, R.A. and Luxton, R.E. 1972 The response of a turbulent boundary layer to a step change in surface roughness. Part 2. Rough to smooth. J. Fluid Mech. 53, 737-757.

Arora, S.C. 1978 An experimental study of the turbulent kinetic energy and the vorticity in a conical diffuser. Ph.D. Thesis, The University of Manitoba.

Arora, S.C. and Azad, R.S. 1978 Turbulent kinetic energy balance in a flow with adverse pressure gradient. Report E25.27, Mech. Eng. Dept., The University of Manitoba.

Arora, S.C. and Azad, R.S. 1980a Turbulent kinetic energy balance in a flow with adverse pressure gradient. AIAA Paper 80-0073.

Arora, S.C. and Azad, R.S. 1980b Applicability of isotropic vorticity theory to an adverse pressure gradient flow. J. Fluid Mech. 97, 385-404.

Azad, R.S. 1982 Turbulent flow in a conical diffuser: overview and implications. Report METR-10, Mech. Eng. Dept., The University of Manitoba.

Azad, R.S. 1983 Corrections to measurements by hot-wire anemometer in proximity of a wall. Report MET-7, Mech. Eng. Dept., The University of Manitoba.

Azad, R.S. and Burhanuddin, S. 1983 Measurements of some feature of turbulence in wall-proximity. Exps. Fluids 1, 149-160.

Azad, R.S. and Hummel, R.H. 1971 Measurement of intermittency factor in diffuser flow. Can. J. Phys. 49, 2917-2930.

Azad, R.S. and Hummel, R.H. 1979 Similarities of turbulence structure in a conical diffuser with other wall-bounded flows. AIAA J. 17, 884-891.

Azad, R.S. and Hummel, R.H. 1981 Structure functions of turbulence in an adverse pressure gradient. Phys. Fluids 24, 1774-1779.

Azad, R.S. and Kassab, S.Z. 1984 Examination of the k^{-1} spectrum in wall-bounded shear flow. Bull. APS 29, 1521.

Azad, R.S. and Kassab, S.Z. 1985a Spectral data in axisymmetric wall-bounded shear flow. Report METR-4, Mech. Eng. Dept., The University of Manitoba.

Azad, R.S. and Kassab, S.Z. 1985b Dissipation of energy in turbulent flow. Report METR-9, Mech. Eng. Dept., The University of Manitoba.

Azad, R.S. and Kassab, S.Z. 1985c Energy budget and shear stress equation in a conical diffuser. Report METR-11, Mech. Eng. Dept., The University of Manitoba.

Azad, R.S. and Kassab, S.Z. 1986a Measurements of small distance in proximity of a wall with a hot wire. Fluid Measurements and Instrumentation Forum, Joint AIAA/ASME Meeting, Atlanta, Georgia, May 11-14, Paper 1-07.

Azad, R.S. and Kassab, S.Z. 1986b A new method of obtaining dissipation. To be Submitted to J. Fluid Mech.

Azad, R.S. and Kassab, S.Z. 1986c Turbulent flow in a conical diffuser: overview and implications. Submitted to J. Fluid Mech.

Azad, R.S., Derksen, R.W. and Kassab, S.Z. 1984 Low Reynolds number turbulent boundary layer. Report METR-12, Mech. Eng. Dept., The University of Manitoba.

Azad, R.S., Kassab, S.Z. and Dang, T.H. 1985 Experimental evaluation of approximation for moments of fluctuating turbulent velocity, namely, $\overline{w^2}$ and $\overline{vw^2}$. Report METR-10, Mech. Eng. Dept., The University of Manitoba.

Azad, R.S., Kassab, S.Z. and Dang, T.H. 1986 Experimental evaluation of approximations for $\overline{w^2}$ and $\overline{vw^2}$. Submitted to AIAA J.

Badri Narayanan, M.A., Raghu, S. and Kamal Poddar 1984 Wall shear fluctuations in a turbulent boundary layer. AIAA J. 22, 1336-1337.

Blackwelder, R.F. and Haritonidis, J.H. 1983 Scaling of the bursting frequency in turbulent boundary layers. J. Fluid Mech. 132, 87-103.

Bradshaw, P. 1965 A compact, null-reading, tilting U-tube micromanometer with a rigid liquid container. J. Sci. Instrum. 42, 677-680.

Bradshaw, P. 1966 The effect of initial condition on the development of a free shear layer. J. Fluid Mech. 26, 225-236.

Bradshaw, P. 1967a The turbulence structure of equilibrium boundary layers. J. Fluid Mech. 29, 625-645. See also NBL Aero Report 1184, 1966.

Bradshaw, P. 1967b Conditions for the existence of an inertial subrange in turbulent flow. NPL Aero Rep. No. 1220. Also ARC R&M 3003.

Bradshaw, P. 1967c The response of a constant-pressure turbulent boundary layer to the sudden application of an adverse pressure gradient. ARC R&M. No. 3575.

Bradshaw, P. 1973 Effects of streamline curvature on turbulent flow. AGARD-AG-169, NATO.

Bradshaw, P. 1975 Review- Complex turbulent flow. Trans.ASME, J. Fluids Eng. 97, 146-154.

Bradshaw, P. 1976 Complex turbulent flows. In Theoretical and Applied Mechanics (Ed. W.T. Koiter), pp. 103-113, North-Holland.

Bradshaw, P. 1978 Research programme on turbulent shear layers. Imperial College Aero. Tech. Note 78-105.

Bradshaw, P. and Ferriss, D.H. 1972 Application of a general method of calculating turbulent shear layers. J. Basic Eng., Trans. ASME 94, 345-353.

Bradshaw, P. and Galea P.V. 1967 Step induced separation of a turbulent boundary layer in incompressible flow. J. Fluid Mech. 27, 111-130.

Bradshaw, P. and Pontikos, N.S. 1985 Measurements in the turbulent boundary layer on an 'infinite' swept wing. J. Fluid Mech. 159, 105-130.

Bradshaw, P. and Wong, F.Y.F. 1972 The reattachment and relaxation of a turbulent shear layer. J. Fluid Mech. 52, 113-135.

Bradshaw, P., Ferriss, D.H. and Atwell, N.P. 1967 Calculation of boundary layer development using the turbulent energy equation. J. Fluid Mech. 28, 593-616.

Bradshaw, P., Cebeci, T. and Whitelaw, J.H. 1981 Engineering calculation methods for turbulent flow. Academic Press.

Brown, K.C. and Joubert, P.N. 1969 The measurement of skin friction in turbulent boundary layers with adverse pressure gradients. J. Fluid Mech. 35, 737-757.

Builtjes, P.J.H. 1975 Determination of the Eulerian longitudinal integral length scale in a turbulent boundary layer. Appl. Sci. Res. 31, 397-399.

Burhanuddin, S. 1980 Measurement of wall shear stress with hot wire anemometer. M.Sc. Thesis, The University of Manitoba.

Castro, I.P. 1973 A highly distorted turbulent free shear layer. Ph.D. Thesis, University of London.

Castro, I.P. and Bradshaw, P. 1976 The turbulence structure of a highly curved mixing layer. J. Fluid Mech. 73, 265-304.

Champagne, F.H. 1978 The fine-scale structure of the turbulent velocity field. J. Fluid Mech. 86, 67-108.

Chandrsuda, C. and Bradshaw, P. 1981 Turbulence structure of a reattaching mixing layer. J. Fluid Mech. 110, 171-194.

Chevray, R. and Kovasznay. L.S.G. 1969 Turbulence measurements in the wake of a thin flat plate. AIAA J. 7, 1641-1643.

Clark, J.A. 1968 A study of incompressible turbulent boundary layers in channel flow. J. Basic Eng., Trans. ASME 90, 445-468.

Coles, D.E. 1956 The law of the wake in the turbulent boundary layer. J. Fluid Mech. 1, 191-226.

Coles, D.E. 1962 The turbulent boundary layer in a compressible fluid. Rand Corp. Rep. R-403-PR.

Comte-Bellot, G. 1965 Ecoulement turbulent entre deux parois paralleles. Publ. Sc. Tech. Min. Air No. 419 (Also Thesis Univ. Grenoble 1963 and Translation into English by P. Bradshaw 1969 ARC No. 31609).

Comte-Bellot, G. and Corrsin, S. 1966 The use of a contraction to improve the isotropy of grid-generated turbulence. J. Fluid Mech. 25, 657-682.

Dang, T.H. 1986 Evaluation of flush mounted film sensors used for the measurements of skin-friction. M.Sc. Thesis, The University of Manitoba (in preparation).

Derksen, R.W. 1981 The response of a hot wire of finite length to fine-scale structure in a turbulent flow. M.Sc. Thesis, The University of Manitoba.

Derksen, R.W. and Azad, R.S. 1983 An examination of hot wire length corrections. Phys. Fluids 26, 1751-1754.

Driscoll, R.J. 1982 The influence of spectral transfer and molecular diffusion on turbulent mixing and combustion. Ph.D. Dissertation, Suny at Buffalo, U.S.A.

Frenkiel, F.N. and Klebanoff, P.S. 1975 On the lognormality of the small-scale structure of turbulence. Boundary-Layer Meteorology 8, 173-200.

Frei, D. and Thomann, H. 1980 Direct measurements of skin friction in a turbulent boundary layer with a strong adverse pressure gradient. J. Fluid Mech. 101, 79-95.

Gessner, F.B. and Mellor, G.L. 1971 Response behaviour of hot wires in shear flow. J. Fluid Mech. 47, 449-468.

Gibson, M.M. 1963 Spectra of turbulence in a round jet. J. Fluid Mech. 15, 161-173.

Gibson, M.M., Verriopoulos, C.A. and Vlachos, N.S. 1984 Turbulent boundary layer on a mildly curved convex surface. Part 1: Mean flow and turbulence measurements. Exps. Fluids 2, 17-24.

Gol'dshtik, M.A. and Kutateladze, S.S. 1969 Calculation of the wall turbulence constant. Soviet Physics-Doklady 14, 194-196.

Granville, P.S. 1977 Drag and turbulent boundary layer of flat plates at low Reynolds number. J. Ship Res. 21, 30-39.

Guitton, D.E. 1974 The effect of high intensity turbulence on the response of a hot wire. CASI Trans. 7, 69-80.

Hama, F.R. 1954 Boundary-layer characteristics of smooth and rough surfaces. Trans. SNAME 62, 333-358.

Hanjalic, K. and Launder, B.E. 1972 Fully developed asymmetric flow in a plane channel. J. Fluid Mech. 51, 301-335.

Hanjalic, K. and Launder, B.E. 1976 Contribution towards a Reynolds-stress closure for low-Reynolds-number turbulence. J. Fluid Mech. 74, 593-610.

Head, M.R. and Bandyopadhyay, P. 1981 New aspect of turbulent boundary-layer structure. J. Fluid Mech. 107, 297-338.

Head, M.R. and Rechenberg, I. 1962 The Preston tube as a means of measuring skin friction. J. Fluid Mech. 14, 1-17.

Heskestad, G. 1965 Hot-wire measurements in a plane turbulent jet. J. Appl. Mech., Trans. ASME 87, 721-734.

Hinze, J.O. 1975 Turbulence. 2nd Ed., McGraw-Hill Book Company.

Huffman, G.D. and Bradshaw, P. 1972 A note on Von Karman constant in low Reynolds number turbulent flows. J. Fluid Mech. 53, 45-60.

Hummel, R.H. 1978 Turbulence structure in a conical diffuser. Ph.D. Thesis, The University of Manitoba.

Irwin, H.P.A.H. 1973 Measurements in a self-preserving plane wall jet in a positive pressure gradient. J. Fluid Mech. 61, 33-63.

Johansson, A.V. and Alfredsson, P.H. 1983 Effects of imperfect spatial resolution on measurements of wall-bounded turbulent shear flows. J. Fluid Mech. 137, 409-421.

Johnson, F.D. and Eckelmann, H. 1984 A variable angle method of calibration for X-probes applied to wall-bounded turbulent shear flow. Exps. Fluids 2, 121-130.

Kader, B.A. 1984 Spectrum of anisotropic pulsations of the velocity in the gradient sublayer of a decelerating turbulent boundary layer. Dokl. Akad. Nauk SSSR 279, 323-327.

Kader, B.A. and Yaglom, A.M. 1984 Turbulent structure of an unstable atmospheric surface layer. Nonlinear and Turbulent Processes in Physics (Ed. R.Z. Sagdeev) 2, 829-845, Harwood Academic Publishers.

Kassab, S.Z., Derksen, R.W. and Azad, R.S. 1985 Remarks on stem configuration of X-array hot-wire probes. DANTEC Inf. 1, 9-10.

Klebanoff, P.S. 1955 Characteristics of turbulence in a boundary layer with zero pressure gradient. NACA Report 1247, 1135-1153.

Klebanoff, P.S. and Diehl, Z.W. 1952 Some features of artificially thickened fully developed turbulent boundary layers with zero pressure gradient. NACA Tech. Rep. No. 1110.

Kline, S.J., Reynolds, W.C., Schraub, F.A. and Runstadler, P.W. 1967 The structure of turbulent boundary layers. J. Fluid Mech. 30, 741-773.

Kolmogoroff, A.N. 1941 Local structure of turbulence in an incompressible fluid at very high Reynolds number. Doklady AN SSSR 30, 299-303.

Kuo, A.Y. and Corrsin, S. 1971 Experiments on internal intermittency and fine-structure distribution functions in fully turbulent fluid. J. Fluid Mech. 50, 285-319.

Lagrini, P.H. and Moffat, R.J. 1986 Structure of transitionally rough and fully rough turbulent boundary layers. J. Fluid Mech. 162, 69-98.

Landweber, L. 1953 The frictional resistance of flat plates in zero pressure gradient. Trans. SNAME 61, 5-32.

Laufer, J. 1954 The structure of turbulence in fully developed pipe flow. NACA Rep. 1174.

Lawn, C.J. 1970a Application of the turbulence energy equation to fully developed flow in simple ducts. CEGB/RD/B/R1575 (B).

Lawn, C.J. 1970b Application of the turbulence energy equation to fully developed flow in simple ducts. CEGB/RD/B/R1575 (C).

Lawn, C.J. 1971 The determination of the rate of dissipation in turbulent pipe flow. J. Fluid Mech. 48, 477-505.

Leslie, D.C. 1980 Analysis of a strongly sheared, nearly homogeneous turbulent shear flow. J. Fluid Mech. 98, 435-448.

Liepmann, H.W. and Laufer, J. 1947 Investigations of free turbulent mixing. NACA TN No. 1257.

Lu, S.S. and Willmarth, W.W. 1973 Measurements of the structure of the Reynolds stress in a turbulent boundary layer. J. Fluid Mech. 60, 481-511.

Lumley, J.L. 1965 Interpretation of time spectra measured in high-intensity shear flows. Phys. Fluids 8, 1056-1062.

Lumley, J.L. 1981 Coherent structures in turbulence. In Transition and Turbulence, pp. 215-242, Academic Press Inc.

Millikan, C.D. 1939 A critical discussion of turbulent flows in channels and circular tubes. Proc. 5th Int. Congr. Appl. Mech. 389-392.

Murlis, J. 1975 The structure of a turbulent boundary layer at low Reynolds number. Ph.D. Thesis, University of London.

Murlis, J., Tsai, H.M. and Bradshaw, P. 1982 The structure of turbulent boundary layers at low Reynolds numbers. J. Fluid Mech. 122, 13-56.

Nakagawa, H., Nezu, I. and Ueda, H. 1975 Turbulence of open channel flow over smooth and rough beds. Proc. JSCE, No. 241, 155-168.

Okwuobi, P.A.C. and Azad, R.S. 1973 Turbulence in a conical diffuser with fully developed flow at entry. J. Fluid Mech. 57, 603-622.

Ozimek, L.G. 1986 A comparison of analog and digital data for measurements of turbulence parameters. M.Sc. Thesis, The University of Manitoba.

Panchev, S. 1969 Exact elementary solution of the spectral equation of nonstratified turbulent shear flow. Phys. Fluids 12, 722-723.

Pao, Y.H. 1965 Structure of turbulent velocity and scalar fields at large wavenumbers. Phys. Fluids 8, 1063-1075.

Patel, V.C. 1965 Calibration of the Preston tube and limitations on its use in pressure gradients. J. Fluid Mech. 23, 185-208.

Patel, V.C. 1973 A unified view of the law of the wall using mixing-length theory. Aero. Quarterly 24, 55-70.

Patel, V.C. and Head, M.R. 1969 Some observations on skin friction and velocity profiles in fully developed pipe and channel flows. J. Fluid Mech. 38, 181-201.

Perry, A.E. and Abell, C.J. 1975 Scaling laws for pipe-flow turbulence. J. Fluid Mech. 67, 257-271.

Perry, A.E. and Abell, C.J. 1977 Asymptotic similarity of turbulence structure in smooth-and rough-walled pipes. J. Fluid Mech. 79, 785-799.

Pozzorini, R. 1976 Das turbulente stromungsfeld in einem langen kreiskegel-diffusor. DISS. ETH 5646, Eduard Truninger AG. Zurich, Switzerland.

Preston, J.H. 1950 The three-quarter radius Pitot-tube flow meter. The Engineer 190, 400-402.

Preston, J.H. 1958 The minimum Reynolds number for a turbulent boundary layer and the selection of a transition device. J. Fluid Mech. 3, 373-384.

Purtell, L.P. 1978 The turbulent boundary layer at low Reynolds number. Ph.D. Thesis, University of Maryland.

Purtell, L.P., Klebanoff, P.S. and Buckley, F.T. 1981 Turbulent boundary layer at low Reynolds number. Phys. Fluids 24, 802-811.

Ramaprian, B.R. and Chandrasekhara, M.S. 1985 LDA measurements in plane turbulent jets. J. Fluids Eng., Trans. ASME 107, 264-271.

Rasmussen, C.G. 1966 Measurement of turbulence characteristics. DISA Inf. 3, 9-20.

Rotta, J.C. 1962 Turbulent boundary layers in incompressible flow. Prog. Aero. Sci. 2, 1-219.

Sabot, J. 1976 Etude de la coherence spatiale et temporelle de la turbulence etablie en conduite circulaire. Dr. es Sci., Universite Claude Bernard, Lyon, France.

Sabot, J. and Comte-Bellot, G. 1972a Memoires des fluctuations longitudinales de vitesse en conduite lisse circulaire. C.R. Acad Sc. Paris, t. 274, Serie A, 1647-1650.

Sabot, J. and Comte-Bellot, G. 1972b Courbes d'iso-correlations spatiales et d'iso-correlations spatio-temporelles relatives aux fluctuations longitudinales de vitesse en conduite lisse circulaire. C.R. Acad Sc. Paris, t. 275, Serie A, 667-670.

Sabot, J. and Comte-Bellot, G. 1974 Temps de coherence de la fluctuation radiale de vitesse en conduite circulaire. C.R. Acad Sc. Paris, t. 278, Serie A, 105-107.

Sabot, J. and Comte-Bellot, G. 1976 Intermittency of coherent structures in the core region of fully developed turbulent pipe flow. J. Fluid Mech. 74, 767-796.

Schlichting, H. 1968 Boundary layer theory. 6th Ed., McGraw-Hill.

Schoenherr, K.E. 1932 Resistance of flat surfaces moving through a fluid. Trans. SNAME 40, 279-313.

Schubauer, G.B. and Klebanoff, P.S. 1946 Theory and application of hot-wire instruments in the investigation of turbulent boundary layers. NACA ACR No. 5K27.

Schubauer, G.B. and Klebanoff, P.S. 1950 Investigation of separation of the turbulent boundary layer. NACA TN No. 2133.

Schultz-Grunow, F. 1940 Neues reibungswiderstandsqesetz fur glatte platten. Luft-Fahrtforschung 17, 239-246 (Available as NACA TM 986, 1941).

Shabaka, I.M.M.A., Mehata, R.D. and Bradshaw, P. 1985 Longitudinal vortices imbedded in turbulent boundary layers Part 1. Single vortex. J. Fluid Mech. 155, 37-57.

Shishov, E.v., Roganov, P.S., Belov, V.M. and Afanasiev, V.N. 1978 Experimental investigation of the turbulent kinetic energy balance in the retarded turbulent boundary layer. Izvestiia Vysshikh Uchebnykh. Zavedenii Aviastsionnaia Tekhnika 3, 108-112.

Simpson, R.L. 1970 Characteristics of turbulent boundary layers at low Reynolds numbers with and without transpiration. J. Fluid Mech. 42, 769-802.

Simpson, R.L. 1976 Comments on "Prediction of turbulent boundary layers at low Reynolds numbers". AIAA J. 14, 1662.

Simpson, R.L., Chew, L.T. and Shivaprased, G. 1981 The structure of separating turbulent boundary layer. Part 2. Higher-order turbulence results. J. Fluid Mech. 113, 53-73.

Singh, D. and Azad, R.S. 1981 Turbulent kinetic energy balance in a conical diffuser. Proc. 7th Symp. on Turbulence, Sep. 21-23, Univ. of Missoure-Rolla, Edited by G.K. Patterson and J.L. Zakin, 21-33.

Smits, A.J., Young, S.T.B. and Bradshaw, P. 1979a The effect of short regions of high surface curvature on turbulent boundary layers. J. Fluid Mech. 94, 209-242.

Smits, A.J., Eaton, J.A. and Bradshaw,P. 1979b The response of turbulent boundary layer to lateral divergence. J. Fluid Mech. 94, 243-268.

Smits, A.J. and Wood, D.H. 1985 The response of turbulent boundary layers to sudden perturbations. Ann. Rev. Fluid Mech. 17, 321-358.

Sovran, G. and Klomp, E. 1967 Experimentally determined optimum geometries for rectilinear diffusers with rectangular, conical or annular cross section. Proc. General Motors Symp. on Fluid Mechanics of Internal Flow (ed.: G. Sovran), Elsevier Pub. Co., 270-319.

Spalding, D.B. 1961 A single formula for the law of the wall. J. Appl. Mech., Trans. ASME 83, 455-458.

Sprenger, H. 1959 Experimentelle untersuchungen an geraden und gekrummten diffusoren. Mitteilung aus dem Institute fur Aerodynamik an der ETH, Zurich, No. 27 (Translation:

Experimental research on straight and curved diffusers. Obtained from the Ministry of Aviation, Gt. Brit.).

Sreenivasan, K.R. 1985 The effect of contraction on a homogeneous turbulent shear flow. J. Fluid Mech. 154, 187-213.

Tchen, C.M. 1953 On the spectrum of energy in turbulent shear flow. Res. Paper 2388, Jour. Res. Nat. Bur. Standards 50, 51-62.

The 1980-81 AFOSR-HTTM Stanford onference on Complex Turbulence Flows. Vol. I. Edited by Kline, S.J., Cantwell, B.J. and Lilley, G.M. Stanford University, 1981.

Townsend, A.A. 1949 Momentum and energy diffusion in the turbulent wake of a cylinder. Proc. Roy. Soc. A197, 124-140.

Townsend, A.A. 1980 The structure of turbulent shear flow. First paperback edition, Cambridge University Press.

Tritton, D.J. 1967 Note on the effect of a nearby obstacle on turbulence intensity in a boundary layer. J. Fluid Mech. 28, 433-437.

Trupp, A.C. 1973 The structure of turbulent flow in triangular array rod bundles. Ph.D. Thesis, The University of Manitoba.

Trupp, A.C., Azad, R.S. and Kassab, S.Z. 1986 Near wall velocity distributions within a straight conical diffuser. Exps. Fluids 4, 1-13.

Ueda, H. and Hinze, J.O. 1975 Fine-structure turbulence in the wall region of a turbulent boundary layer. J. Fluid Mech. 67, 125-144.

Weir, A.D., Wood, D.H. and Bradshaw, P. 1981 Interacting turbulent shear layers in a plane jet. J. Fluid Mech. 107, 237-260.

Wieghardt, K. and Tillman, W. 1944 On the turbulent friction layer for rising pressure. Kaiser Wilhelm Institute fur stromengsforschung, Gottingen, U & M 6617. see also NACA 1314, 1951.

White, B.R. 1981 Low-Reynolds-number turbulent boundary layers. J. Fluids Eng., Trans. ASME 103, 624-630.

Wood, D.H. and Bradshaw, P. 1982 A turbulent mixing layer constrained by a solid surface. Part 1. Measurements before reaching the surface. J. Fluid Mech. 122, 57-89.

Wood, D.H. and Bradshaw, P. 1984 A turbulent mixing layer constrained by a solid surface. Part 2. Measurements in the wall-bounded flow. J. Fluid Mech. 139, 347-361.

Wyngaard, J.C. and Lumley, J.L. 1967 A sharp cutoff spectral differentiator. J. Appl. Meteorol. 6, 952-955.

Wygnanski, I. and Fiedler, H. 1969 Some measurements in the self-preserving jet. J. Fluid Mech. 38, 577-612.

Wygnanski, I. and Fiedler, H. 1970 The two-dimensional mixing region. J. Fluid Mech. 41, 327-361.

APPENDIX A

REMARKS ON STEM CONFIGURATION OF X-ARRAY HOT-WIRE PROBES

When one measures the turbulence parameters close to a wall with an in-line probe, such as DISA 55P51, one finds the smallest distance to the wall approached by the probe is about 3 mm.[8] This distance of 3 mm is a large distance if it is compared with the physical field there. This situation arises due to the probe holder tube having a diameter of 6 mm. By using probes that have prongs bent at right angles to the stem, a distance to the wall closer than 3 mm can be approached. But a comparison of results from the right-angled probes with the in-lined probe reveals significant difference in their readings. This note concerns aerodynamic interference of probe stems.

To study the aerodynamic interference of the probe stem, the flow selected was a boundary layer developing on the inside of a 27 cm diameter hydraulically smooth brass pipe (see chapter 6). The in-lined probe was a DISA 55P51 and the right angled probes were a DISA 55P53 (for u-v plane) and a DISA 55P54 (for u-w plane). The sensing wire of these probes was platinum plated tungsten of nominal length of 1.25 mm and nominal diameter of 5 μm and its supports were

---

[8] This Appendix is based on the paper by Kassab, Derksen and Azad (1985).

gold plated. The probes and their supports together with mounting tube geometries for the 55P51 and 55P53 are shown in figure A.1. The 55P54 is not shown in the figure, since it is similar in geometry to the 55P53.

First the results of mean velocity for all three probes are presented in figure A.2 and this figure shows that the velocity profiles are exactly the same for all three probes. It means that mean field is not disturbed by the variation of stem geometry.

Data for Reynolds stresses are presented next. The turbulence intensities are shown in figure 6.4a. In all cases the root mean squire (RMS) values of fluctuating normal velocities divided by the same free stream velocity belonging to the right angle probes denote roughly 5 to 10% lower than the values obtained by the in-line probe. The two right angled probes can measure the value of $\overline{(u^2)^{1/2}}/U$ only in common, this value has the same magnitude for both probes because they have similar geometry. The value of $\overline{(u^2)^{1/2}}/U$ is higher for DISA 55P51 than for two right angled probes, namely, DISA 55P53 and DISA 55P54 and this can only be due to stem interference. Physically the Reynolds shear stress coefficients are most revealing turbulence parameters. One in particular, usually occuring in two-dimensional or axisymmetric flow, is $R_{12} = \overline{-uv}/(\overline{u^2}\,\overline{v^2})^{1/2}$ and its maximum value reported by Klebanoff (1955) is 0.50, by Lu and Willmarth (1973) is 0.45, and

Chandrsuda and Bradshaw (1981) is about 0.45 to 0.50. The most accepted value between 0.45 and 0.50 may be the value 0.47 which has been used by Hanjalic and Launder (1976) in their low Reynolds number model. This value was obtained by X-array probe DISA 55P51 (see figure A.3). The results for Reynolds shear coefficient, R_{12}, are shown in figure A.3 for two relevant X-array probes for comparison. It can be seen from the figure that the maximum value of R_{12}, obtained by the right angle probe, DISA 55P53, is 0.37. Approximately more than 20% discrepancy in the maximum value of R_{12} is possible due to aerodynamic interference of the stem geometry.

Results in figures 6.4a and A.3 clearly demonstrate that readings taken by X-array probes, whose prongs are bent at right angles to the stem, are lower in value than readings taken by the probe with parallel prongs to the stem under identical mean field conditions. These figures show only the turbulence field where the difference exits, but the mean field shown in figure A.2 does not show any difference at all. The whole geometry of the right angle bent probe is producing an aerodynamic interference and in turn giving smaller values of R_{12}. A similar qualitative conclusion has been made by Tritton (1967).

APPENDIX B

EXPERIMENTAL EVALUATION OF APPROXIMATIONS FOR $\overline{w^2}$ AND $\overline{vw^2}$.

Assumptions involved in assessment of any physical situation should be reduced to a minimum for increasing knowledge of a subject.[9] The purpose of this Appendix is to evaluate assumptions usually made for some moments of turbulence fluctuating velocity one of these moments requires additional time to measure whereas the other is difficult to measure as well as being time consuming. The following assumptions are generally made by researchers [for example, Bradshaw (1966, 1967a), Lawn (1970a), Antonia and Luxton (1971, 1972), Shishov et al. (1978), Smits et al. (1979a, b), Chandrsuda and Bradshaw (1981), Murlis et al. (1982) and Ramaprian and Chandrasekhara (1985)] in turbulence regarding $\overline{w^2}$ and $\overline{vw^2}$:

$$\overline{w^2} = 0.5(\overline{u^2} + \overline{v^2}) \qquad \text{(B.1)}$$

$$\overline{vw^2} = 0.5(\overline{u^2 v} + \overline{v^3}) \qquad \text{(B.2)}$$

Eqs. (B.1) and (B.2) affect the mean and turbulent transport of the turbulent kinetic energy. They are examined in light of experimental measurements in three flows, namely, boundary layer, fully developed pipe flow and also in

---

[9] This Appendix is based on the report by Azad, Kassab and Dang (1985) and the paper by Azad, Kassab and Dang (1986).

diffuser flow which was fed with fully developed pipe flow. Details regarding these three flows are given in chapters 6 and 7.

The measurement of triple correlation, $\overline{vw^2}$, first outlined by Townsend (1949) and later followed by others [for example, Wygnanski and Fiedler (1969, 1970), Hanjalic and Launder (1972) and Irwin (1973)], was adopted in the present work. Briefly, the method requires that the X-wire should be placed in the flow in such a way that its plane is parallel to the flow and it is at an angle of 45^0 to both the y— and z-axes. Detailed derivation is given in Wygnanski and Fiedler (1969).[10]

Figure B.1 shows the results for the low Reynolds number turbulent boundary layer, $R_\theta = (U_\infty \theta)/\nu = 2.76*10^3$, in which U_∞ is the free stream velocity, θ is the momentum thickness and ν is the kinematic viscosity of a fluid. Figure B.1a shows the value of $\overline{w^2}/(\overline{u^2} + \overline{v^2})$ to be 0.4 instead of the value of 0.5 usually assumed, except some variations in intermittent region ($y/\delta > 0.4$). In figure B.1b the value of $\overline{vw^2}/(\overline{u^2v} + \overline{v^3})$ drops linearly from about 1.0 near the wall to 0.2 at $y/\delta = 0.4$ and remains at this value through out the boundary layer.

---

[10] There is a misprint in the final form in Wygnanski and Fiedler (1969), v^2 was incorrectly replaced by u^2.

The results in fully developed pipe flow are given in figure B.2. The results of Dang (1986) are also shown for the same pipe flow for two values of the pipe Reynolds number, Re = $1.14*10^5$ and $2.31*10^5$, and for two values of L/D, 78 and 98. The Reynolds number, Re is based on mean velocity, U_b, at a cross-section, the pipe diameter D, and kinematic viscosity ν, i.e., Re = $(U_b D)/\nu$. The value of $\overline{w^2}/(\overline{u^2} + \overline{v^2})$ is not equal to 0.5 but varys from about 0.41 at the center of the pipe to about 0.35 at r/R =0.9 (see figure B.2a), where r is the distance from the pipe axis and R is the radius of the pipe. Finally this value increases to 0.4 near the pipe wall. The results pertaining to $\overline{vw^2}/(\overline{u^2v} + \overline{v^3})$ shown in figure B.2b remain nearly constant at 0.2 from the pipe axis to r/R = 0.6 and increase to a value of nearly 1.0 near the pipe wall. Both the quantities, i.e., $\overline{w^2}/(\overline{u^2} + \overline{v^2})$ and $\overline{vw^2}/(\overline{u^2v} + \overline{v^3})$ clearly demonstrate that the flow is fully developed and independent of Reynolds number over the range tested. In addition, credence is added to the measurements since the present results and Dang's (1986) results have been obtained independently over three year period.

These two quantities have been measured at six different axial locations of a diffuser and are reported in Azad et al. (1985). For conciseness, only one location that is thought to be representative of the behaviour of these two quantities has been selected for reportage in this note.

This position is located at a distance of 42 cm from the inlet of the diffuser. The results for $\overline{w^2}/(\overline{u^2} + \overline{v^2})$ shown in figure B.3a monotonically decrease from 0.38 at the axis of the diffuser to 0.33 at $r/R_{LOC} = 0.8$ and then increases rather rapidly to a value of 0.48 near the wall of the diffuser. Since the sign of $\overline{vw^2}$ is not the same as $(\overline{u^2v} + \overline{v^3})$ across the radius as they are in fully developed pipe flow and boundary layer, the results for $\overline{vw^2}$ and $0.5(\overline{u^2v} + \overline{v^3})$ are plotted in figure B.3b with different symbols. It can be seen from the figure that these quantities are far apart from each other from the axis to $r/R_{LOC} = 0.8$. A similar trend has been observed at other locations of the diffuser [see Azad et al. (1985)].

The expressions given by Eqs.(B.1) and (B.2) are not valid as demonstrated by the present measurements in three turbulent shear flows. The above inference is also corroborated by others [for example, Wood and Bradshaw (1982, 1984), Townsend (1980) and Andreopoulos and Wood (1982)]. In particular, Wood and Bradshaw (1982) obtained $\overline{vw^2} = 0.20(\overline{u^2v} + \overline{v^3})$ across the whole turbulent mixing layer and subsequently used this finding in their further study [Wood and Bradshaw (1984)]. It can be inferred from Table 5.2 given by Townsend (1980) that $\overline{w^2}/(\overline{u^2} + \overline{v^2}) = 0.37$ for the laboratory equilibrium layer, and 0.63 for the atmospheric equilibrium layer. Finally Andreopoulos and Wood (1982) compared $\overline{w^2}$ with $0.5(\overline{u^2} + \overline{v^2})$ in their figure 9 and

found that the approximation $\overline{w^2} = 0.5(\overline{u^2} + \overline{v^2})$ was erroneous.

Apart from these, Lawn (1971) has deduced from the measurements of Laufer (1954) that $\overline{vw^2} \cong 0.5\overline{v^3} \cong 0.5\overline{u^2v}$ and in turn used $\overline{vw^2} = 0.25(\overline{u^2v} + \overline{v^3})$. Nakagawa et al. (1975) has approximated $\overline{vw^2} = \overline{v^3}$. Besides these there are other assumptions [see Heskestad (1965), Guitton (1974)] available in the literature.

The above discussions of the assumptions concerning two parameters, $\overline{w^2}$ and $\overline{vw^2}$ clearly indicate that none of the assumptions really work in all the turbulent flows. Hence generalization in turbulence is very risky. In other words, the quantity required has to be measured.

APPENDIX C

FULLY DEVELOPED TURBULENT PIPE FLOW

Fully developed pipe flow was chosen to be the inlet flow to the diffuser in the present study since the flow there is supposed to have attained a physical equilibrium condition. Before discussing diffuser flow it would be better to examine whether pipe flow used satisfied the conditions for the fully developed pipe flow.

Until recently, flow developed in pipes was believed to be solely determined by a flat plate like growth of the wall boundary layer. Therefore, the peakedness of the velocity profile, defined as the ratio between the maximum value and the area mean, was thought to increase gradually until the boundary layers meet at the pipe centreline. But, the mean velocity is not a sufficient description of any turbulent shear flow. Apart from this, there are other necessary conditions for fully developed turbulent flow in a pipe, i.e. all physical quantities are independent of downstream distance. These conditions are:

1. Minimum Reynolds number to ensure fully turbulent flow.
2. Linear static pressure drop along the pipe wall.
3. The lack of downstream evolution of the skewness factors.

4. The insensitivity of turbulent intensity profile to the entry conditions.
5. The length, L, from the pipe inlet to the measuring section, should be more than the resultant length L_1+L_2, where L_1 is the length required by initial boundary layers to meet and L_2 is the length able to ensure the renewal of the turbulence.

In the present study, the above conditions are discussed in detail and are examined with respect to the present pipe flow.

The values of ratio U_b/U_c, where U_b is the bulk or mean velocity at a x-section of the pipe in the longitudinal direction and U_c is the centreline mean velocity, are given in Table C.1. The present values of U_b/U_c change from 0.82 to 0.83 in the range of Reynolds number, $Re = U_bD/\nu$, from $8.07*10^4$ to $2.30*10^5$. These values of ratio are the same as of Okwuobi and Azad (1973). Nikuradse [reference in Schlichting (1968, p. 563)] obtained values of U_b/U_c in the range 0.81-0.83 for $2.3*10^4 < Re < 1.10*10^6$ and L/D = 120, Lawn (1971) reported values of U_b/U_c in the range 0.806-0.833 for $3.50*10^4 < Re < 2.50*10^5$ and L/D = 59, and finally Sabot (1976) also mentioned values of U_b/U_c = 0.82 and 0.83 for Re = $5.58*10^4$ and $1.12*10^5$ respectively [see also Sabot and Comte-Bellot (1976)]. Comparing the above results that of in Table C.1 indicate that the present pipe flow is fully developed.

Secondly, the minimum Reynolds number, Re, required to ensure fully turbulent flow was investigated thoroughly for the case of pipe and channel flows by Patel and Head (1969). Their three criteria, namely, skin friction-Reynolds number relation, log law with universal constants and disappearance of intermittency, did not lead to a unique minimum value of Reynolds number above which fully turbulent flow can be established. But figures 13 and 14 and Table 1 in their paper show that this Reynolds number should be greater than 10^4. In the present study the minimum Reynolds number, Re = $8.07*10^4$, i.e. the present pipe flow satisfies this requirement. Further, the coefficient of friction:

$$C_f = \tau_w/(0.5\rho U_b^2) = 2(u^*/U_b)^2$$

(where τ_w is the wall shear stress and equal to ρu^{*2}, u^* is the wall friction velocity and ρ is the fluid density) is shown in figure C.1 and the present results are in agreement with the well known Blasius friction law:

$$C_f = 0.079Re^{-1/4}$$

Moreover, Figure C.2 shows the velocity distribution in U^+ and y^+ coordinates for different Reynolds numbers. In this figure, the log law is given as

$$U^+ = A \ln y^+ + B$$

where $U^+ = U/u^*$, U is the local mean velocity in the longitudinal direction, u^* is the friction velocity, A and B

are constant and $y^+ = (yu^*)/\nu$, y is the distance from the wall and perpendicular to it. Constant A is chosen to be 1/0.41, but constant B is obtained as the best fit to pipe data and is found to be 5.45. This value of B is the same as the asymptotic value found by Patel and Head (1969) for the flow in a pipe that was fully turbulent.

Another necessary condition for the flow in the pipe to be fully developed is that the static pressure drop along the pipe wall should be linear. This condition required accurate measurement of the wall static pressure. Therefore, sixteen static pressure holes, 1.0 mm diameter each, were drilled in four sets. Each set contains four taps placed 90^0 apart. For Re = $1.15*10^5$, the wall static pressure measured by each hole was examined separately and the results are given in figure C.3a. Two holes give unexpected static pressure readings. These readings have been attributed to the drilling defects and a decision was made to close them. Their readings, first measured, are marked "out" in figure C.3a. The mean wall static pressure was observed by inter-connecting the holes of each set to give a single reading. The results of the mean output for the four sets are indicated by a continuous lines in figure C.3a and they agree with the reading of the individual hole of each corresponding set. These results are presented also in figure C.3b and they give a linear static pressure drop along the pipe wall.

Regarding the condition of the lack of the downstream evolution of the skewness factors as a necessary condition for the turbulent flow to be fully developed in a pipe [see Comte-Bellot (1965)], figure C.4 shows the skewness factor in the longitudinal direction $S(u) = \overline{u^3}/\overline{(u^2)^{3/2}}$ at three different locations. This figure shows that the measured quantities are the same for the three locations and in turn the flow is fully developed (although it is weak support because of the short distance between the three locations). However, Dang (1986), using the same set-up as the present one, recently did the measurements at two locations, namely, L/D = 78 and 98, for two Reynolds numbers, $Re = 1.14*10^5$ (the same as the present study) and the other at $Re = 2.31*10^5$. The comparison of his results and the present results for some of the second and third moments, namely, $\overline{w^2}$ and $\overline{vw^2}$ is given in Appendix B. The present and Dang's (1986) results clearly demonstrate that the pipe flow is fully developed and also it is independent of Reynolds number over the range tested.

Next, the insensitivity of turbulent intensity profile to the entry conditions was checked in a similar way as Perry and Abell (1975) but with different approach. They checked their fully developed pipe flow for a possible lack of axisymmetry caused by entry conditions by measuring $\overline{(u^2)^{1/2}}$ at fixed radii and rotating the entrance assembly relative to the pipe. In the present study, the measurements were

made across the pipe. The results for turbulence intensity are shown in figure C.5 and clearly demonstrate that the flow is axisymmetric and there is no effect of the entry conditions at the measuring location.

The last condition required for a flow in a pipe to be fully developed turbulent is the pipe total length, L, which should be larger than the resultant length L_1+L_2, where L_1 is the length required by initial boundary layer to close and L_2 is the length able to ensure the renewal of the turbulence as proposed by Sabot and Comte-Bellot (1976). They have examined this condition experimently [see for example, Sabot and Comte-Bellot (1972a, b, 1974)], stated that $L_1 \cong L_2 \cong 35D$ for their fully developed pipe flow. Their pipe diameter, D, was 10 cm and their highest Reynolds number, Re, was $1.12*10^5$. In the present study, D = 10.16 cm (4 inch), and Re $=1.15*10^5$ and are very close to Sabot and Comte-Bellot values. Therefore, for the present study ,L_1 and L_2 should be the same(or nearly the same) as their values, i.e. L/D should be > 70. This means that our flow is fully developed because L/D = 78.

Finally, after examining all the above necessary conditions for fully developed pipe flow, it can be concluded that the pipe flow under investigation in the present study was fully developed.

APPENDIX D

NEAR-WALL VELOCITY DISTRIBUTION WITHIN A STRAIGHT CONICAL DIFFUSER

The near-wall velocity distribution in a conical diffuser flow have been measured, and the purpose of this appendix is simply to communicate these experimental results.[11] The present experimental results involve three types of measurement at various stations located between the inlet and outlet of the axisymmetric diffuser. These measurements were wall static pressure, mean velocity distributions normal to the diffuser wall in the near-wall region, and local wall shear stress. The first two types of measurement are routine. However, measurements of local wall shear stress were made using Preston tubes of various size, but the accuracy of such measurements in an adverse pressure gradient is subject to some debate.

A thorough review of the available methods which have been used to obtain the wall shear stress in adverse pressure gradient is given by Trupp et al. (1986). In summary, subsequent to Patel's (1965) work, two methods have been proposed for employing Preston tubes in turbulent boundary layers involving medium to strong adverse pressure gradients. Each approach begins by using the calibration of

---

[11] This Appendix is based on the paper by Trupp, Azad and Kassab (1986).

Patel (1965), and is then followed by a correction procedure. The first approach is exemplified in the paper by Brown and Joubert (1969) who formalized the procedure in which wall shear stress is obtained by plotting the friction velocity obtained by Patel's calibration against Preston tube diameter and extrapolating to zero diameter. Formally extrapolating to zero probe diameter is not possible, then the friction velocities obtained using Preston tubes of various size with Patel's calibration, are simply plotted and then a quasi-mean line is drawn favouring the smaller tubes [e.g., see Bradshaw and Wong (1972)]. The second method is due to Frei and Thomann (1980) who investigated the errors of Preston tubes in adverse pressure gradients by comparing their results to those obtained by direct measurement of skin friction using a floating element technique.

In view of different considerations [details are given in Trupp et al. (1986)], the present wall shear stress obtained by simply averaging all the Preston tubes readings (see figure 7.2). This mean value is used for the examination of velocity distributions.

Mean velocity measurements were made at 17 stations located along the diffuser as indicated in Table D.1. At each station, the Pitot tube/hot-wire traverse was in the y_w direction, and measurements were made between the wall and y_w = 20 mm.

All the data are shown in figure D.1 in U^+, y^+ format using the local friction velocities listed in Table D.1. The stations have been numbered to facilitate discussion. The y^+ values for u^*d_p/ν are shown by arrows at each station for both the smallest and largest Preston tubes. Also for each station, a log law line of standard form:

$$U^+ = A \ln y^+ + B ,$$

has been drawn with slope A set to $(\kappa)^{-1}$ and the intercept B determined by arbitrarily shifting the line so as to pass through the data in the vicinity of $y^+ = 30$.

From a close examination of the data presented in figure D.1, the following observations can be made,

1. The hot-wire and Pitot tube results are generally in good agreement except for the last few stations where the Pitot tube results are consistently lower than the hot-wire data in the region $40 < y^+ < 120$. The maximum discrepancies reflected in figure D.1 are only of the order 6 to 8%.
2. The velocity distribution for the fully developed pipe flow agrees closely with Spalding's (1961) law of the wall for both the fully turbulent and buffer regions.
3. Departures from the law of the wall begin as soon as the flow enters the diffuser. This is seen first (station 1) in the buffer region, and later

(beginning with station 2) in the outer portion of the fully turbulent region. There is rapid erosion of the width of the log law such that by station 6 there is little evidence of a log law of any substantial thickness. However, beginning at about station 11, the width of the log region appears to begin to increase and the departures in the outer region become progressively less. Hence in the final stages of the diffuser, the log law appears to re-emerge.

4. For station 5 (for example), the entire velocity distribution can be represented by two straight lines which are joined by a blending region in the vicinity of $y^+ = 100$.
5. For stations 8 to 17 inclusive, data appear at $y^+ < 5$ which do not conform to the viscous sub-layer specification, $U^+ = y^+$. These measurements were made at locations having high turbulence intensities, hence true mean velocities are likely to be somewhat lower than the measured values. In addition, it is well known for the immediate near-wall region, that any errors in u* can have a significant influence on velocity distributions in U^+, y^+ coordinates. Accordingly, the data here may not be accurate.

The velocity distributions, as determined by hot-wire measurements only, were examined in more detail for stations

1 to 17 inclusive. The results of this study are summarized in Table D.1. Three regional types were identified; viz, log law regions, half-power law regions (both inner and outer) and linear regions. As noted in Table D.1, there is some over-lap in adjacent regions. This stems simply from the well-known fact for curve-fitting that a given set of data can often be represented adequately by more than one form.

For the log law regions, assuming the experimental friction velocities to be fairly accurate, there is evidence that the log law slopes are generally higher than the conventional slope and the log regions are generally quite narrow. For the inner half-power law regions, the attendant coefficients correlate with both the local friction velocities and the kinematic pressure gradients. Due to the axisymmetric flow factor and lack of moving equilibrium, these coefficients differ from the standard values for equilibrium boundary layers subject to adverse pressure gradients. The linear regions basically form blending regions between the inner and outer half-power regions (where the latter exists). The coefficients here also correlate with either the local wall shear stress or the kinematic pressure gradient.

TABLE 2.1

PRESTON TUBES DIMENSIONS

No.	d_p [mm]	d_p/d_1
1	0.508	0.700
2	1.067	0.714
3	2.032	0.825
4	3.175	0.680
5	4.750	0.701

d_p is the Preston tube outside diameter

d_1 is the Preston tube inside diameter

TABLE 2.2

DIMENSIONS OF FOUR OF THE STANDARD DISA 55P05 BOUNDARY LAYER PROBES USED IN THE PRESENT STUDY

No.	length,(l) [mm]	diameter,(d) [μm]	l/d
1	1.177	5.766	204
2	1.192	5.681	210
3	1.177	5.596	210
4	1.161	5.935	196

TABLE 2.3

DIMENSIONS OF THE WIRES USED TO EXAMINE THE SPATIAL RESOLUTION OF A HOT WIRE

No.	length,(l) [mm]	diameter,(d) [μm]	l/d
1	0.30	5.68	53
2	0.60	5.51	109
3	1.18+	5.75	205
4	1.85	5.47	338
5	2.45	5.51	445
6	0.62*	2.54	243

+ Mean dimensions obtained from Table 2.2.

* This wire has been used to examine l/d effect.

In all cases, the total length between the pronges was 3 mm.

TABLE 6.1

MEAN QUANTITIES OF THE LOW-REYNOLDS-NUMBER TURBULENT BOUNDARY LAYER

U_∞ ms^{-1}	δ mm	δ^* mm	θ mm	H δ^*/θ	R_θ $U_\infty\theta/\nu$	$C_f^*10^3$	Δ	Δ'
4.27	46	7.35	5.46	1.346	1466	3.918	$-1.289*10^{-3}$	-0.112
8	46	7.35	5.46	1.346	2756	3.341	$-7.427*10^{-4}$	-0.112
12	46	7.35	5.46	1.346	4125	3.168	$-5.097*10^{-4}$	-0.112

$C_f = 2[u^*/U_\infty]^2$

$\Delta = [\nu/(\rho u^{*3})](dP_s/dx)$.

$\Delta' = (\delta^*/\tau_w)(dP_s/dx)$.

TABLE 6.2

FRICTION VELOCITY, u*

	Cross-Plot	Preston Tubes					Slope
U_∞ ms^{-1}	u* ms^{-1}	0.508 mm	1.067 mm	2.032 mm	3.175 mm	4.750 mm	u* ms^{-1}
4	0.189+	---	0.182	0.188	0.191	0.181	0.16++
8	0.328	0.303	0.318	0.325	0.327	0.325	0.279
12	0.478	0.416	0.454	0.461	0.458	0.460	---

+ U_∞ = 4.27 [ms^{-1}].

++ from Burhanuddin (1980).

TABLE C.1

FULLY DEVELOPED PIPE FLOW MEAN VELOCITY DATA

No.	$Re*10^{-5}$	U_b $[ms^{-1}]$	U_b/U_c
1	0.807	12.71	0.820
2	1.15	18.06	0.817
3	1.39	21.89	0.823
4	1.61	25.34	0.816
5	1.80	28.33	0.828
6	1.98	31.16	0.828
7	2.30	36.27	0.830

TABLE D.1

u* VALUES AND y^+ RANGES AT DIFFERENT STATIONS

St.	x_w cm	u* ms^{-1}	log	inner half-power	linear	outer half-power
1	1	0.820	50-310 (56)	---	---	---
2	3	0.795	30-140 (54)	---	---	330-1000$^+$
3	6	0.642	8$^-$-70 (44)	35-130	---	330-800$^+$
4	9	0.565	7$^-$-65 (39)	30-180	---	330-700$^+$
5	12	0.483	6$^-$-65 (33)	25-100	60-170	300-600$^+$
6	15	0.425	5$^-$-60 (29)	15-160	80-250	270-530$^+$
7	18	0.380	5$^-$-60 (26)	20-120	60-270	250-480$^+$
8	21	0.345	4$^-$-60 (24)	20-75	60-260	190-430$^+$
9	24	0.316	4$^-$-60 (22)	20-90	50-260	150-400$^+$
10	30	0.272	3$^-$-55 (19)	20-110	50-340$^+$	---
11	36	0.242	3$^-$-35 (17)	20-120	50-240	---
12	42	0.220	3$^-$-35 (15)	20-120	50-190	---
13	48	0.201	3$^-$-20 (14)	20-120	50-250$^+$	---
14	54	0.188	2$^-$-20 (13)	20-130	50-230$^+$	---
15	60	0.176	2$^-$-20 (12)	20-160	100-220$^+$	---
16	66	0.170	2$^-$-20 (12)	20-150	130-210$^+$	---
17	71	0.164	2$^-$-20 (11)	20-130	120-210$^+$	---

NOTES:
1) The listed u* values correspond to the mean value line in figure 7.2 which was obtained by averaging the four Preston tube readings.
2) All data for y^+ bounds are approximate.
3) Superscript (+) indicates end of data; range may be continue.
4) Numbers in brackets in the log column are the local values of $(u^* d_p/\nu)$ for the smallest Preston tube (d_p = 1.067 mm).

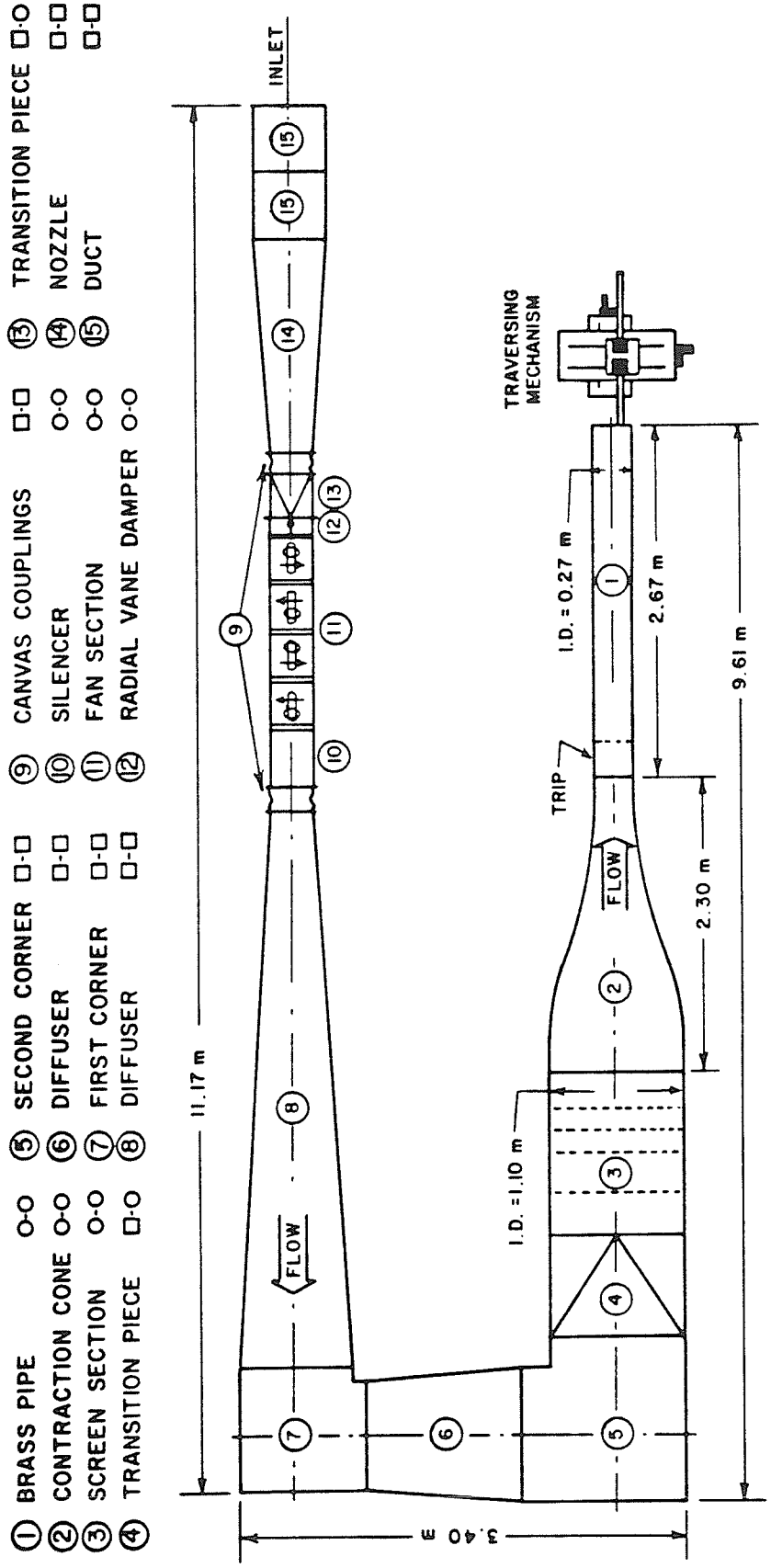

Figure 2.1 Plan view of wind tunnel for turbulent boundary layer on a pipe wall.

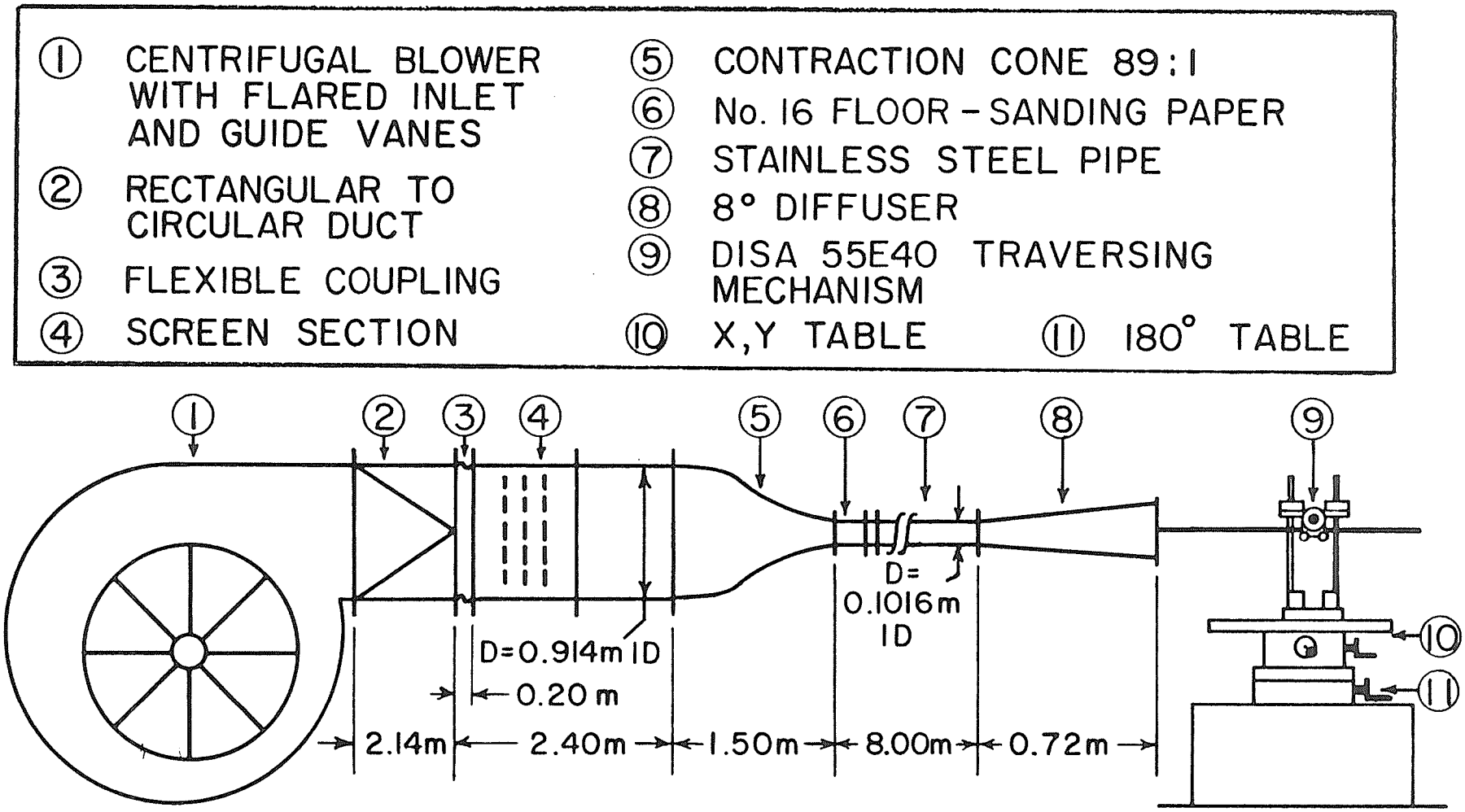

Figure 2.2 Tunnel for the studies of fully developed pipe flow and diffuser flow.

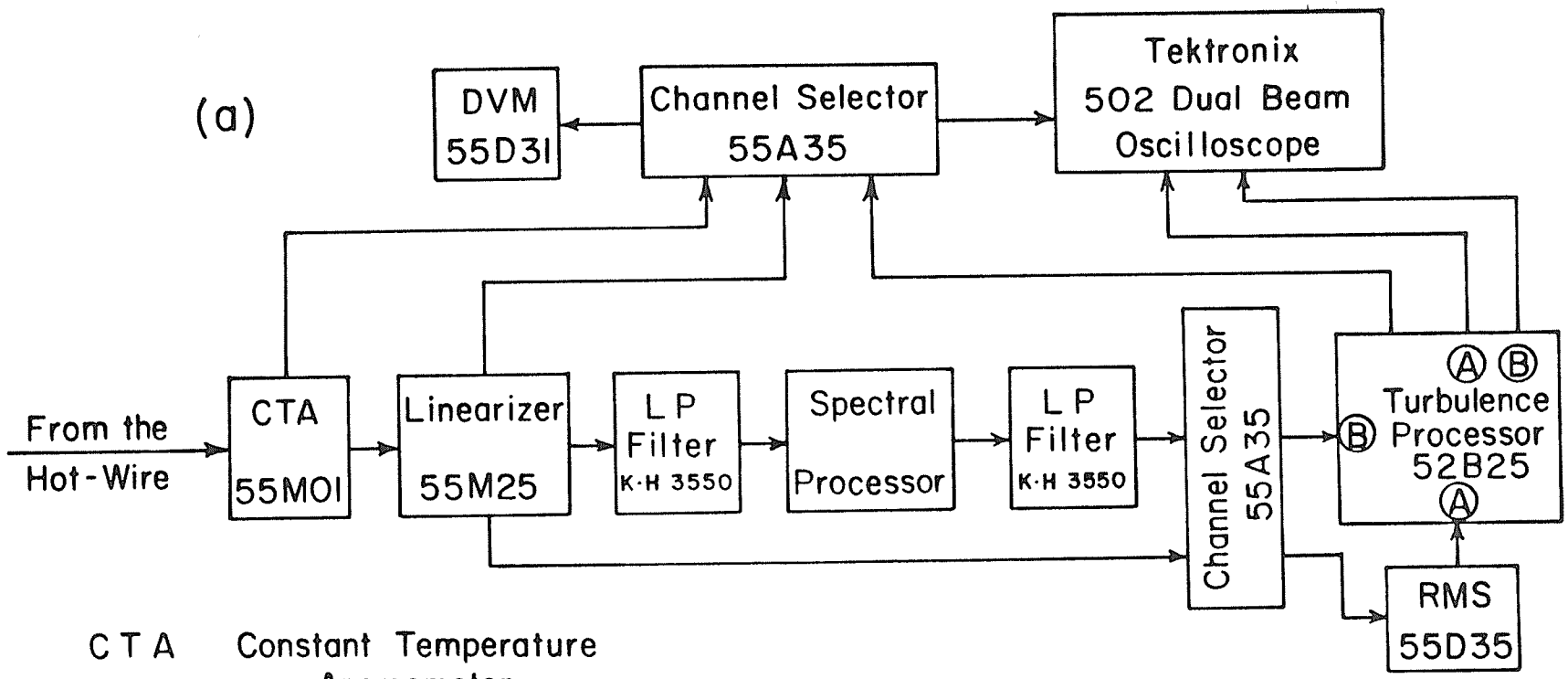

C T A Constant Temperature Anemometer

L P Low Pass

R M S Root Mean Square

D V M Digital Voltmeter

K·H Krohn · Hite

Figure 2.3 Block diagram for a single wire measurements (a) Set-up(a).

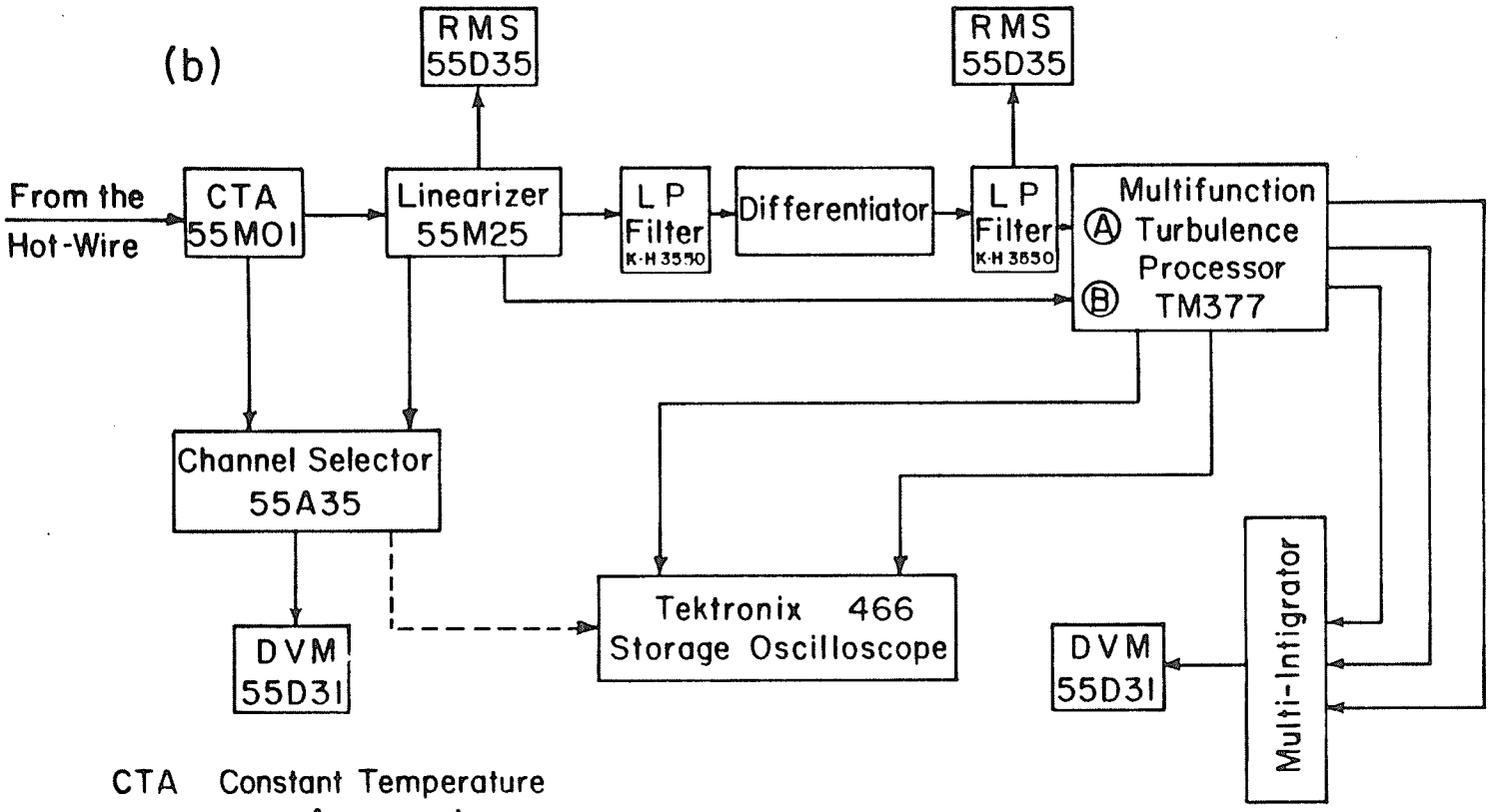

CTA Constant Temperature Anemometer

L P Low Pass

RMS Root Mean Square

DVM Digital Voltmeter

K·H Krohn·Hite

Figure 2.3 Block diagram for a single wire measurements (b) Set-up(b).

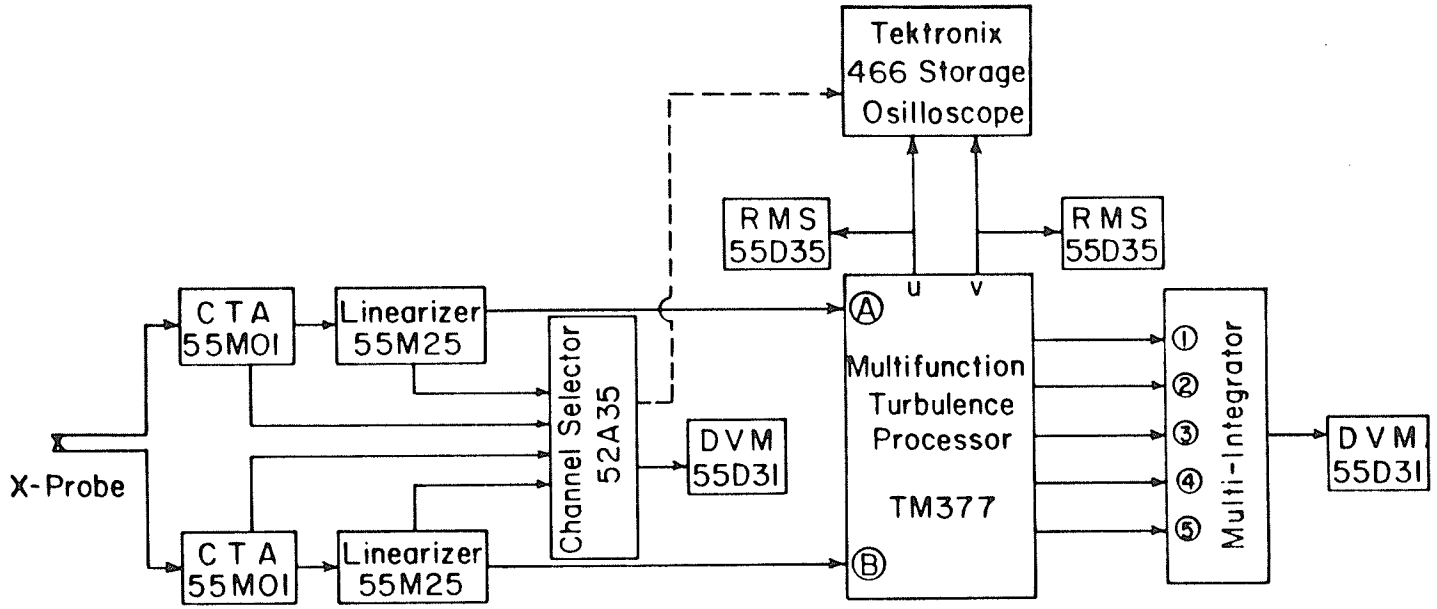

CTA Constant Temperature Anemometer

RMS Root Mean Square

DVM Digital Voltmeter

① $\frac{\overline{u^2}}{10}$, $\frac{\overline{u^3}}{100}$, $\frac{\overline{u^4}}{1000}$, $\frac{\overline{uv}}{10}$

② $\frac{\overline{v^2}}{10}$ $\frac{\overline{v^3}}{100}$ $\frac{\overline{v^4}}{1000}$ $\frac{\overline{uv^2}}{100}$

③ $\frac{\overline{uv^3}}{1000}$, $\frac{\overline{u^3v}}{1000}$, $\frac{\overline{u^2v^2}}{1000}$, $\frac{\overline{u^2v}}{100}$

④ U

⑤ V

Figure 2.4 Block diagram for X-wire measurements.

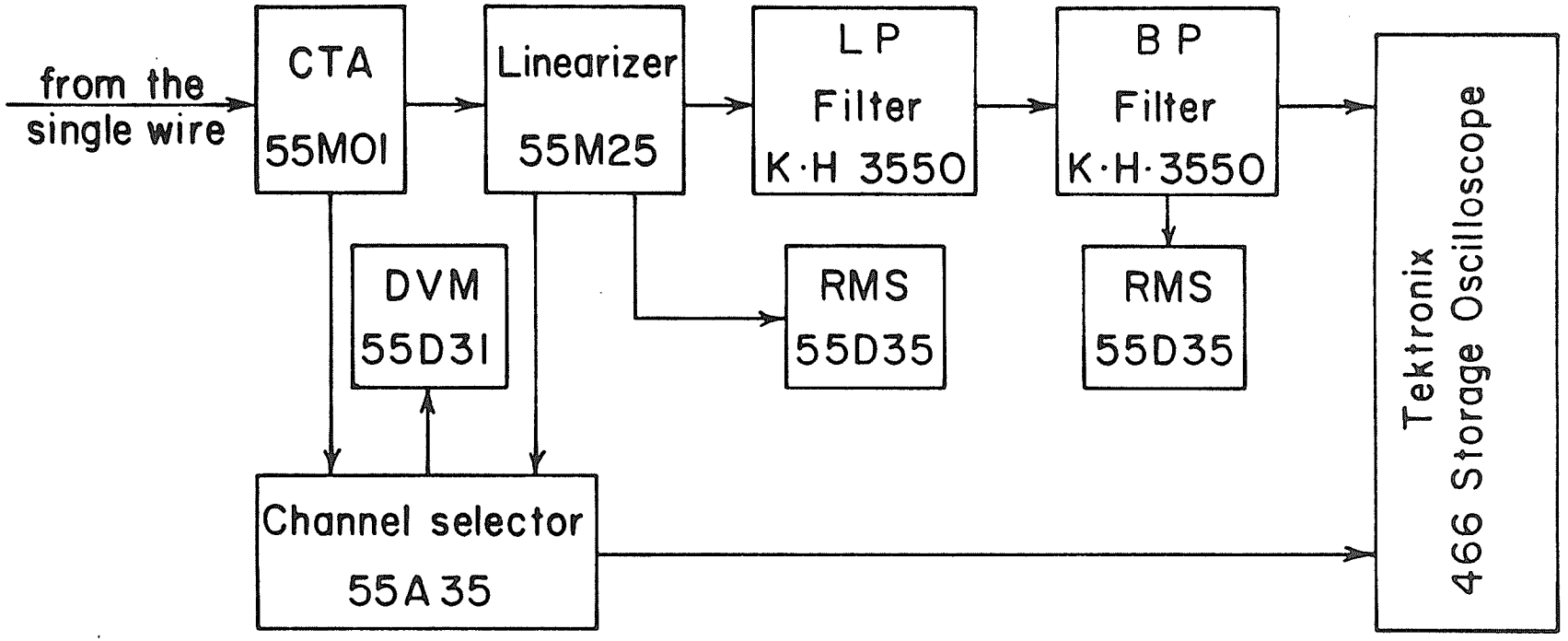

Figure 2.5 Block diagram for spectra measurements.

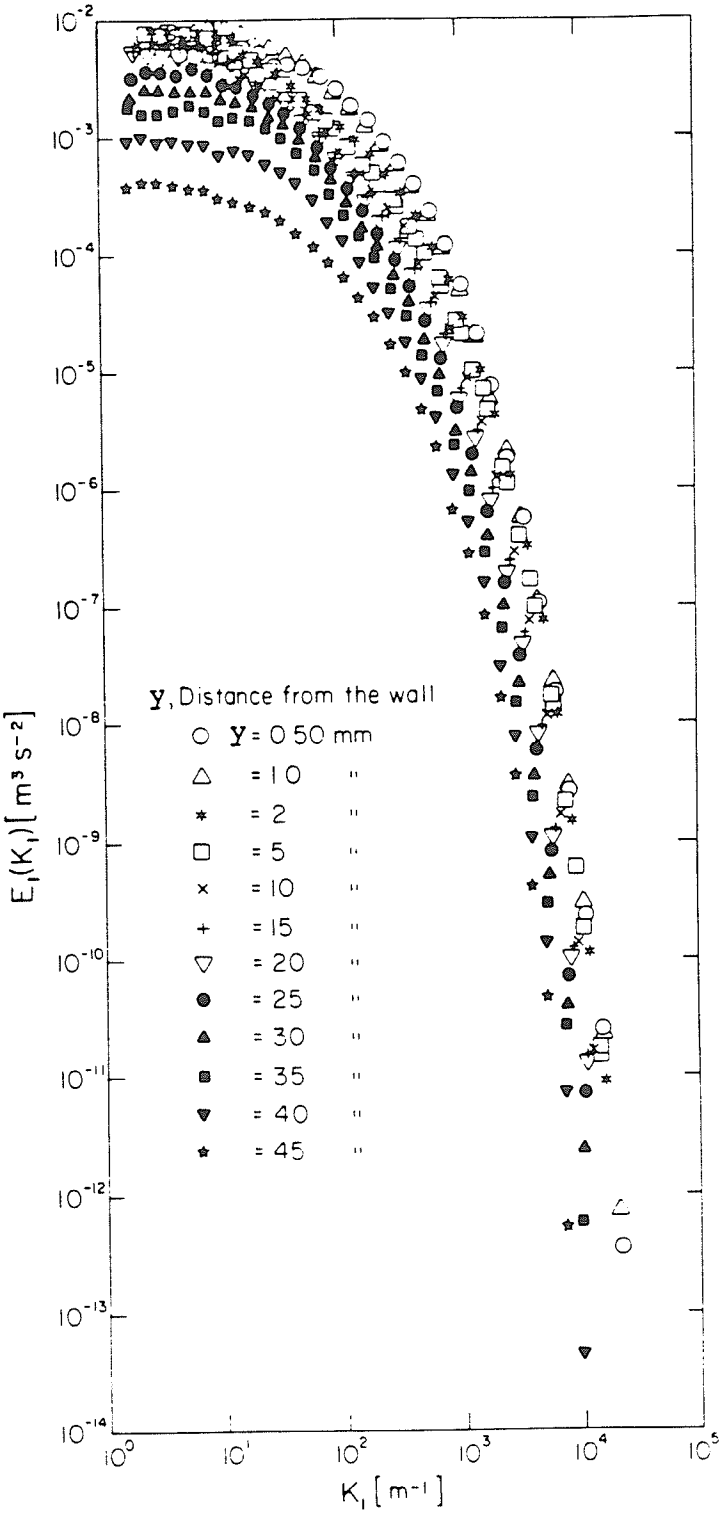

Figure 3.1 $\overline{u^2}$-spectra in the boundary layer, $\bar{R}_\theta$ = 2756.

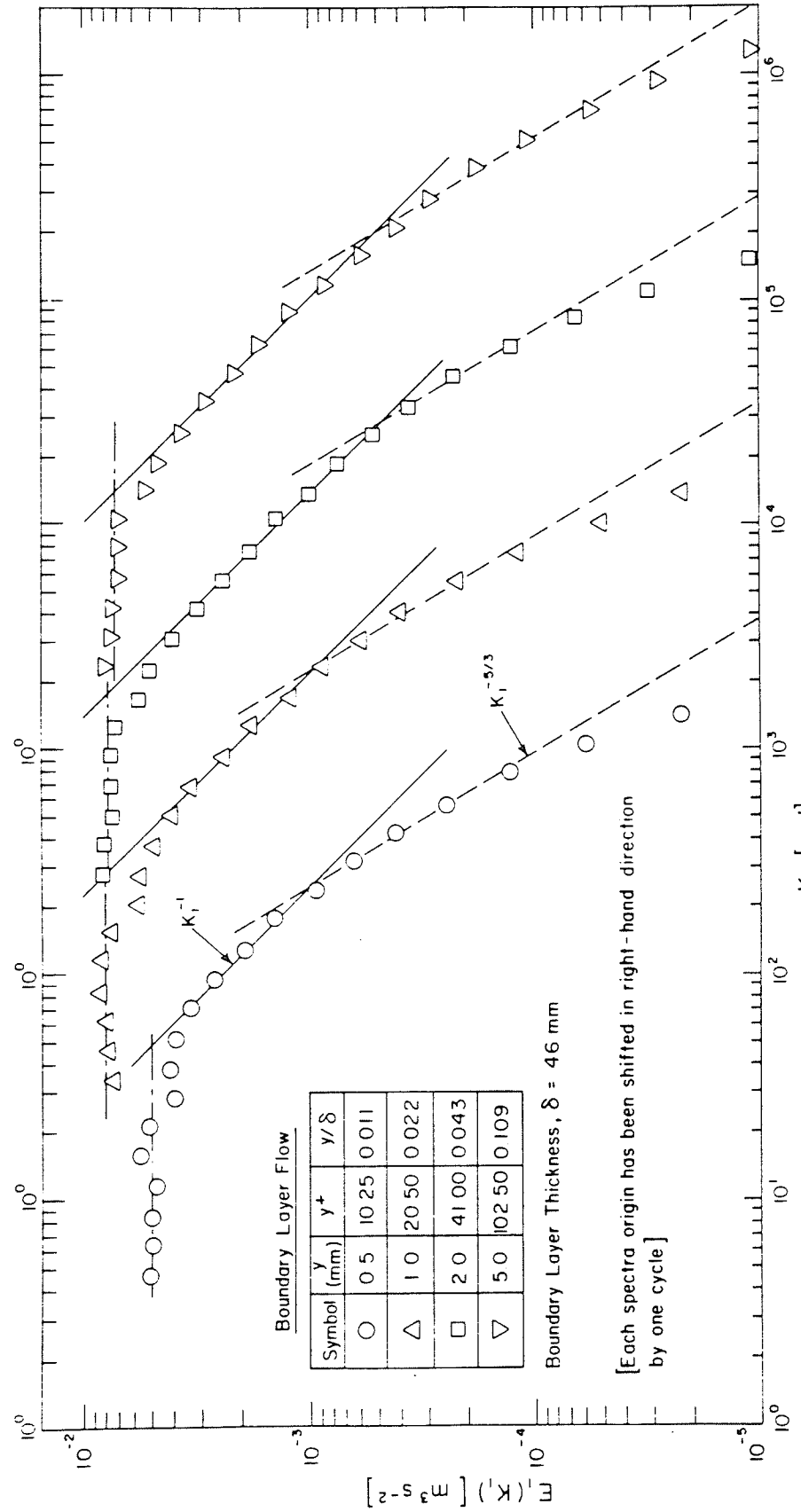

Figure 3.2 $\overline{u^2}$-spectra in a turbulent boundary layer.
y/δ = 0.011, 0.022, 0.043 & 0.109.

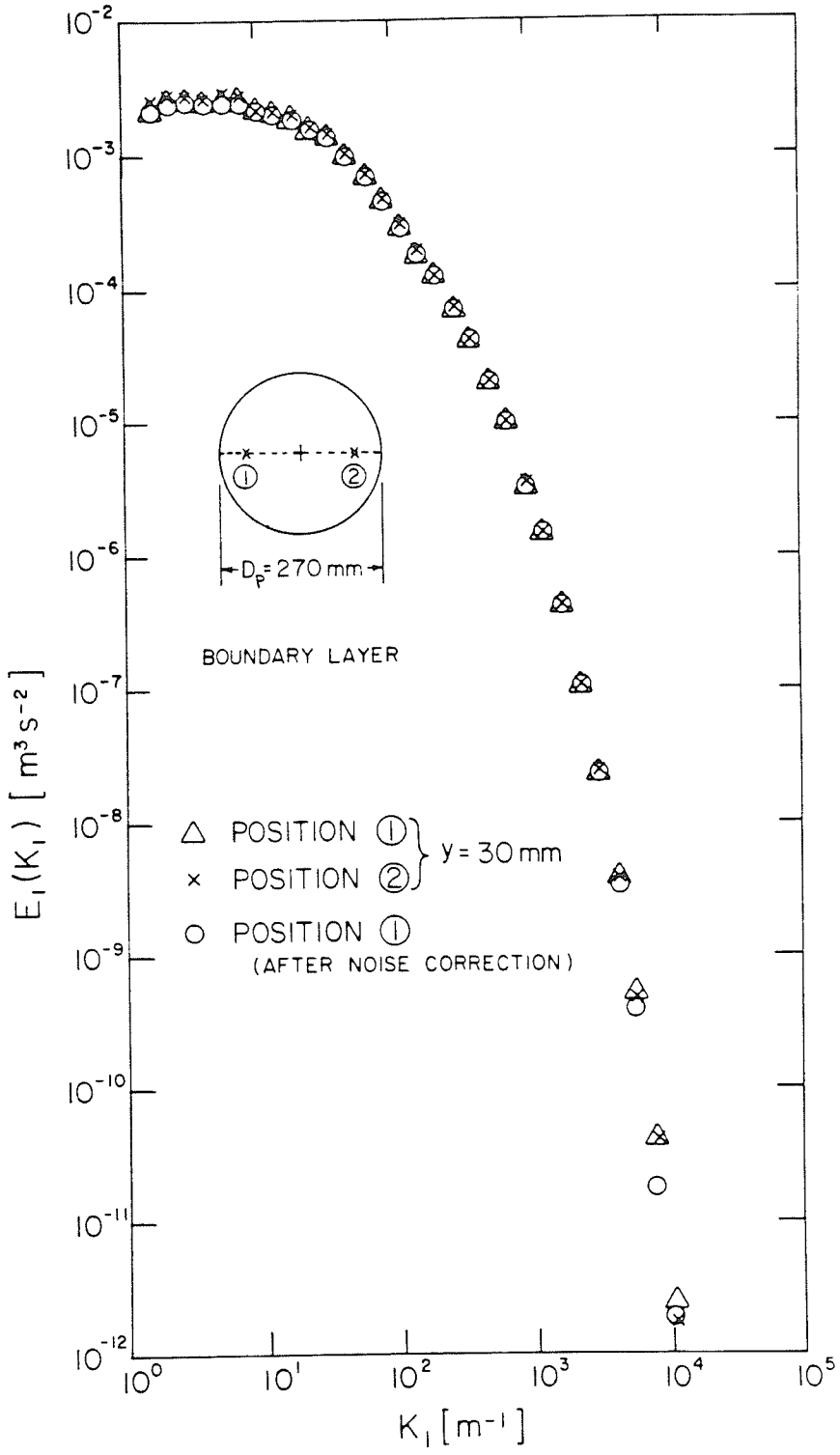

Figure 3.3 Symmetrical $\overline{u^2}$-spectra to test the symmetry of the flow and the noise correction.

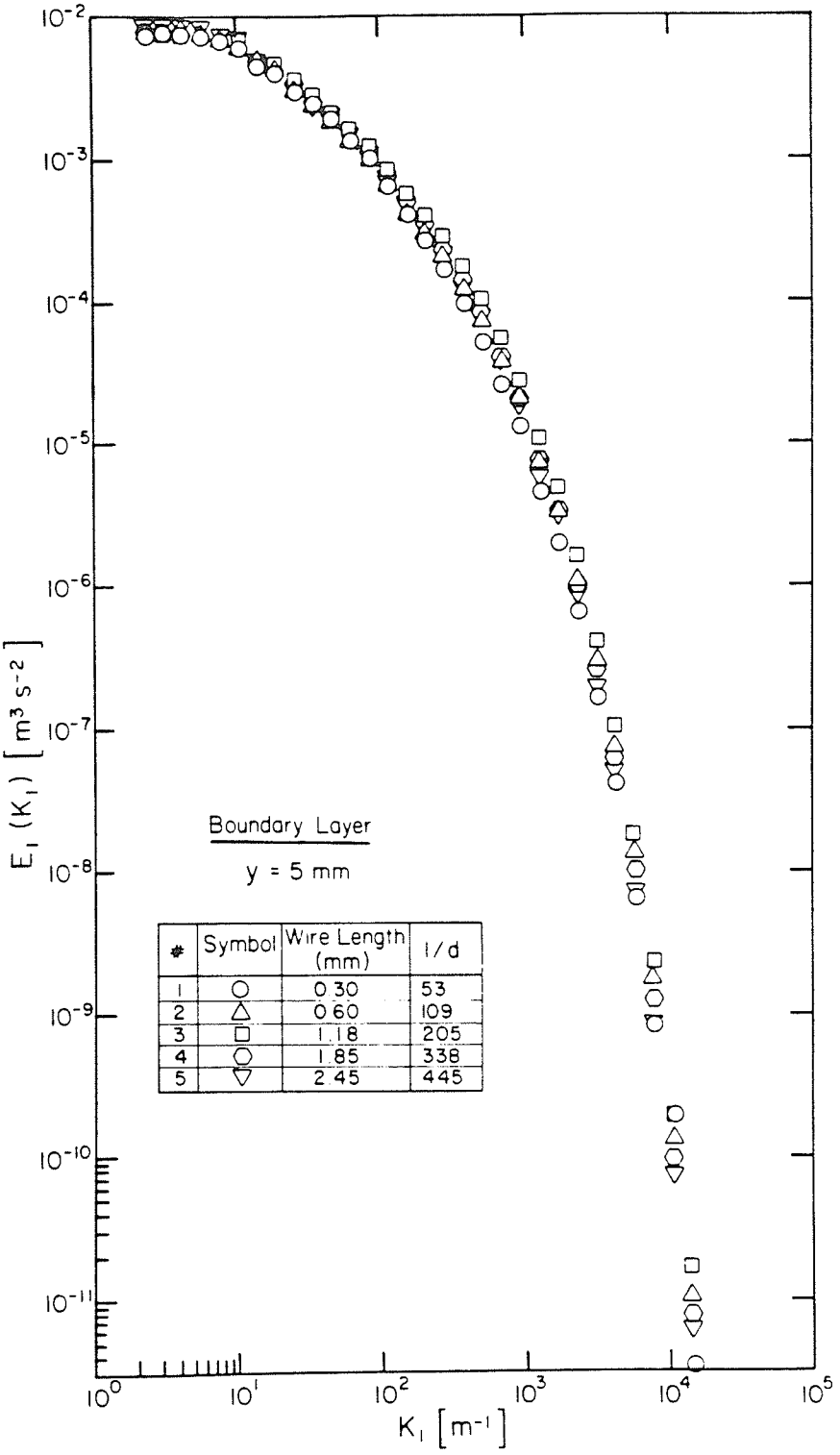

Figure 3.4 $\overline{u^2}$-spectra for different l/d ratios in the boundary layer, R_θ = 2756.

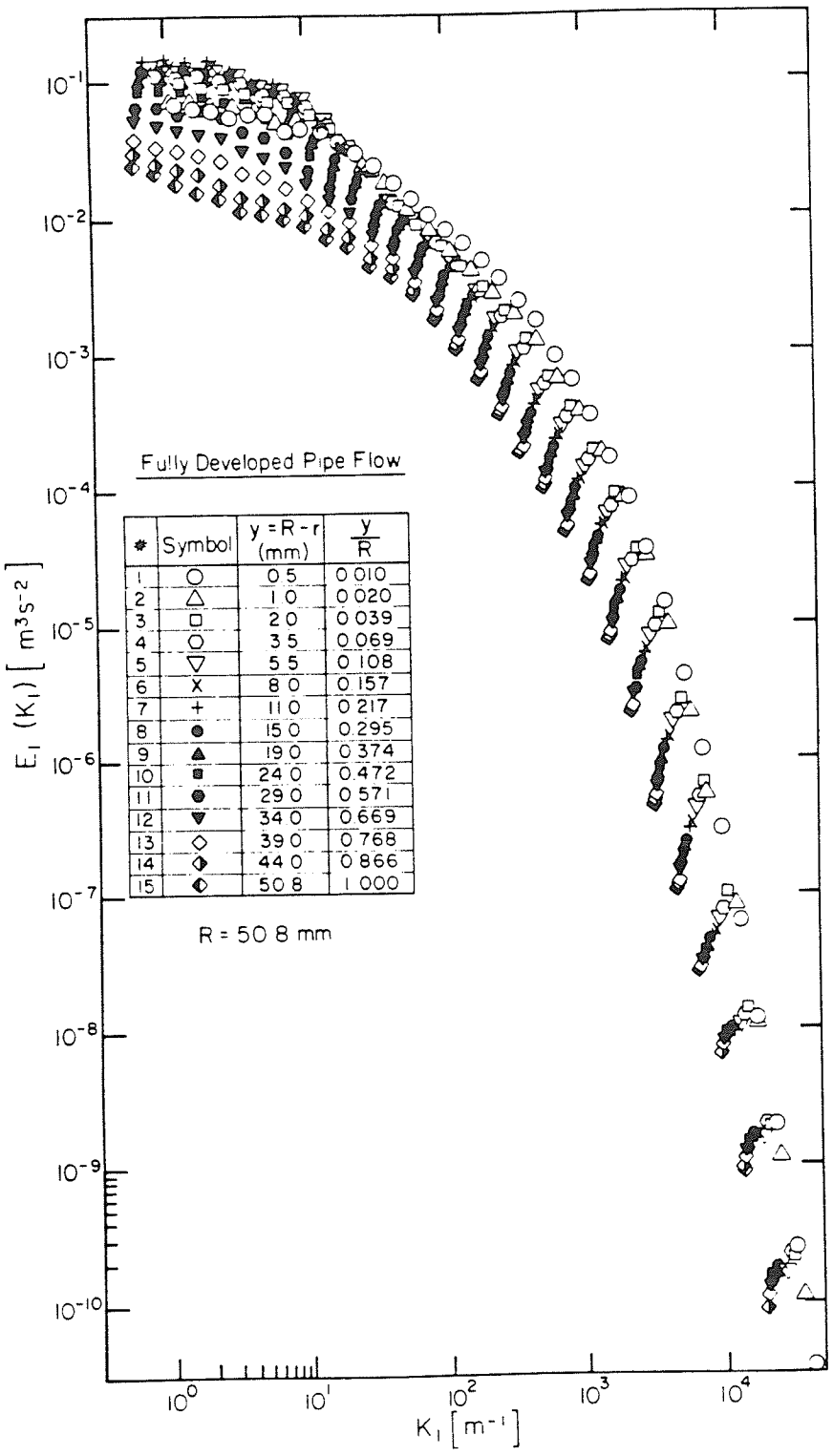

#	Symbol	y = R - r (mm)	y/R
1	○	0 5	0 010
2	△	1 0	0 020
3	□	2 0	0 039
4	○	3 5	0 069
5	▽	5 5	0 108
6	X	8 0	0 157
7	+	11 0	0 217
8	●	15 0	0 295
9	▲	19 0	0 374
10	■	24 0	0 472
11	⬢	29 0	0 571
12	▼	34 0	0 669
13	◇	39 0	0 768
14	◑	44 0	0 866
15	◐	50 8	1 000

Figure 3.5 $\overline{u^2}$-spectra in fully developed pipe flow, Re = $1.15*10^5$.

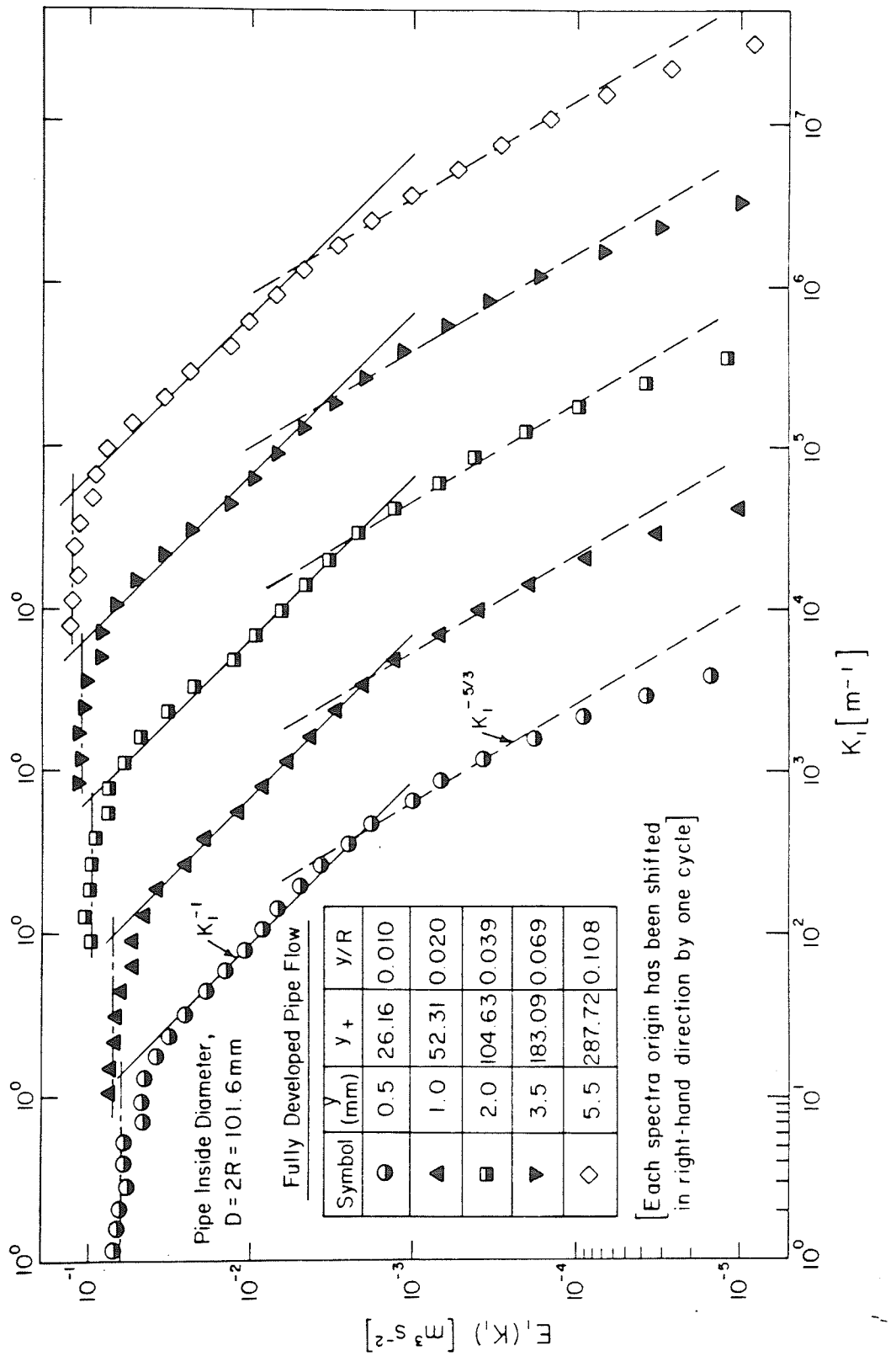

Figure 3.6 $\overline{u^2}$-spectra in fully developed pipe flow.
y/R = 0.010, 0.020, 0.039, 0.069 & 0.108.

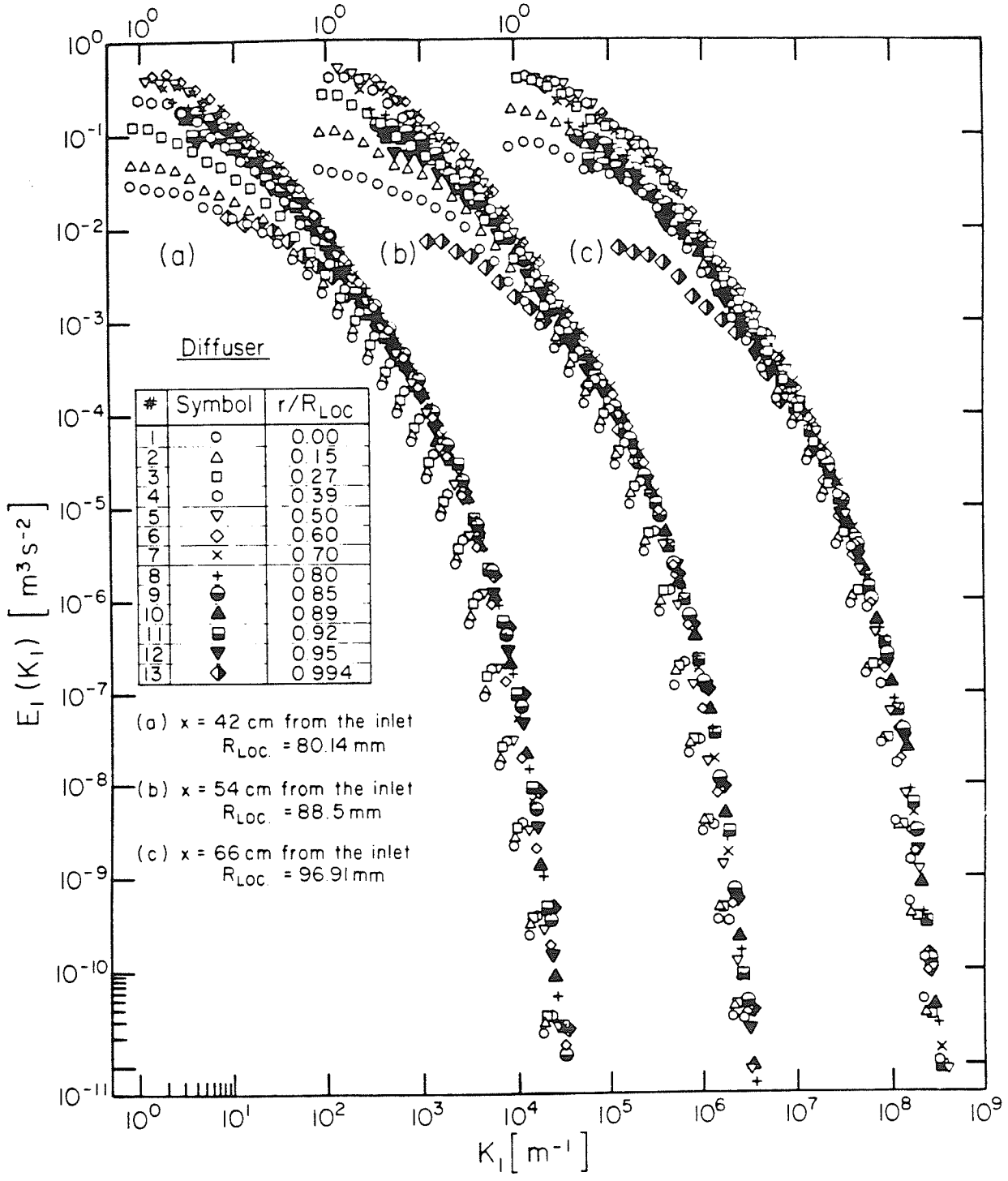

Figure 3.7 $\overline{u^2}$-spectra in diffuser flow at three different locations.

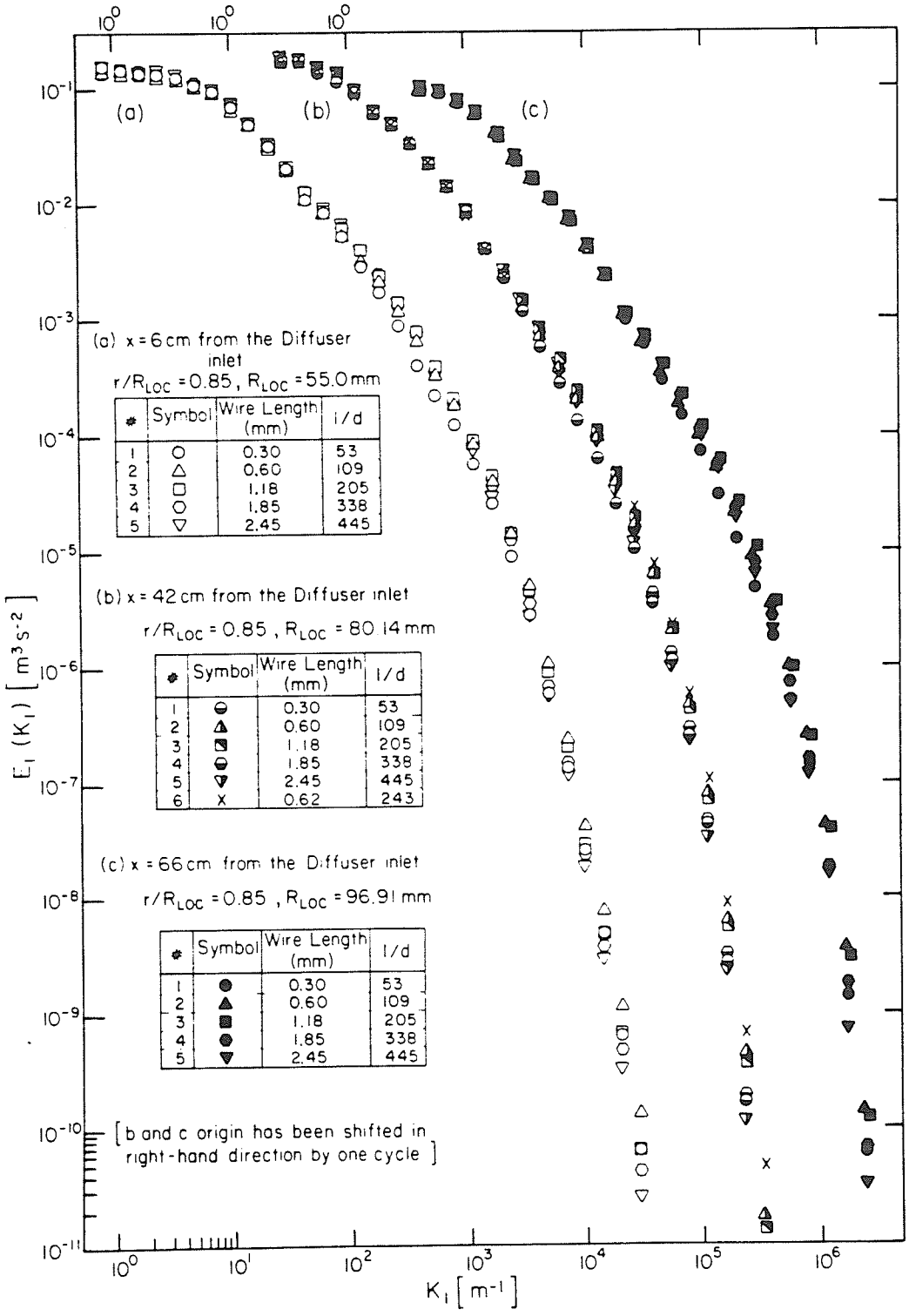

#	Symbol	Wire Length (mm)	l/d
1	○	0.30	53
2	△	0.60	109
3	□	1.18	205
4	○	1.85	338
5	▽	2.45	445

#	Symbol	Wire Length (mm)	l/d
1	◒	0.30	53
2	◭	0.60	109
3	◪	1.18	205
4	◒	1.85	338
5	▽	2.45	445
6	x	0.62	243

#	Symbol	Wire Length (mm)	l/d
1	●	0.30	53
2	▲	0.60	109
3	■	1.18	205
4	●	1.85	338
5	▼	2.45	445

Figure 3.8 $\overline{u^2}$-spectra at three different locations for different l/d ratios.

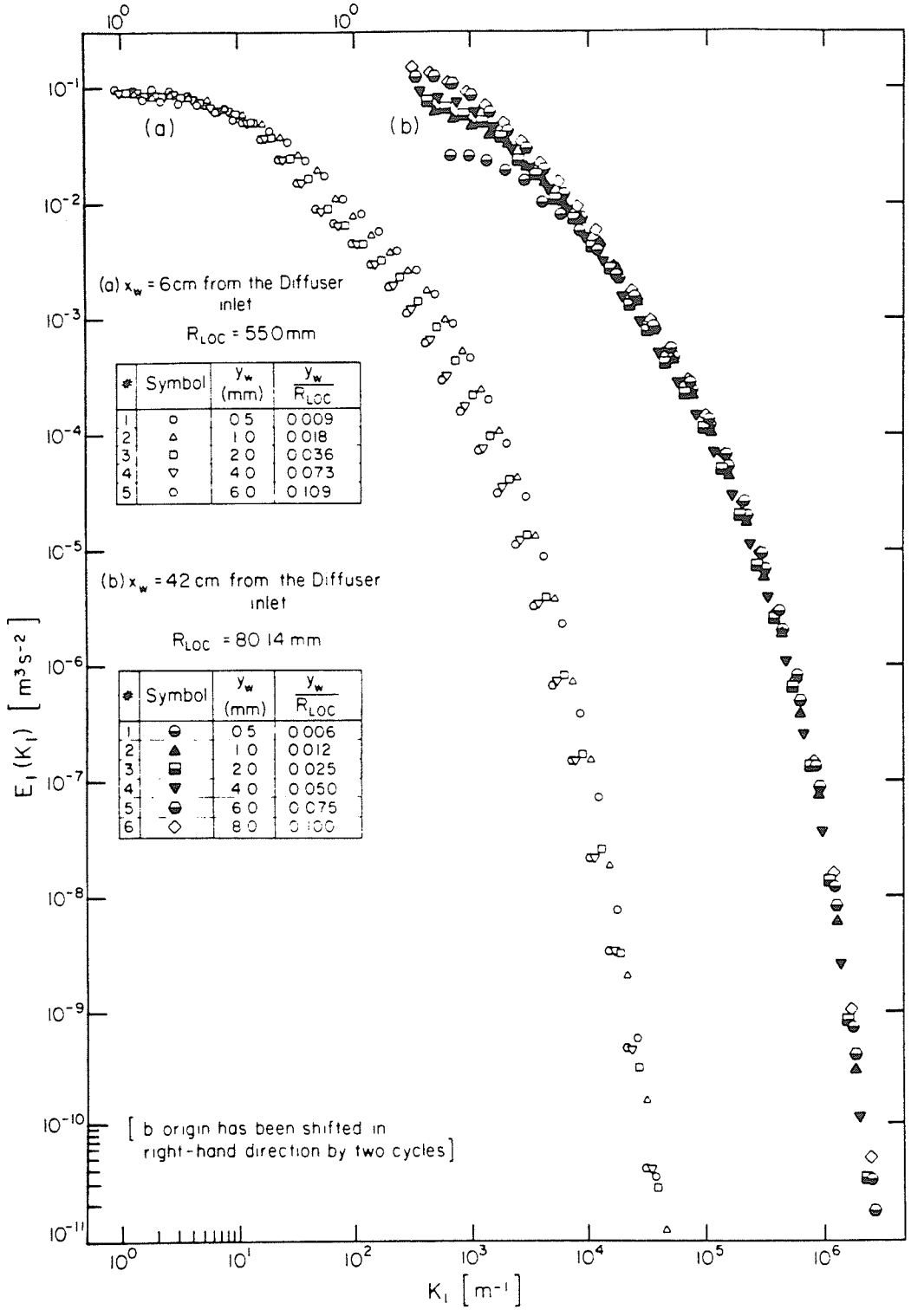

#	Symbol	y_w (mm)	$\frac{y_w}{R_{LOC}}$
1	○	0 5	0 009
2	△	1 0	0 018
3	□	2 0	0 036
4	▽	4 0	0 073
5	○	6 0	0 109

#	Symbol	y_w (mm)	$\frac{y_w}{R_{LOC}}$
1	◒	0 5	0 006
2	▲	1 0	0 012
3	■	2 0	0 025
4	▼	4 0	0 050
5	◒	6 0	0 075
6	◇	8 0	0 100

Figure 3.9 $\overline{u^2}$-spectra measured on line perpendicular to the wall of the diffuser for two different locations

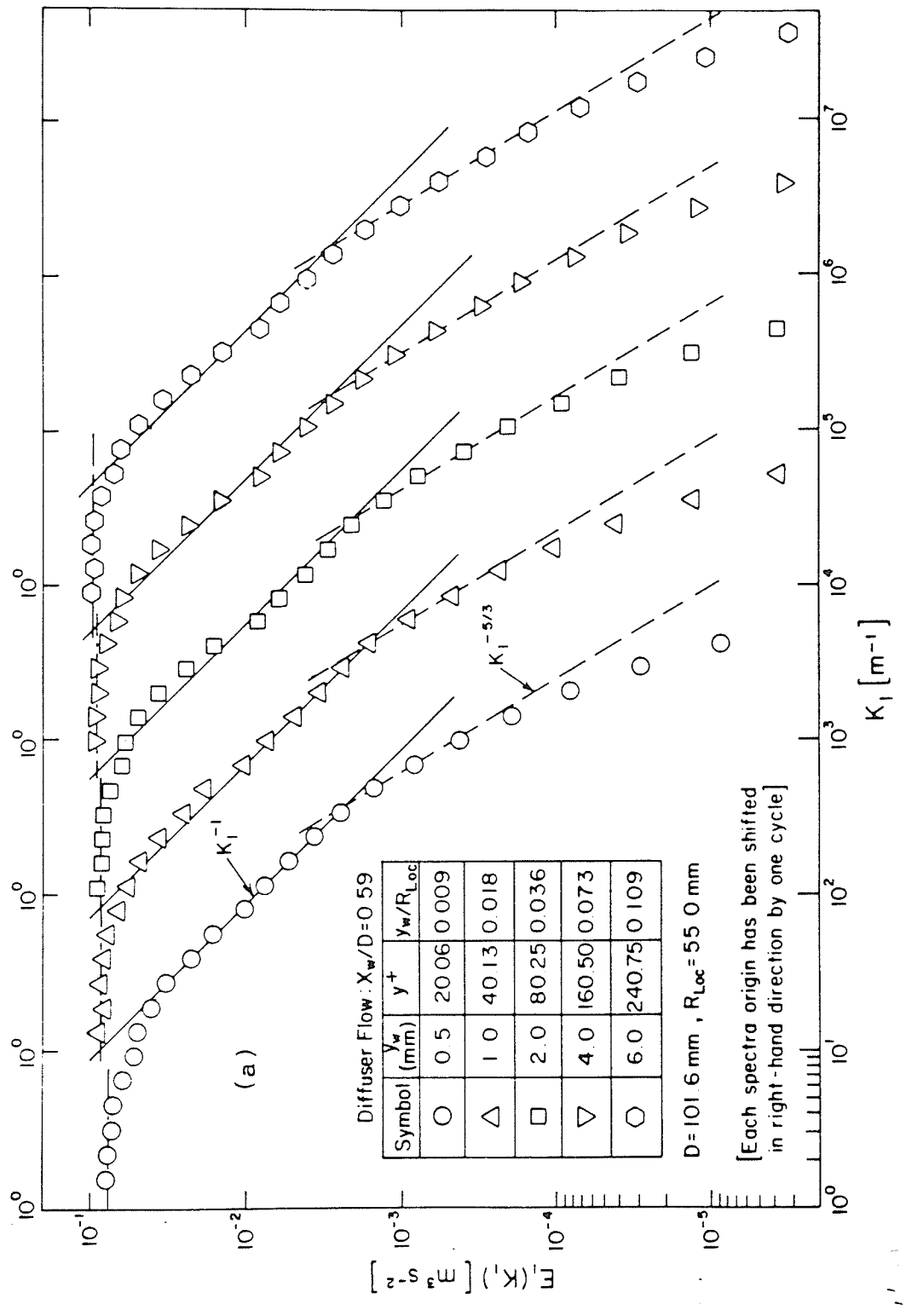

Figure 3.10 $\overline{u^2}$-spectra to emphasize the initial spectral laws in diffuser flow.
(a) $x_w/D = 0.59$.

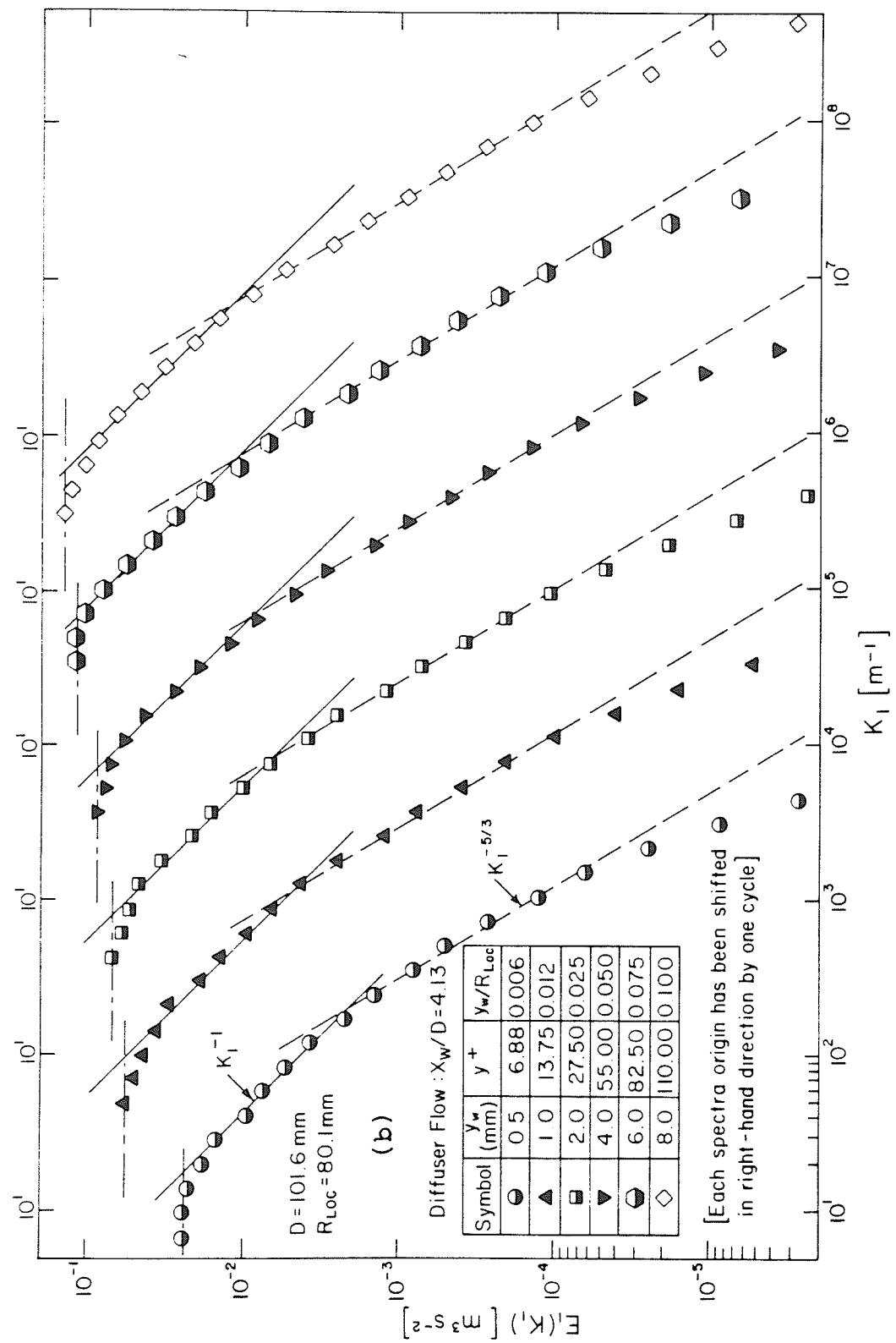

Symbol	y_w (mm)	y^+	y_w/R_{Loc}
◑	0.5	6.88	0.006
◭	1.0	13.75	0.012
◨	2.0	27.50	0.025
▼	4.0	55.00	0.050
◐	6.0	82.50	0.075
◇	8.0	110.00	0.100

Figure 3.10 $\overline{u^2}$-spectra to emphasize the initial spectral laws in diffuser flow.
(b) x_w/D = 4.13.

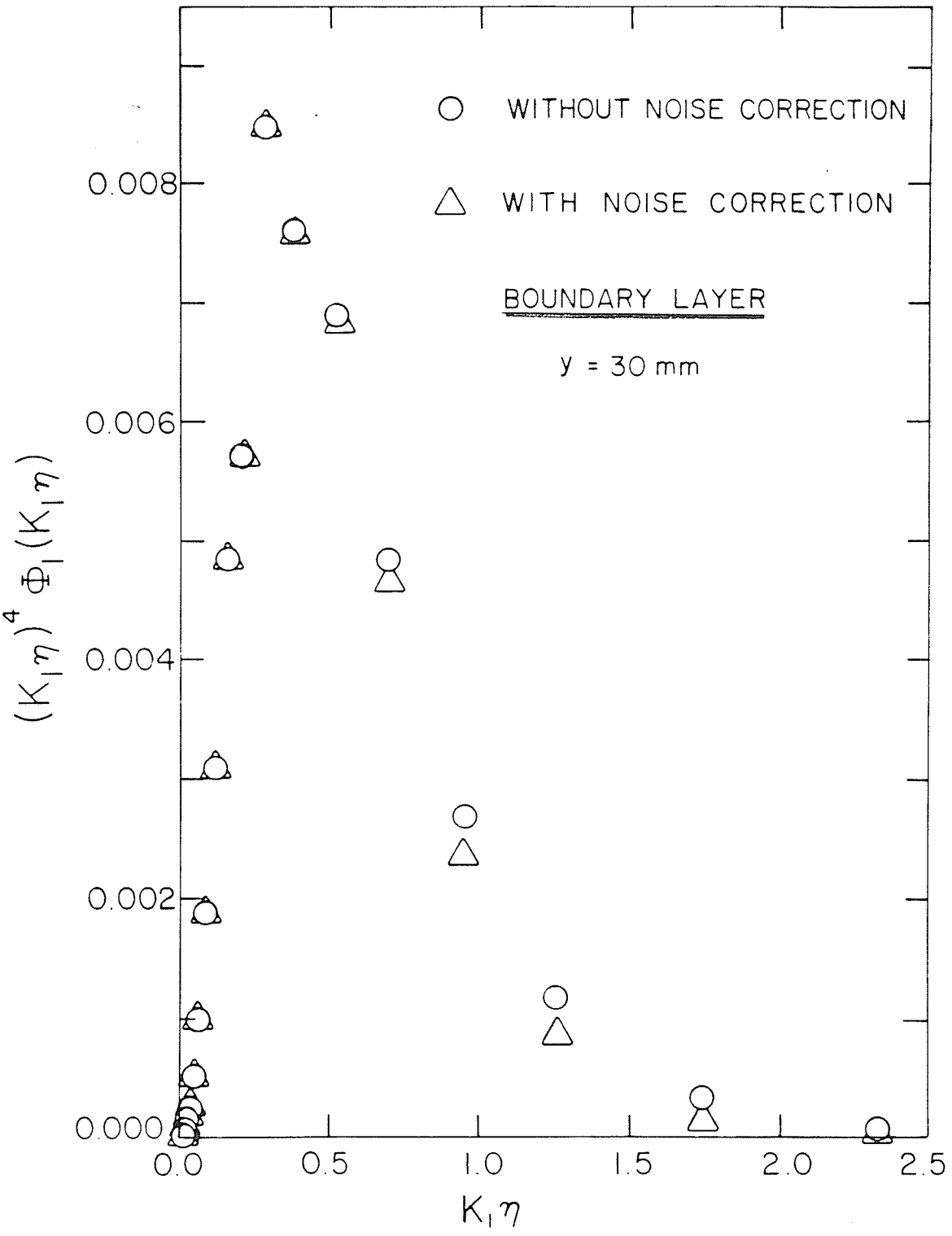

Figure 3.11 Fourth-order non-dimensional spectra to show the accuracy of spectra measurements at high wavenumber.

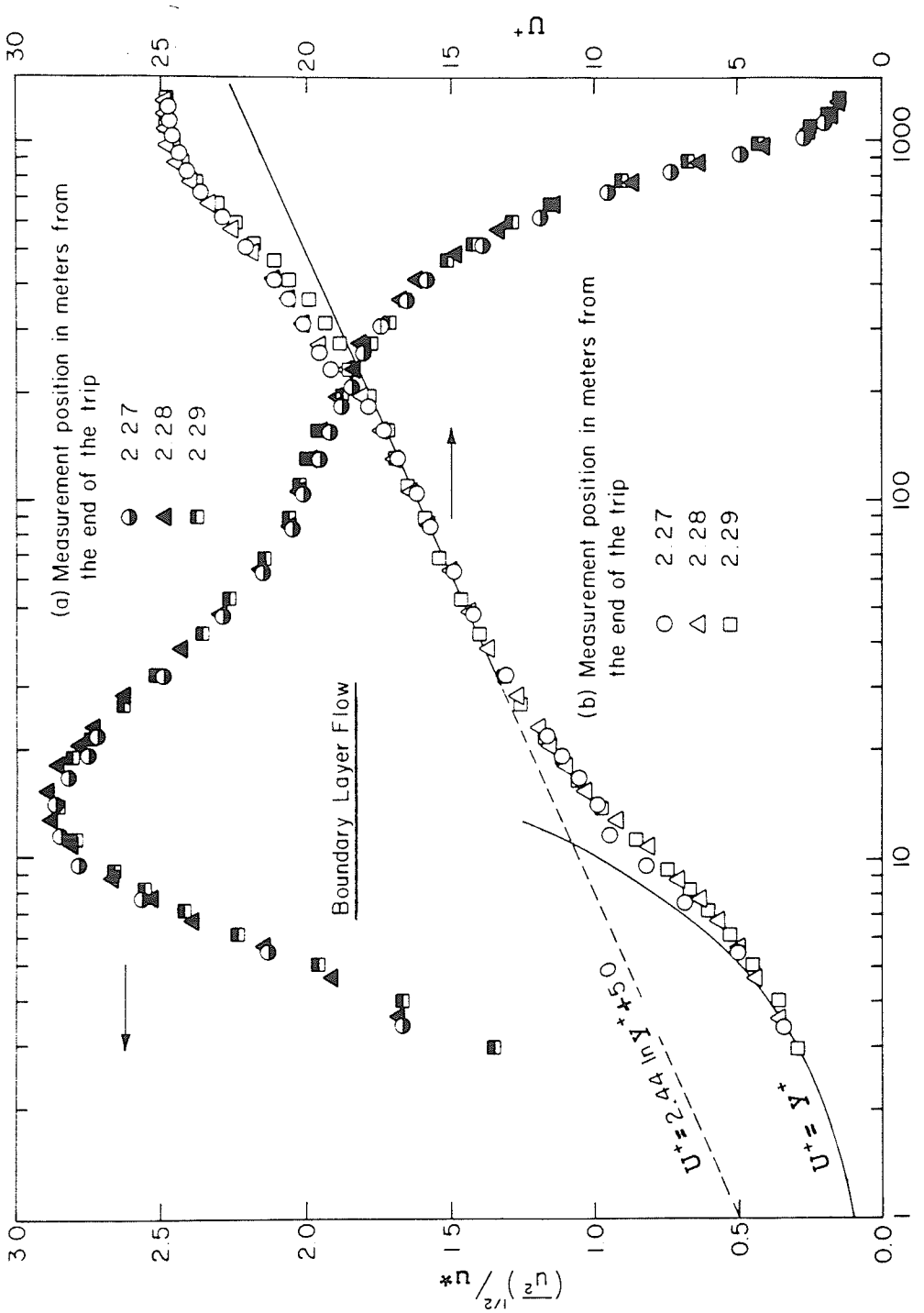

Figure 4.1 The non-dimensional mean velocity profile and fluctuating velocity distribution in the boundary layer flow.

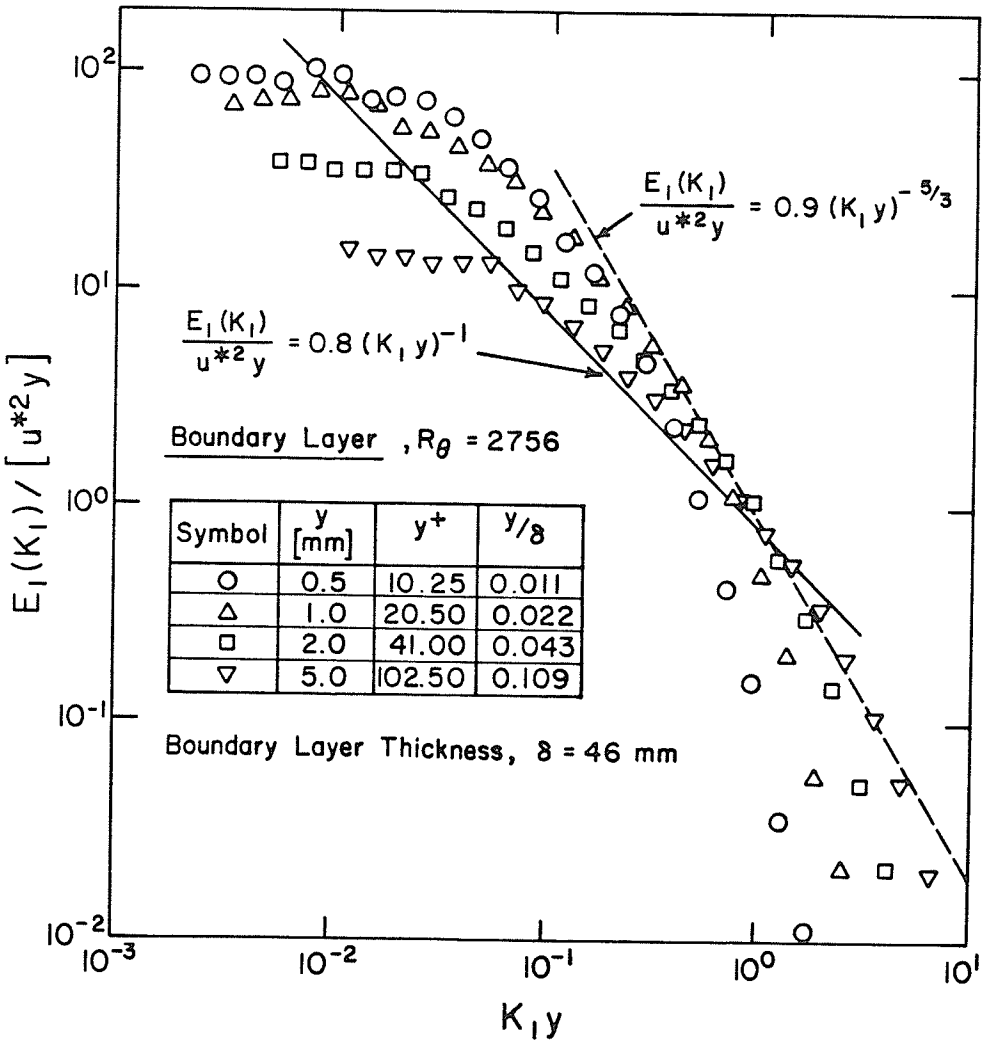

Figure 4.2 Normalized values of longitudinal spectrum $E_1(k_1)$ in the boundary layer.

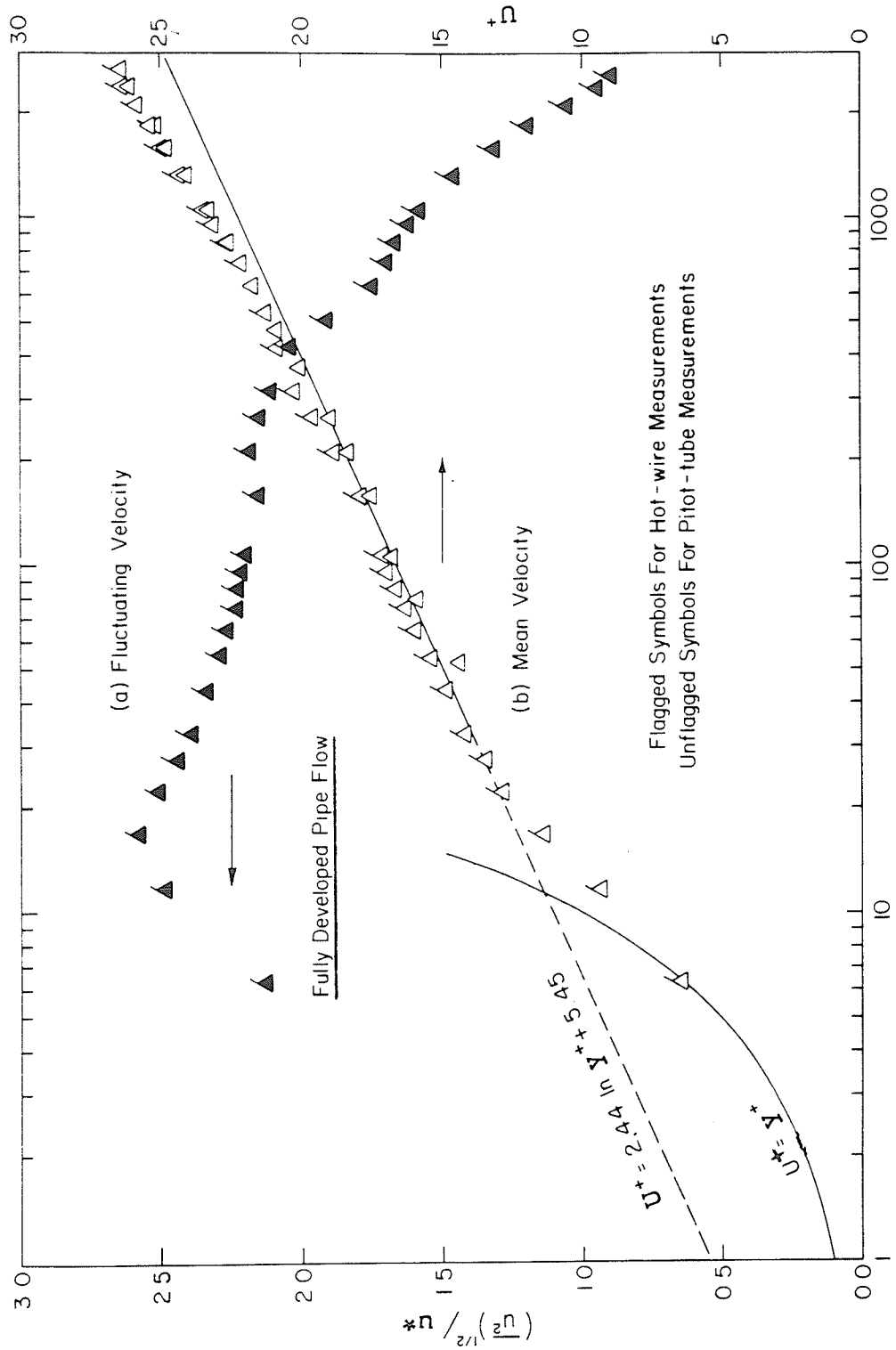

Figure 4.3 The non-dimensional mean velocity profile and fluctuating velocity distribution in the fully developed pipe flow.

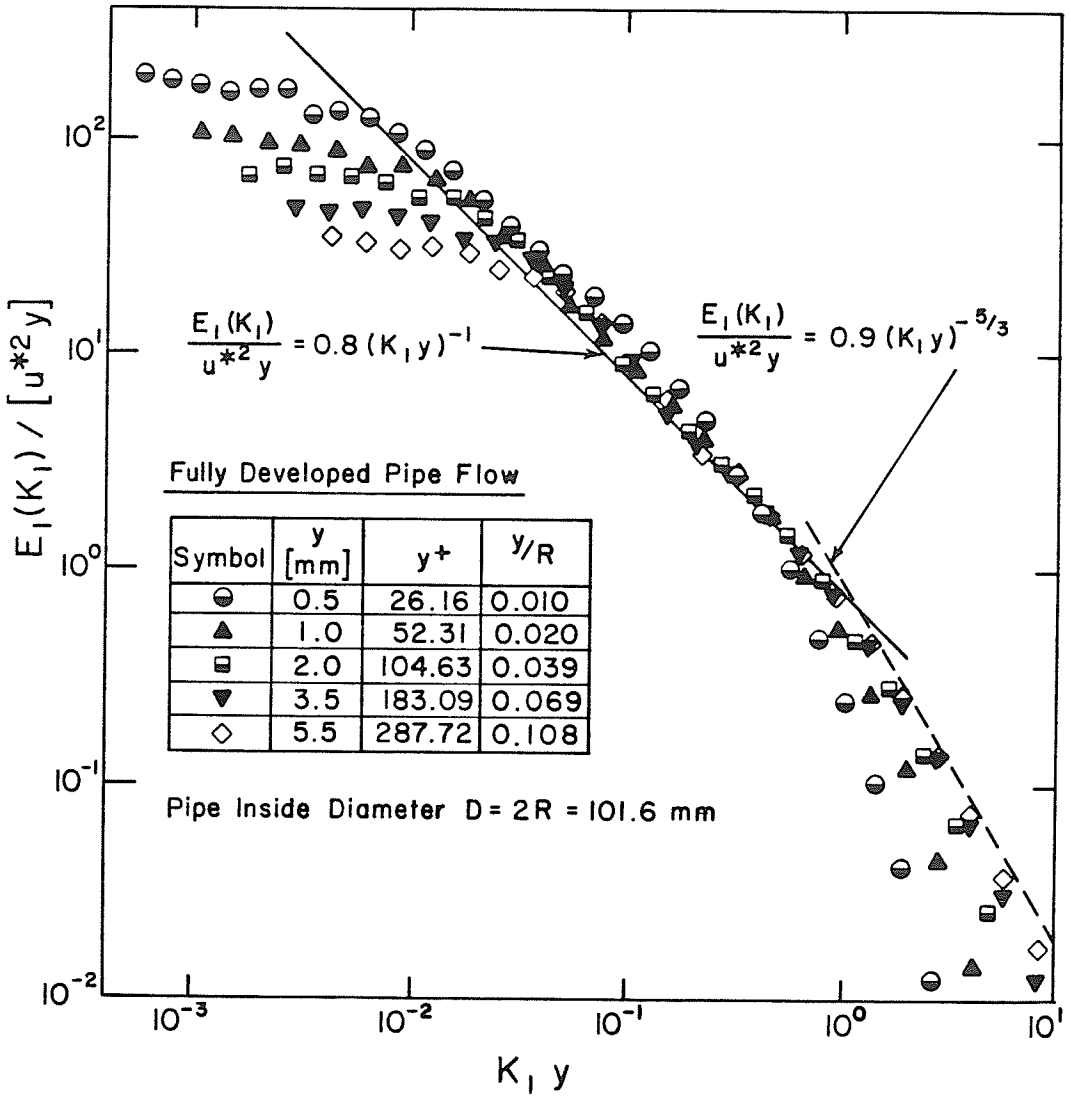

Symbol	y [mm]	y+	y/R
◒	0.5	26.16	0.010
▲	1.0	52.31	0.020
▣	2.0	104.63	0.039
▼	3.5	183.09	0.069
◇	5.5	287.72	0.108

Figure 4.4 Normalized values of longitudinal spectrum $E_1(k_1)$ in the fully developed pipe flow.

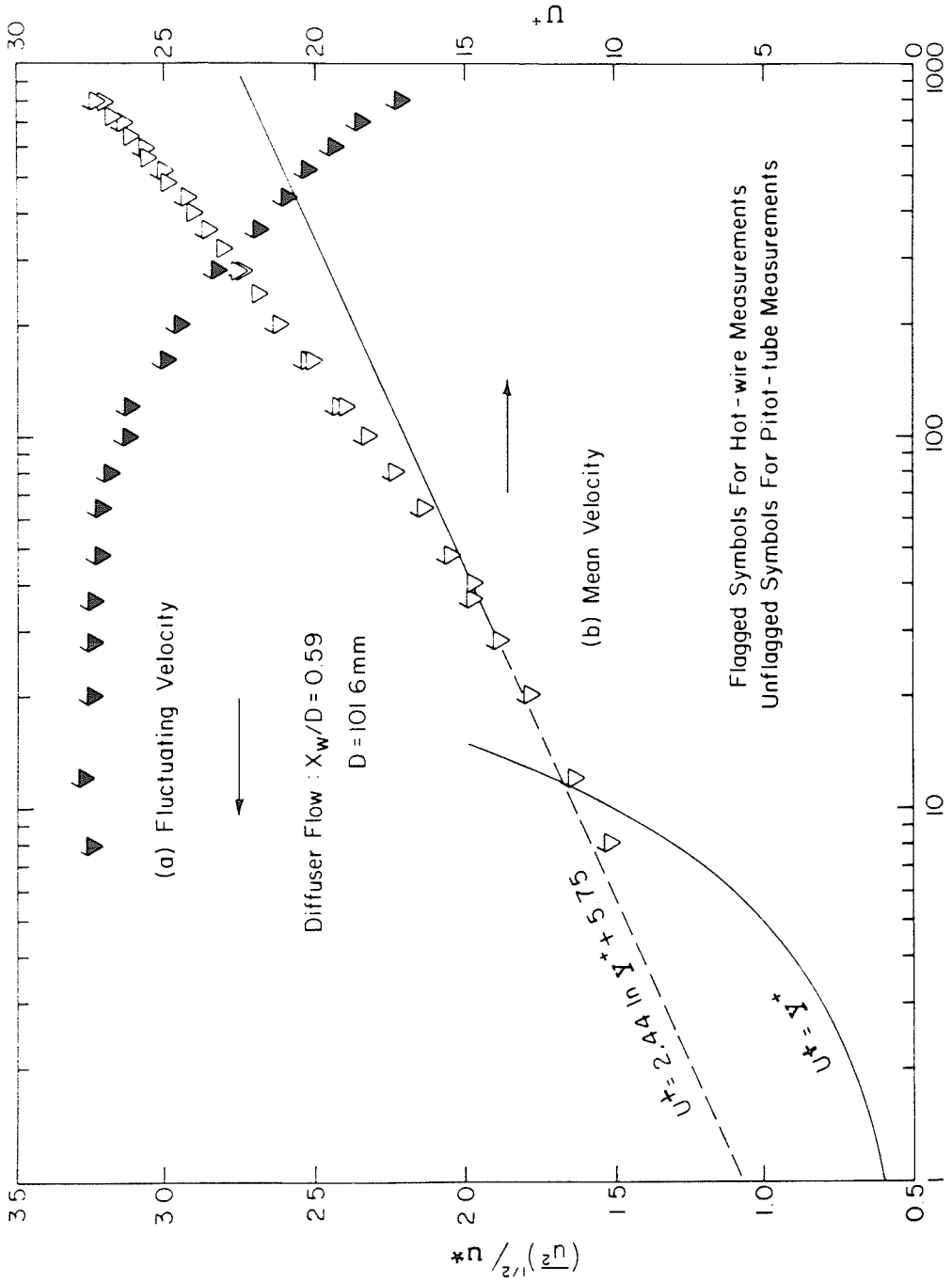

Figure 4.5 The non-dimensional mean velocity profile and fluctuating velocity distribution in the diffuser at $x_w/D = 0.59$

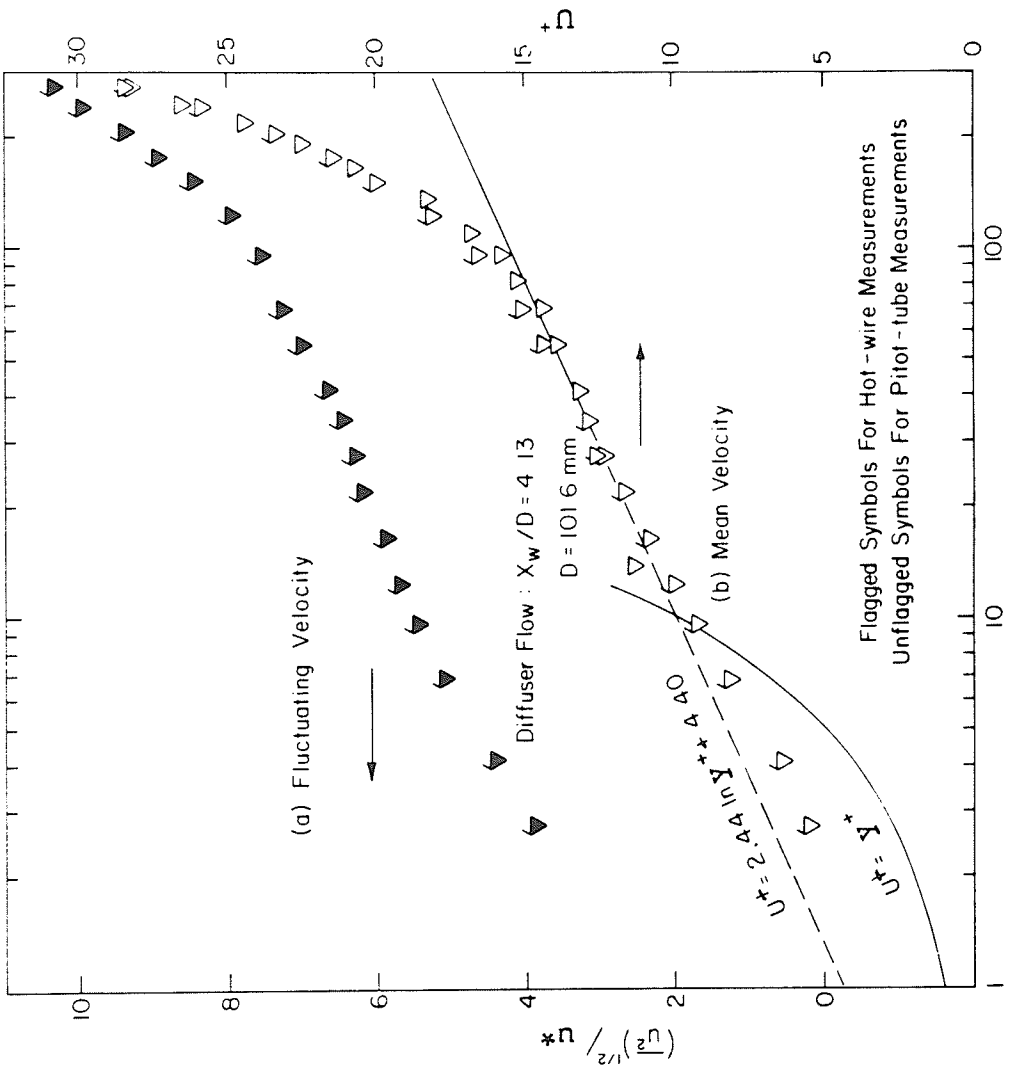

Figure 4.6 The non-dimensional mean velocity profile and fluctuating velocity distribution in the diffuser at $x_w/D = 4.13$

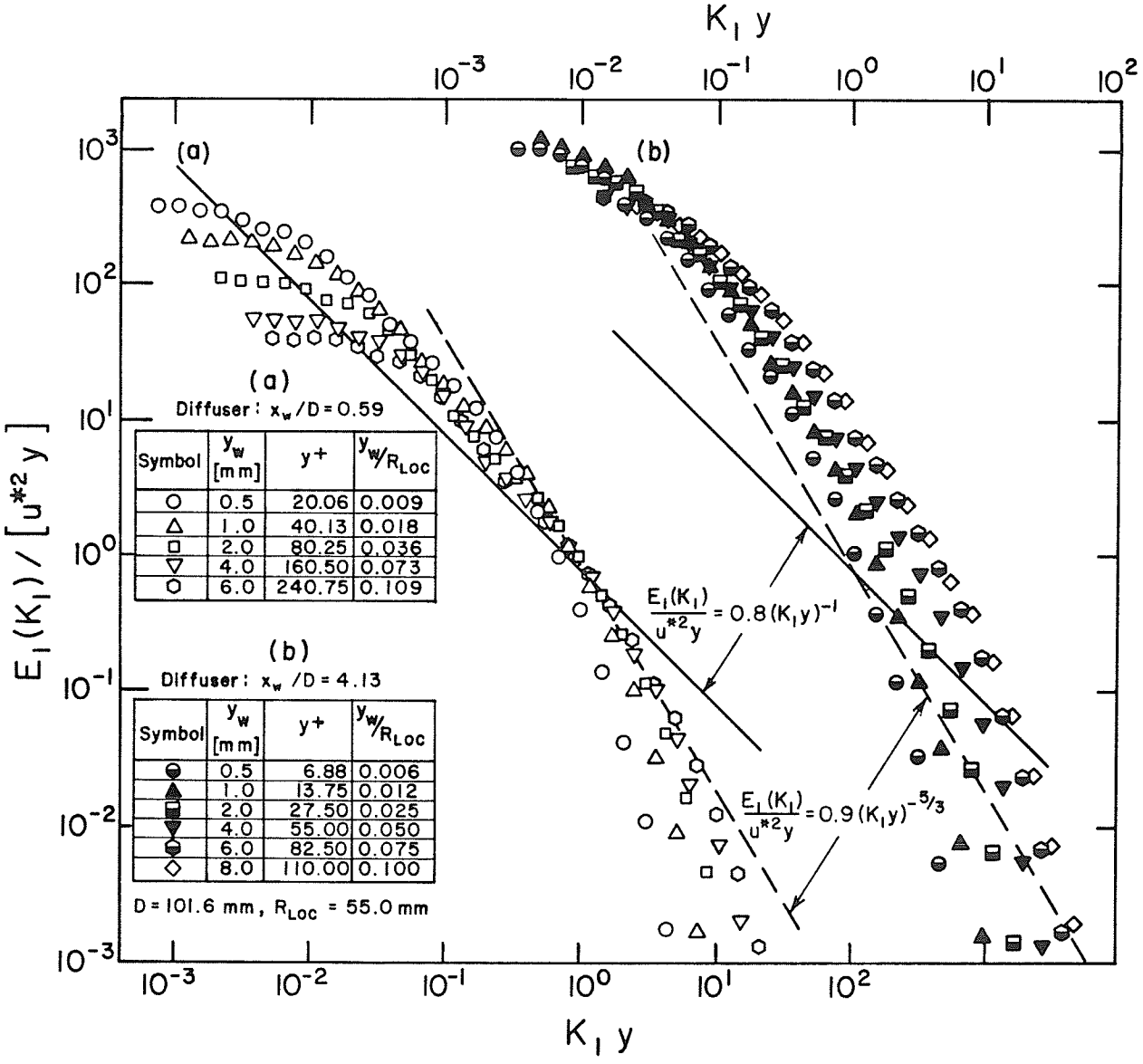

Figure 4.7 Normalized values of longitudinal spectrum $E_1(k_1)$ in the present diffuser flow at x_w/D = 0.59 & 4.13.

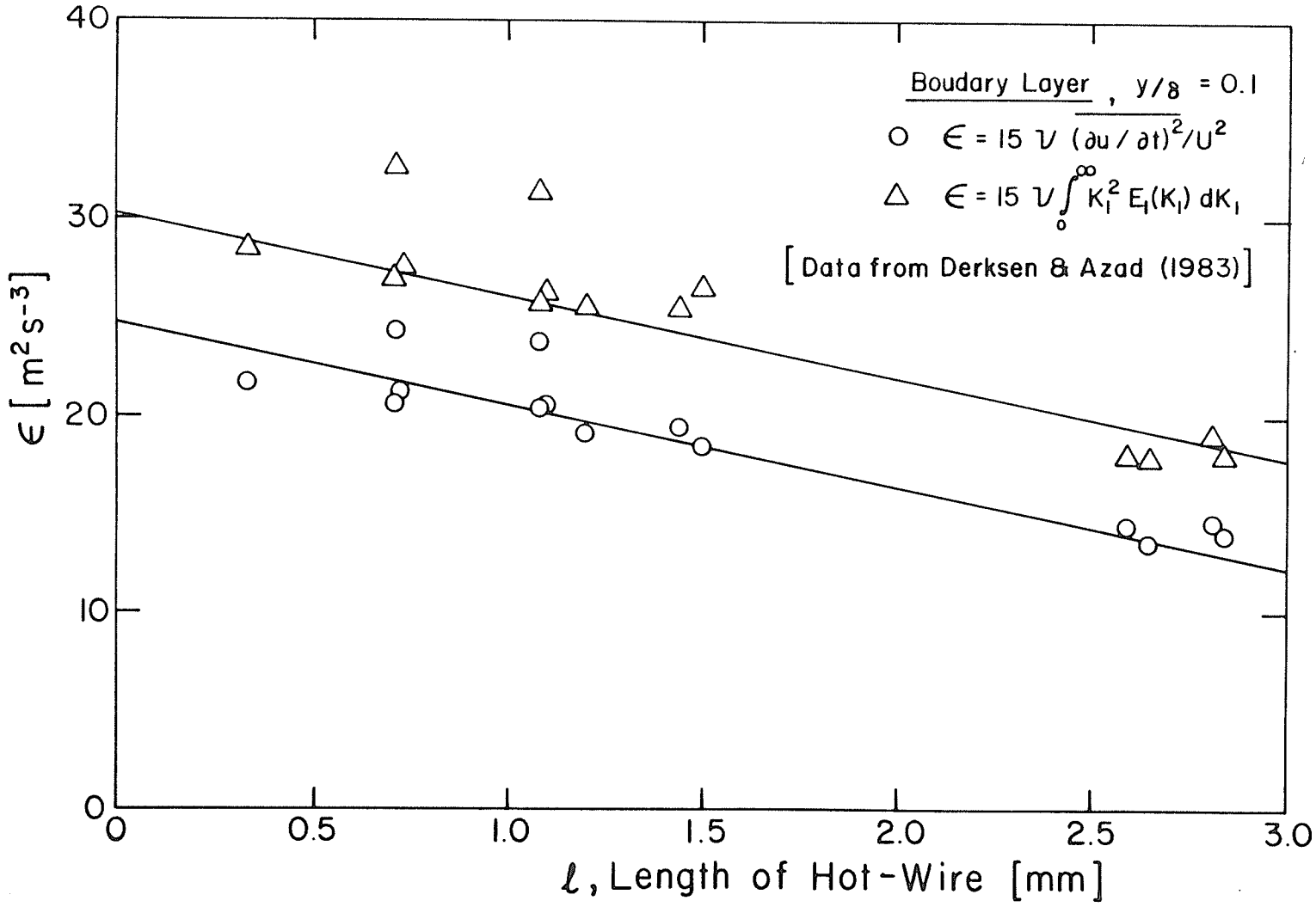

Figure 5.1 Dissipation obtained from spectra and from $\partial u/\partial t$ for different lengths of the hot wire in boundary layer flow.

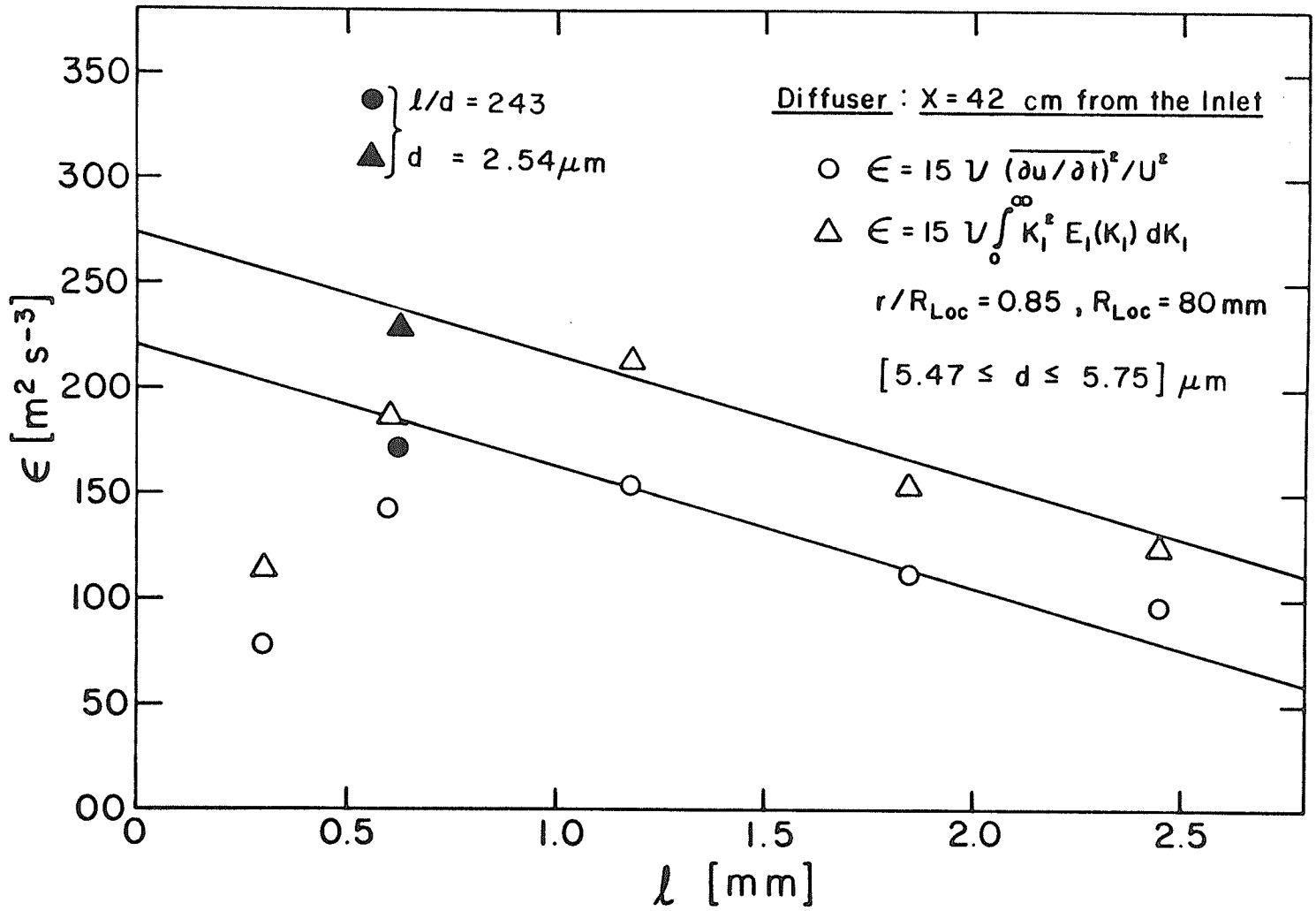

Figure 5.2 Dissipations obtained from spectra and from $\partial u/\partial t$ for different lengths of the hot wire in diffuser flow at x = 42 cm, $r/R_{Loc.}$ = 0.85 and $R_{Loc.}$ = 8 cm.

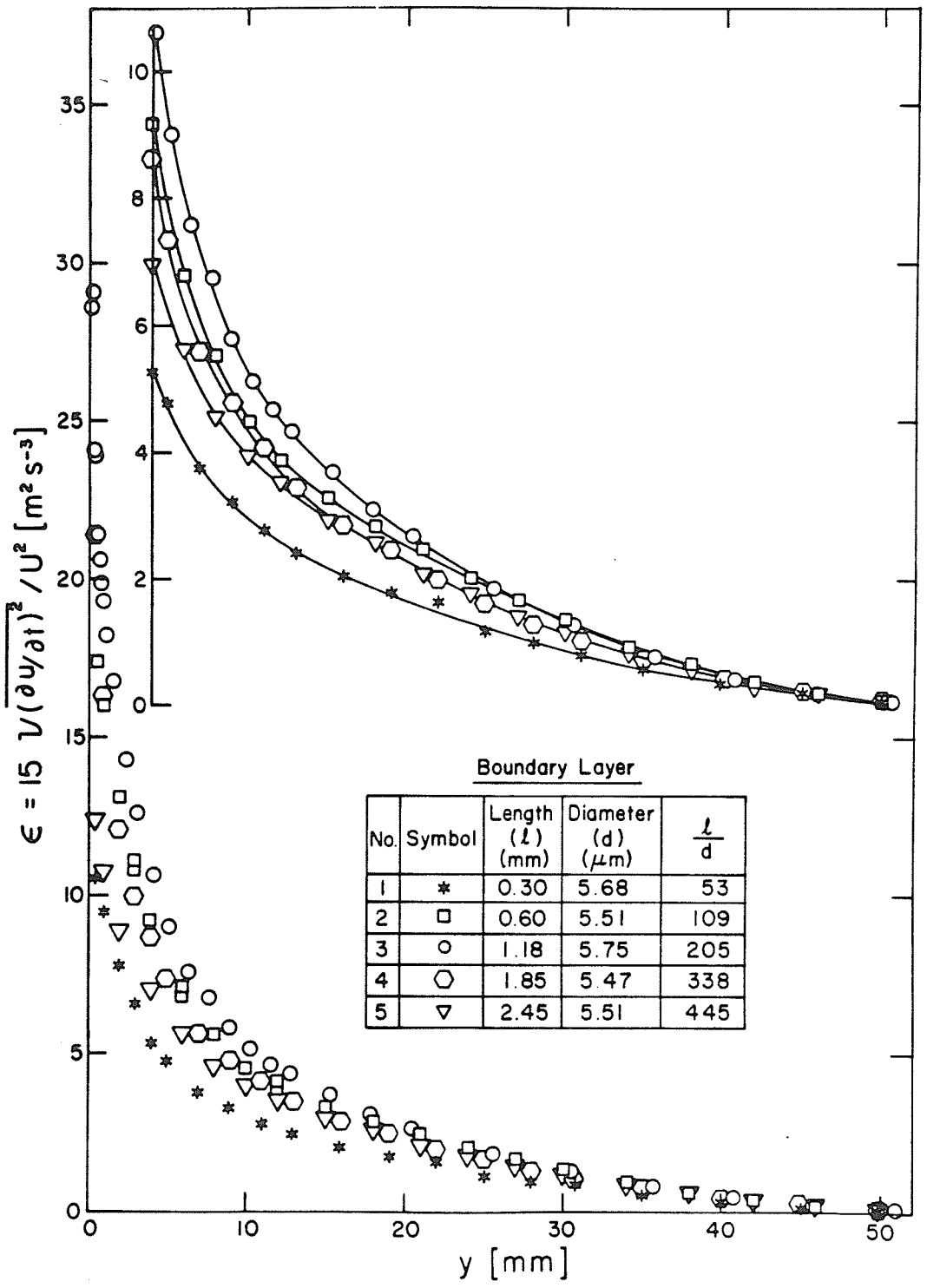

Figure 5.3 Dissipations from $\partial u/\partial t$ across the boundary layer with different hot wires.

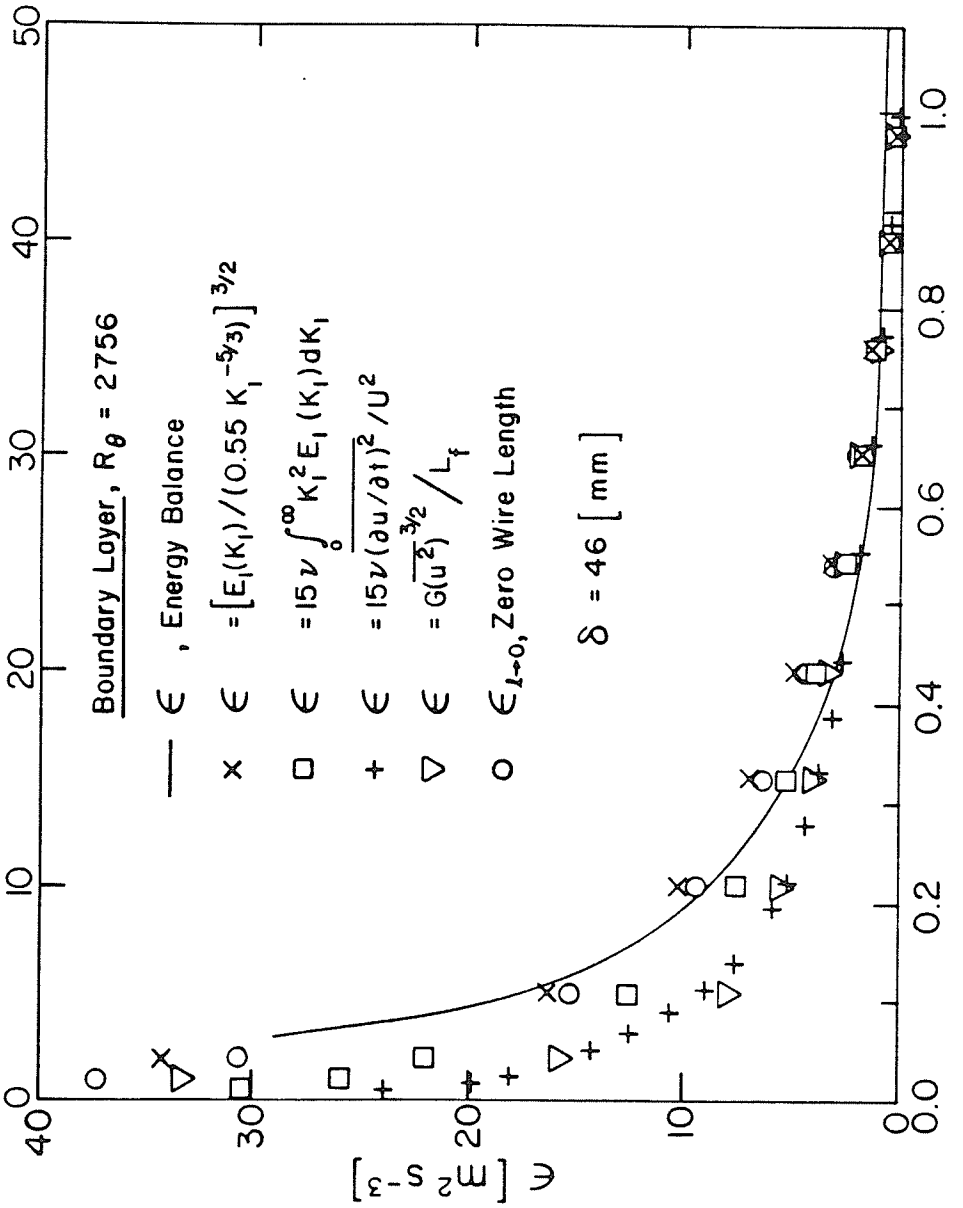

Figure 5.4 Different methods of obtaining dissipation rate in turbulent boundary layer.

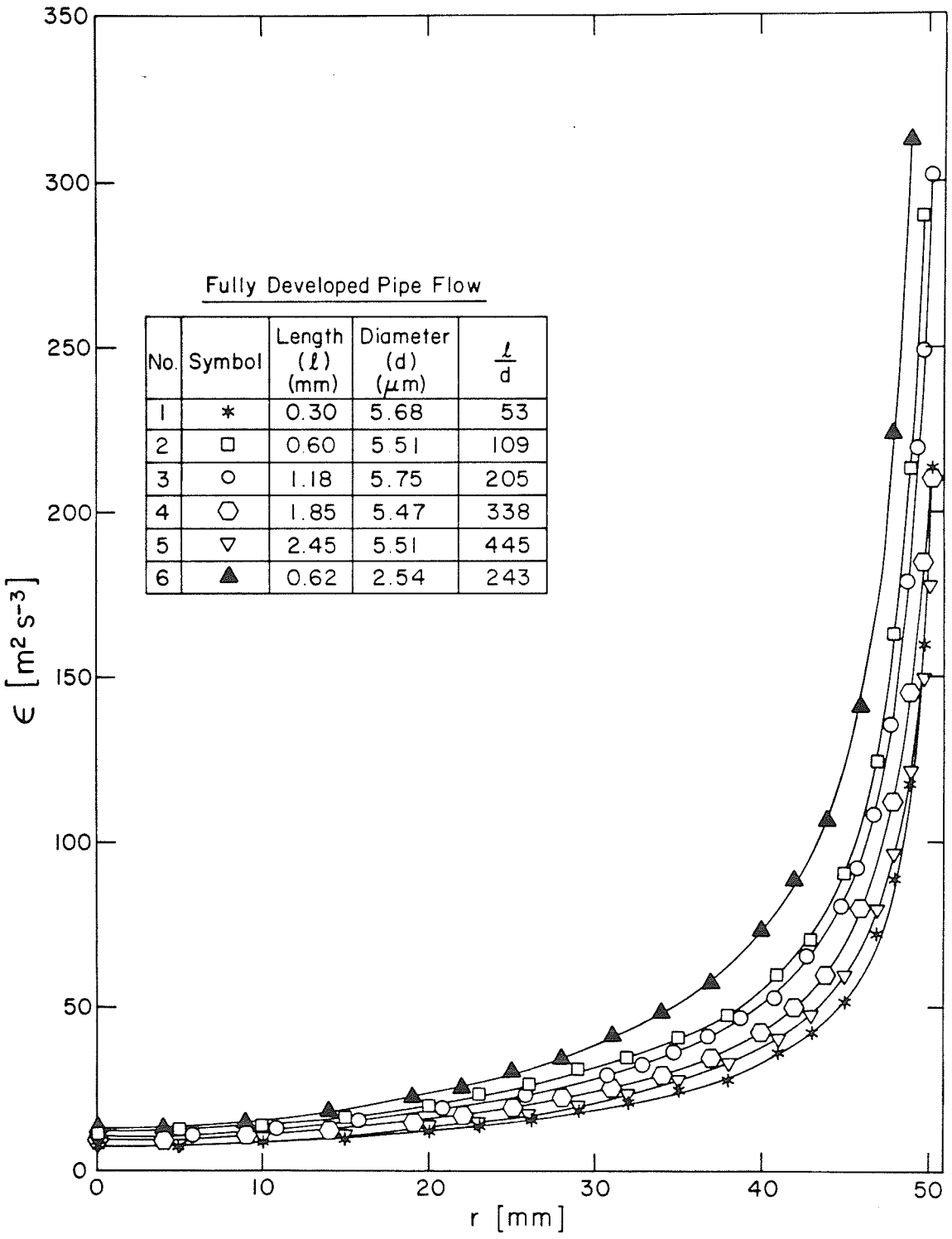

Figure 5.5 Dissipation from $\partial u/\partial t$ with different hot wires in a fully developed pipe flow.

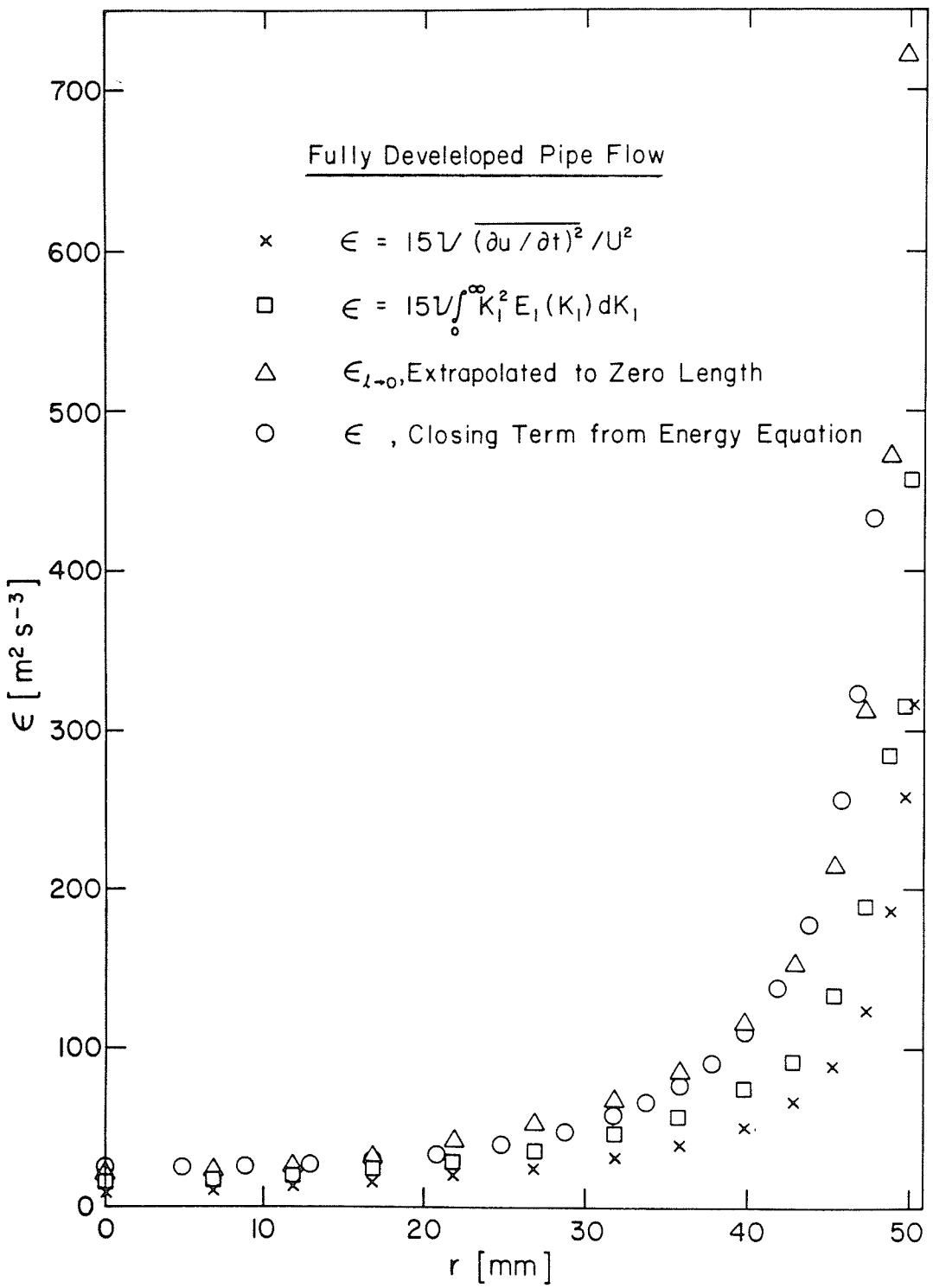

Figure 5.6 Different methods of obtaining dissipation rate in a fully developed pipe flow.

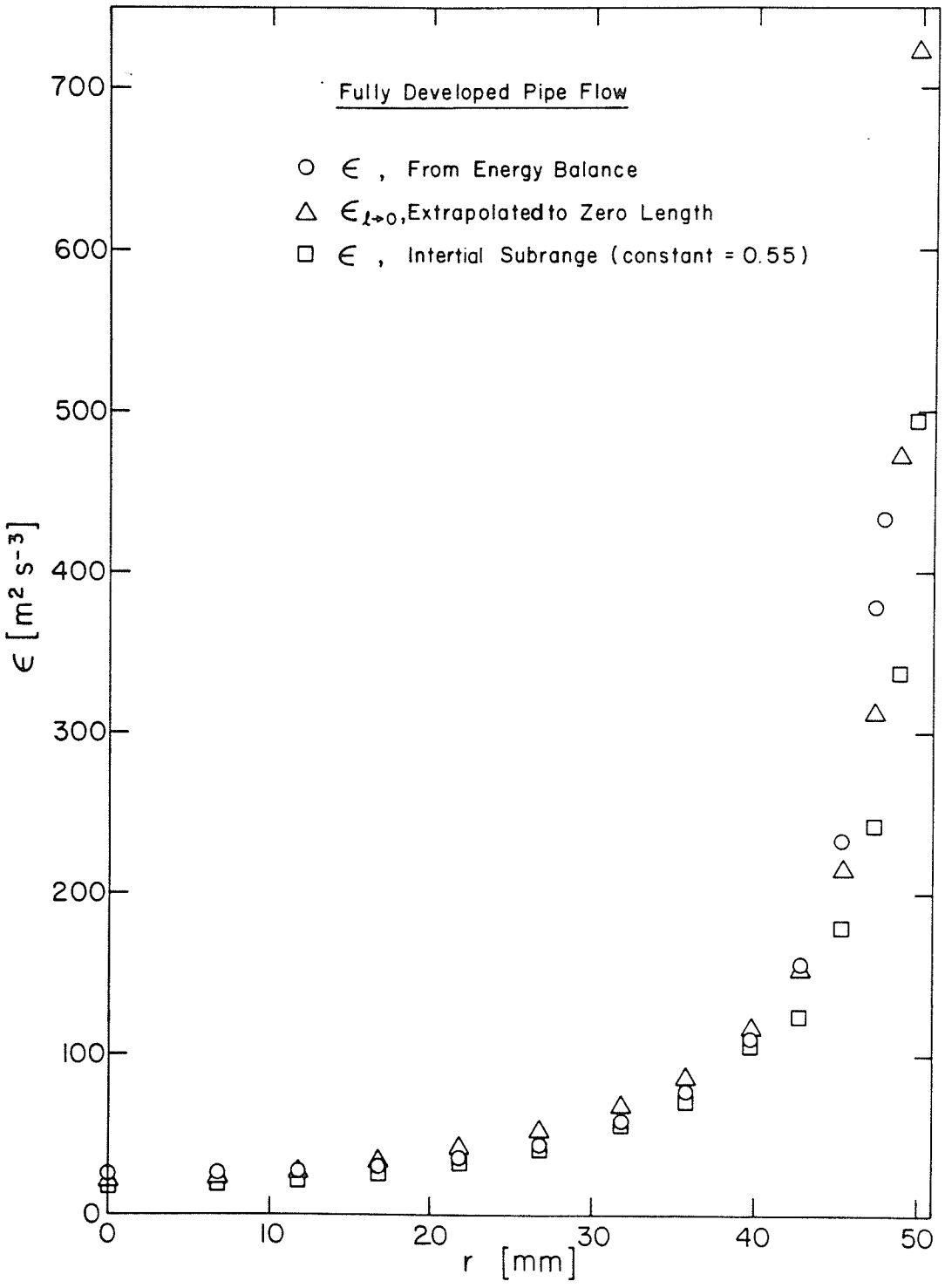

Figure 5.7 Assessment of dissipation rate by comparing three promising methods in a fully developed pipe flow.

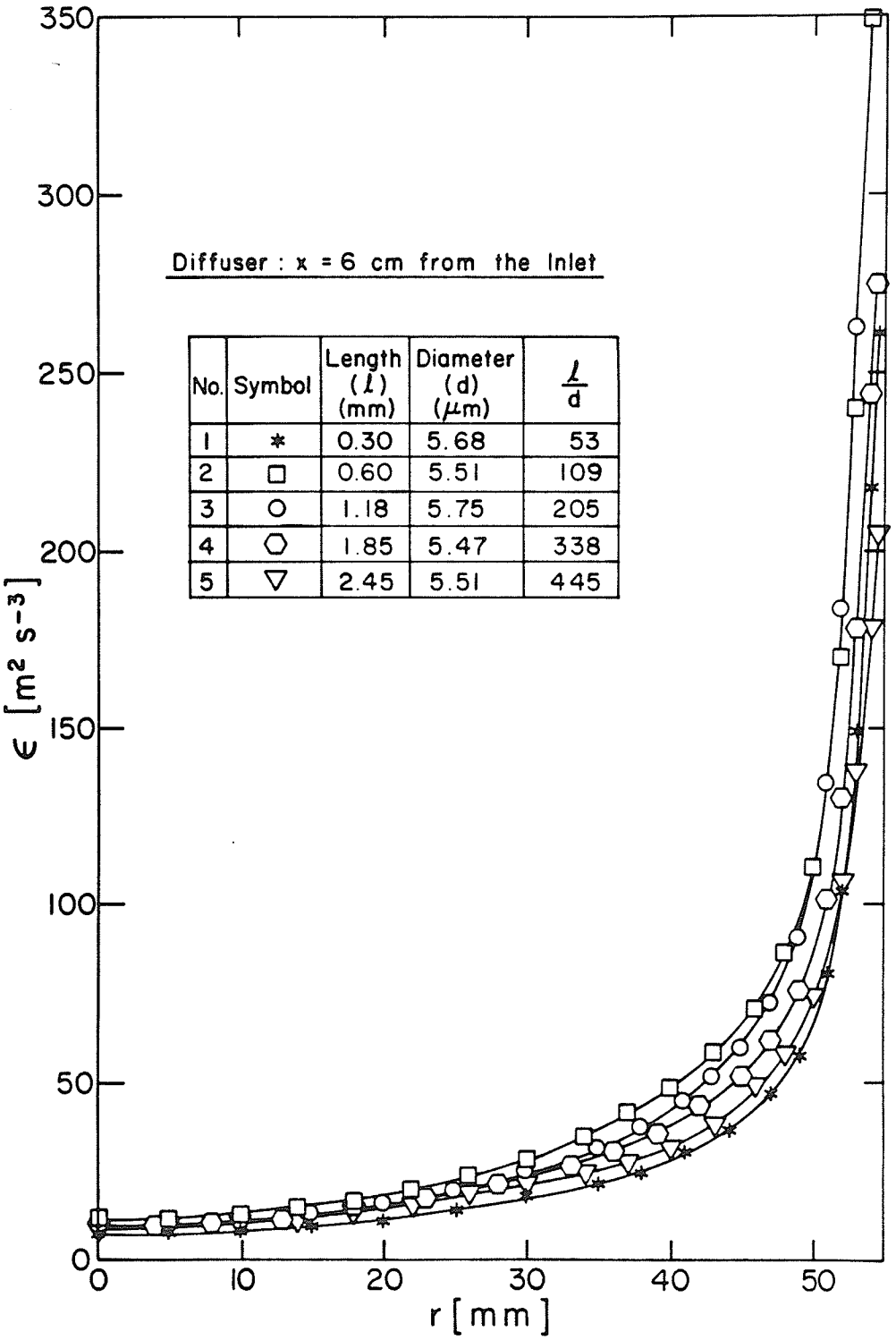

Figure 5.8 Dissipation from $\partial u/\partial t$ with different hot wires in a diffuser flow at x = 6 cm.

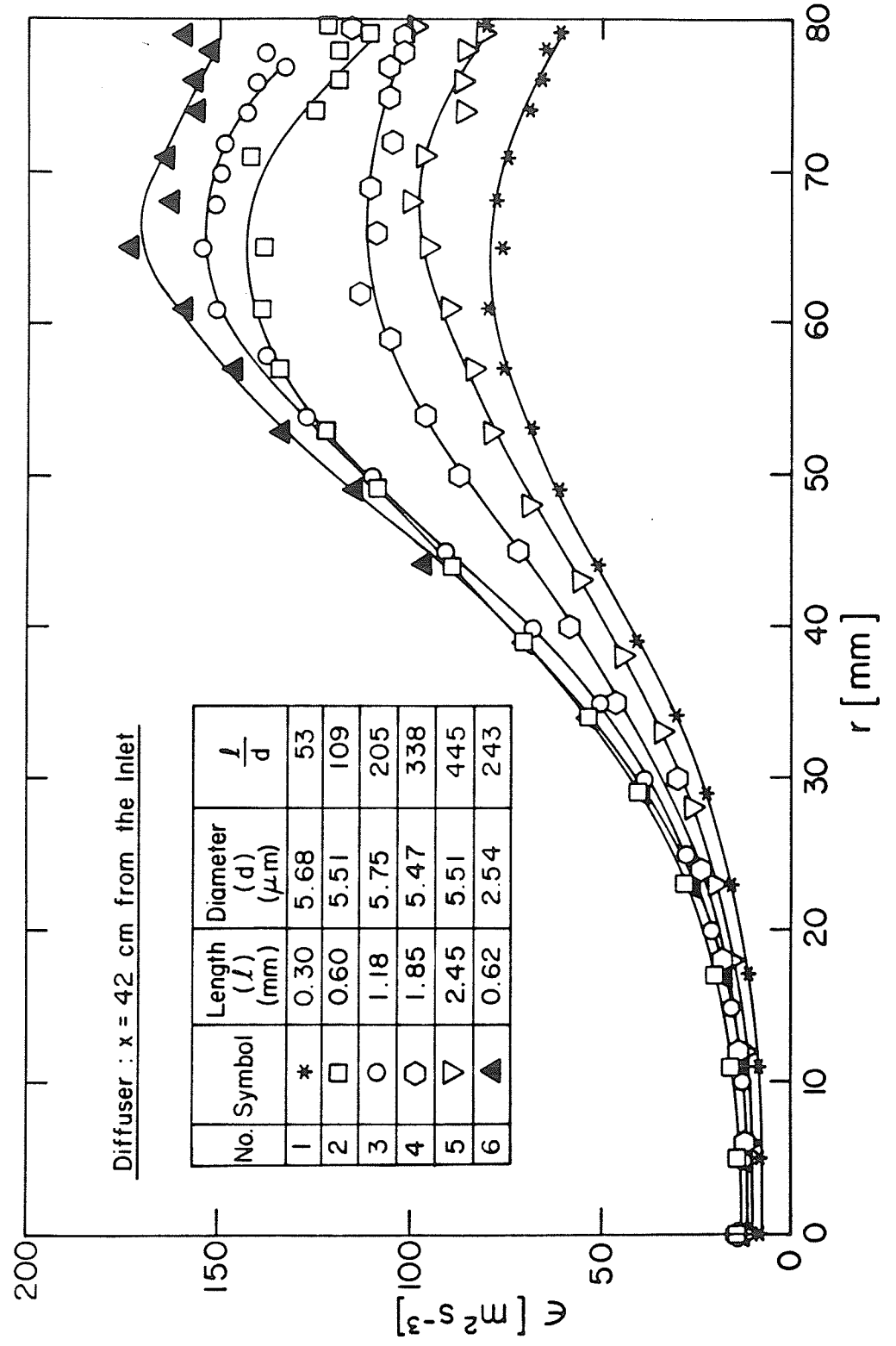

Figure 5.9 Dissipation from $\partial u/\partial t$ with different hot wires in a diffuser flow at x = 42 cm.

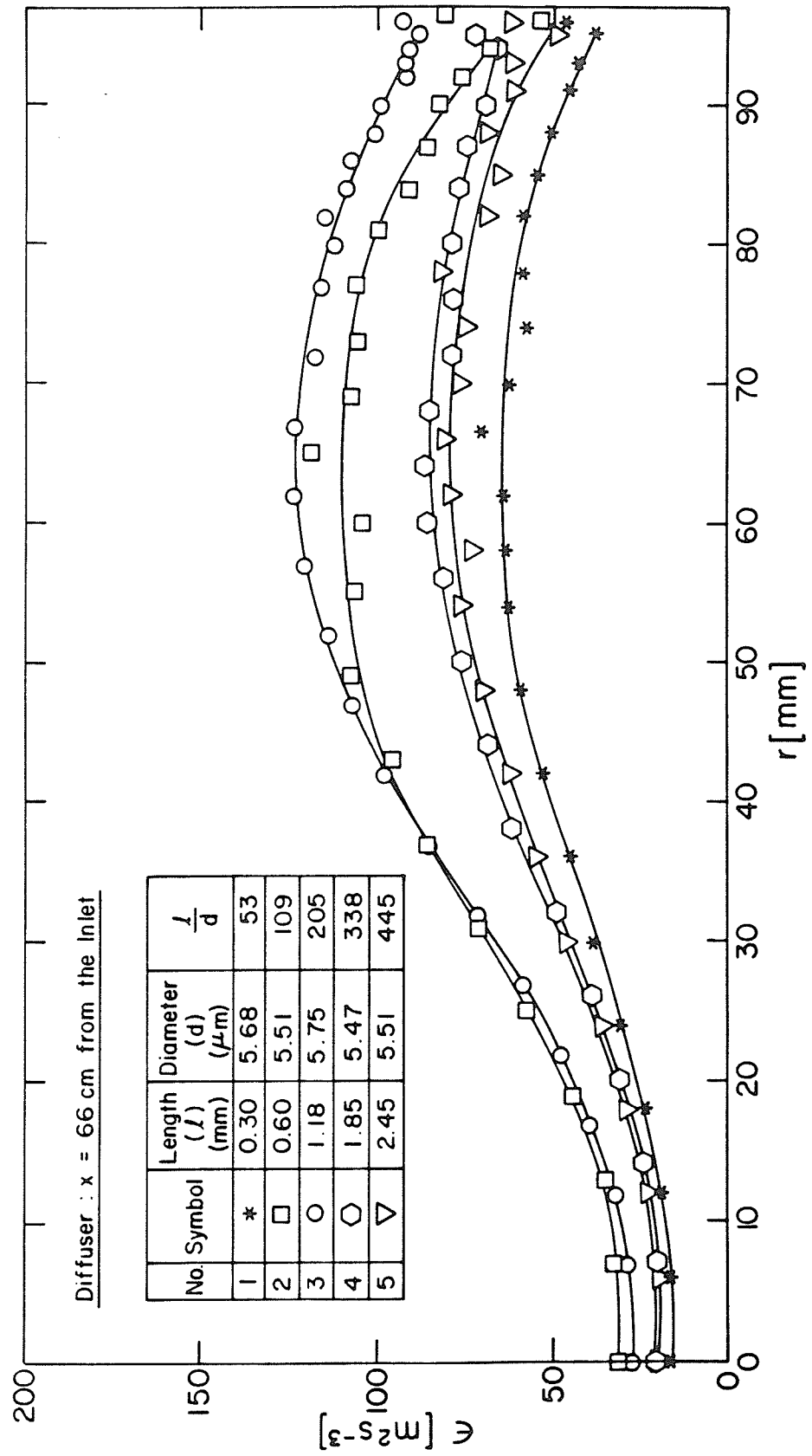

Figure 5.10 Dissipation from $\partial u/\partial t$ with different hot wires in a diffuser flow at x = 66 cm.

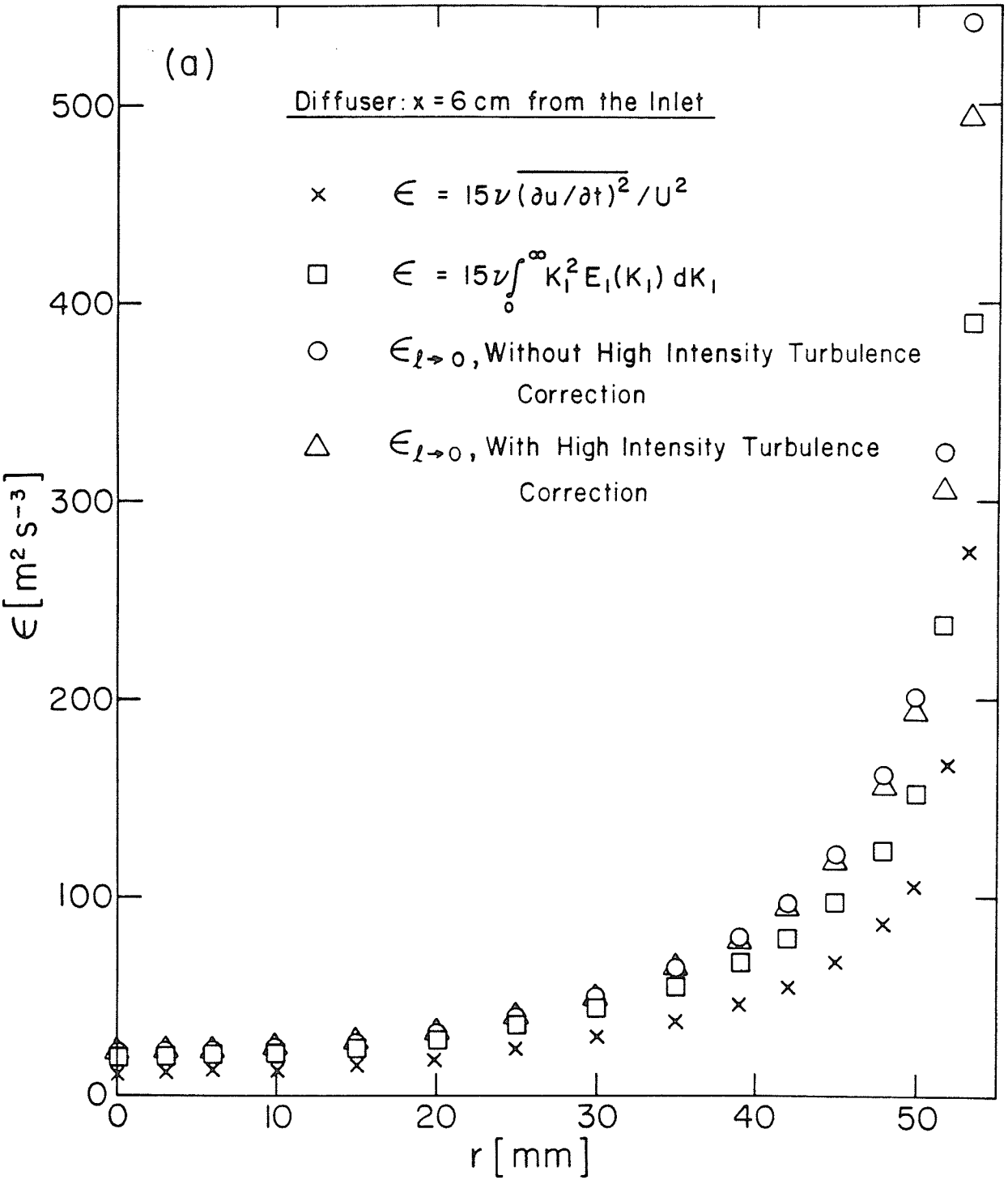

Figure 5.11a Different methods of obtaining dissipation rate in a diffuser flow at x = 6 cm.

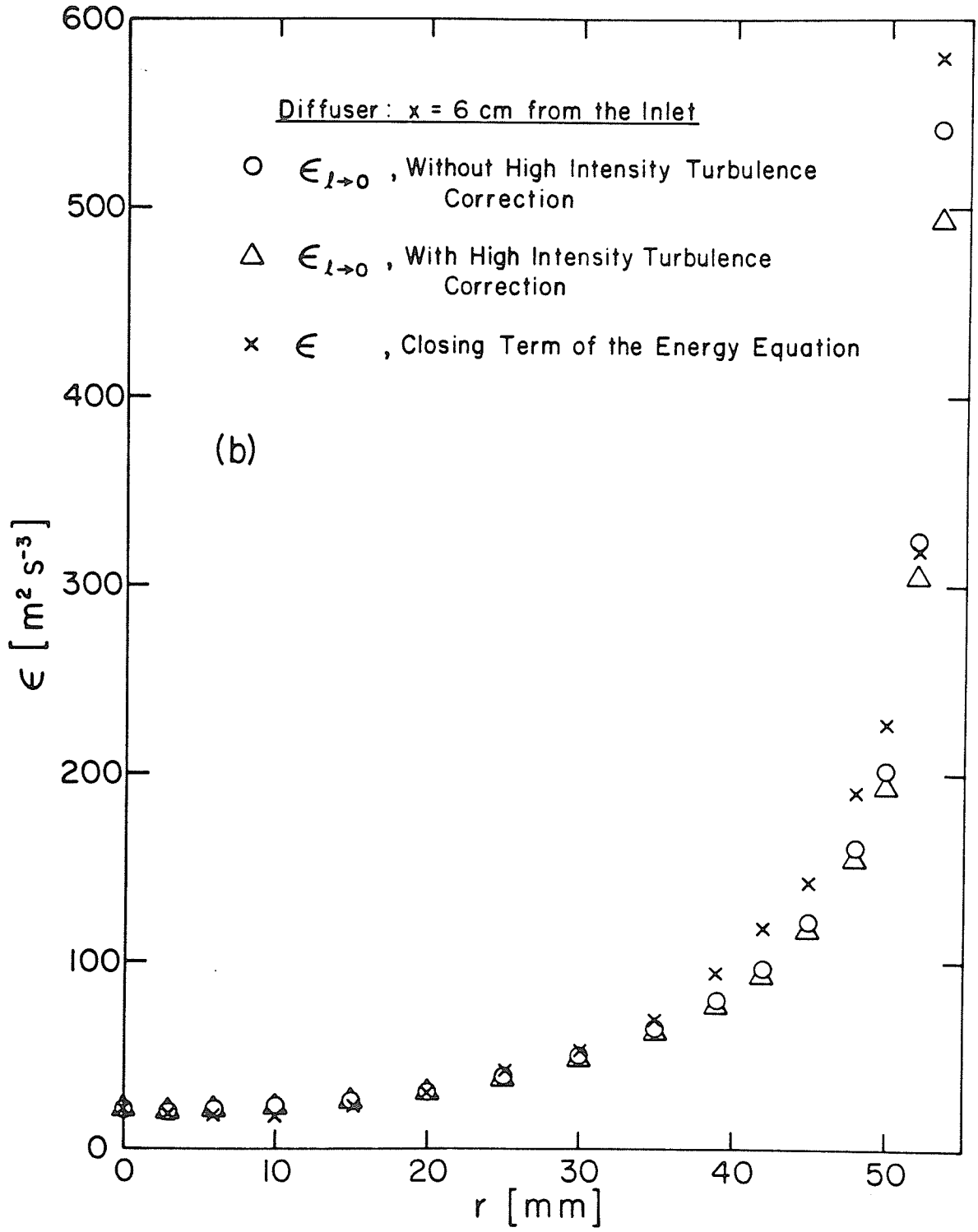

Figure 5.11b Assessment of dissipation rate by comparing present methods with the dissipation rate obtained from the closing term of the turbulent energy equation in a diffuser flow at x = 6 cm.

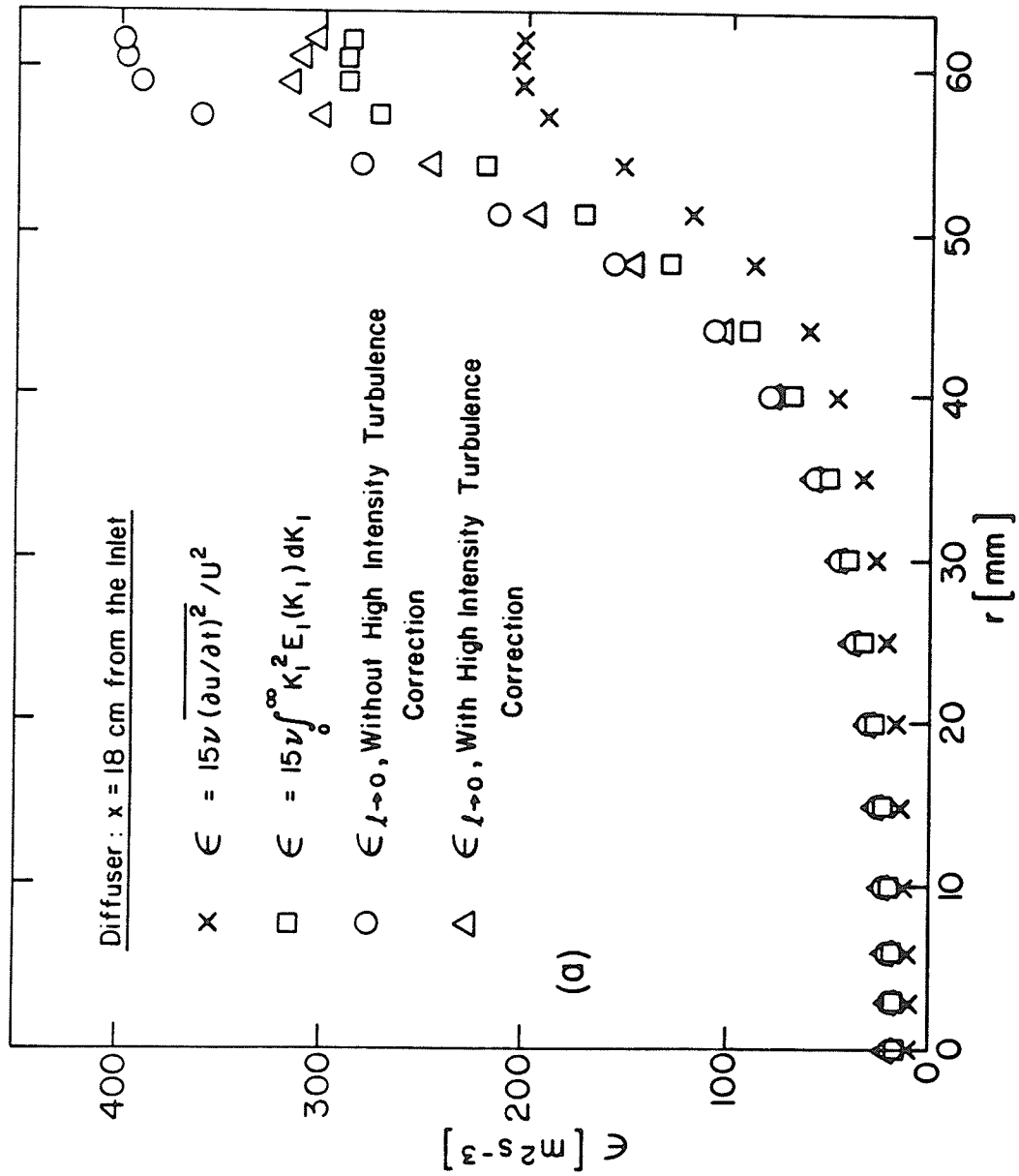

Figure 5.12a Different methods of obtaining dissipation rate in a diffuser flow at x = 18 cm.

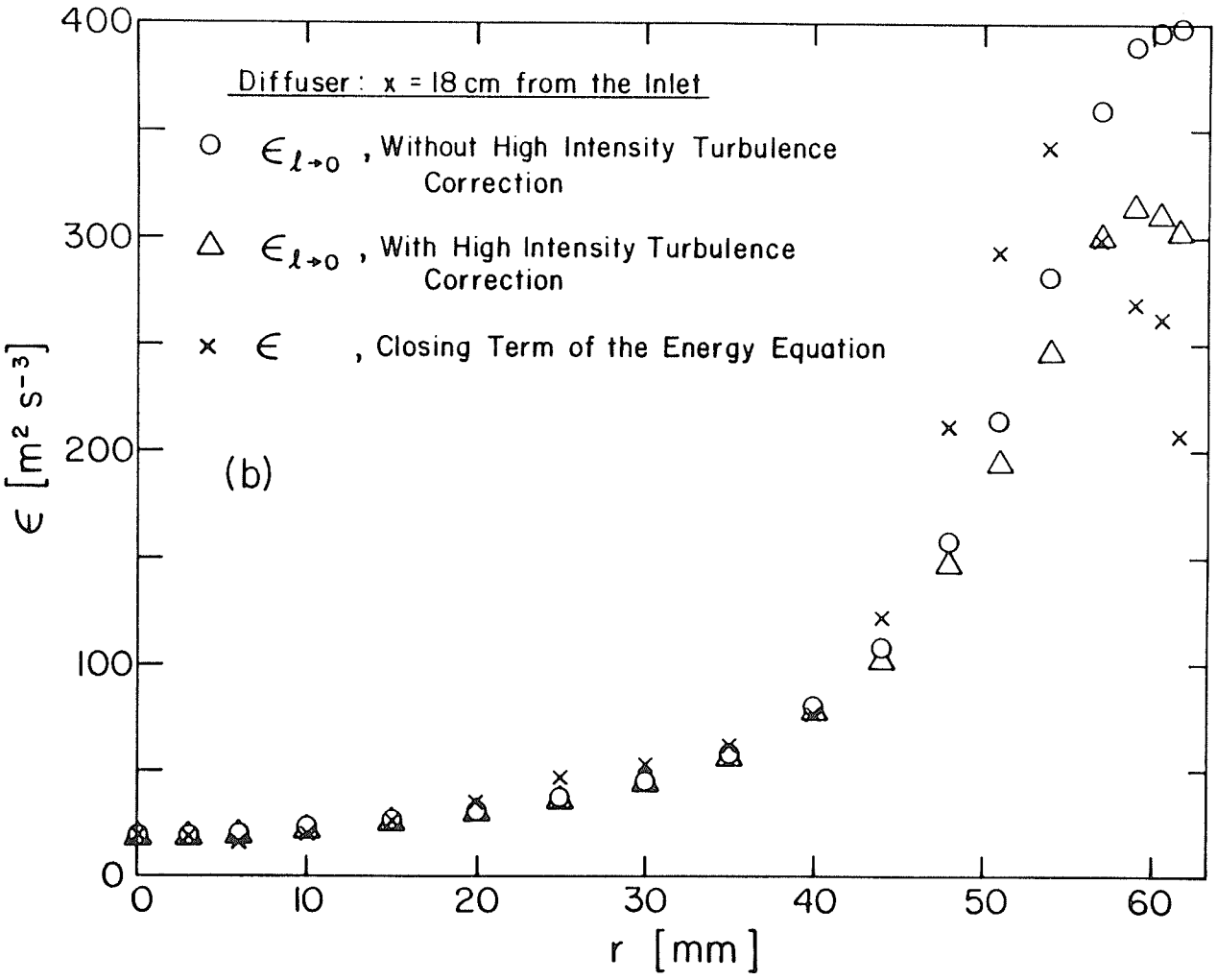

Figure 5.12b Assessment of dissipation rate by comparing present methods with the dissipation rate obtained from the closing term of the turbulent energy equation in a diffuser flow at x = 18 cm

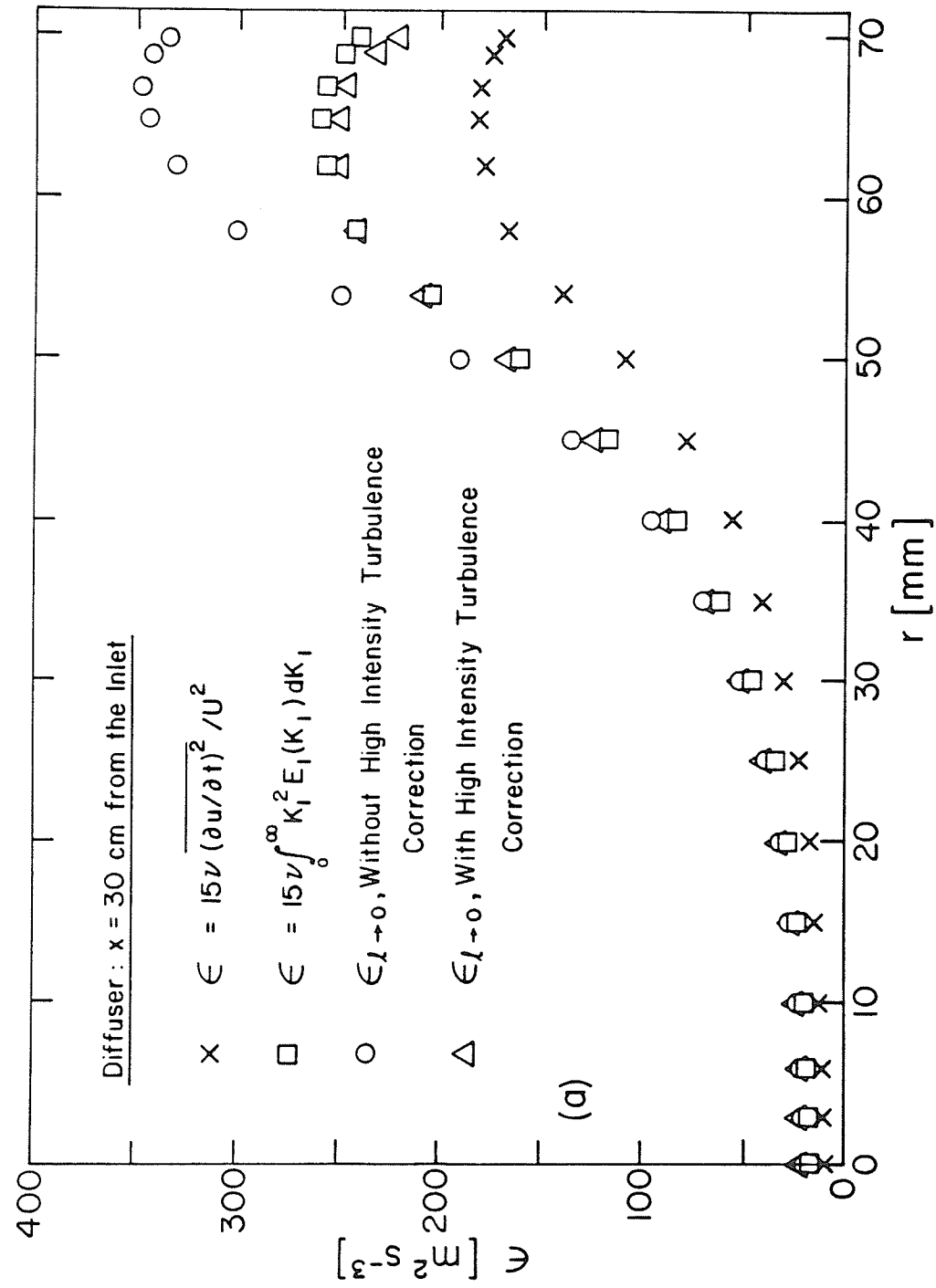

Figure 5.13a Different methods of obtaining dissipation rate in a diffuser flow at x = 30 cm.

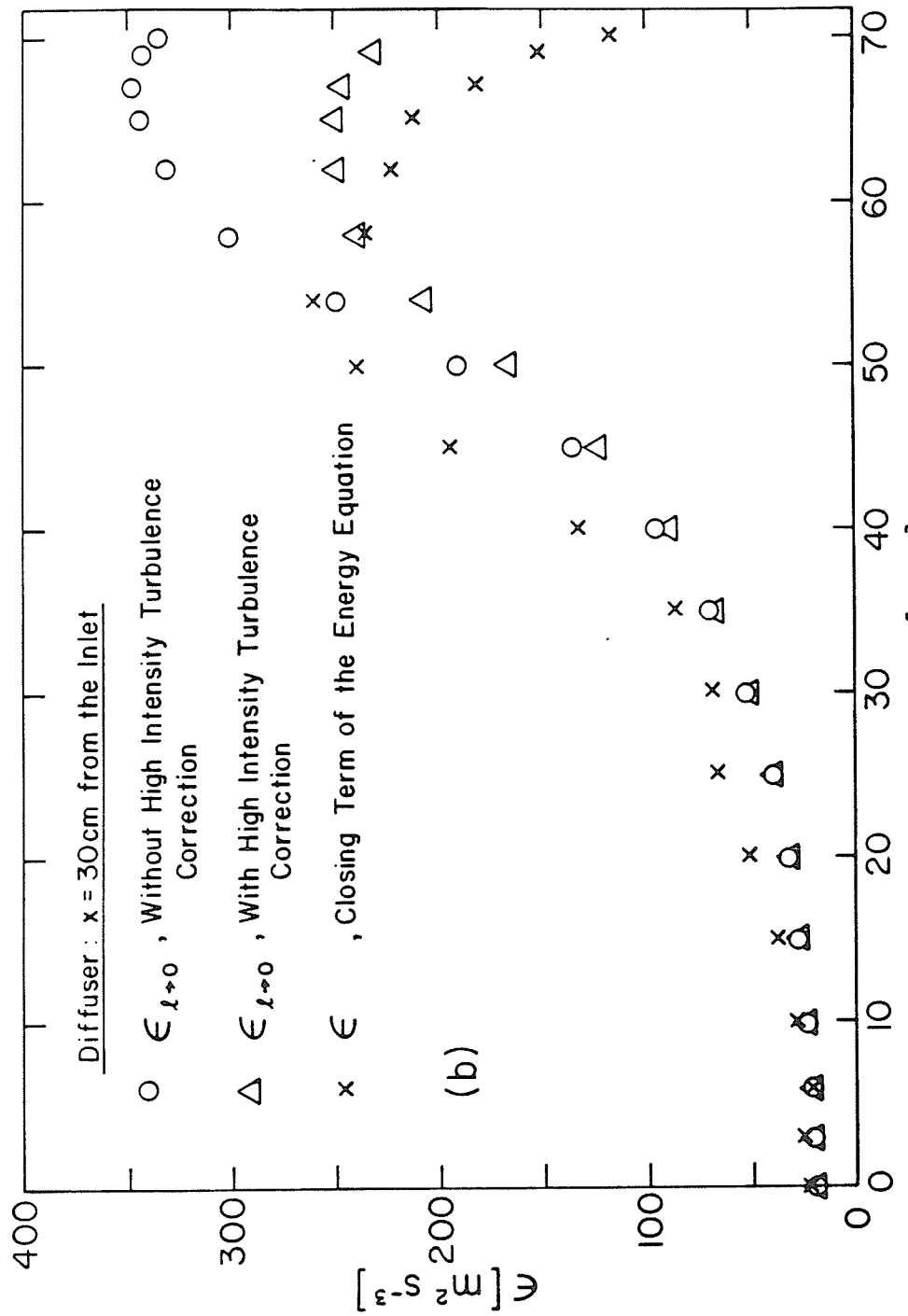

Figure 5.13b Assessment of dissipation rate by comparing present methods with the dissipation rate obtained from the closing term of the turbulent energy equation in a diffuser flow at x = 30 cm

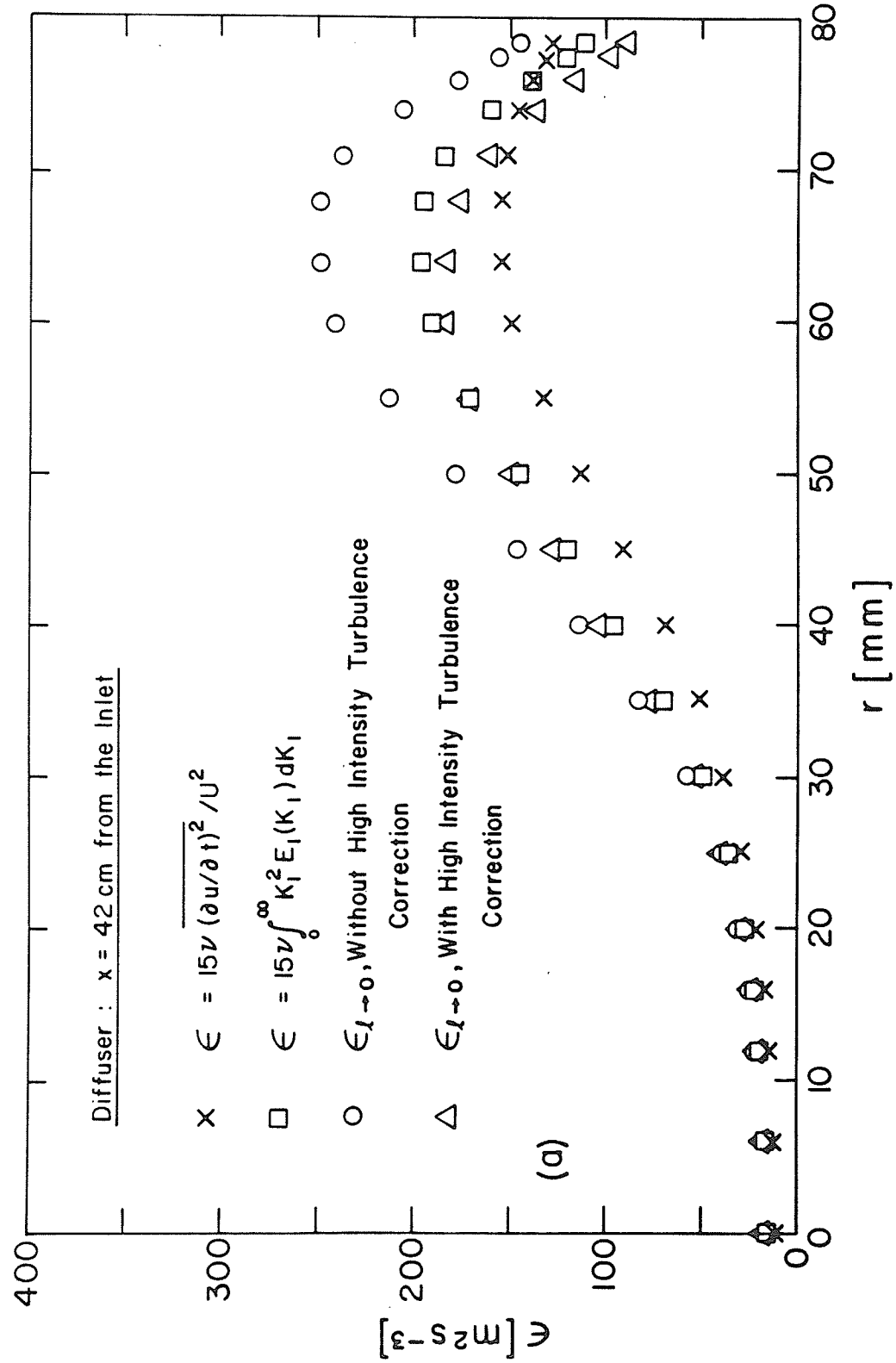

Figure 5.14a Different methods of obtaining dissipation rate in a diffuser flow at x = 42 cm.

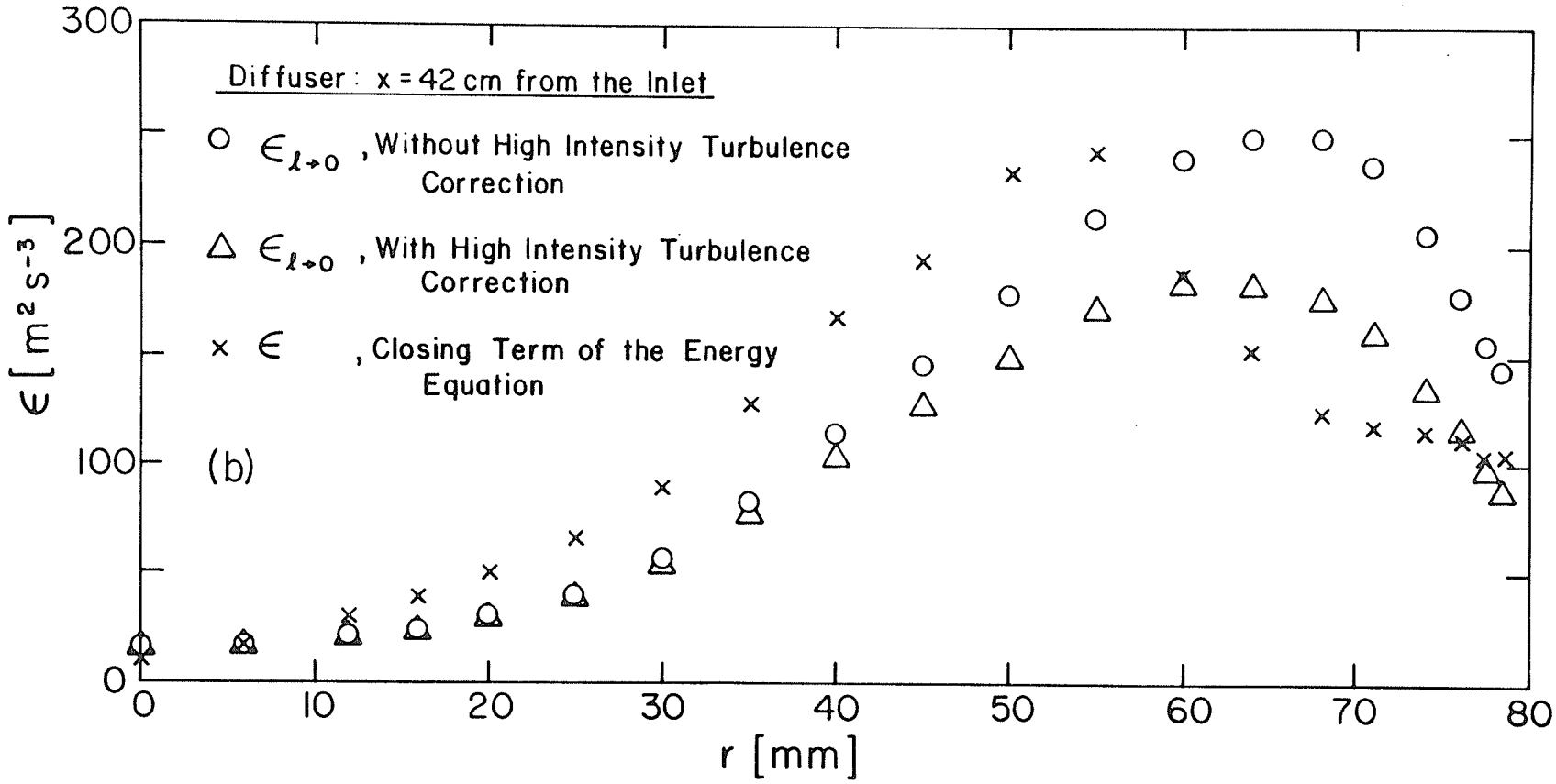

Figure 5.14b Assessment of dissipation rate by comparing present methods with the dissipation rate obtained from the closing term of the turbulent energy equation in a diffuser flow at x = 42 cm

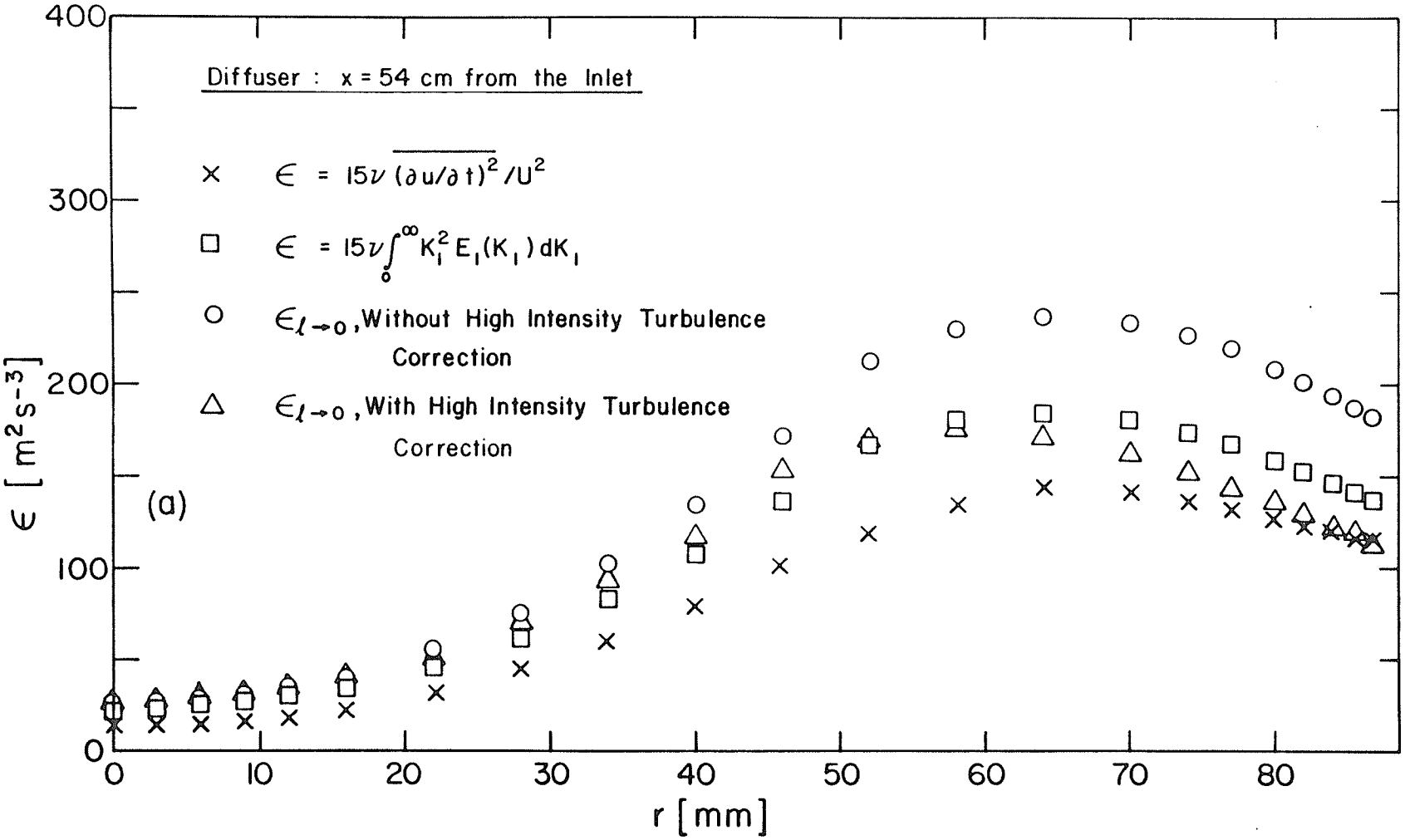

Figure 5.15a Different methods of obtaining dissipation rate in a diffuser flow at x = 54 cm.

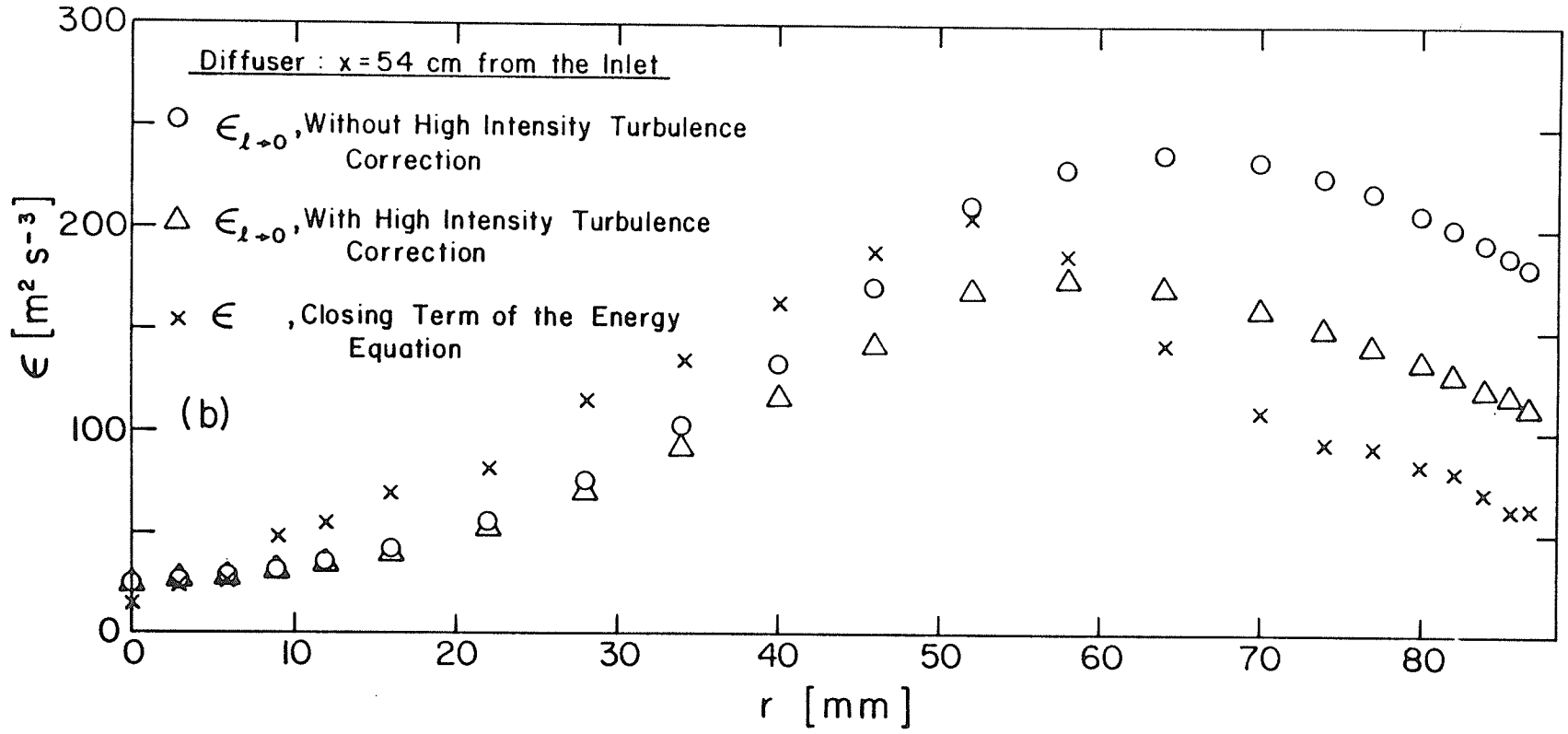

Figure 5.15b Assessment of dissipation rate by comparing present methods with the dissipation rate obtained from the closing term of the turbulent energy equation in a diffuser flow at x = 54 cm

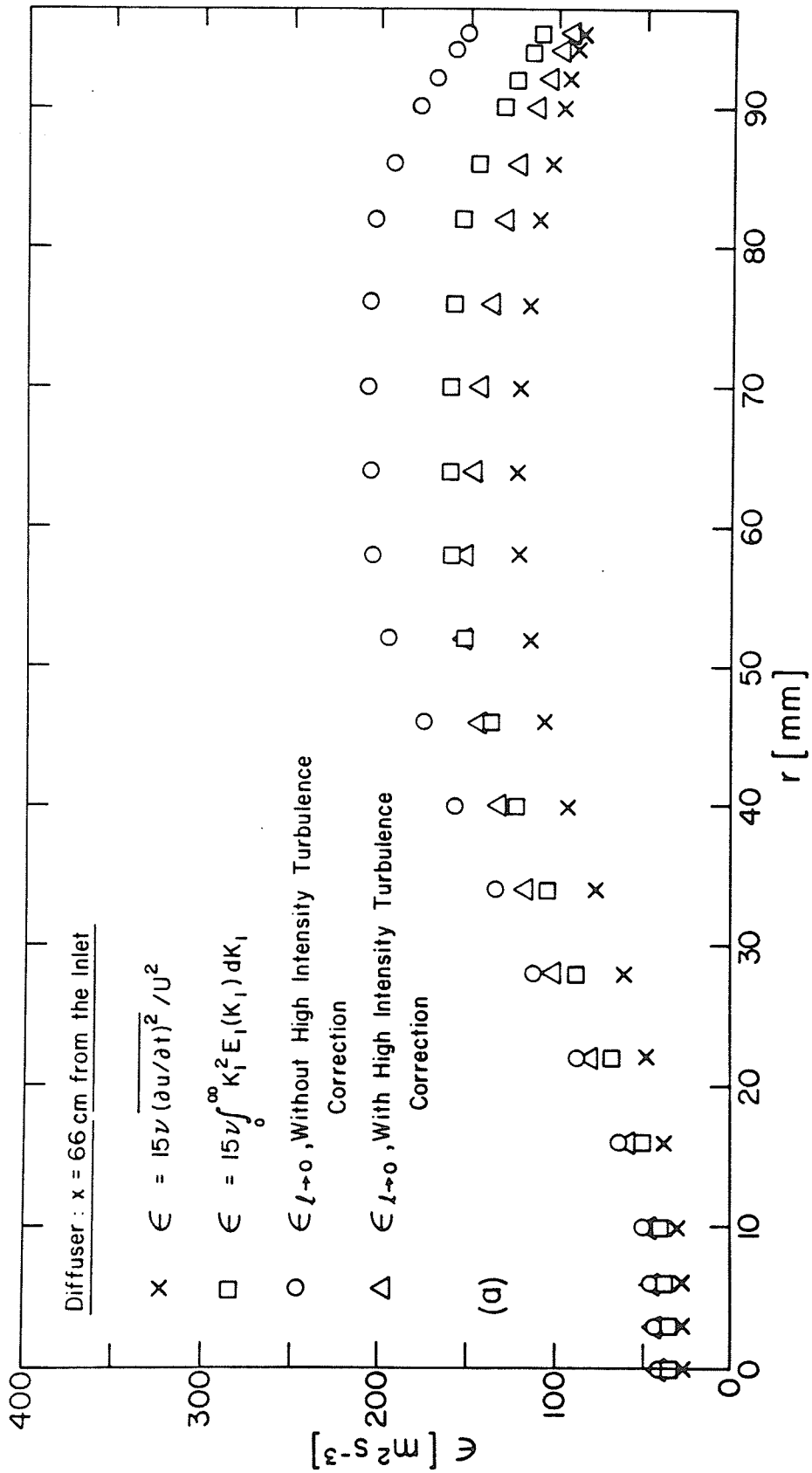

Figure 5.16a Different methods of obtaining dissipation rate in a diffuser flow at x = 66 cm.

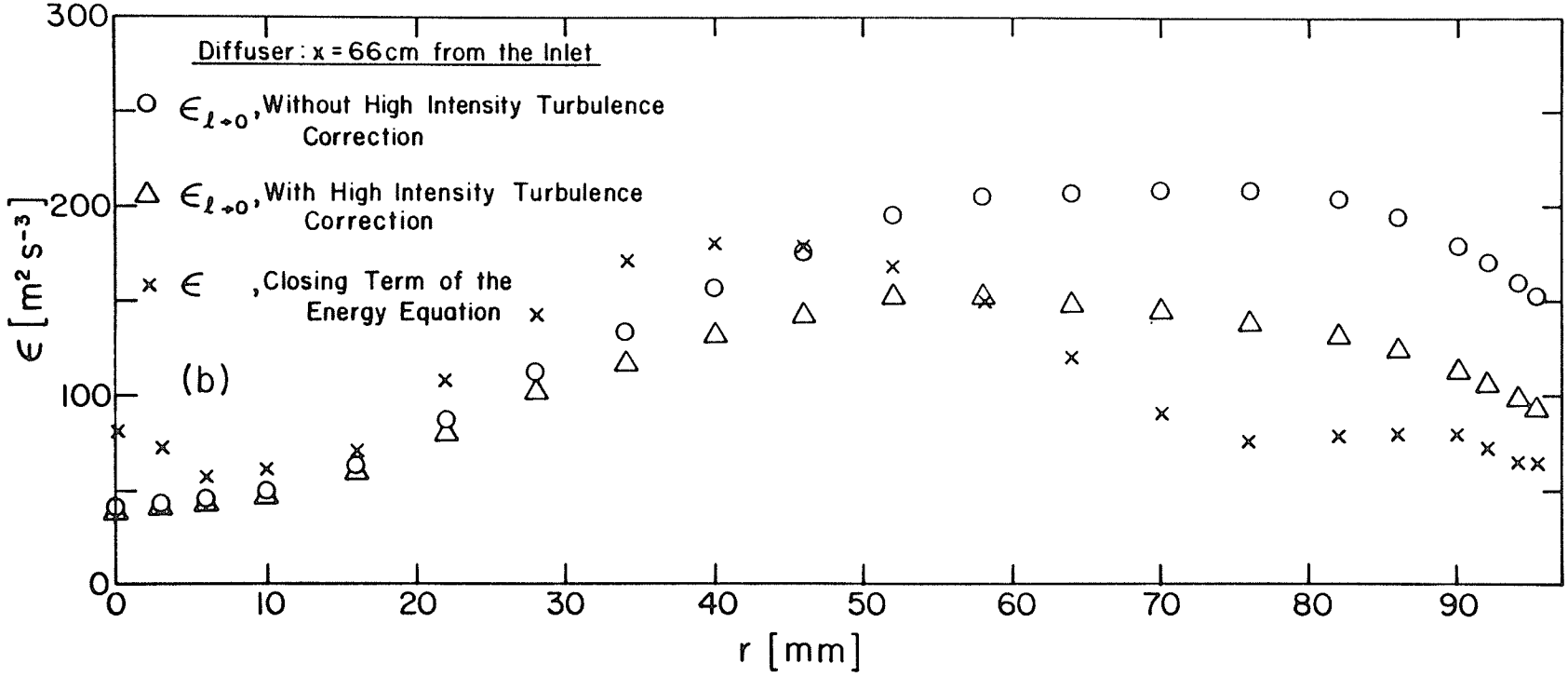

Figure 5.16b Assessment of dissipation rate by comparing present methods with the dissipation rate obtained from the closing term of the turbulent energy equation in a diffuser flow at x = 66 cm

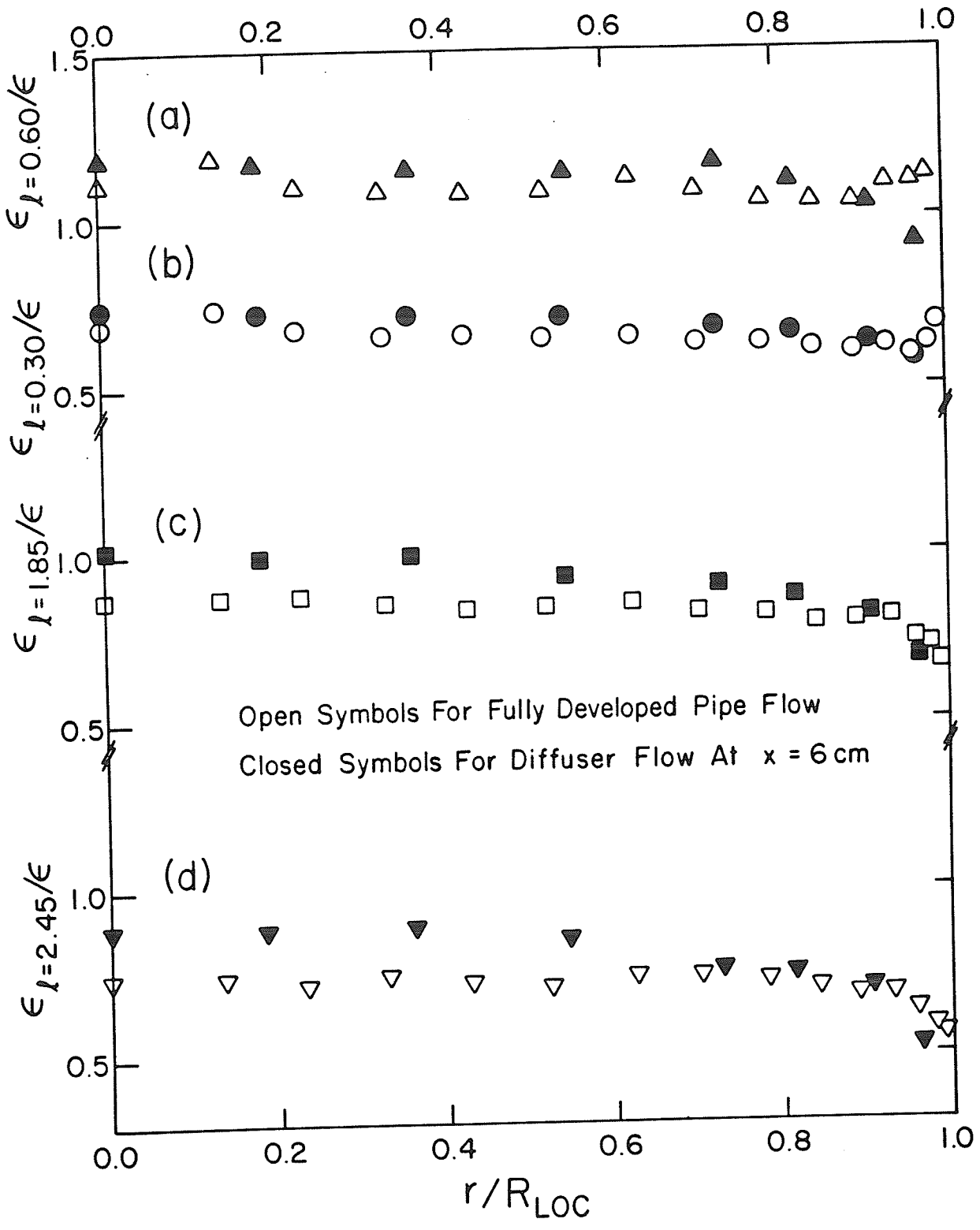

Figure 5.17 Ratio of dissipation obtained between the different lengths of wire and standard wire plotted against non-dimensional radial distance.

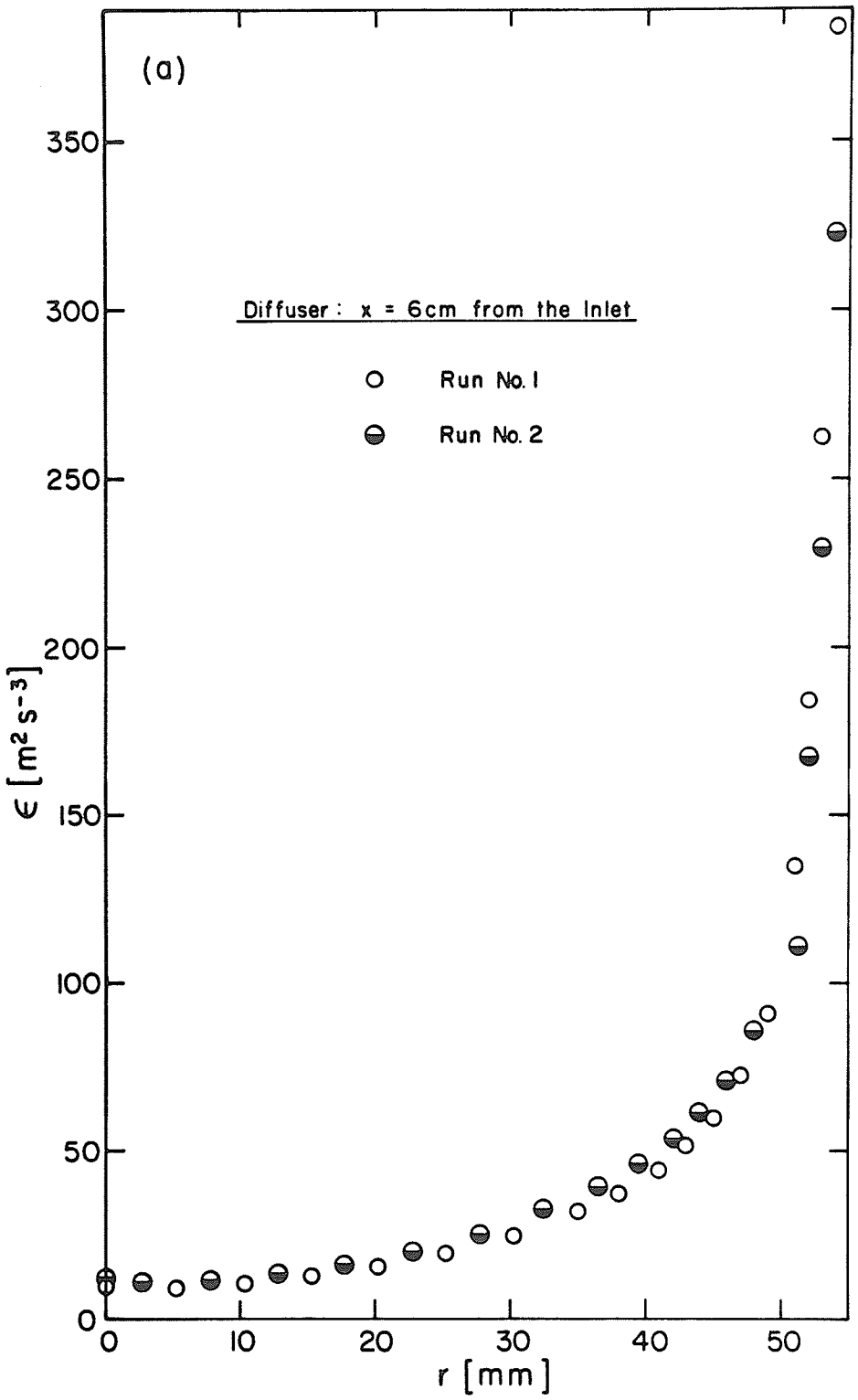

Figure 5.18 Dissipation rate obtained from the measurements of $\partial u/\partial t$ with standard boundary layer probe in a diffuser flow
(a) x = 6 cm.

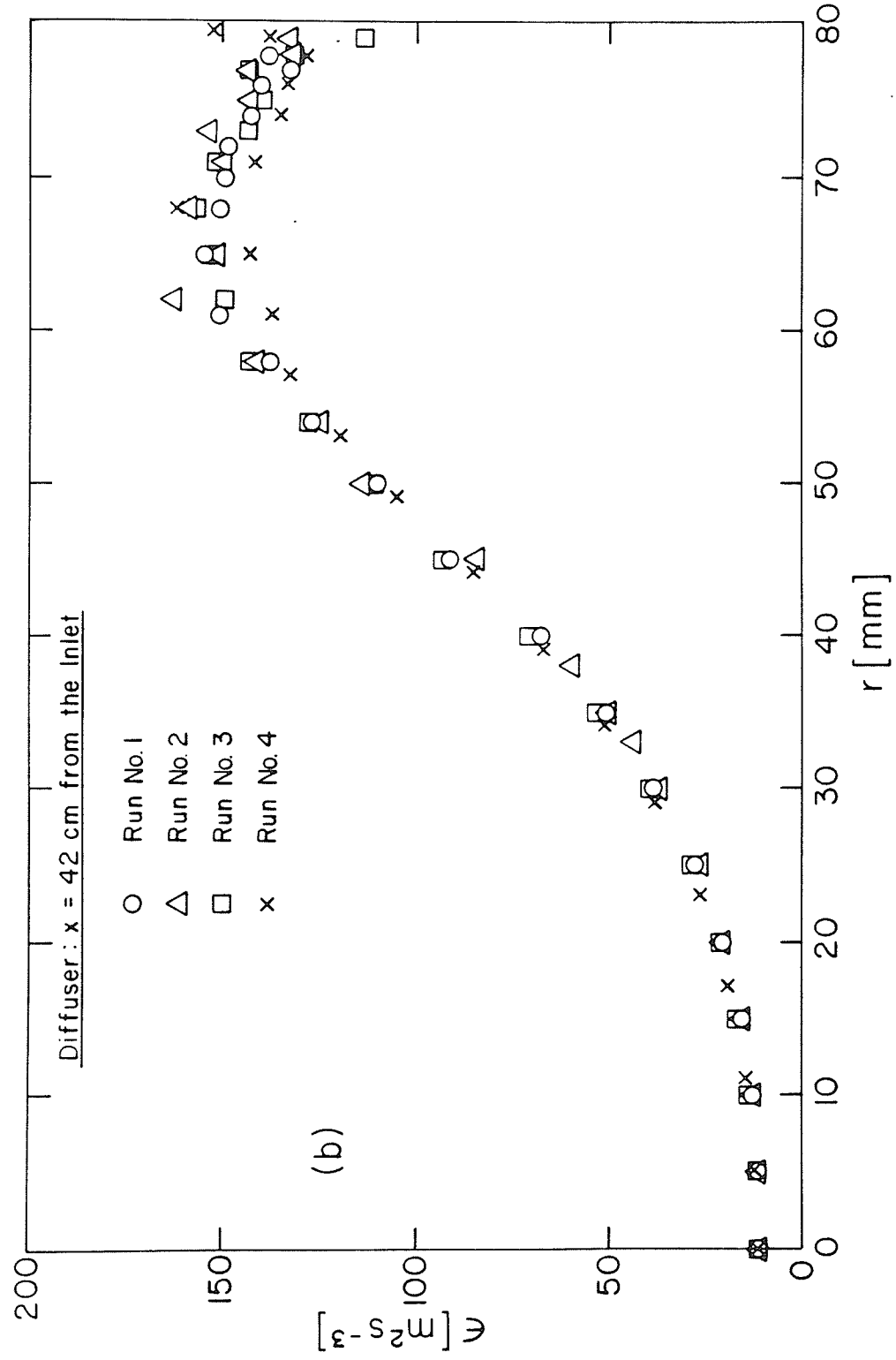

Figure 5.18 Dissipation rate obtained from the measurements of $\partial u/\partial t$ with standard boundary layer probe in a diffuser flow
(b) x = 42 cm.

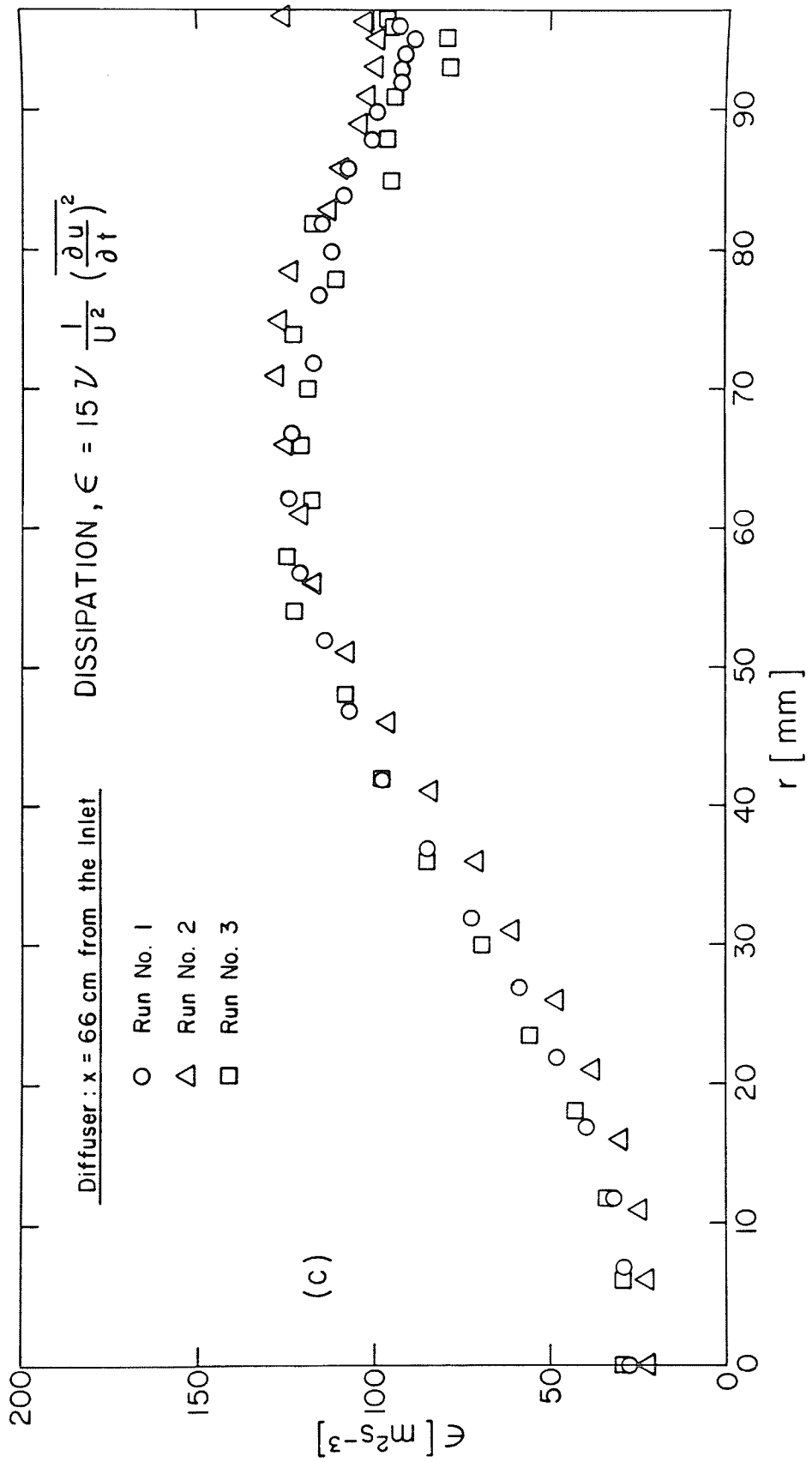

Figure 5.18 Dissipation rate obtained from the measurements of $\partial u/\partial t$ with standard boundary layer probe in a diffuser flow
(c) x = 66 cm.

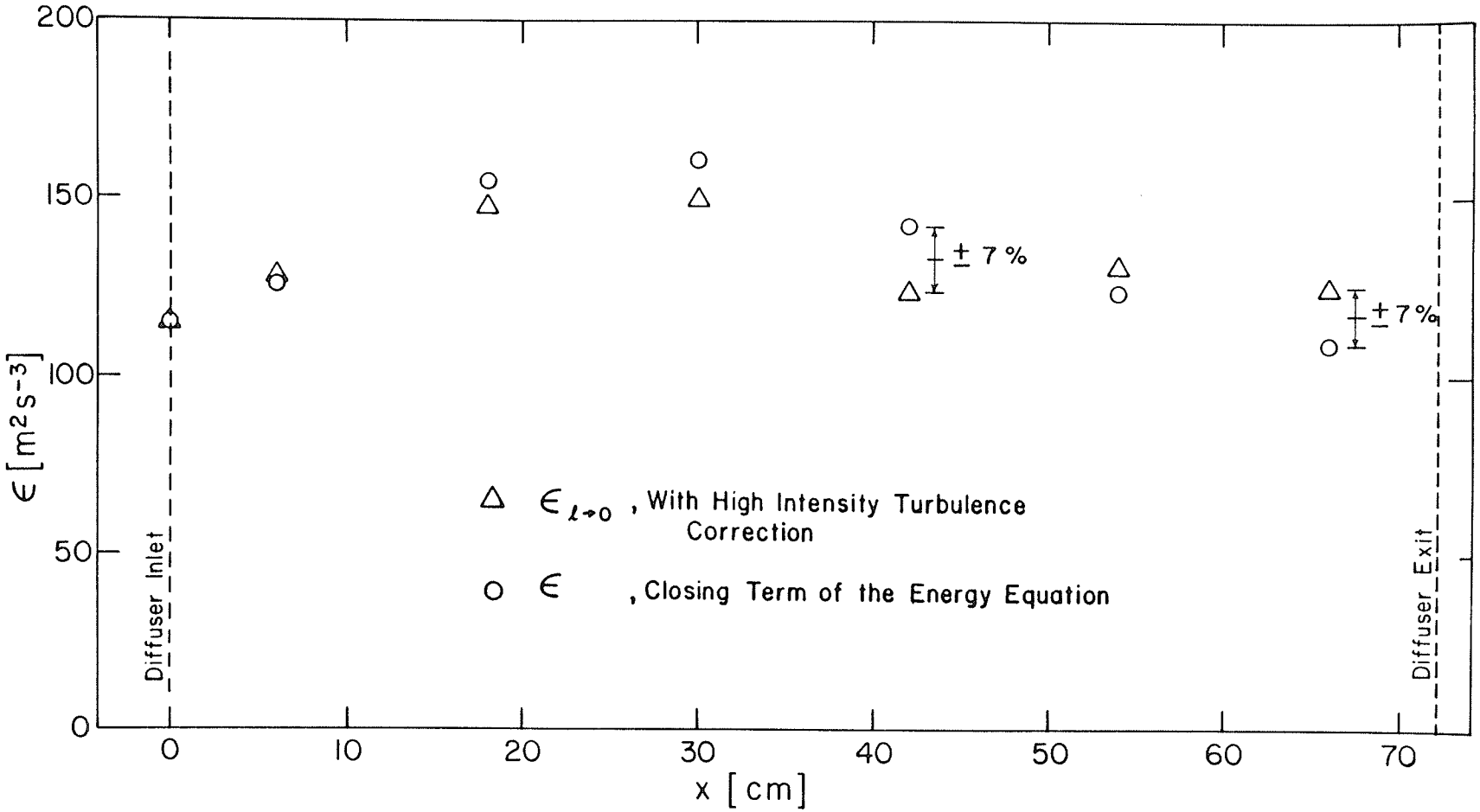

Figure 5.19 Area integrated value of dissipation rate obtained by extrapolation to zero length and then corrected for high intensity turbulence compared with the one obtained from the closing term of the turbulent energy equation.

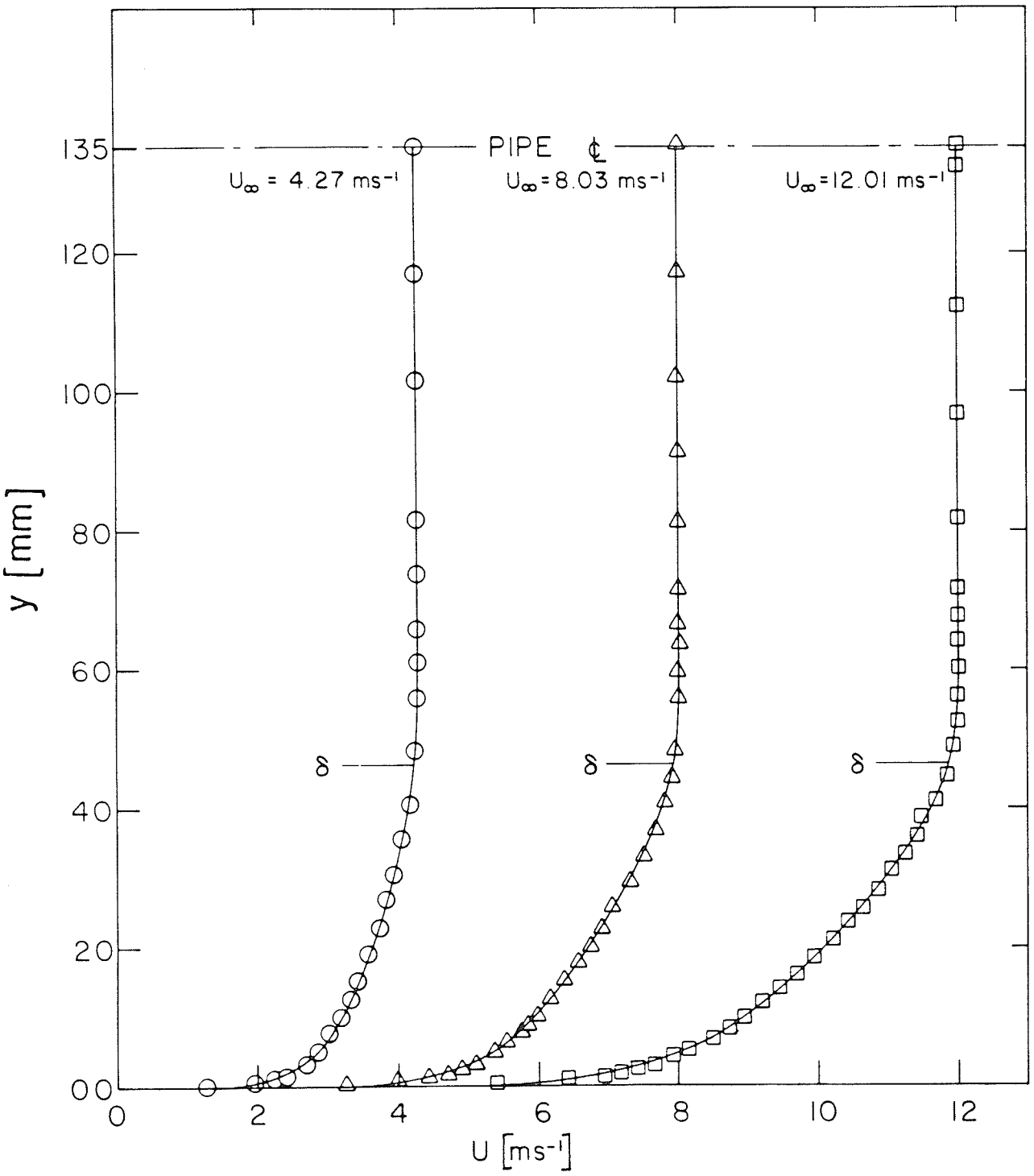

Figure 6.1 Mean velocity profiles for different free-stream velocities.

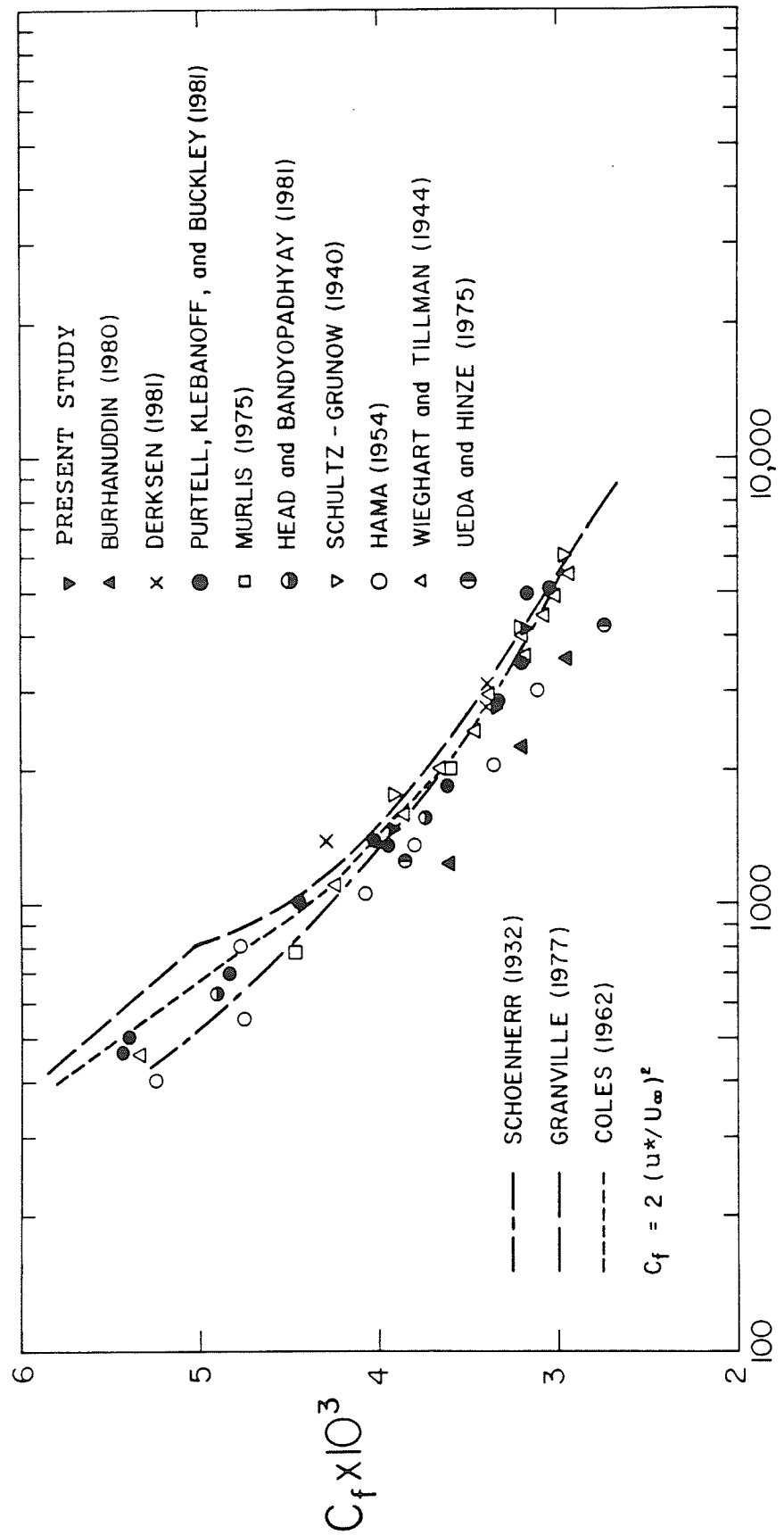

Figure 6.2 Skin friction coefficient variation with Reynolds number.

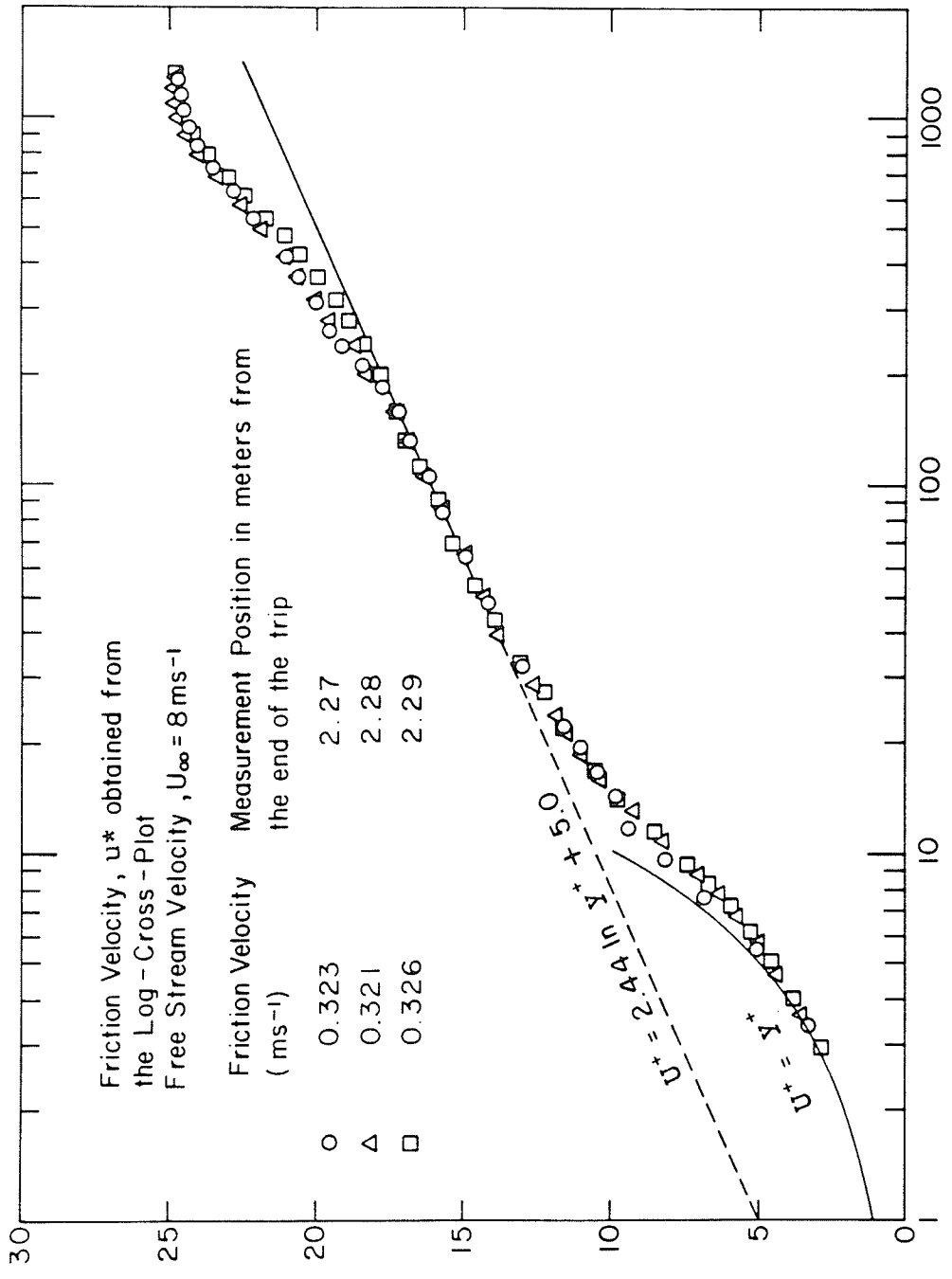

Figure 6.3 Distribution of U^+ versus y^+ in the boundary layer.

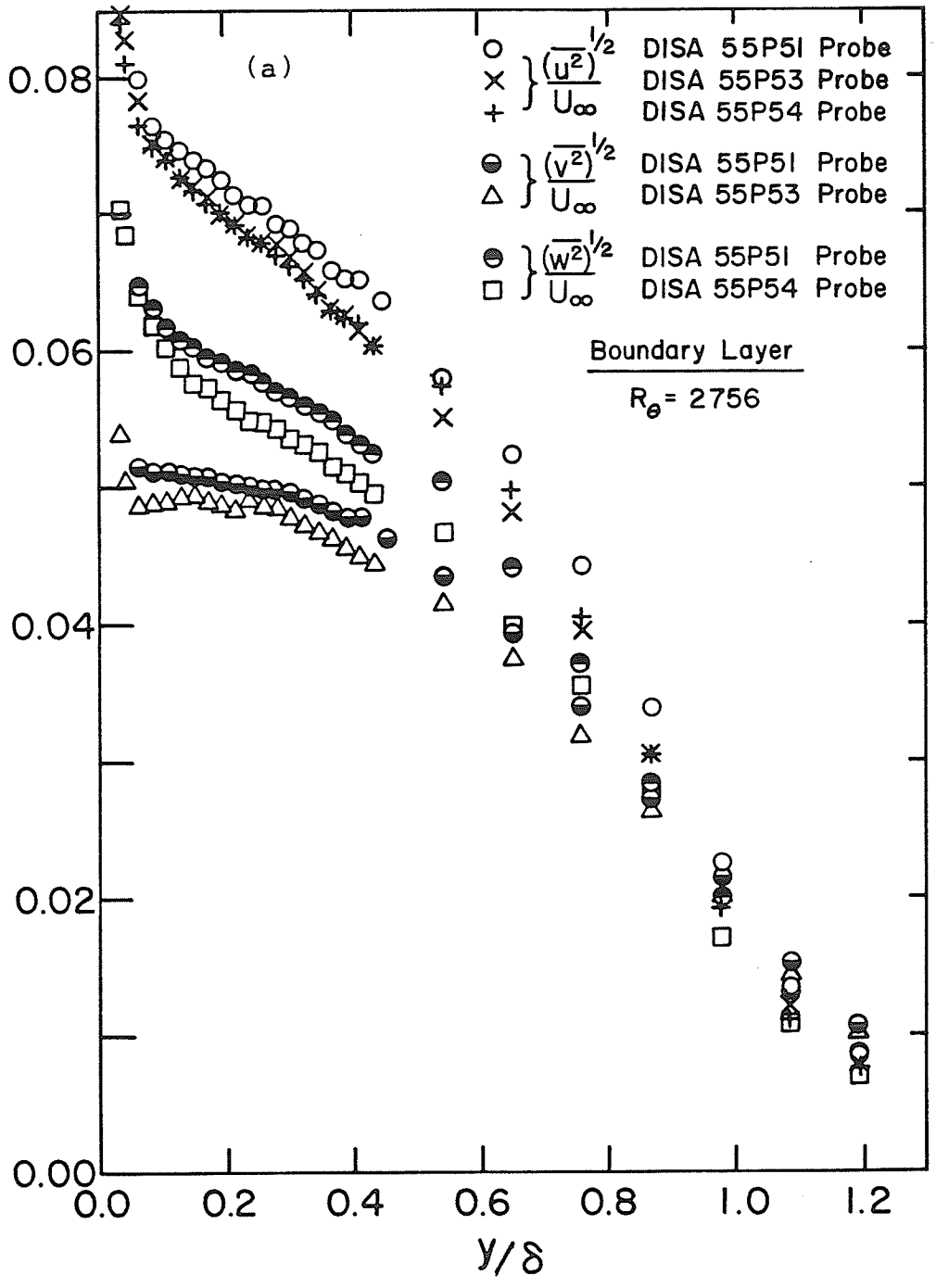

Figure 6.4 Distribution of the u, v, w fluctuations normalized by the free stream velocity. (a) Results away from the wall.

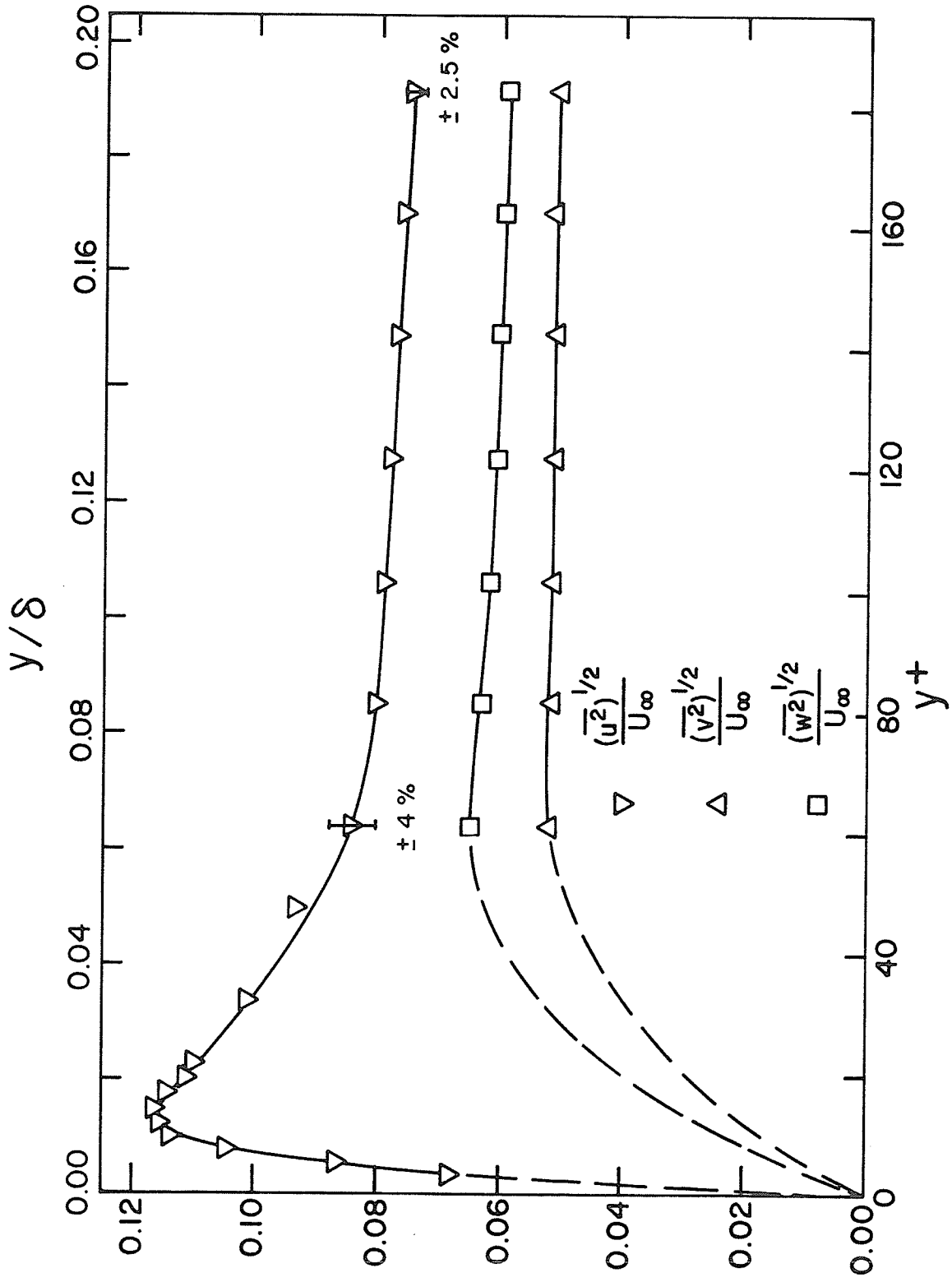

Figure 6.4 Distribution of the u, v, w fluctuations normalized by the free stream velocity. (b) Results in the vicinity of the wall.

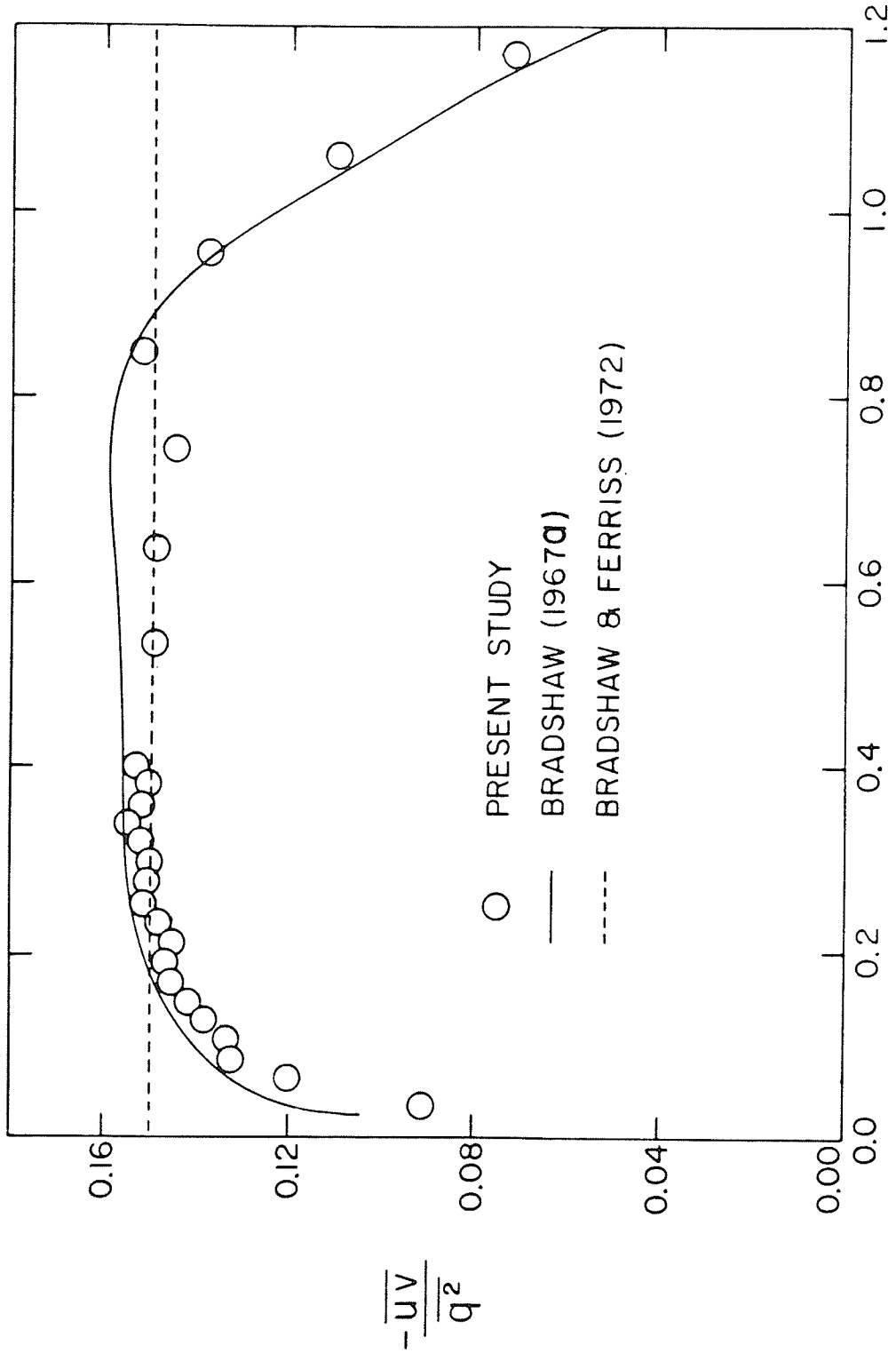

Figure 6.5 Distribution of stress-energy ratio across the boundary layer.

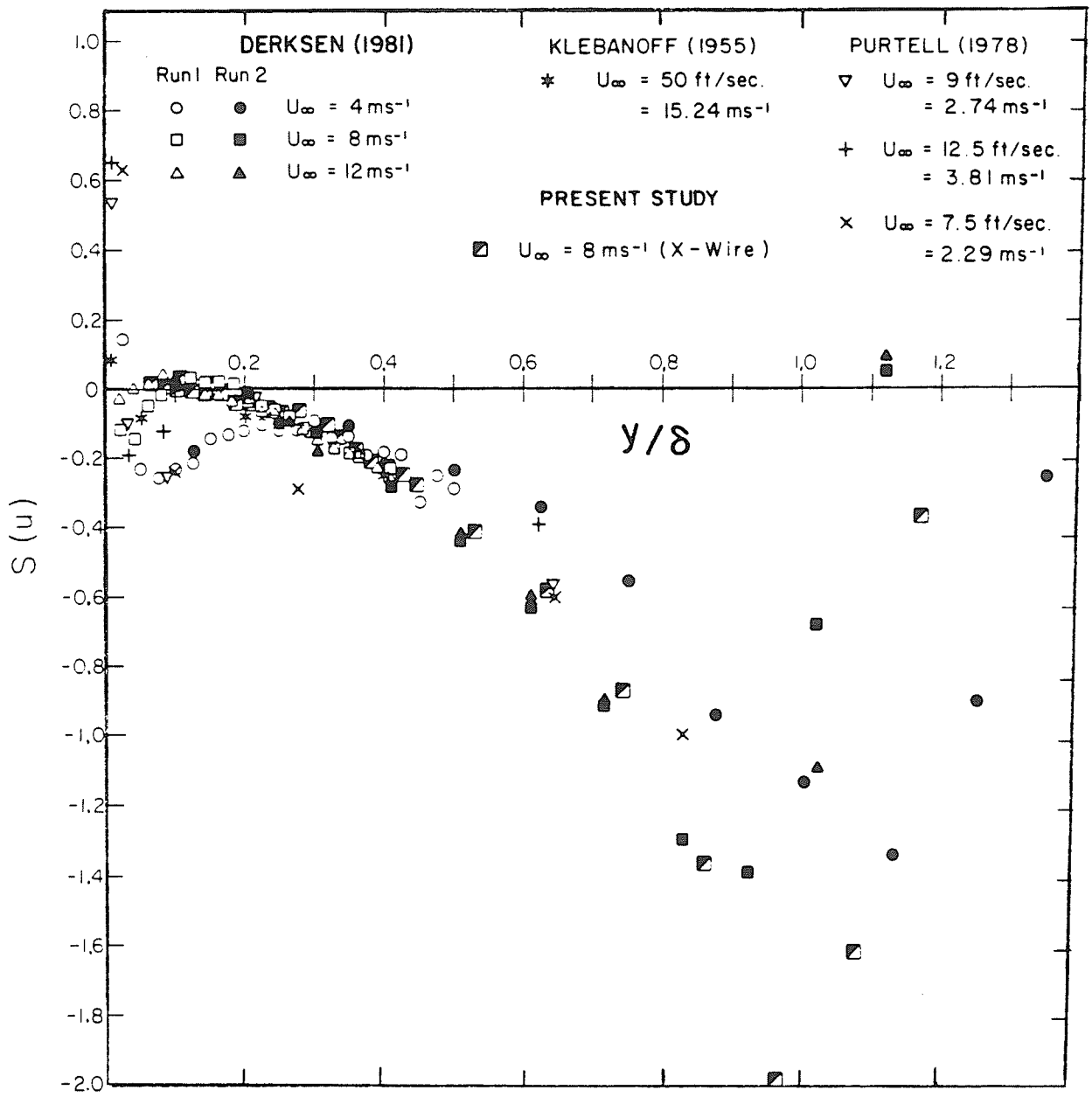

Figure 6.6 Skewness of u, $S(u) = \overline{u^3}/\overline{(u^2)^{3/2}}$.

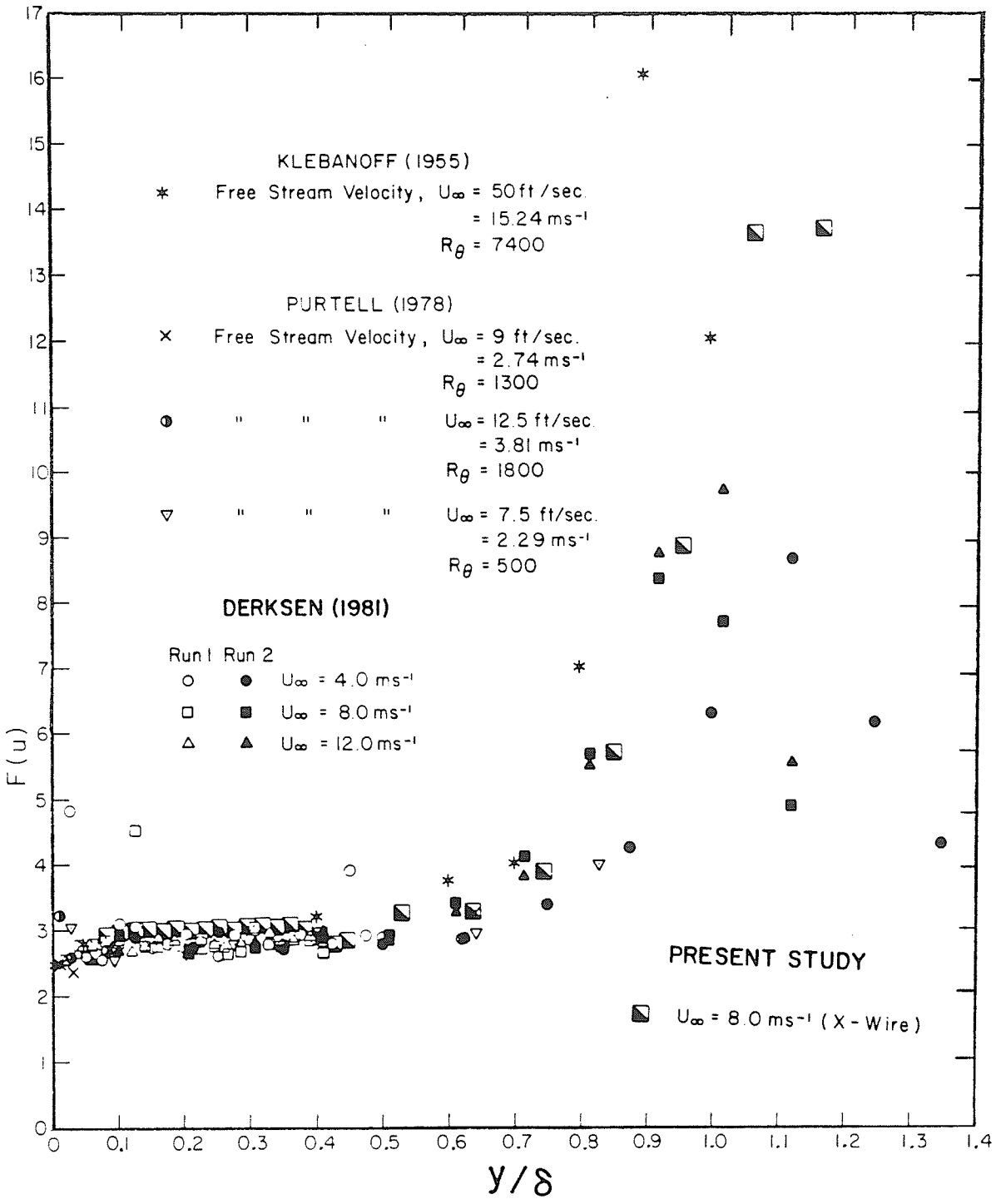

Figure 6.7 Flatness factor of u, $F(u) = \overline{u^4}/(\overline{u^2})^2$.

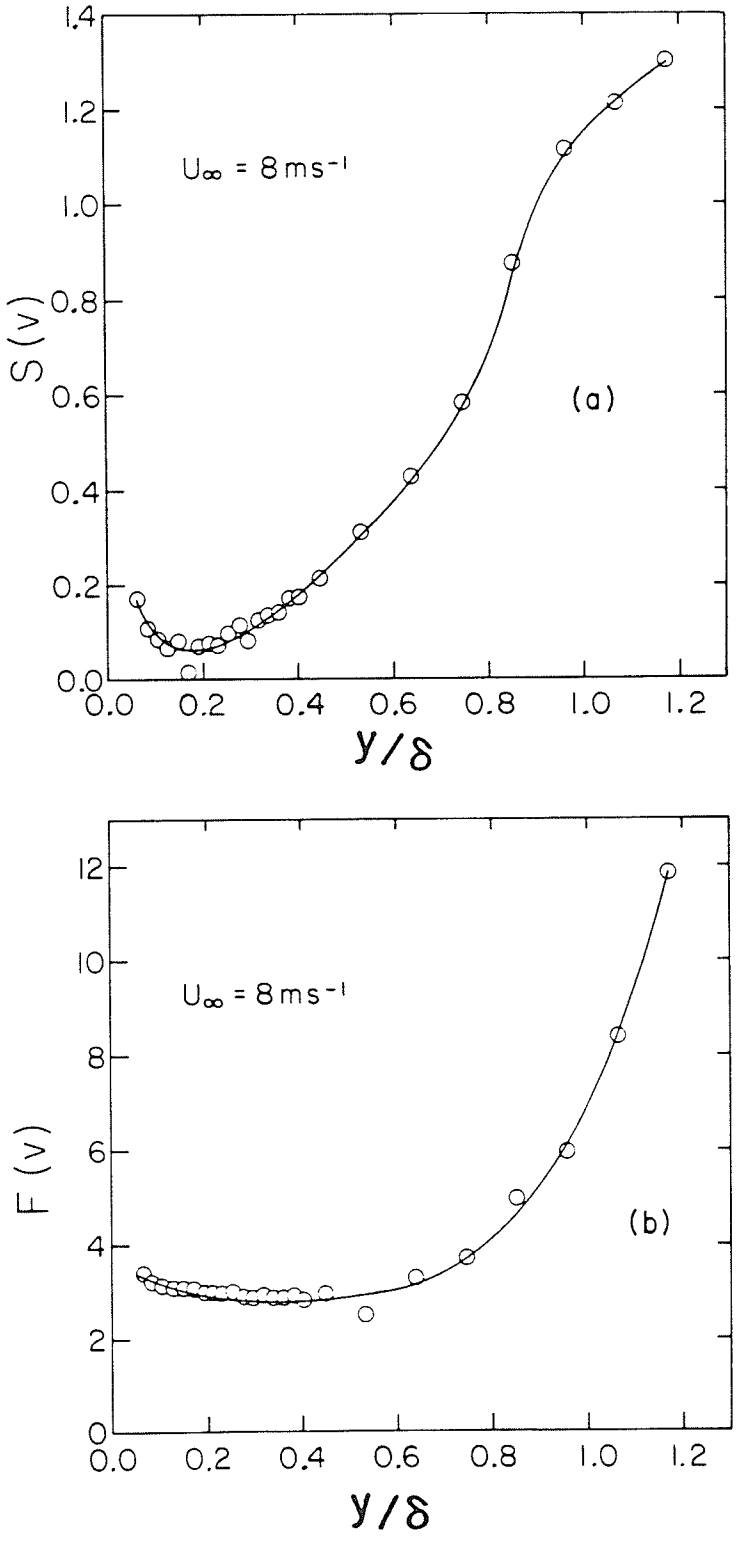

Figure 6.8 Higher-order moments of the normal fluctuating velocity component in the boundary layer.
(a) Third order.
(b) Fourth order.

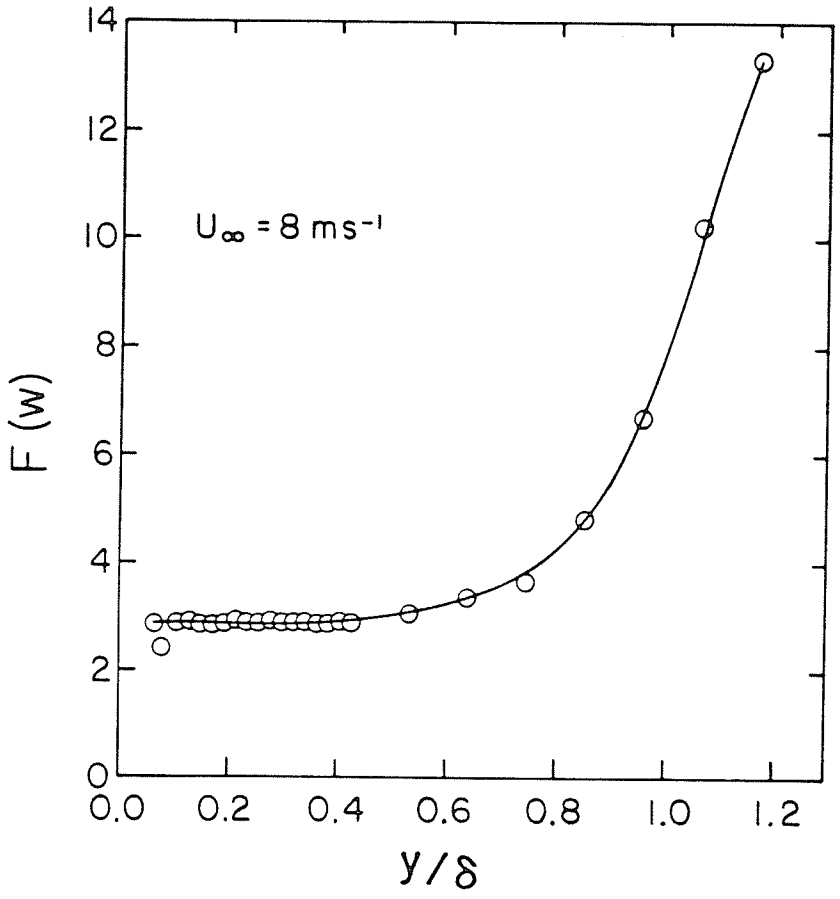

Figure 6.9 Flatness factor of w, $F(w) = \overline{w^4}/\overline{(w^2)^2}$

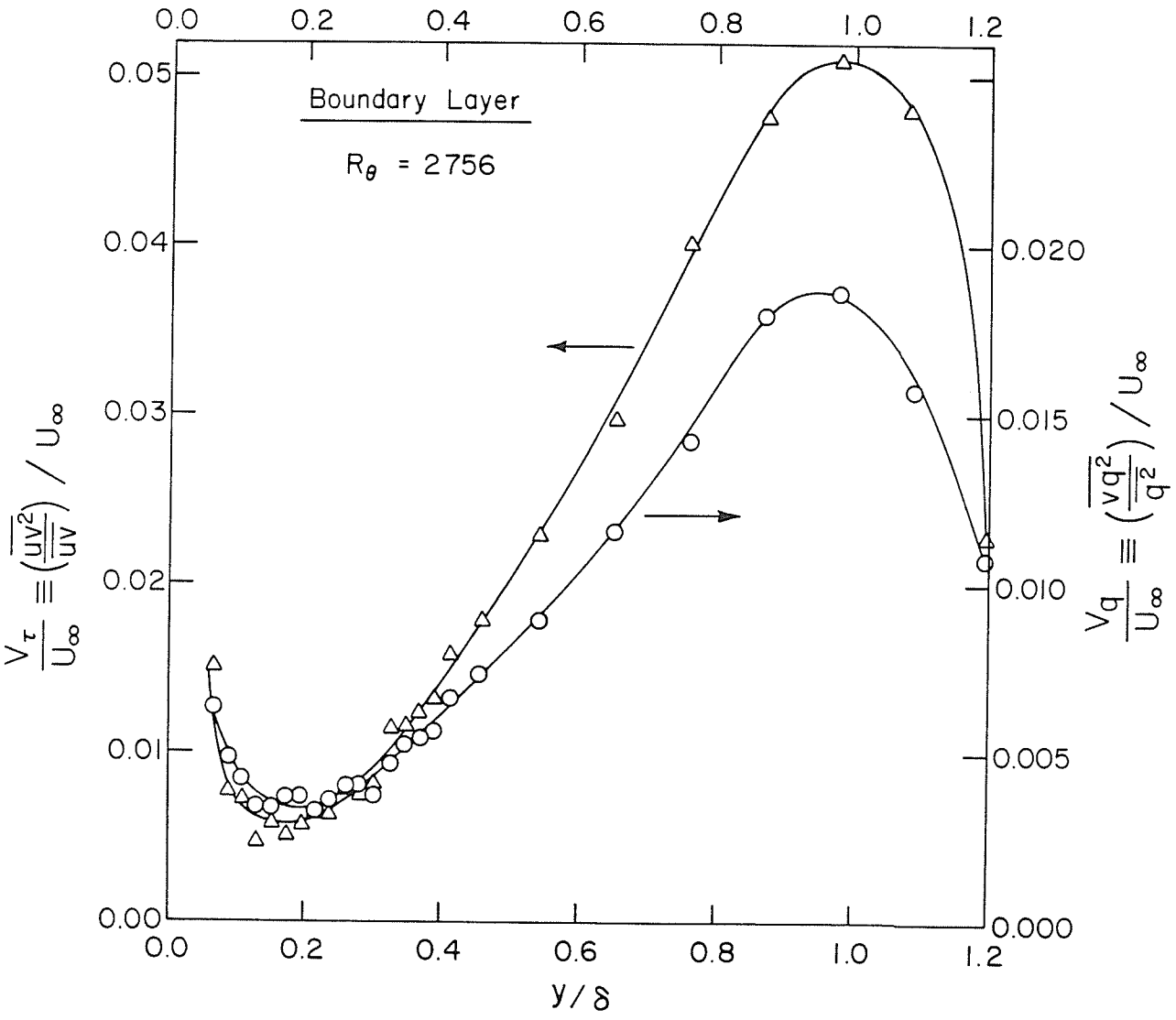

Figure 6.10 Profiles of turbulent transport velocity of $\overline{q^2}$, $V_q = \overline{vq^2}/\overline{q^2}$ and of $\overline{uv}$, $V_\tau = \overline{uv^2}/\overline{uv}$, expressed nondimensionally in relation to U_∞.

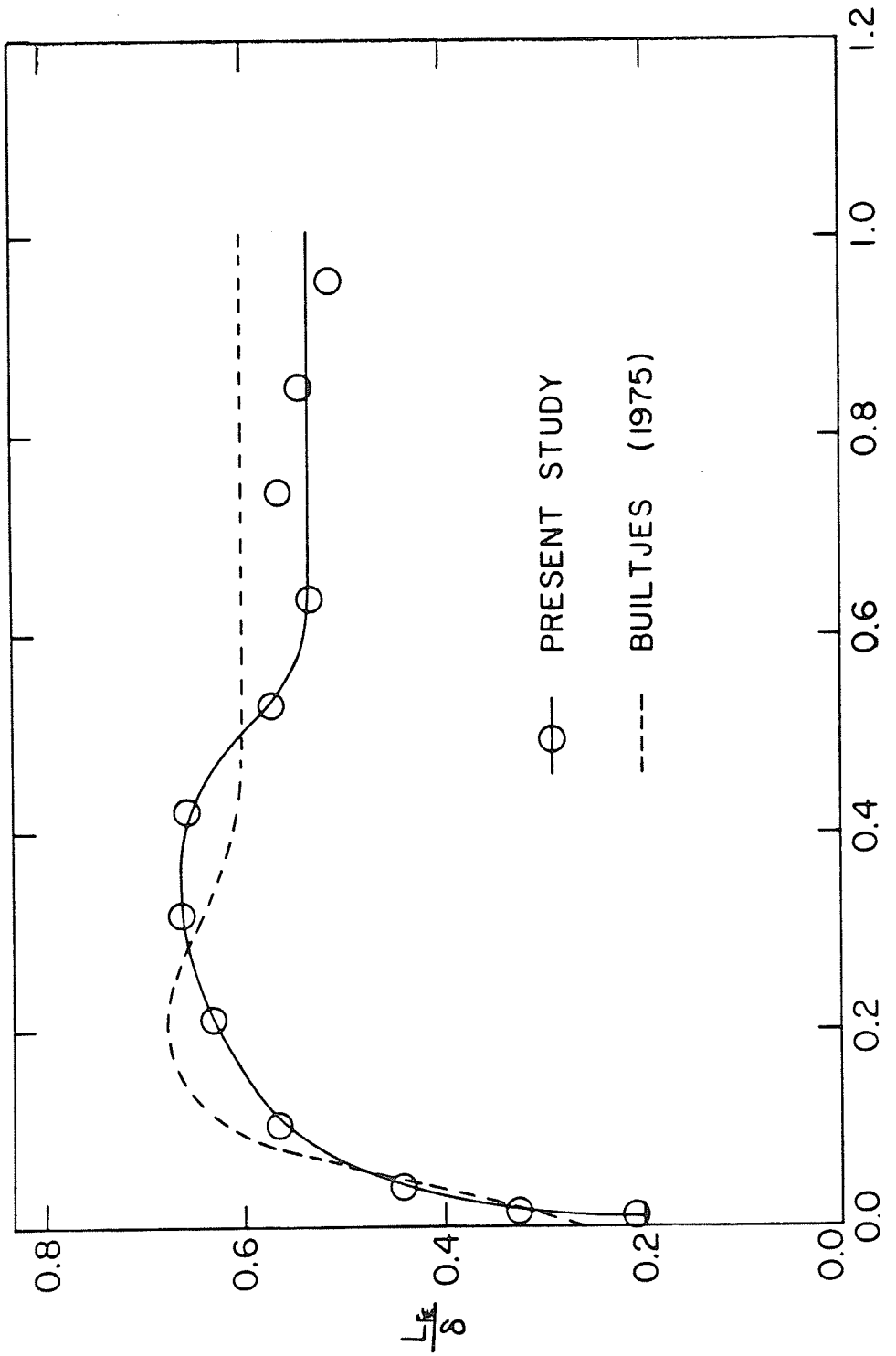

Figure 6.11 The integral scale of the longitudinal turbulent component velocity.

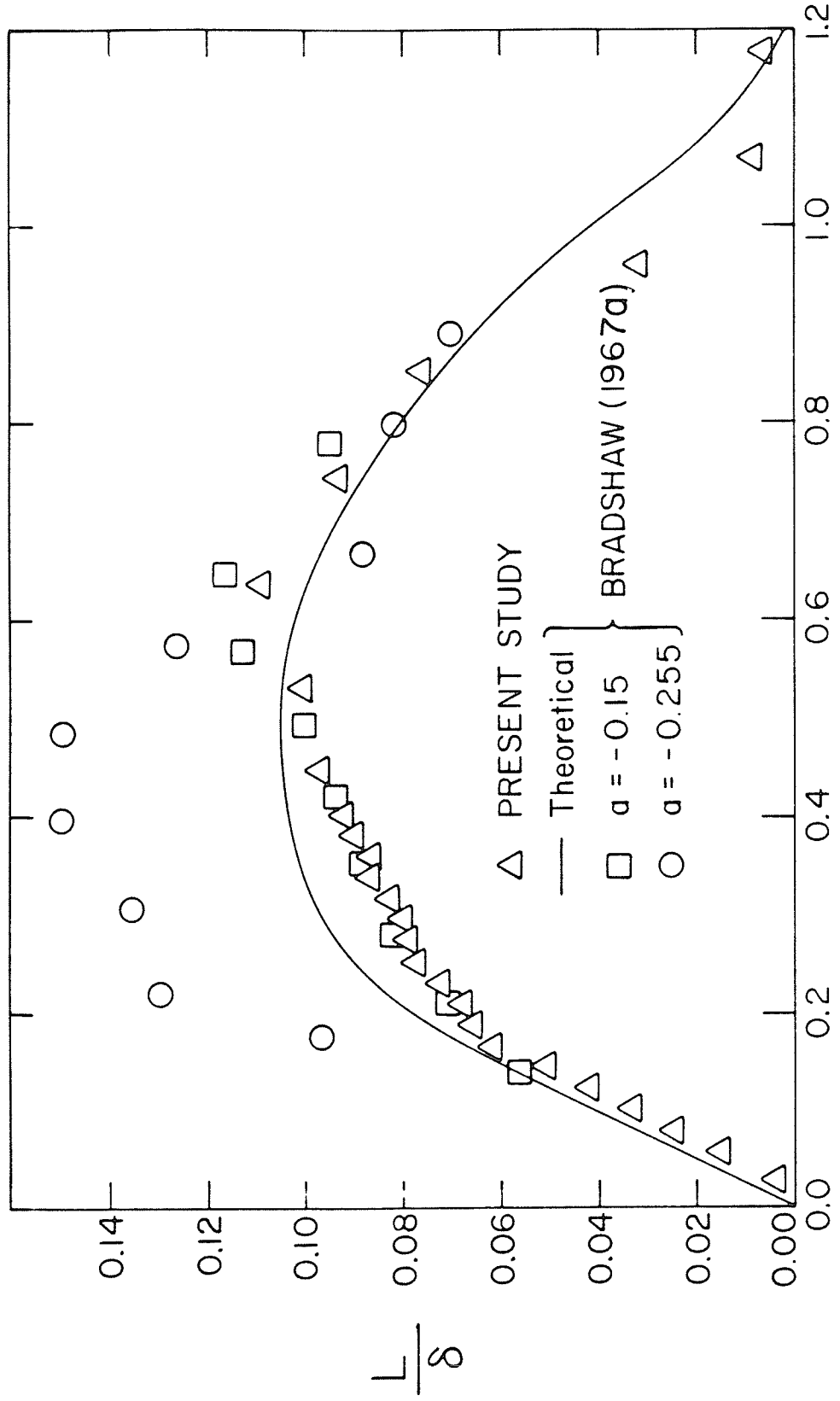

Figure 6.12 Dissipation length parameter, $L = \overline{(-uv)^{3/2}}/\epsilon$, expressed nondimensionally in relation to δ.

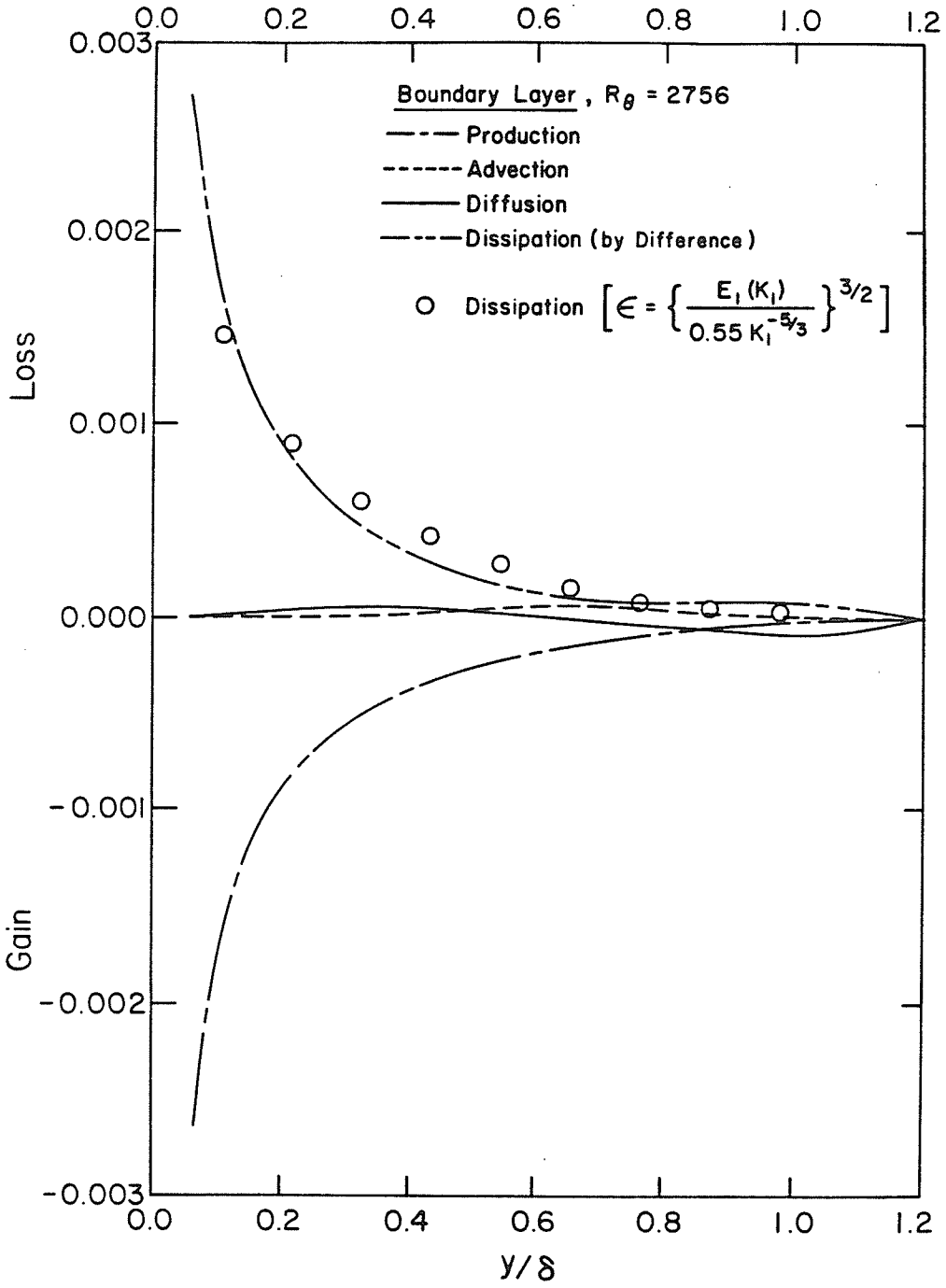

Figure 6.13 Turbulent energy balance across the boundary layer, all terms made dimensionless by U_∞^3/δ.

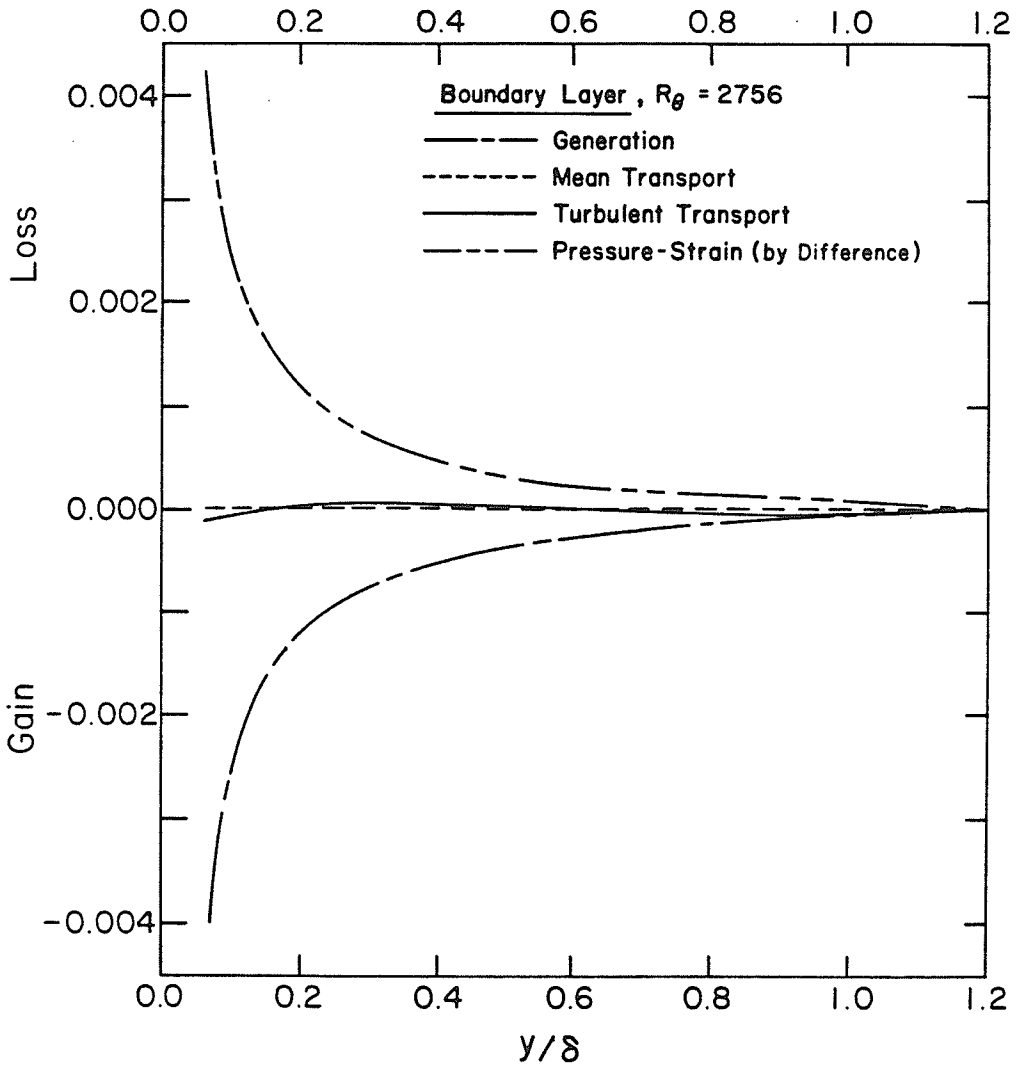

Figure 6.14 Shear stress balance across the boundary layer, all terms made dimensionless by U_∞^3/δ.

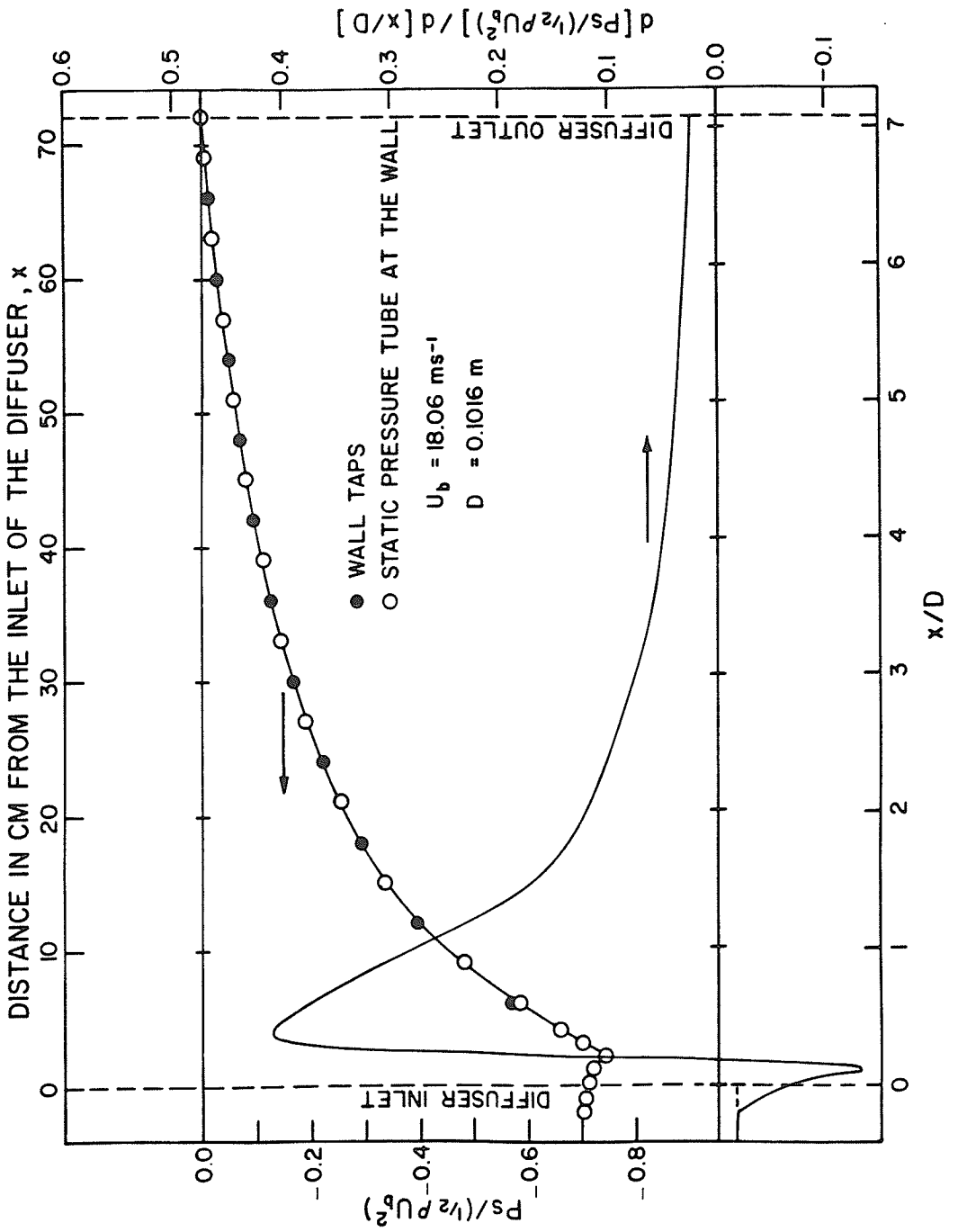

Figure 7.1 Surface pressure and its gradient in fully developed pipe flow and in diffuser flow.

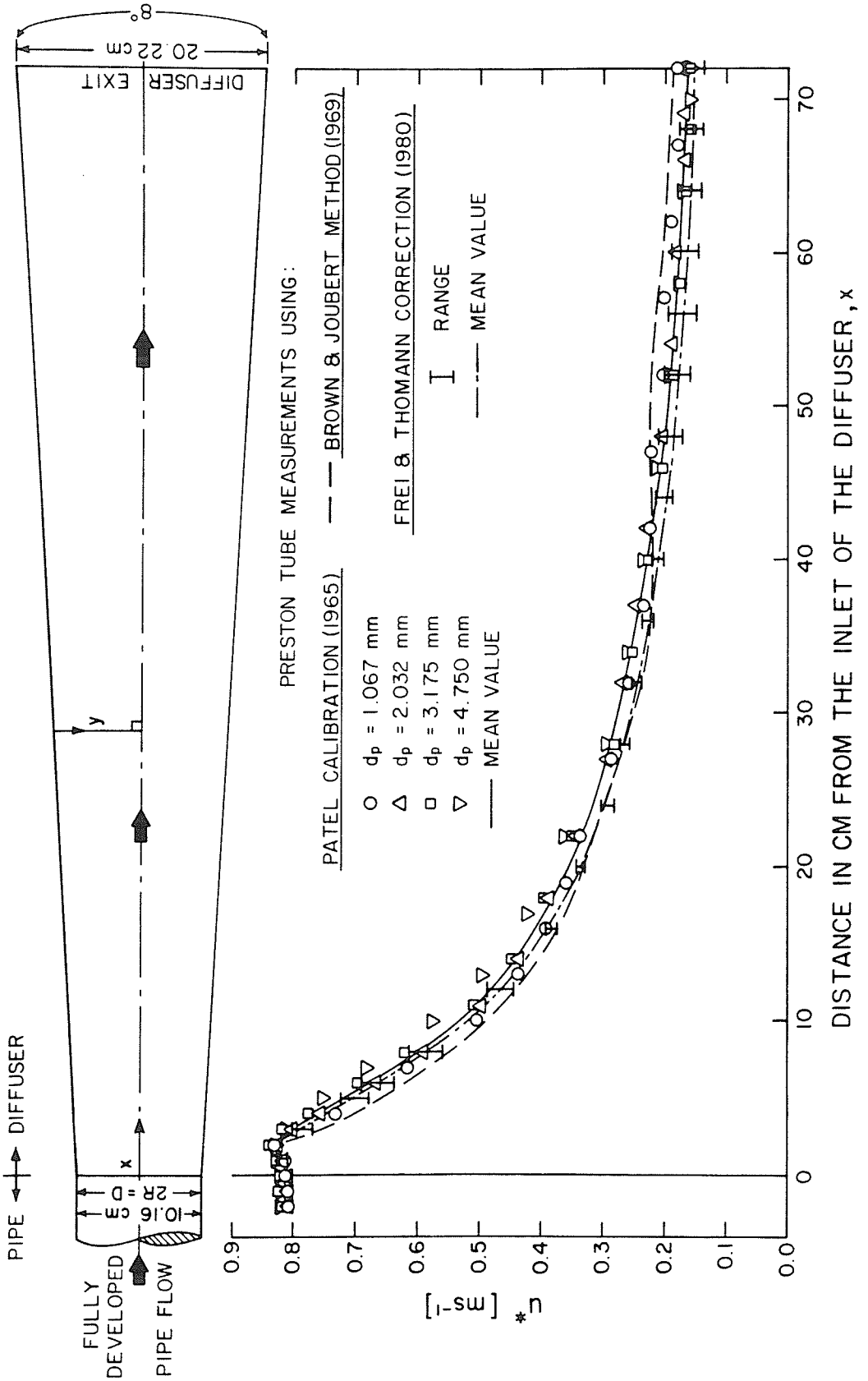

Figure 7.2 Friction velocity in fully developed pipe flow and in conical diffuser flow.

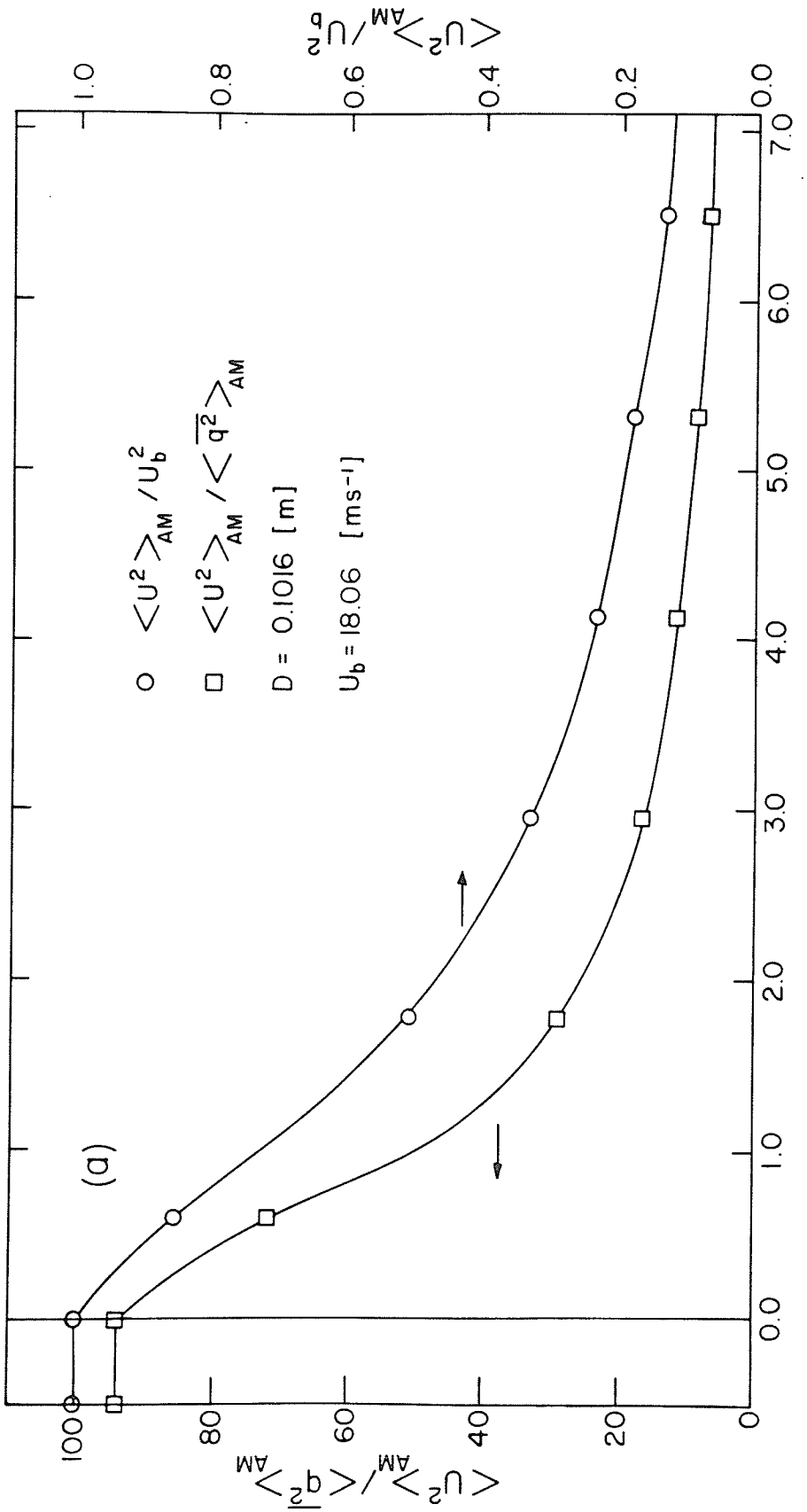

Figure 7.3a Area weighted mean values of twice the mean and turbulent kinetic energies per unit mass along the axial distance of the diffuser.

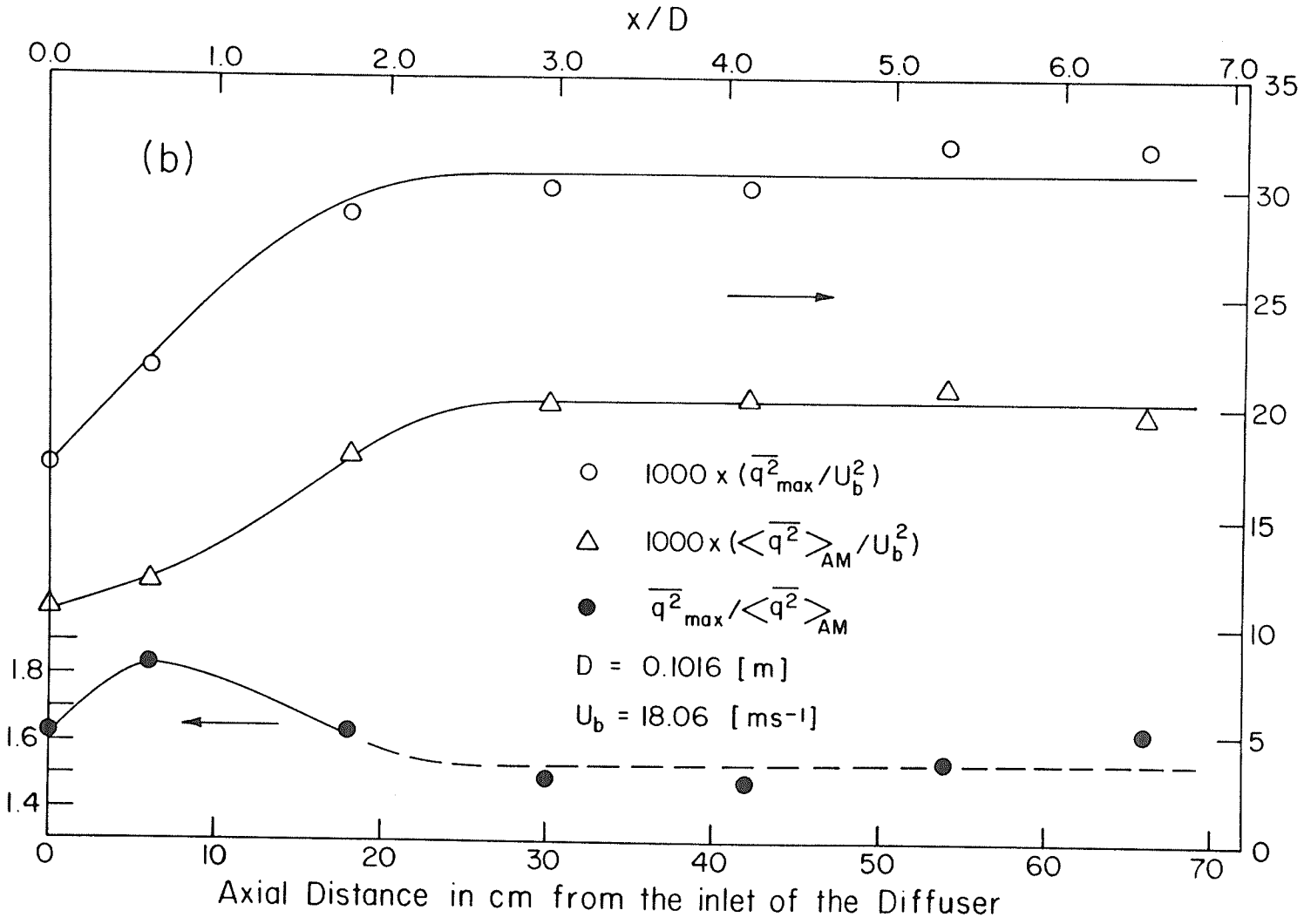

Figure 7.3b Variation of $\langle\overline{q^2}\rangle_{AM}$ and $\overline{q^2}_{max}$ along the axial length of the diffuser.

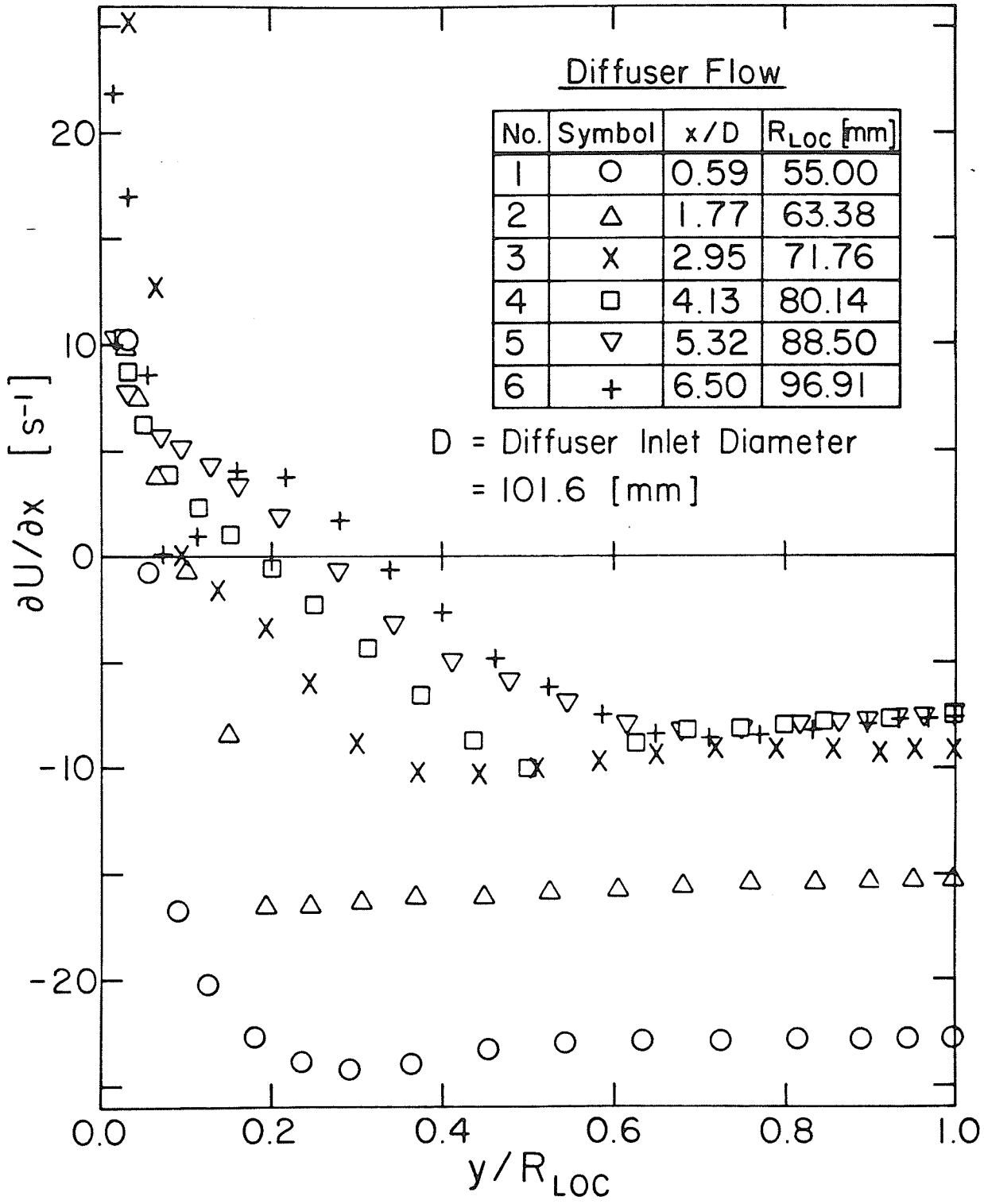

Figure 7.4 Rate of normal strain, $\partial U/\partial x$.

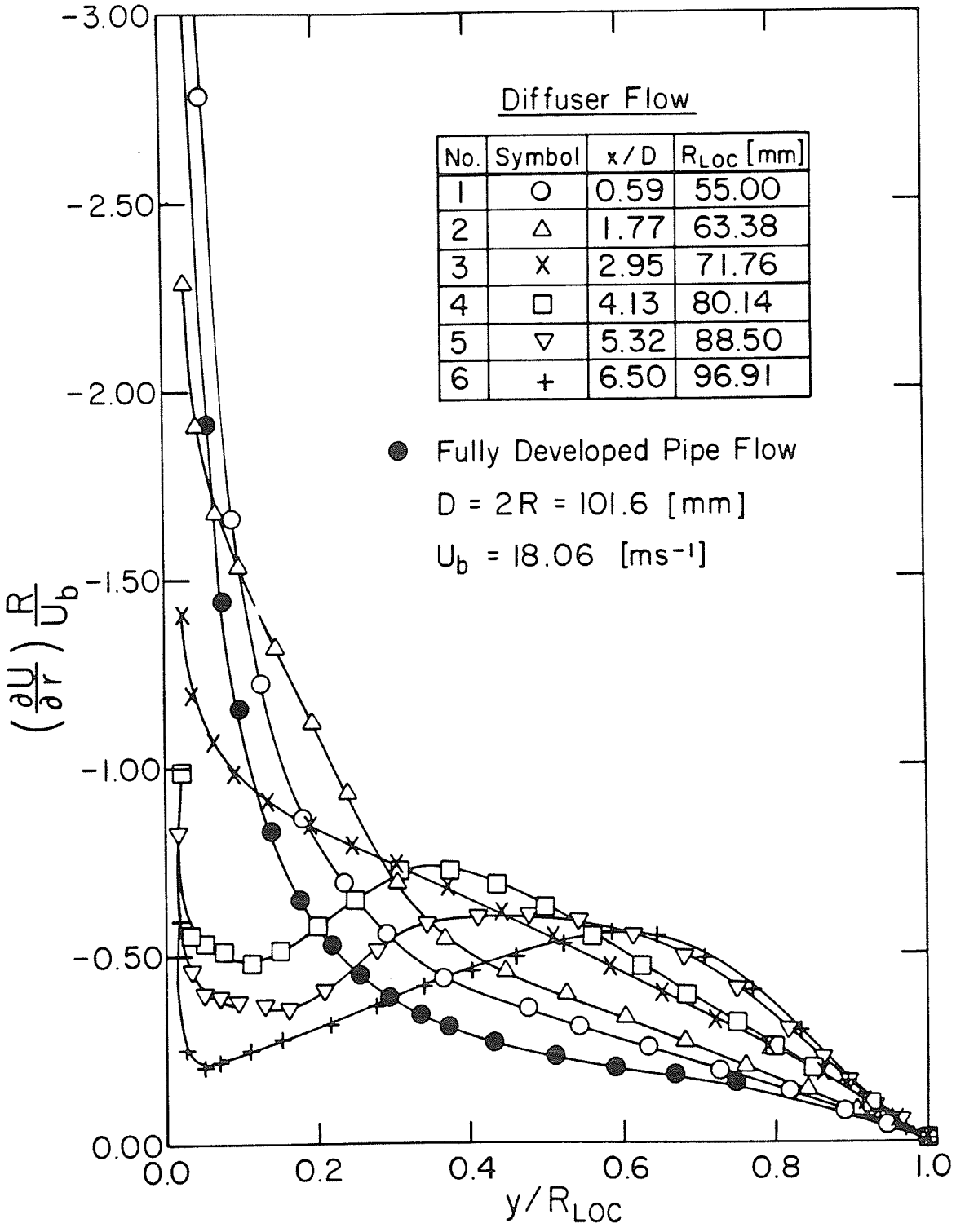

Figure 7.5 Basic rate of shear strain, ∂U/∂r.

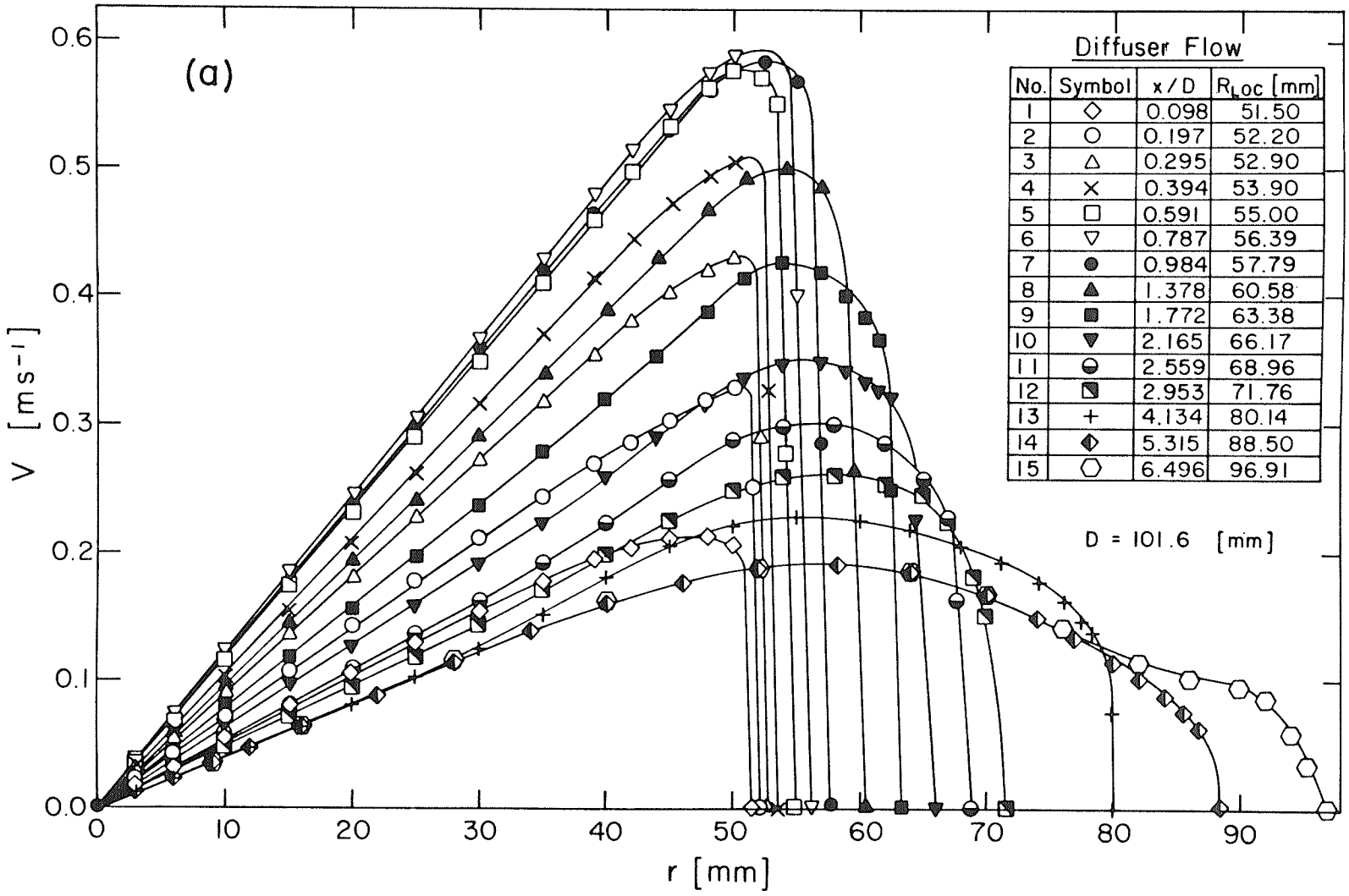

Figure 7.6a Transverse mean velocity V across different locations in the diffuser.

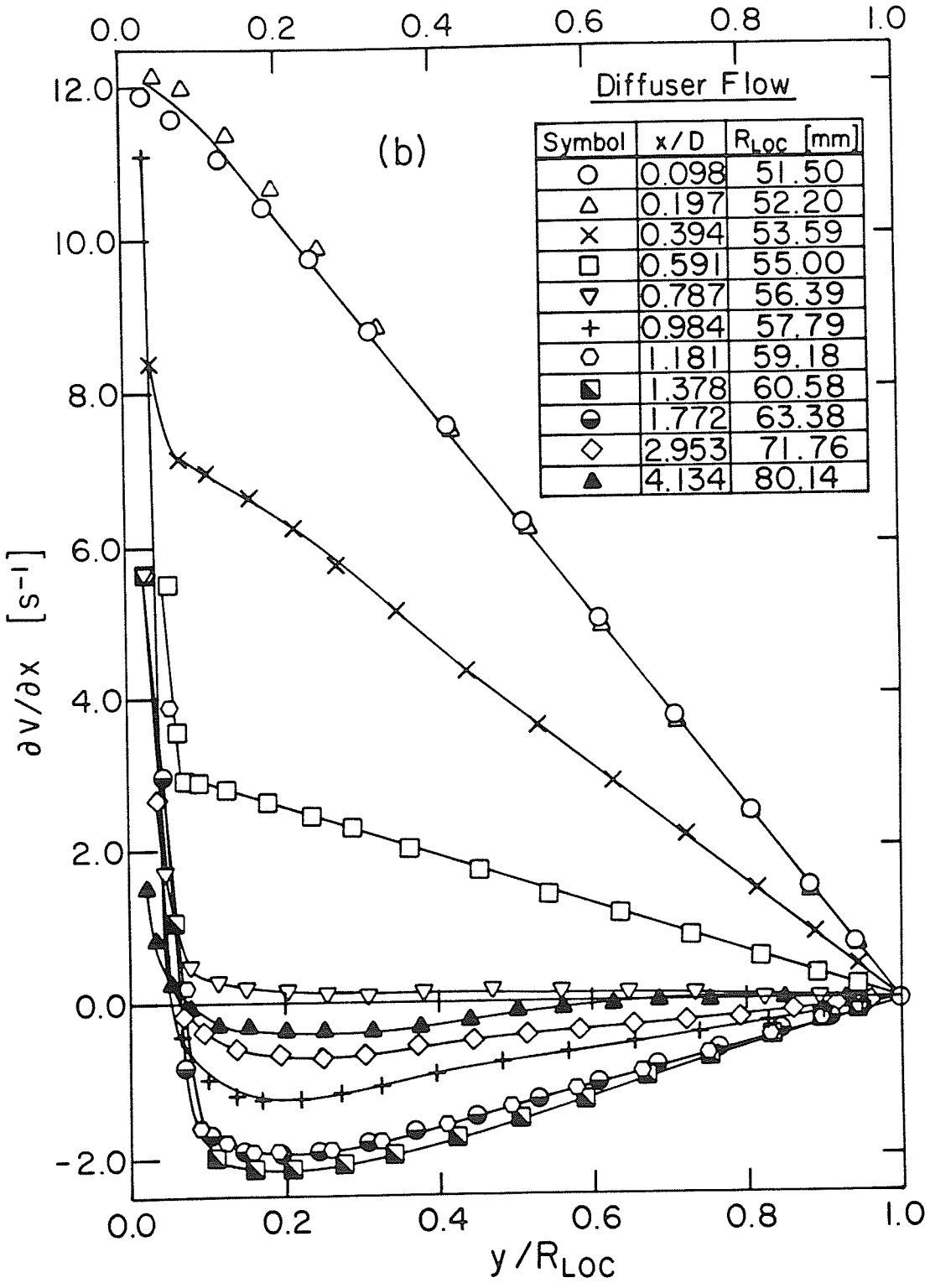

Figure 7.6b Extra strain-rate $\partial V/\partial x$ in the diffuser.

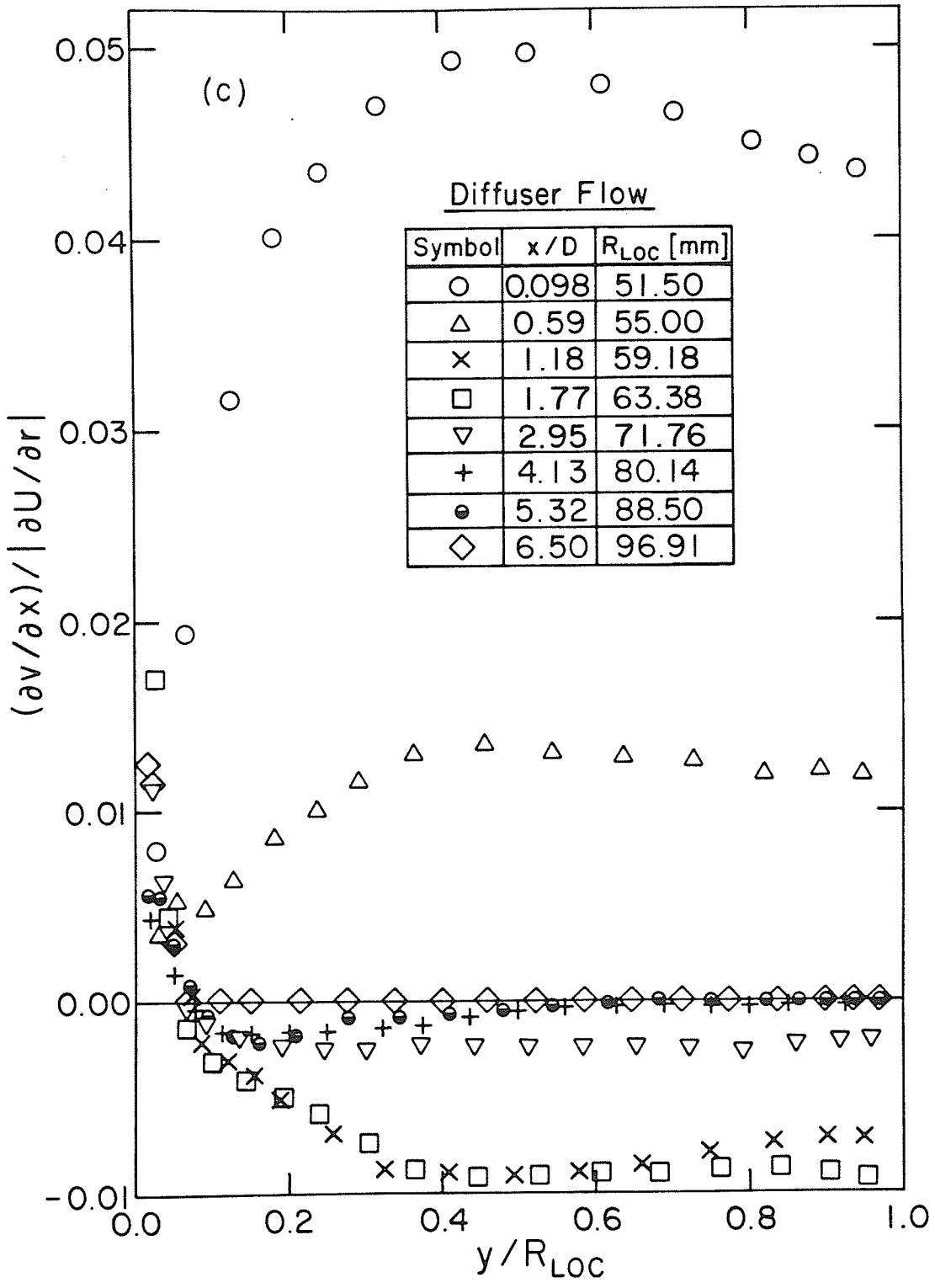

Figure 7.6c Extra strain-rate non-dimensionalized by main strain-rate in a diffuser flow.

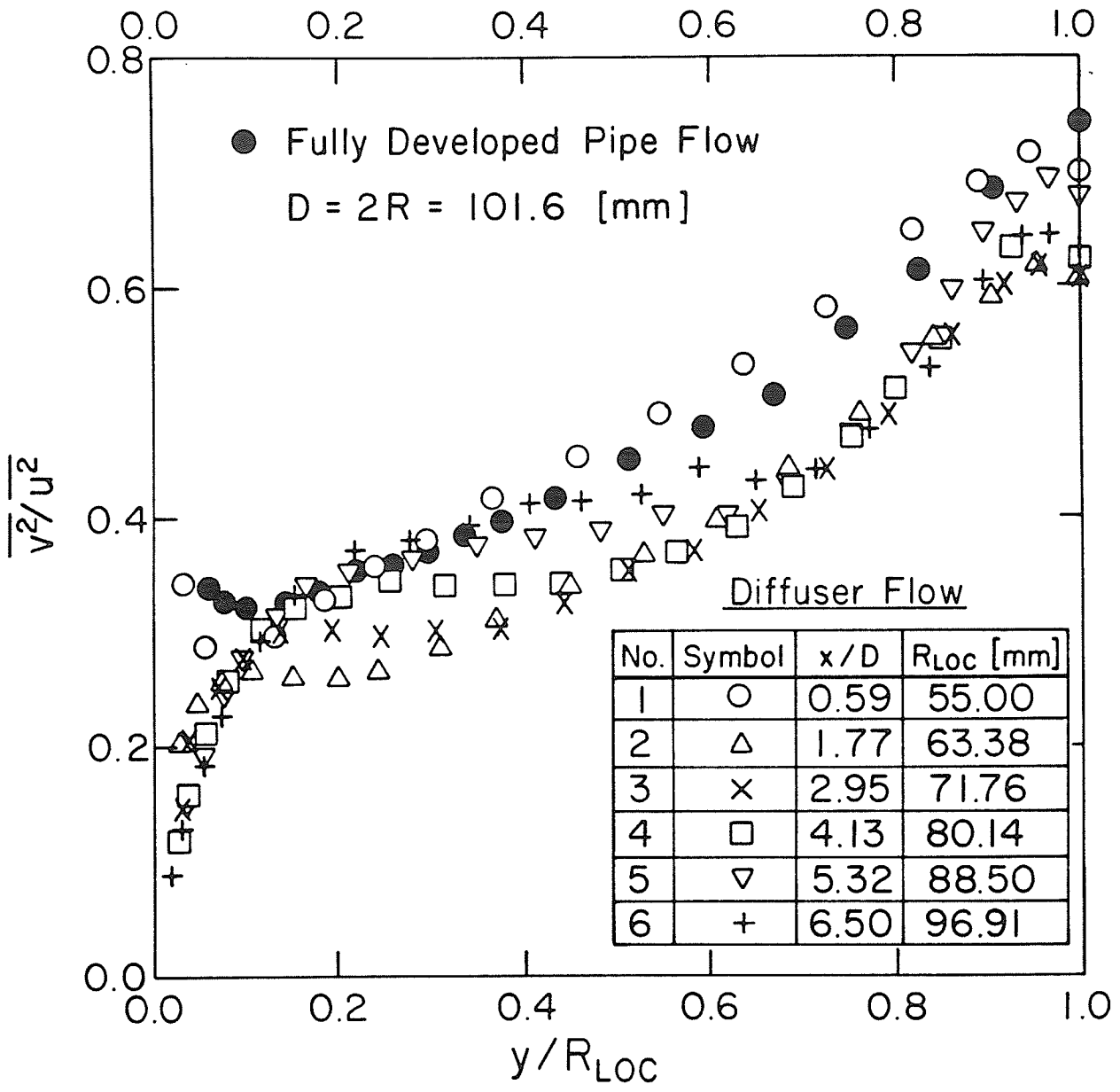

Figure 7.7 Ratio of transverse to longitudinal mean-square turbulent intensity in diffuser and pipe flow.

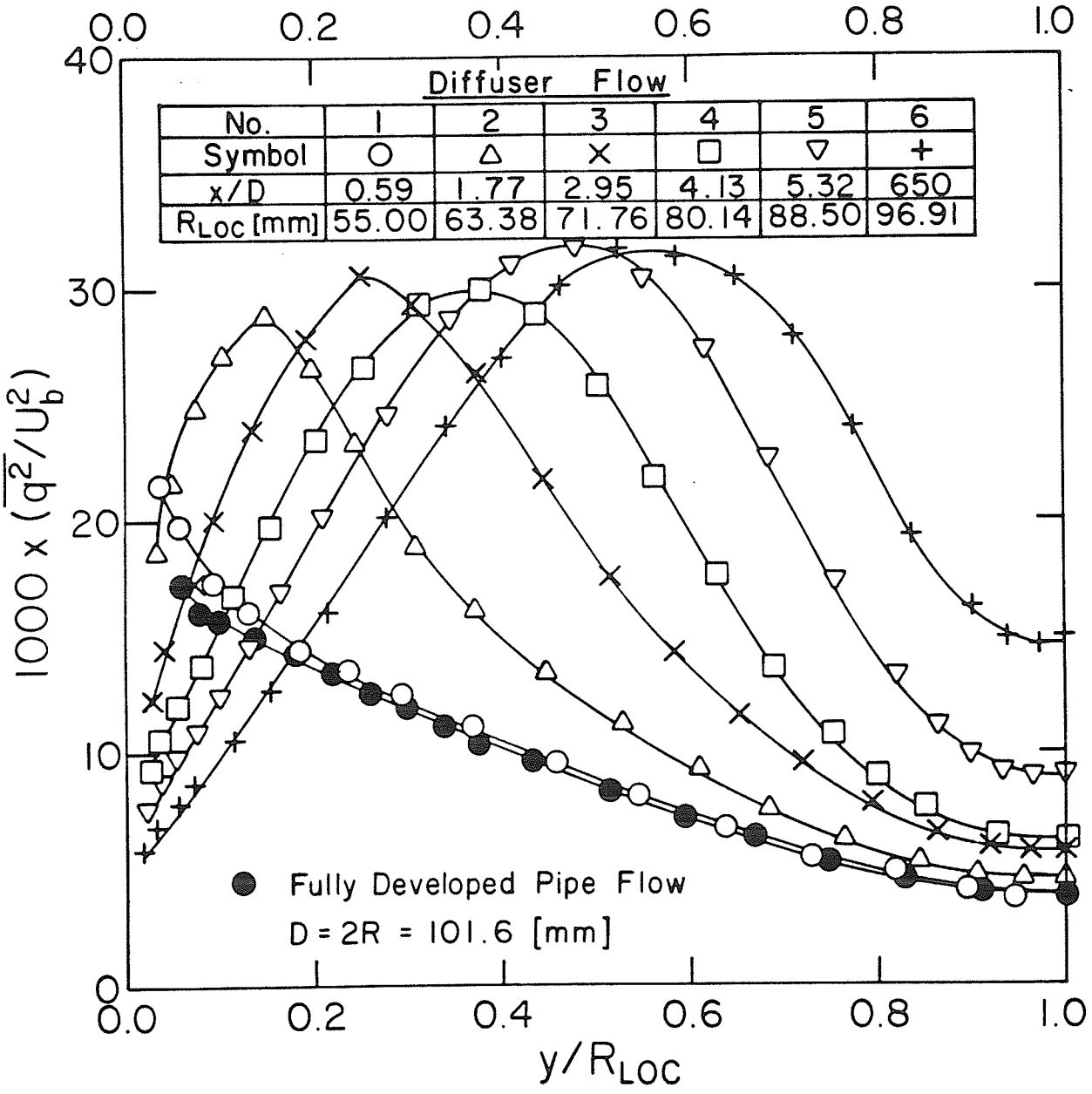

Figure 7.8 Profiles of turbulent energy $\overline{q^2} = 0.5(\overline{u^2}+\overline{v^2}+\overline{w^2})$.

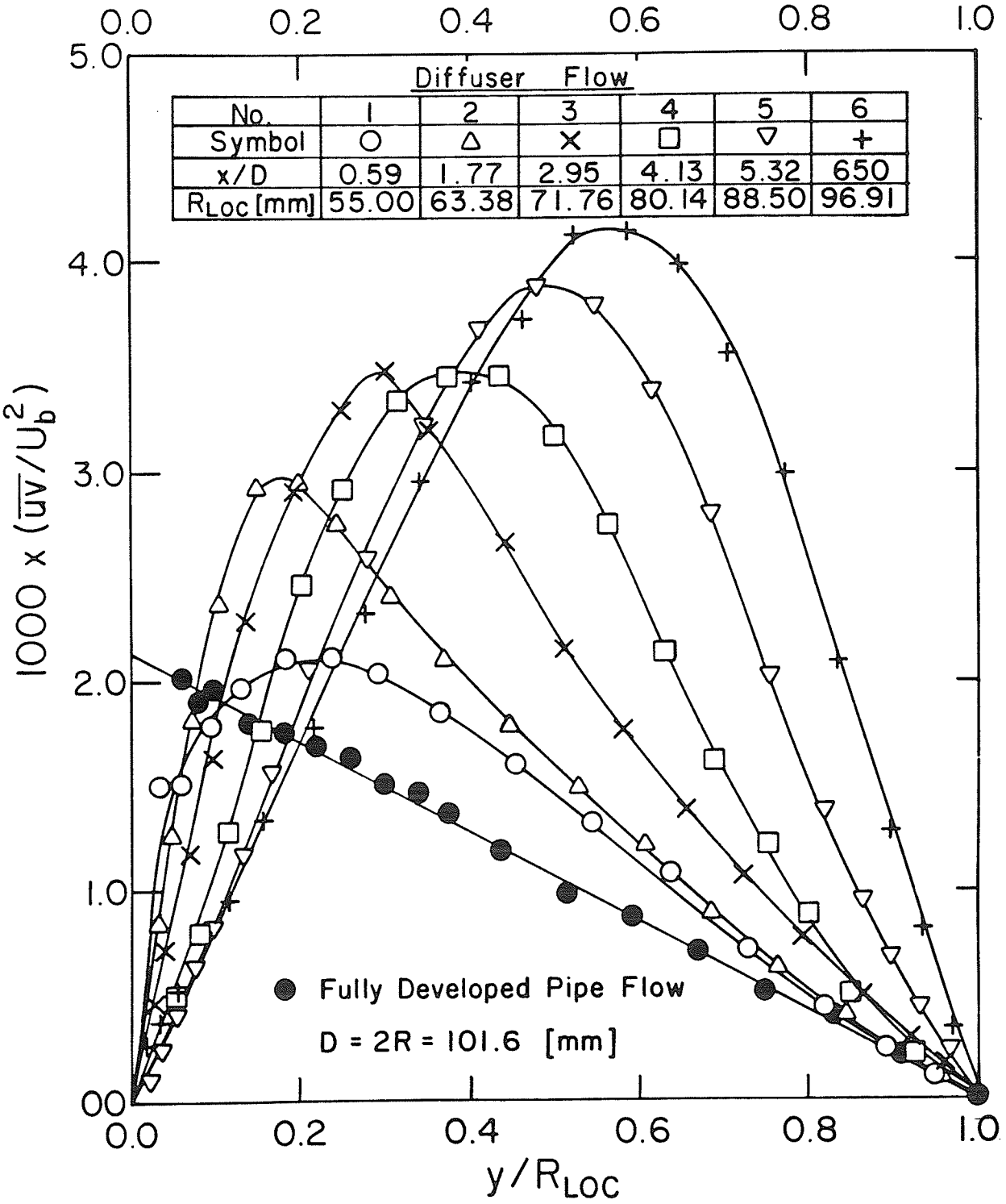

Figure 7.9 Shear-stress profiles.

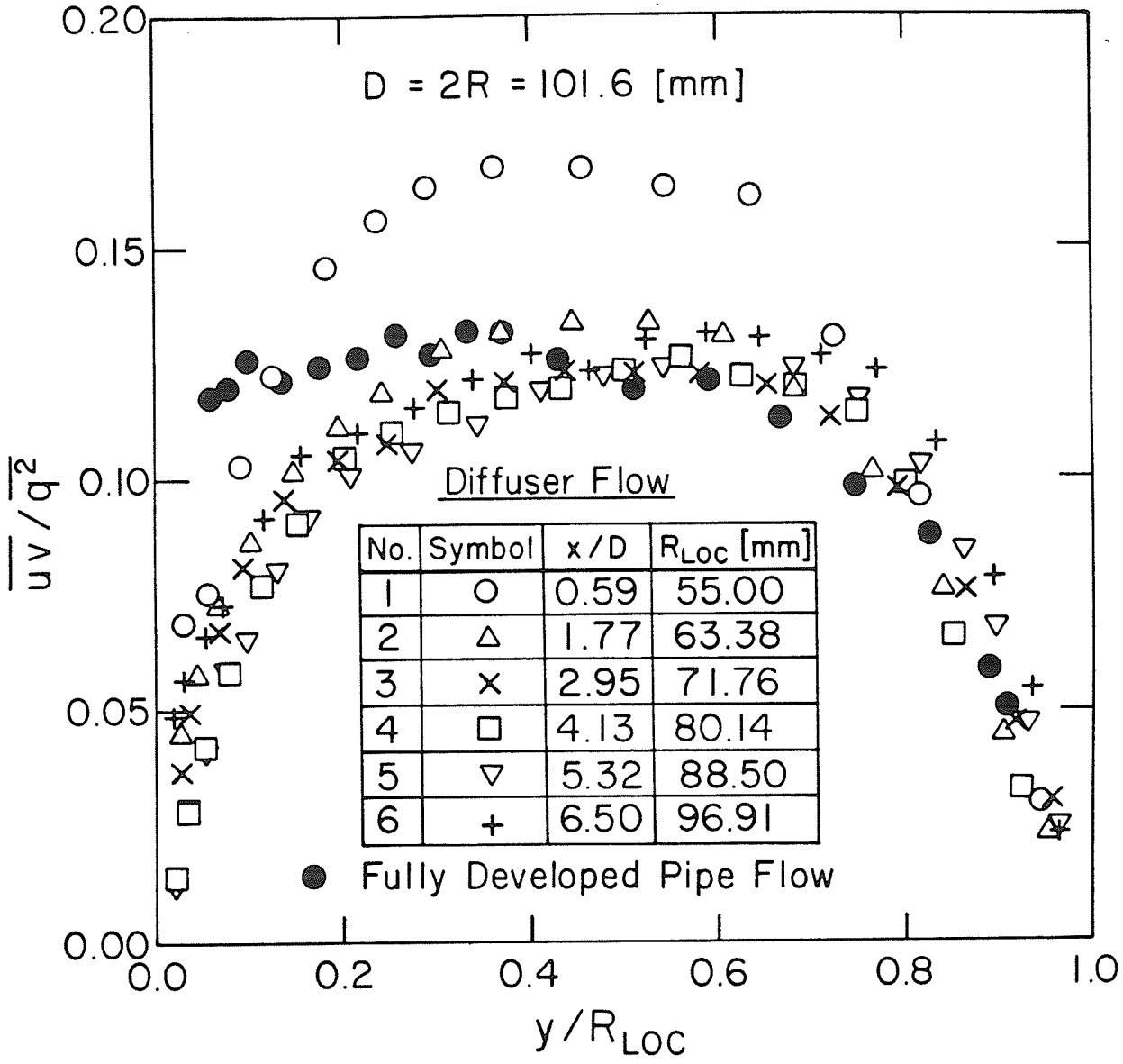

Figure 7.10 Stress-energy ratio $a_1 = \overline{uv}/\overline{q^2}$.

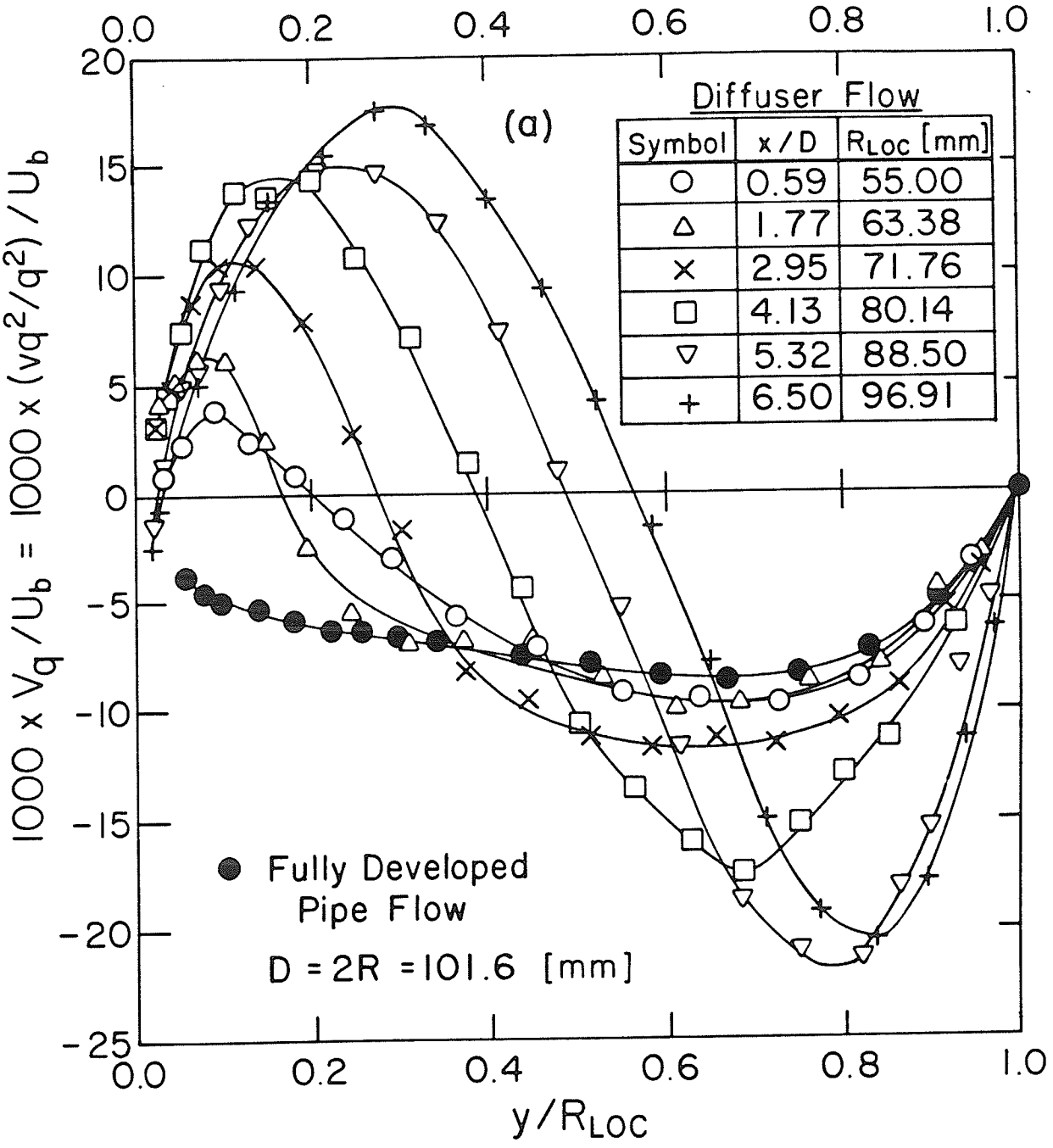

Figure 7.11a Profiles of turbulent transport velocity of $\overline{q^2}$, $V_q/U_b = \overline{vq^2}/(\overline{q^2}U_b)$.

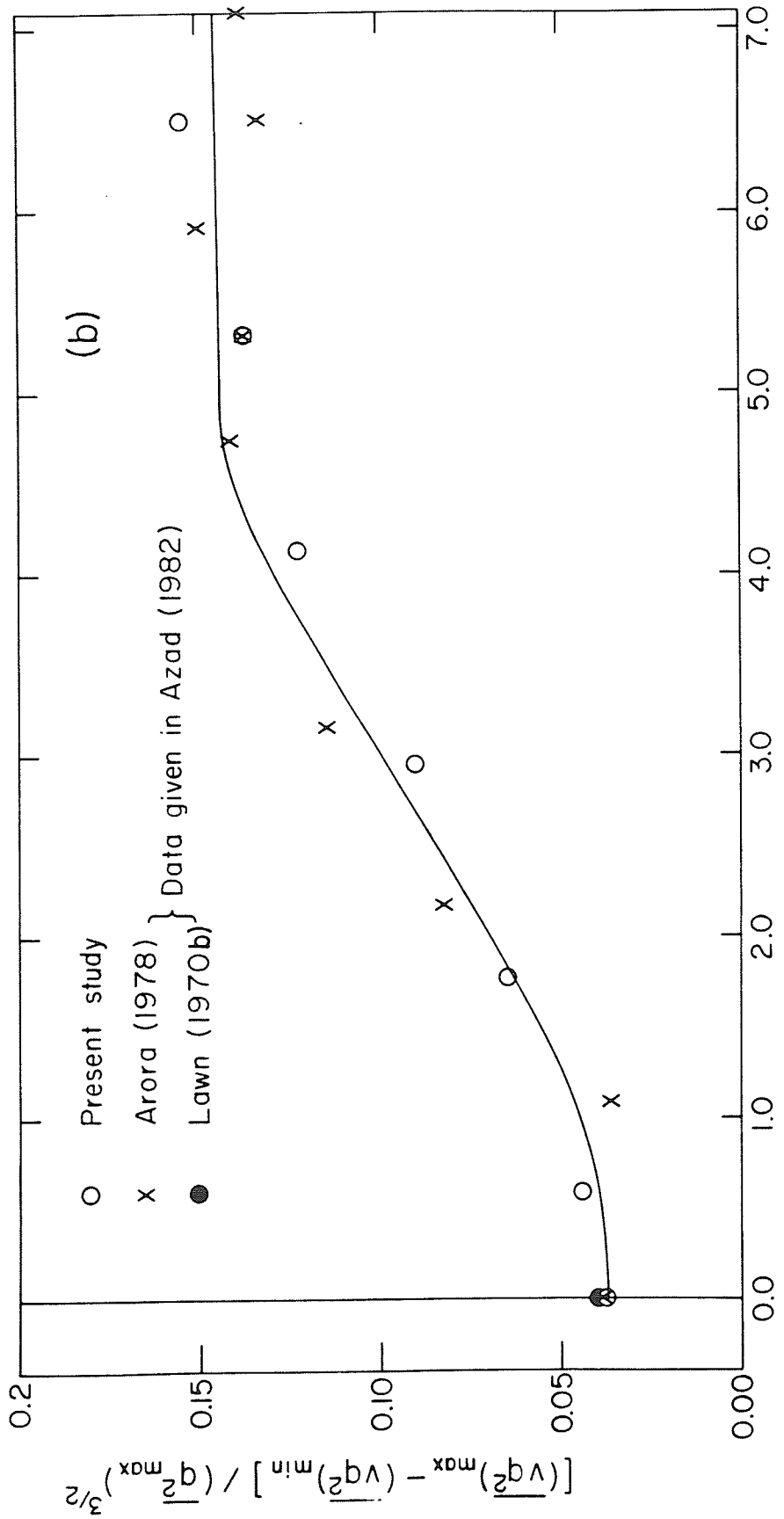

Figure 7.11b Relative strength of large eddies, $[(\overline{vq^2})_{max} - (\overline{vq^2})_{min}]/(\overline{q^2})^{3/2}_{max}$.

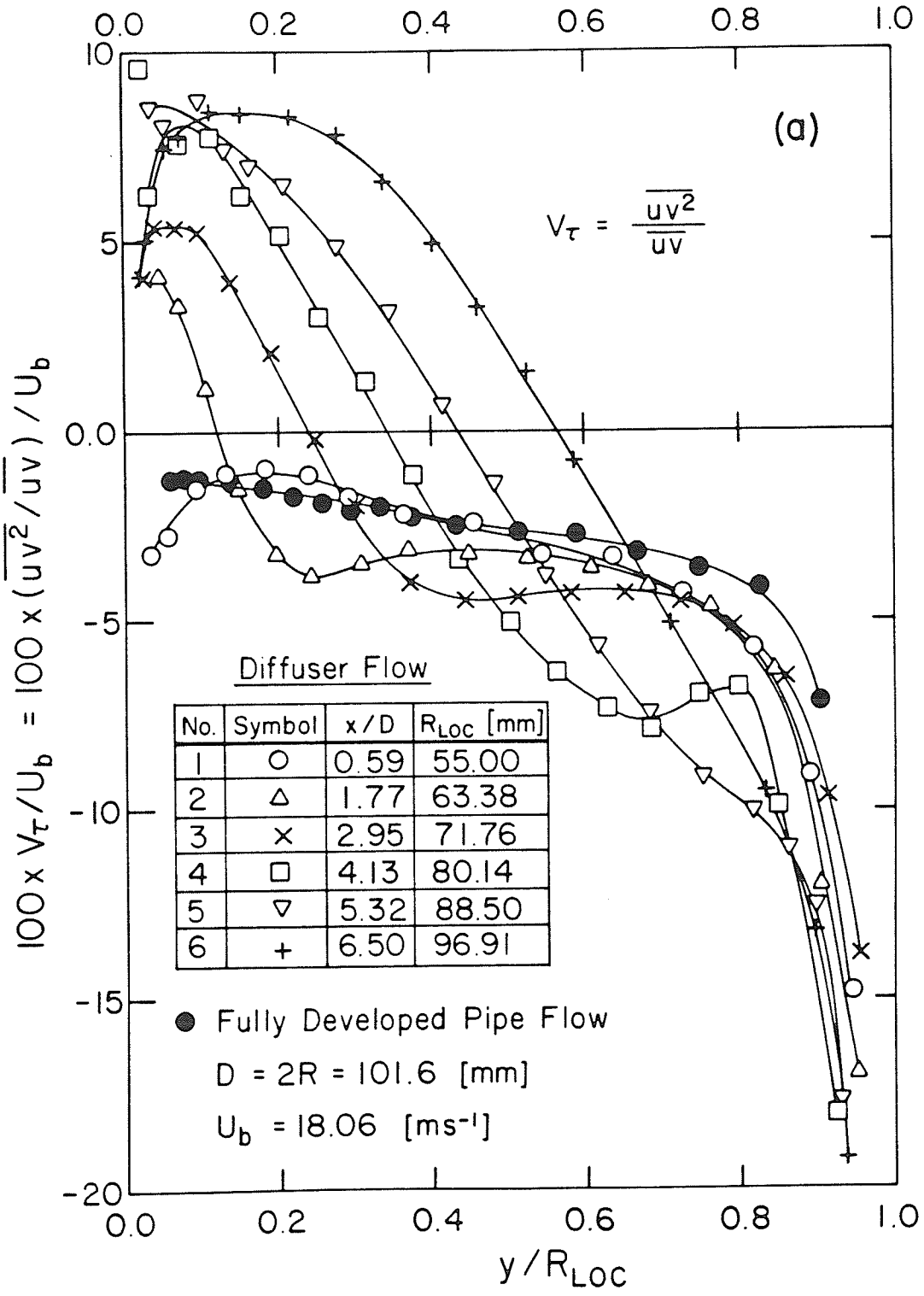

Figure 7.12a Profiles of turbulent transport velocity of $\overline{uv}$, $V_\tau/U_b = \overline{uv^2}/(\overline{uv}U_b)$.

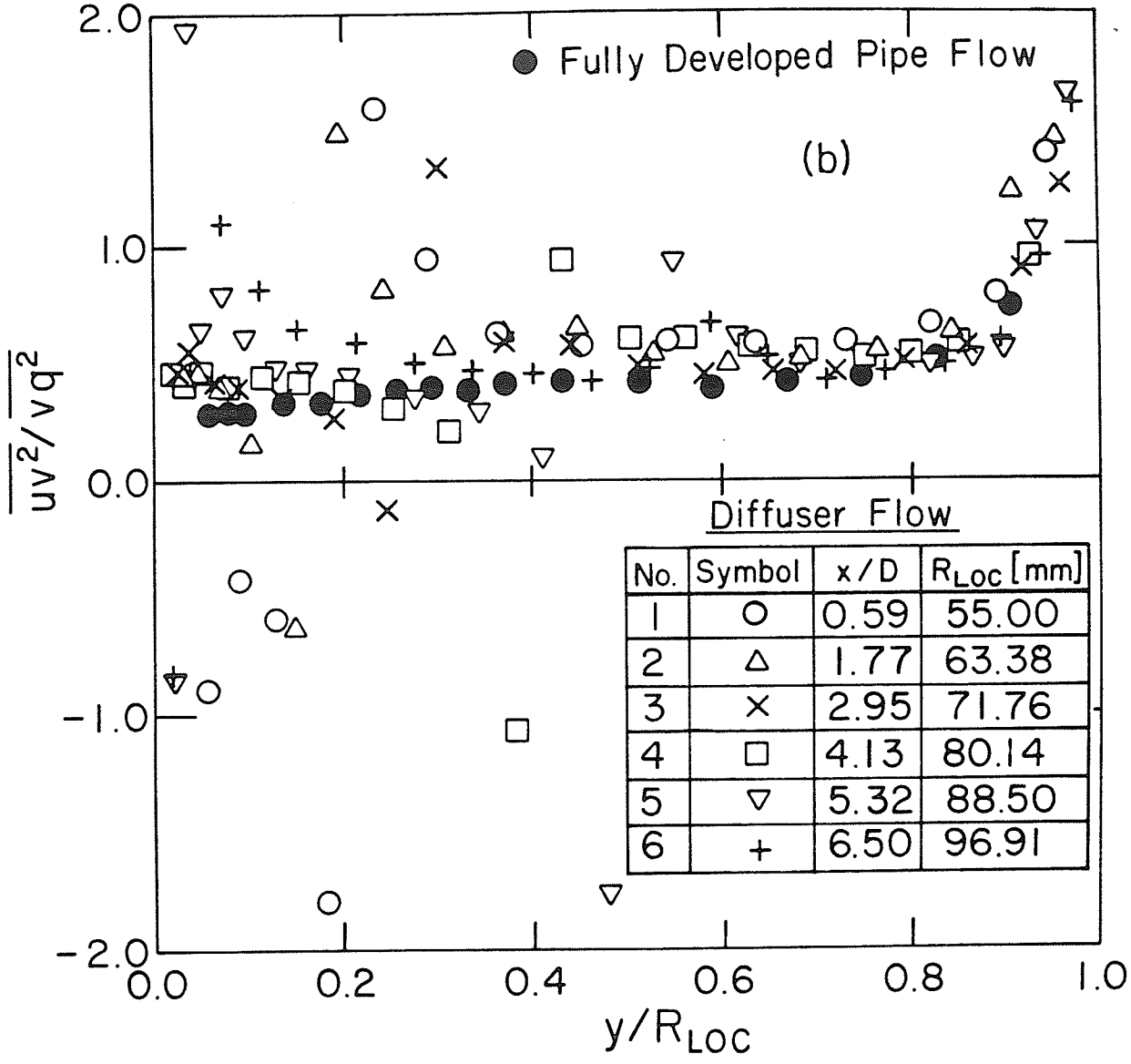

Figure 7.12b Ratio of triple products, $\overline{uv^2}/\overline{vq^2}$.

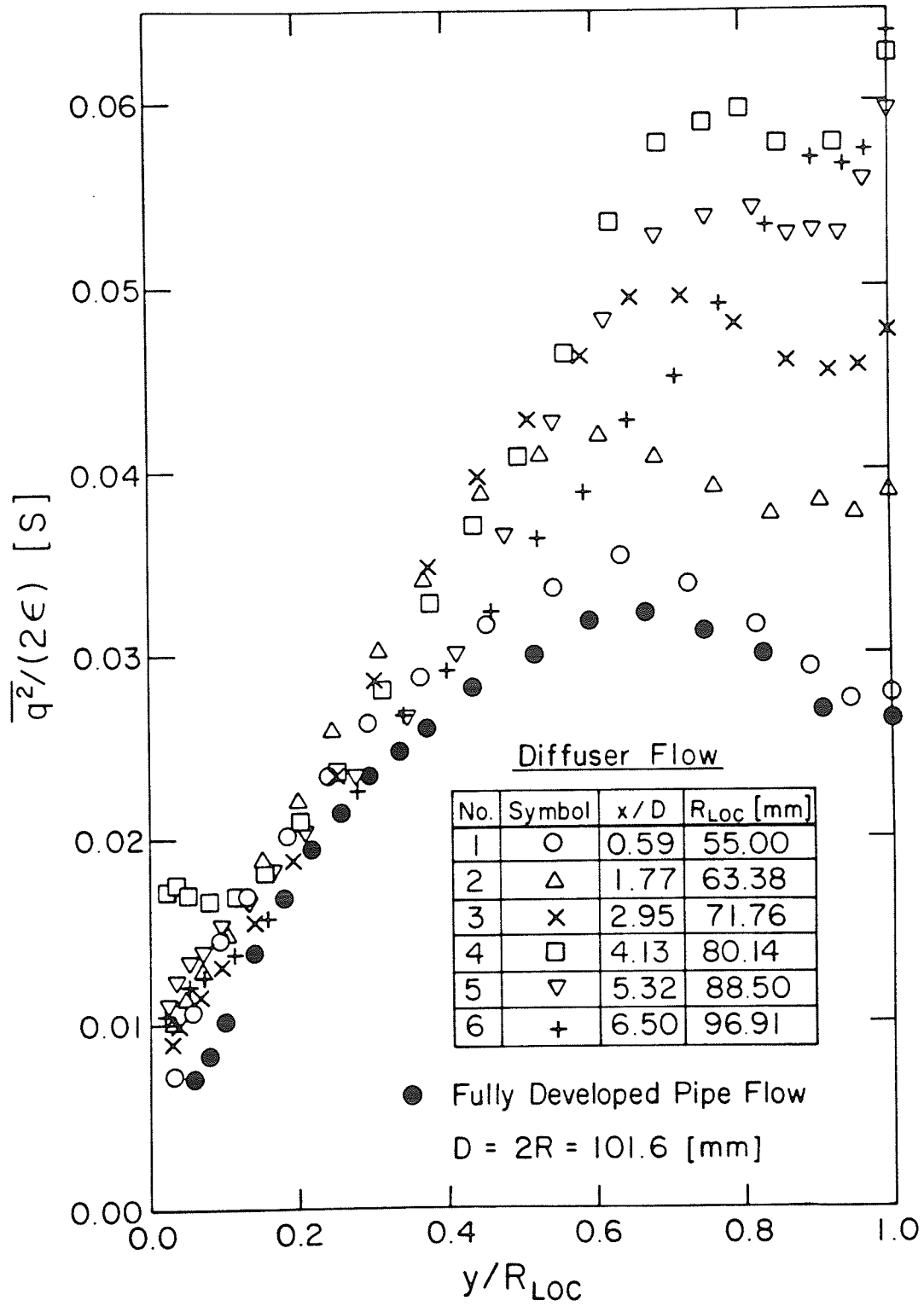

Figure 7.13 The time scale $\tau = \overline{q^2}/(2\epsilon)$.

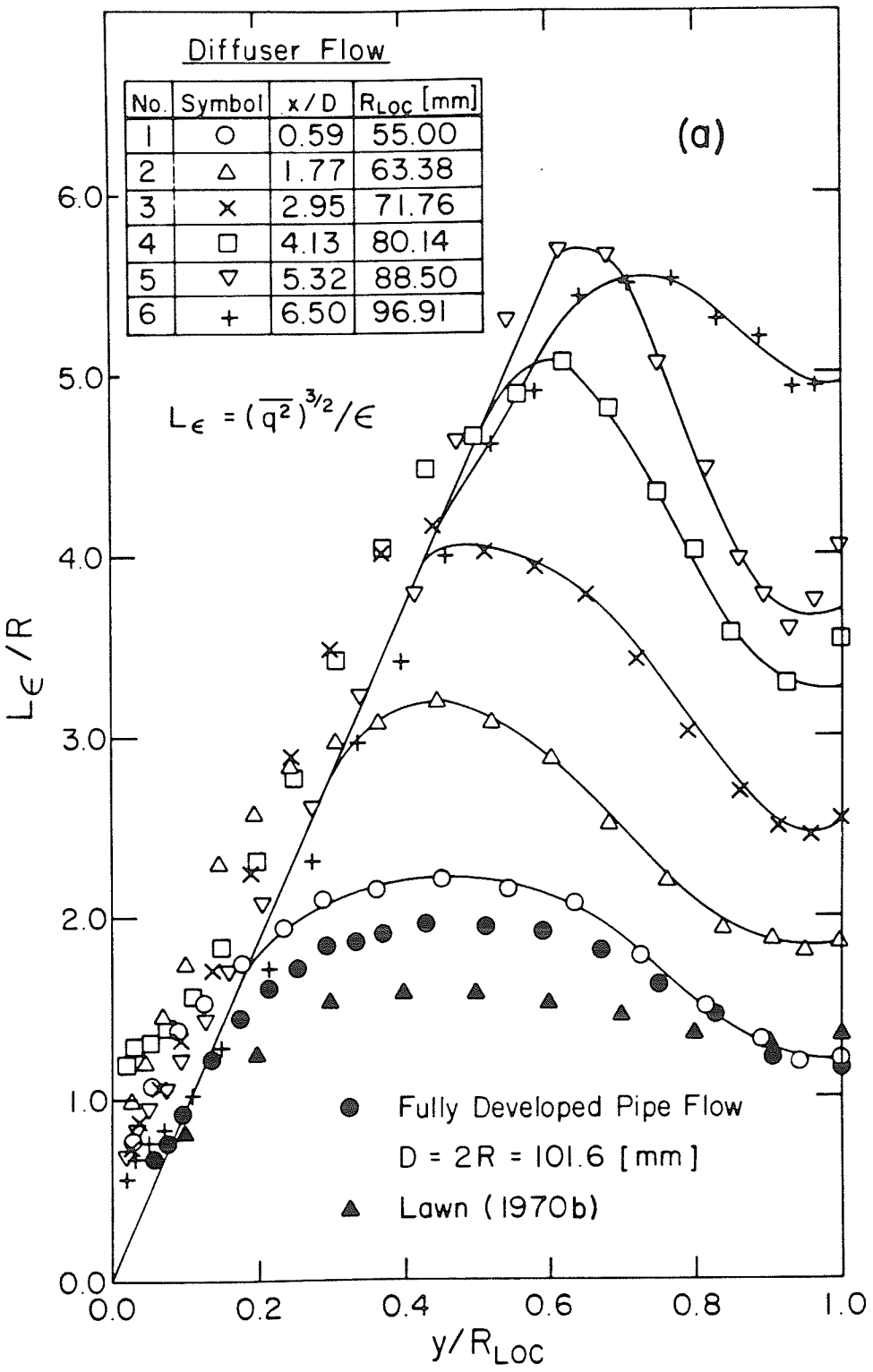

Figure 7.14a Dissipation length scale, $L_\epsilon = (\overline{q^2})^{3/2}/\epsilon$.

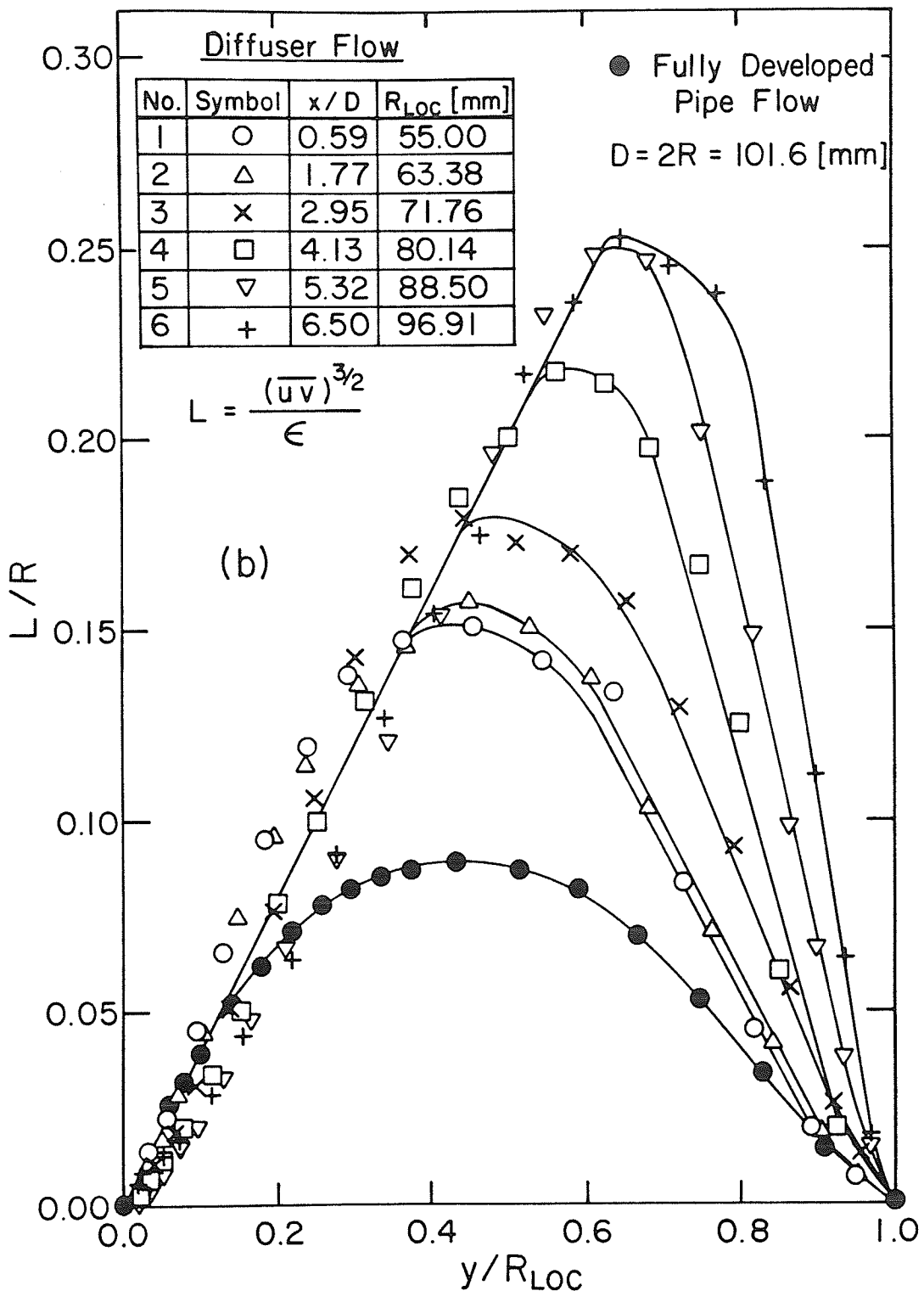

Figure 7.14b Dissipation length scale, $L = (\overline{uv})^{3/2}/\epsilon$.

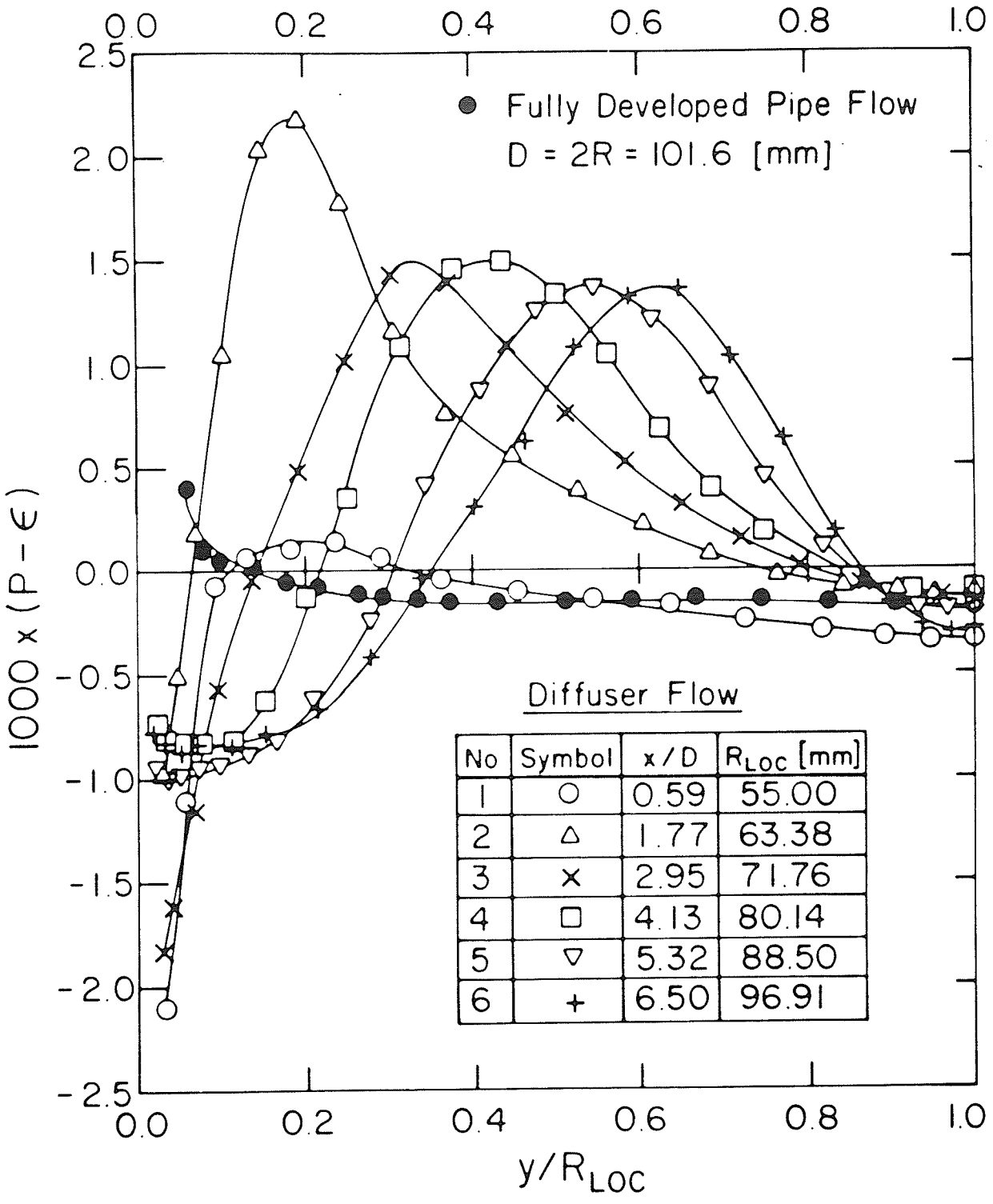

No	Symbol	x/D	R_{LOC} [mm]
1	○	0.59	55.00
2	△	1.77	63.38
3	×	2.95	71.76
4	□	4.13	80.14
5	▽	5.32	88.50
6	+	6.50	96.91

Figure 7.15 Profiles of the difference of production, P and dissipation, ϵ. P and ϵ are nondimensionalized by R/U_b^3. R = 0.0508 m and U_b = 18.06 ms^{-1}.

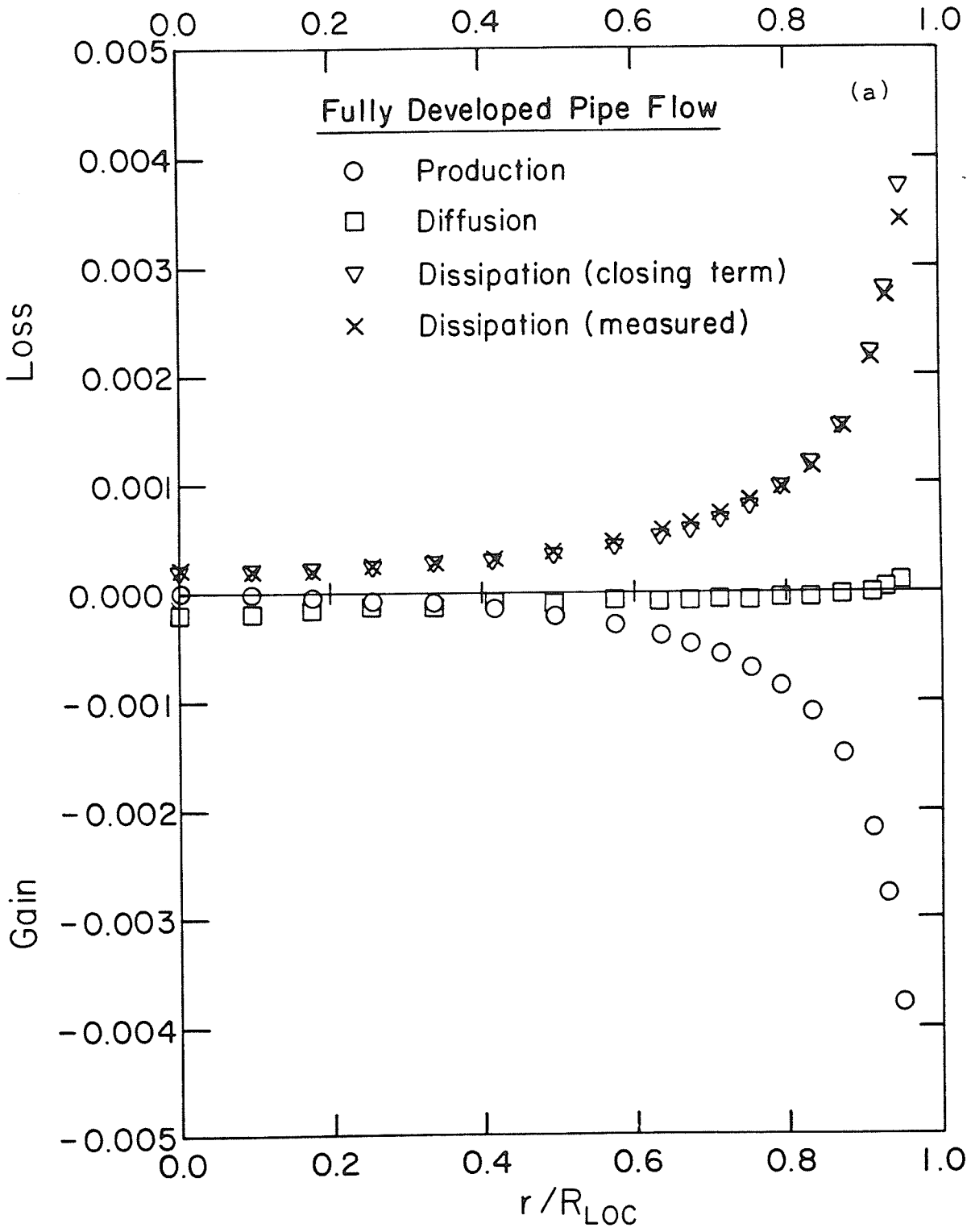

Figure 7.16 Turbulent energy balance.
(a) Fully developed pipe flow.
All terms made dimensionless by R/U_b^3.

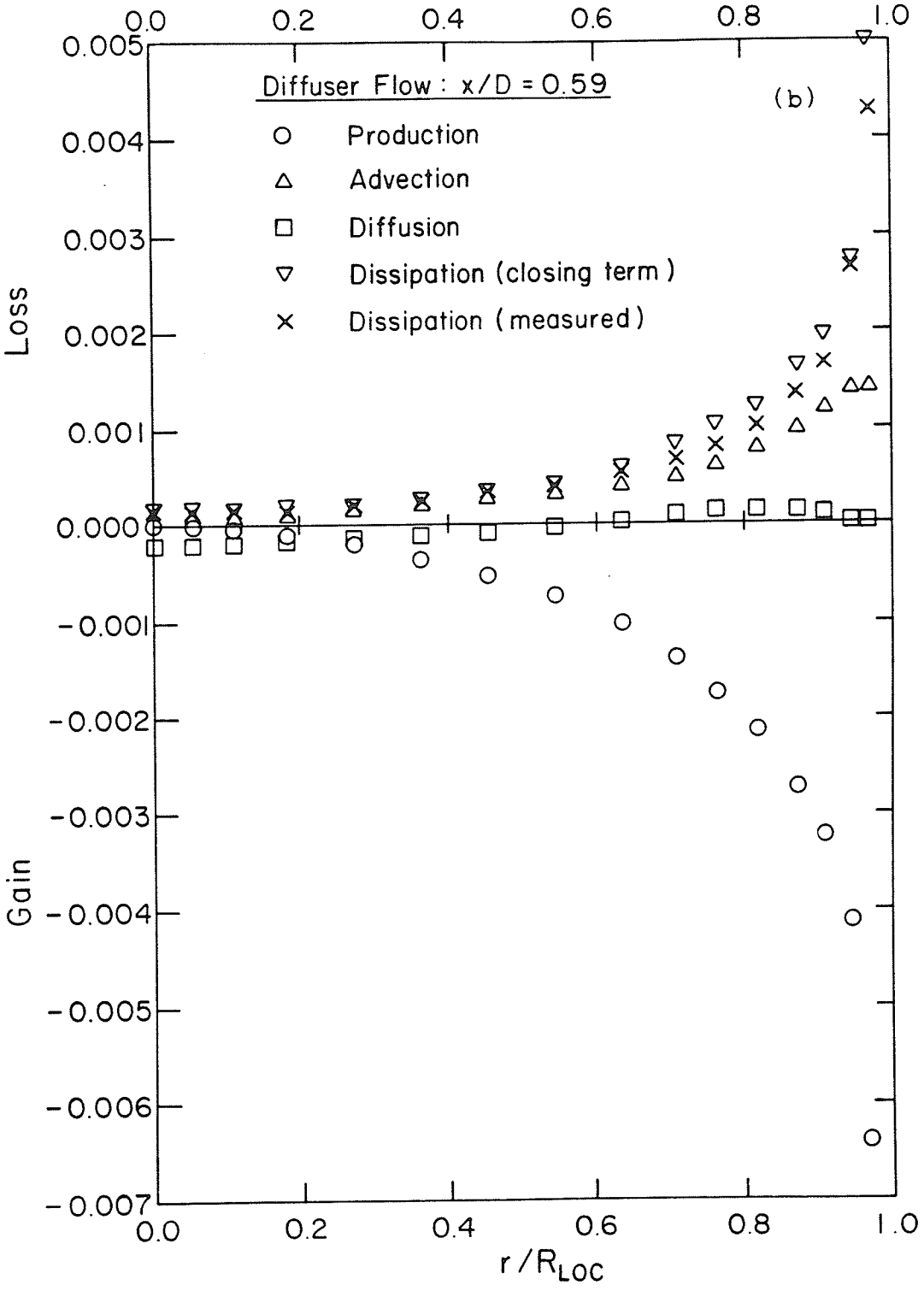

Figure 7.16 Turbulent energy balance.
(b) Diffuser flow: x/D = 0.59.
All terms made dimensionless by R/U_b^3.

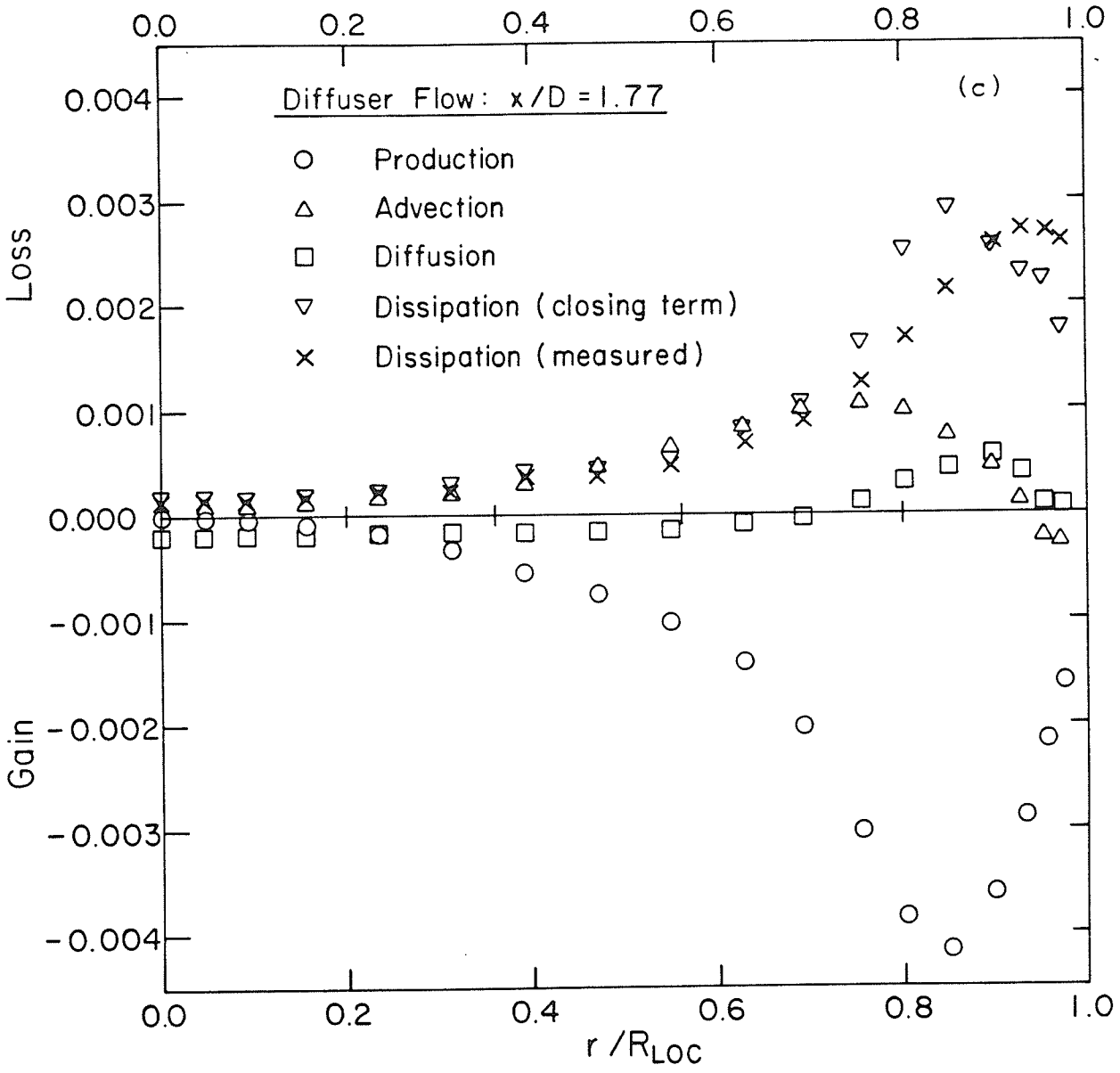

Figure 7.16 Turbulent energy balance.
(c) Diffuser flow: x/D = 1.77.
All terms made dimensionless by R/U_b^3.

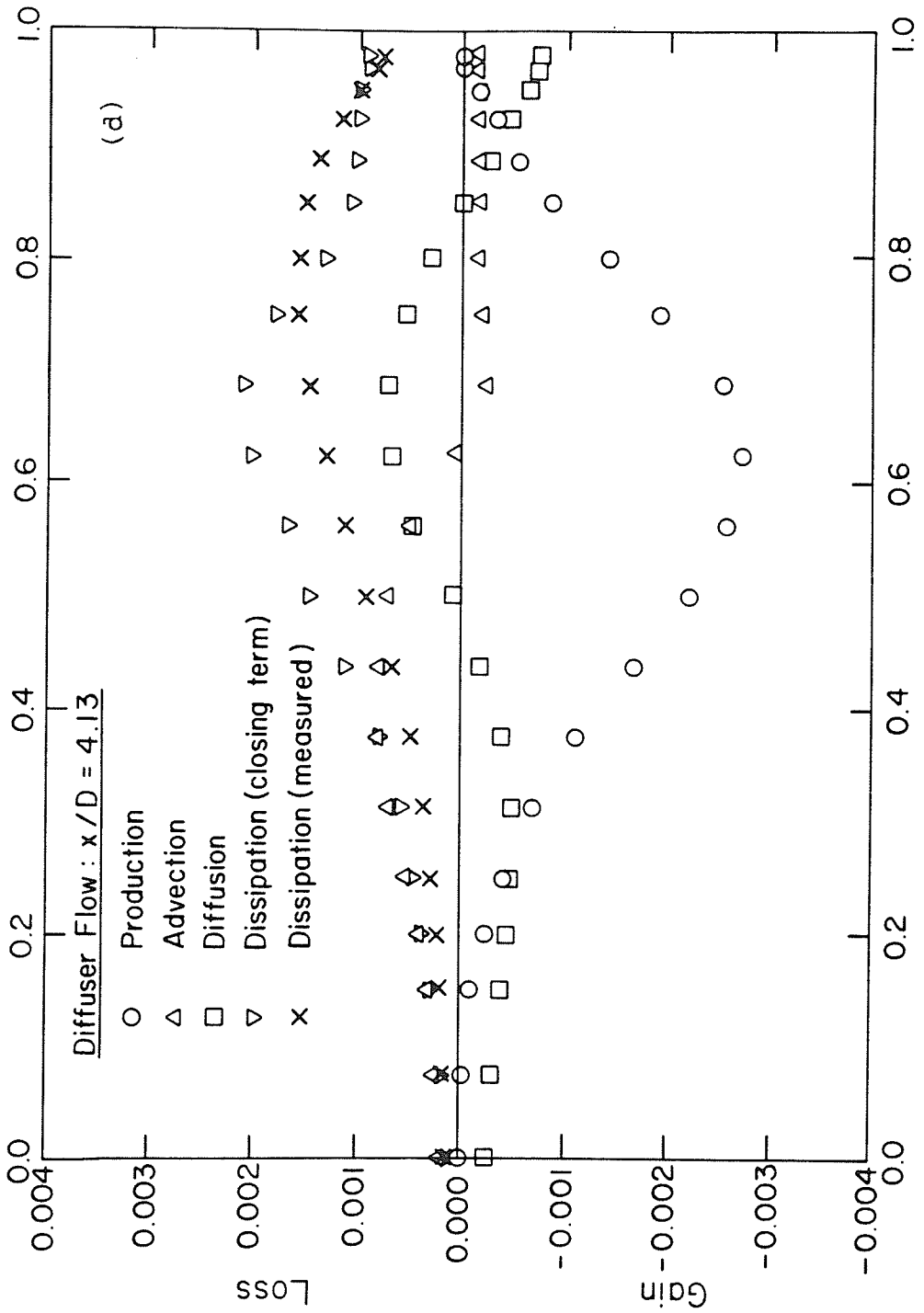

Figure 7.16 Turbulent energy balance.
(d) Diffuser flow: x/D = 4.13.
All terms made dimensionless by R/U_b^3.

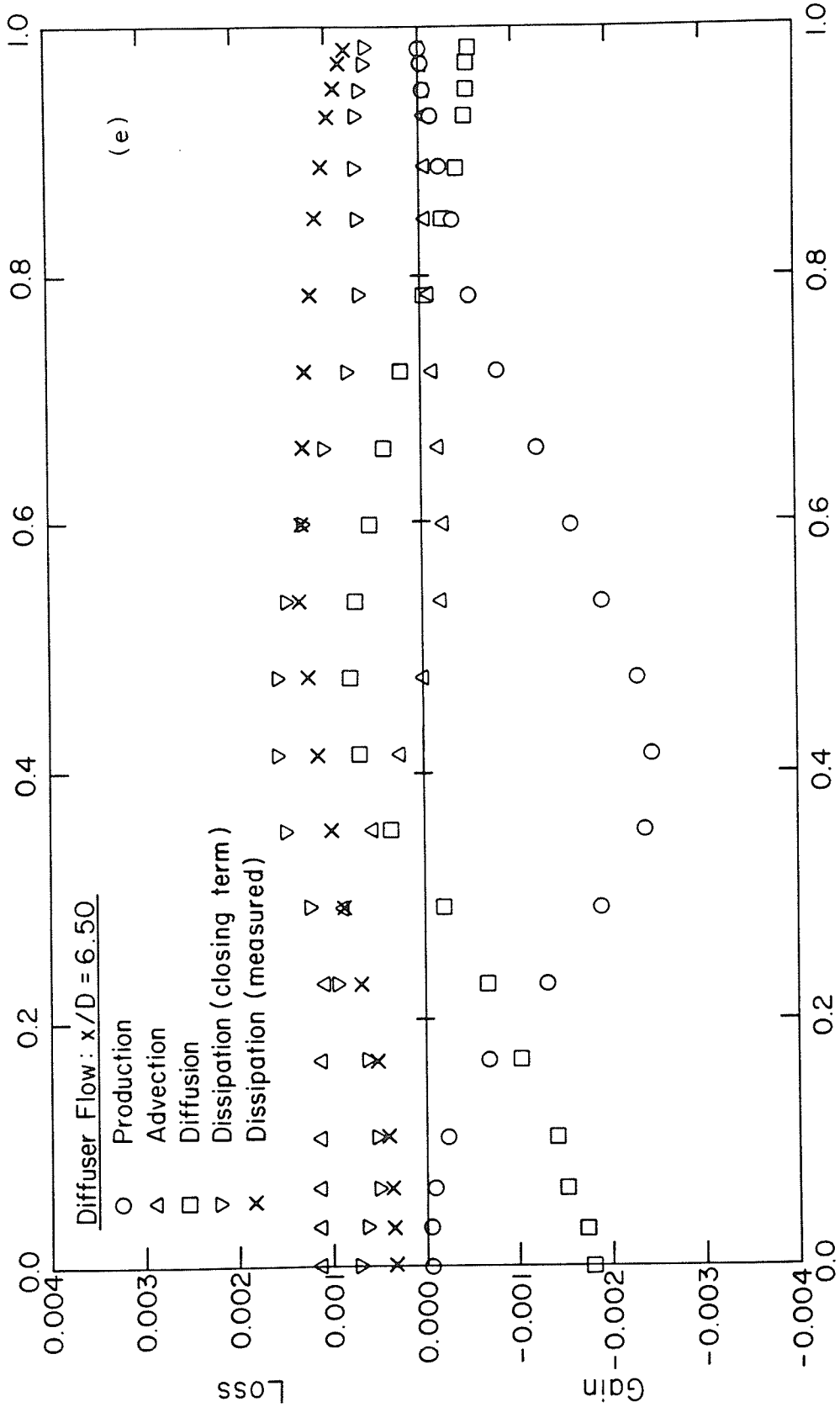

Figure 7.16 Turbulent energy balance.
(e) Diffuser flow: x/D = 6.50.
All terms made dimensionless by R/U_b^3.

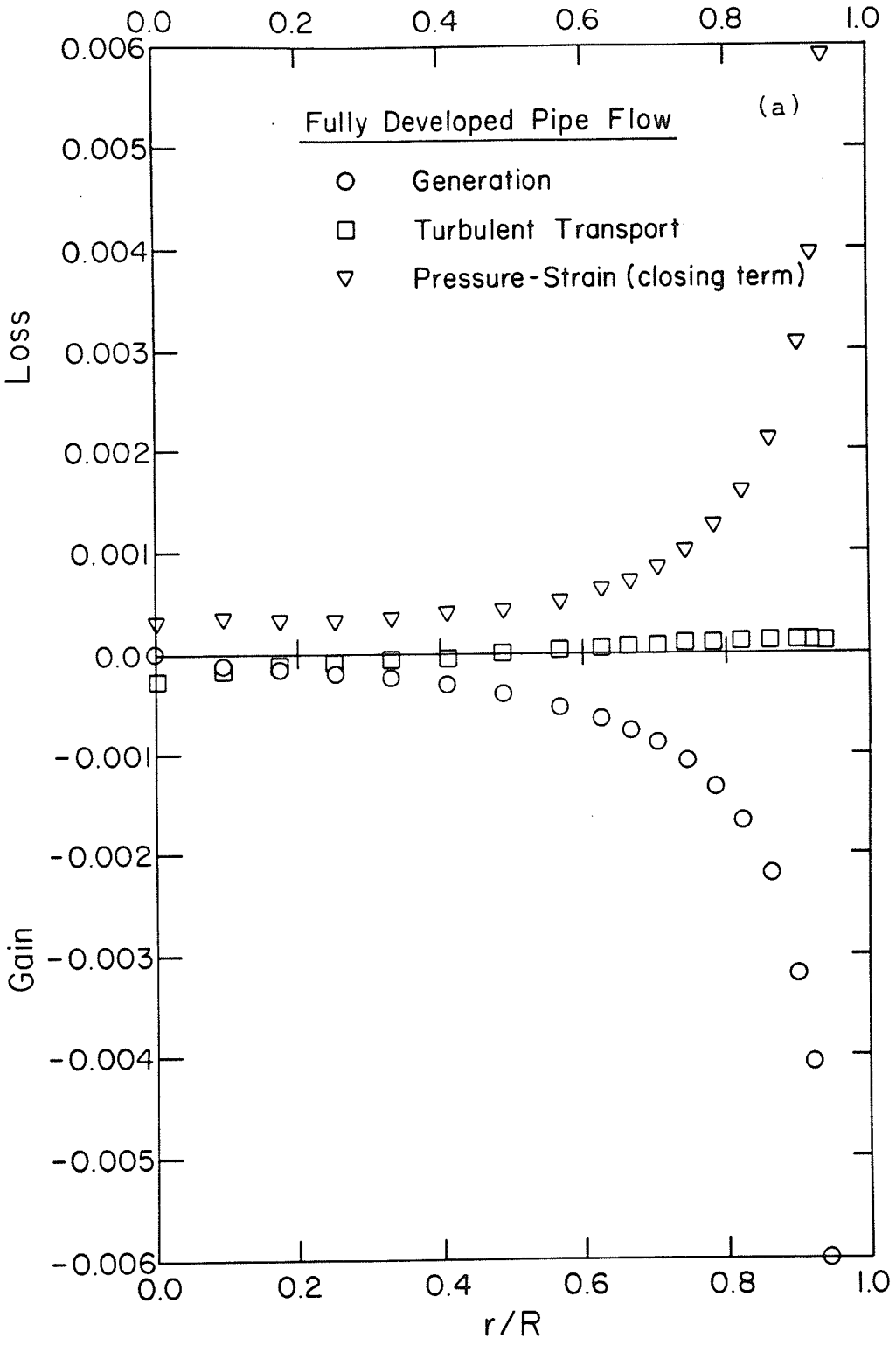

Figure 7.17 Shear stress balance.
(a) Fully developed pipe flow.
All terms made dimensionless by R/U_b^3.

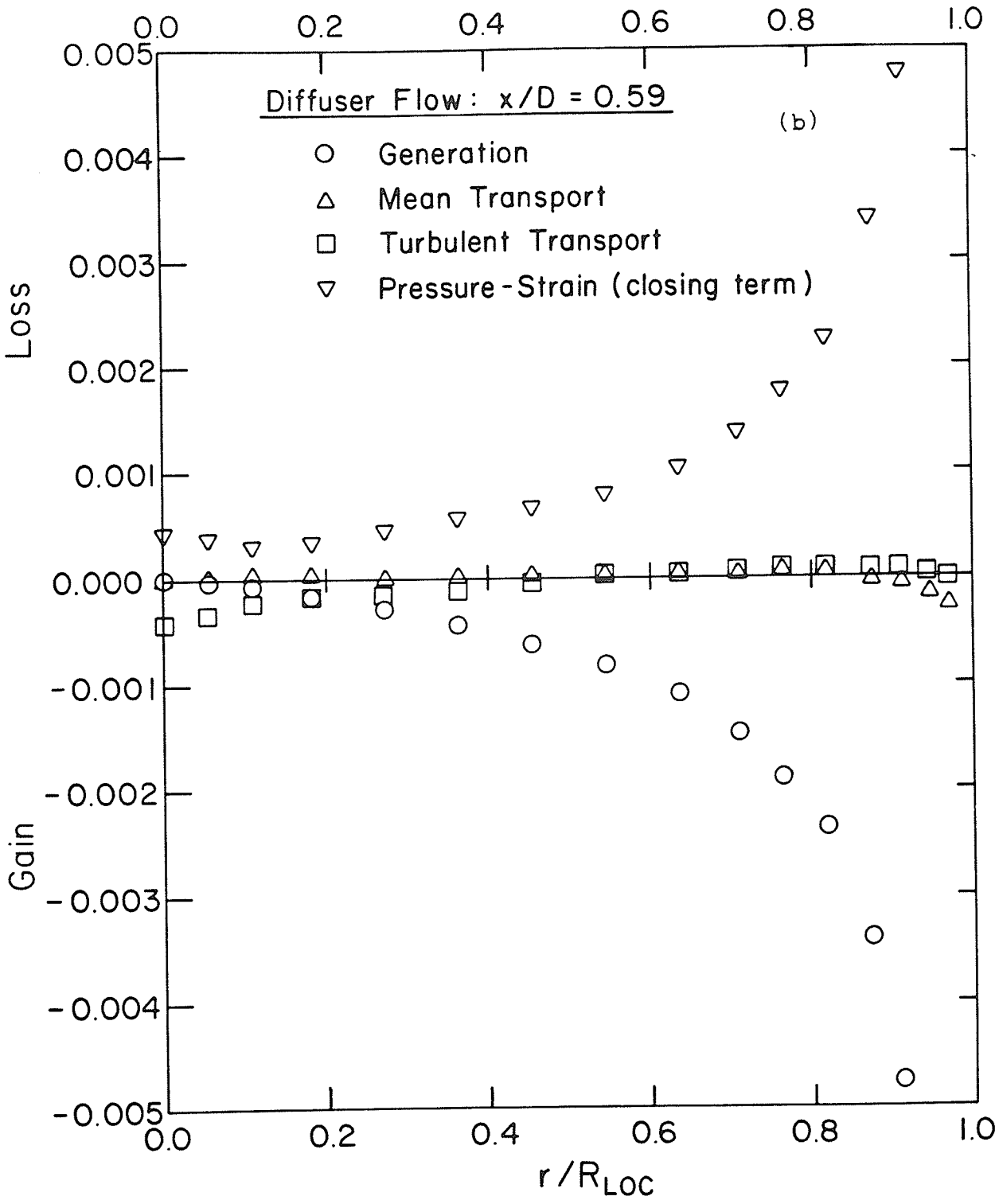

Figure 7.17 Shear stress balance.
(b) Diffuser flow: x/D = 0.59.
All terms made dimensionless by R/U_b^3.

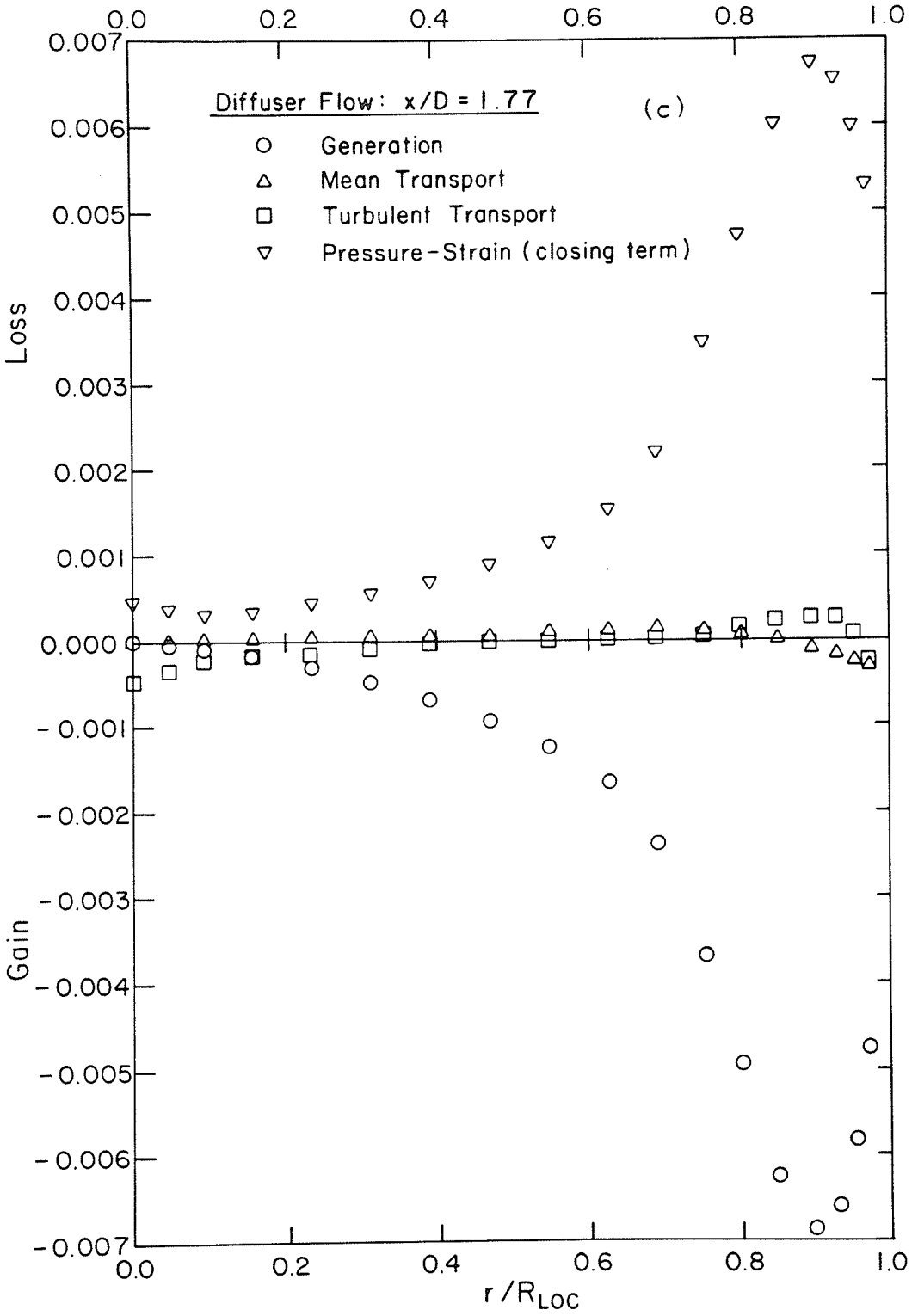

Figure 7.17 Shear stress balance.
(c) Diffuser flow: x/D = 1.77.
All terms made dimensionless by R/U_b^3.

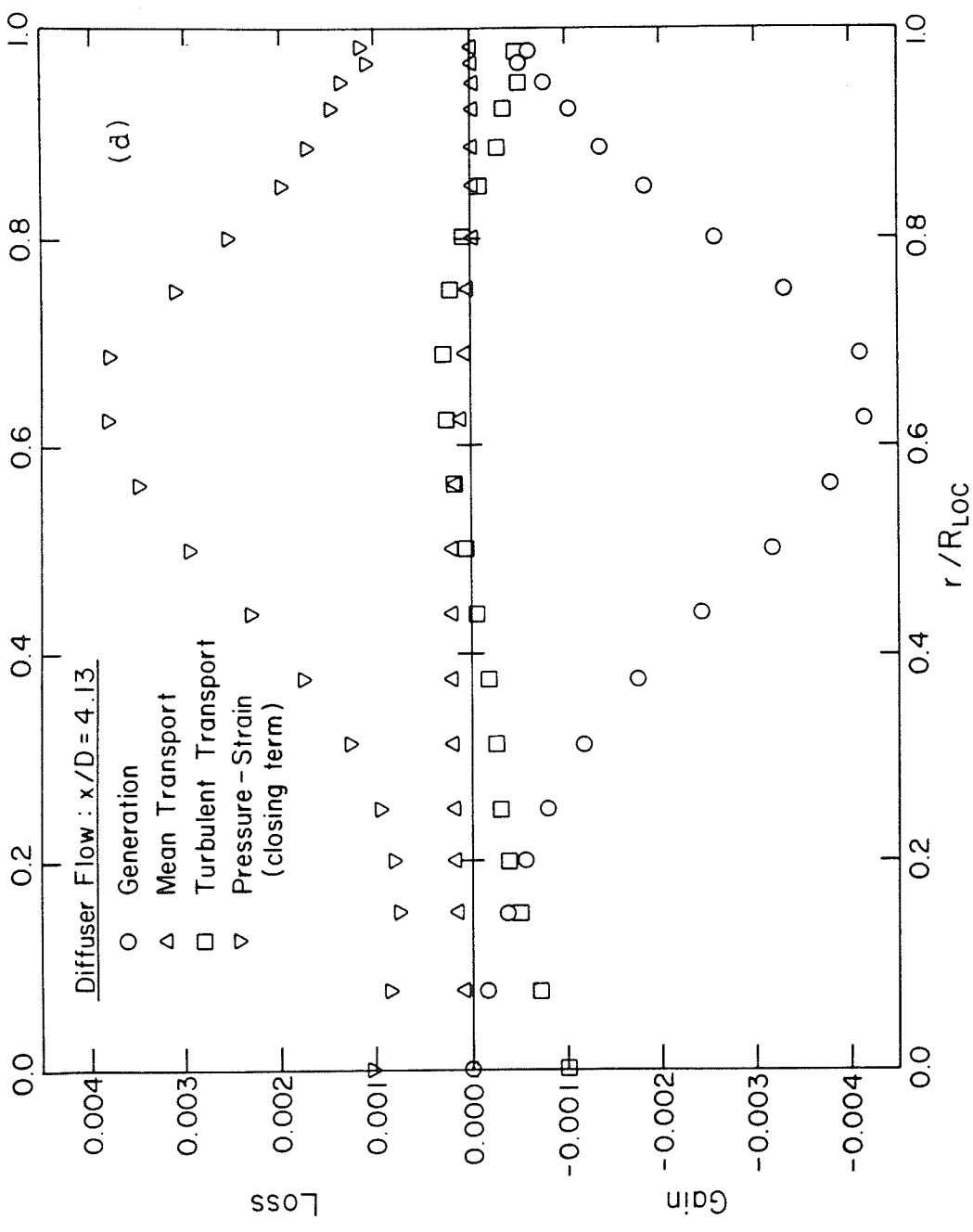

Figure 7.17 Shear stress balance.
(d) Diffuser flow: x/D = 4.13.
All terms made dimensionless by R/U_b^3.

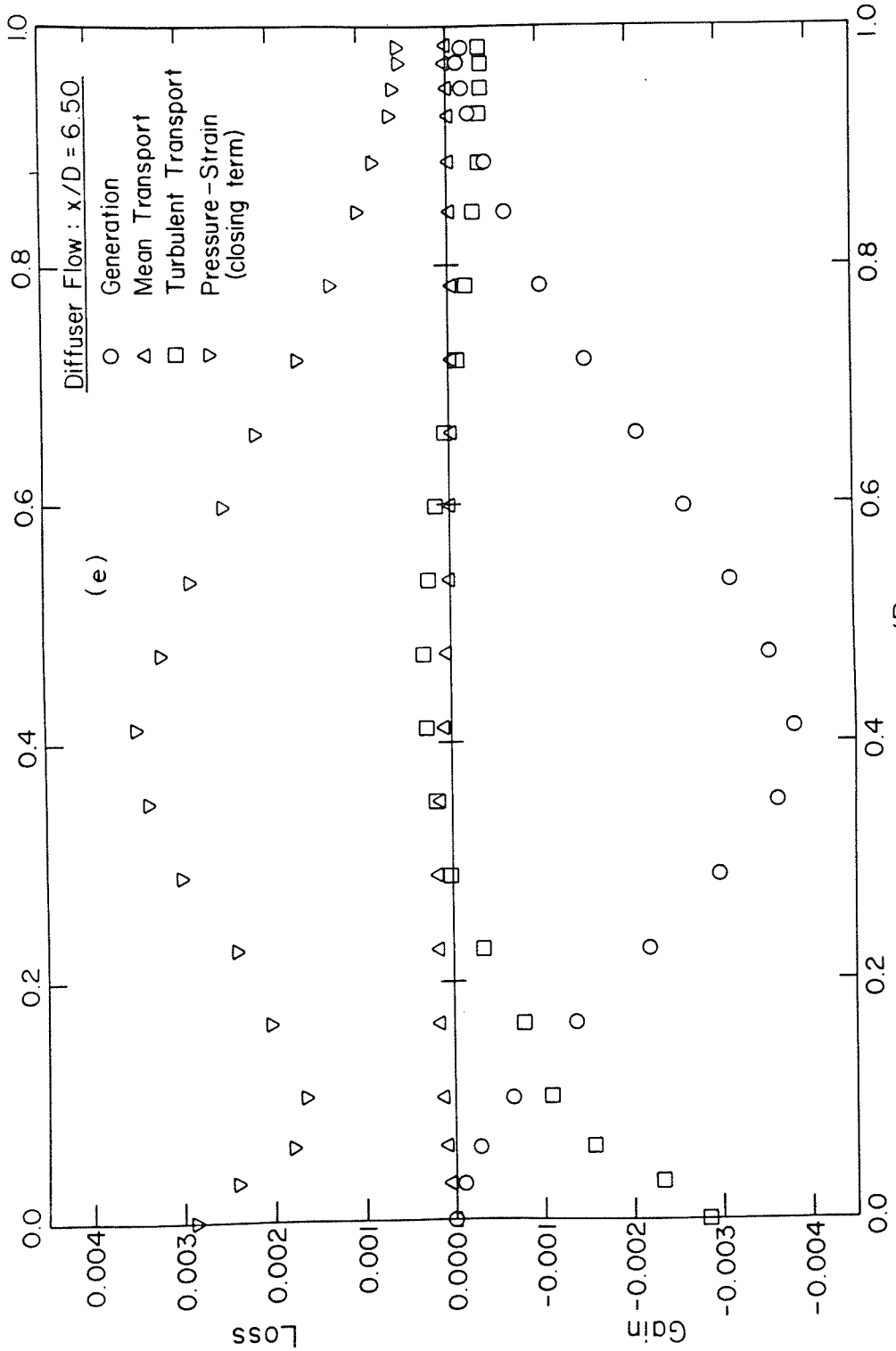

Figure 7.17 Shear stress balance.
(e) Diffuser flow: $x/D = 6.50$.
All terms made dimensionless by R/U_b^3.

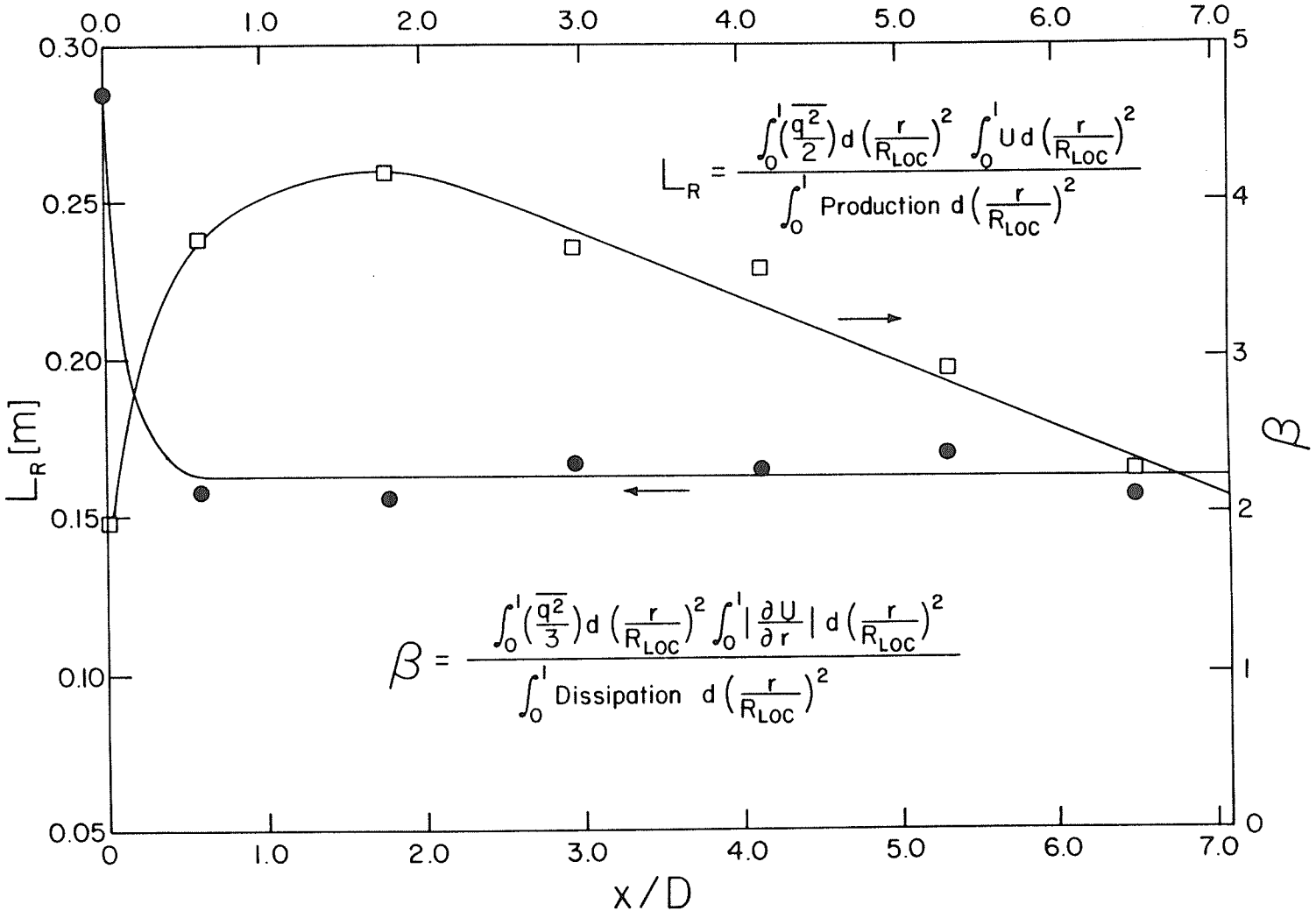

Figure 7.18 strain parameter, β, and relaxation length scale, L_R.

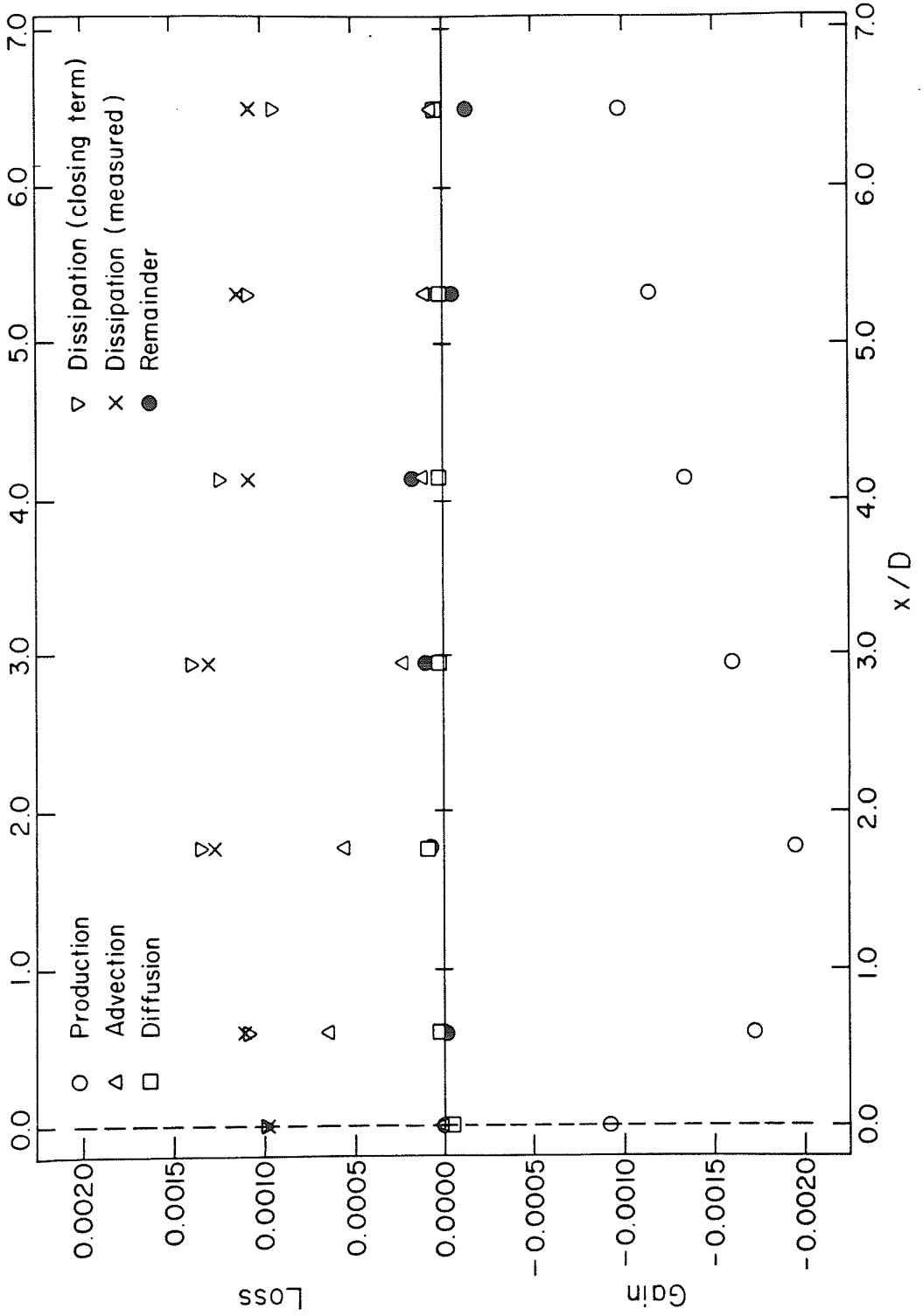

Figure 7.19 Area integrated values of terms of turbulent energy equation along the diffuser. All terms made dimensionless by R/U_b^3.

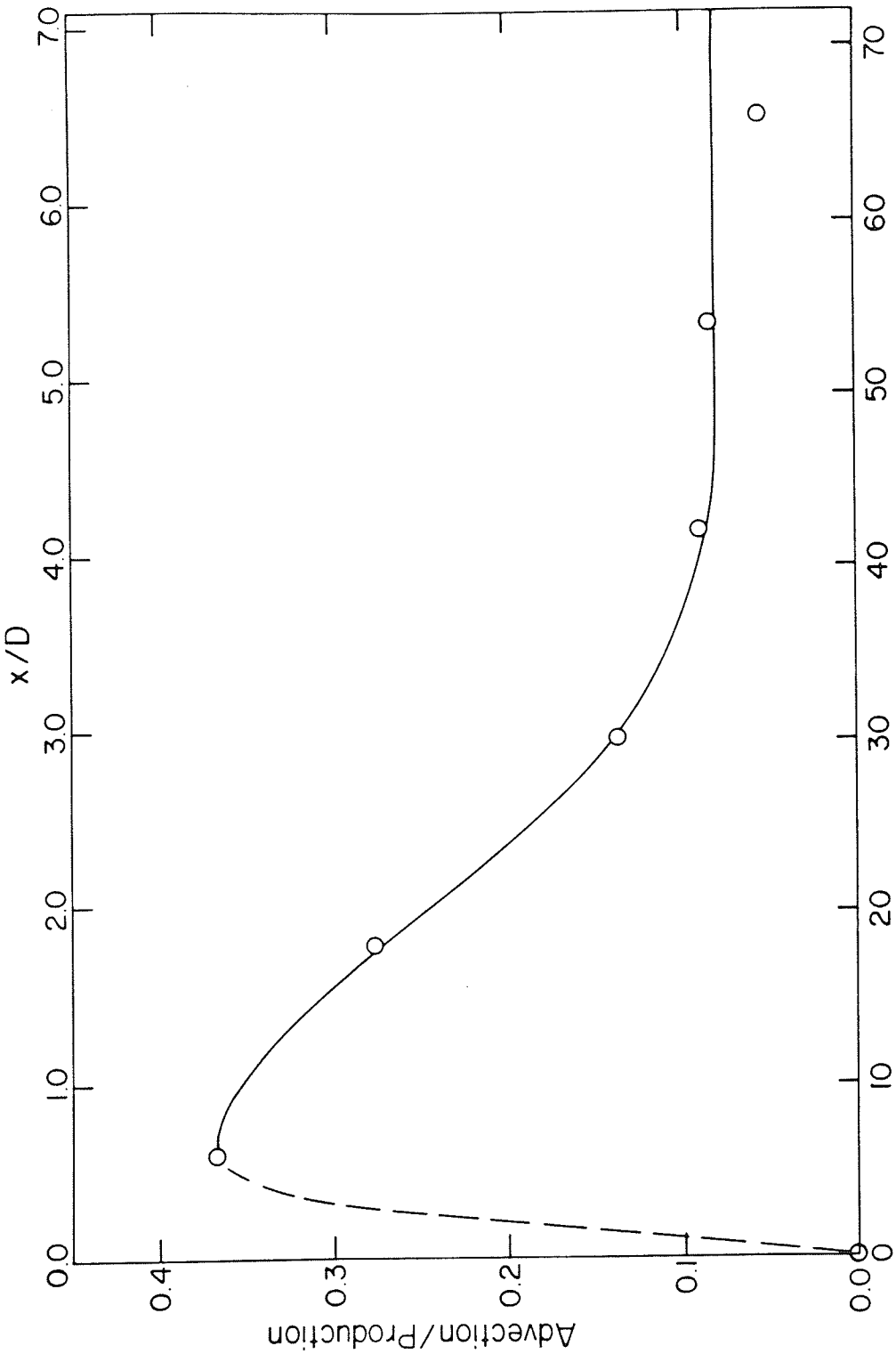

Figure 7.20 The ratio of advection to production.

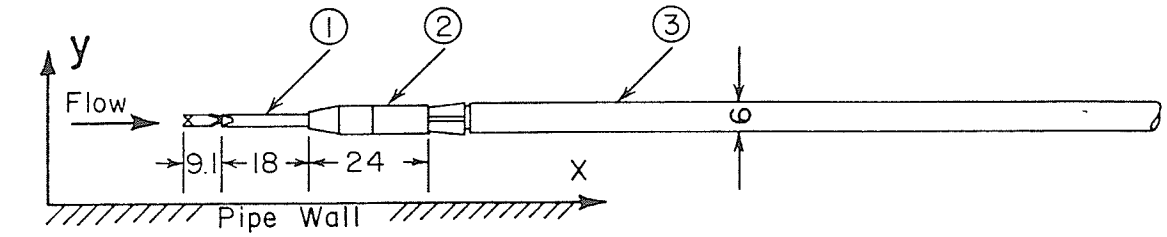

(a) x - array DISA 55P51 PROBE TOGETHER WITH ITS SUPPORT AND MOUNTING TUBE

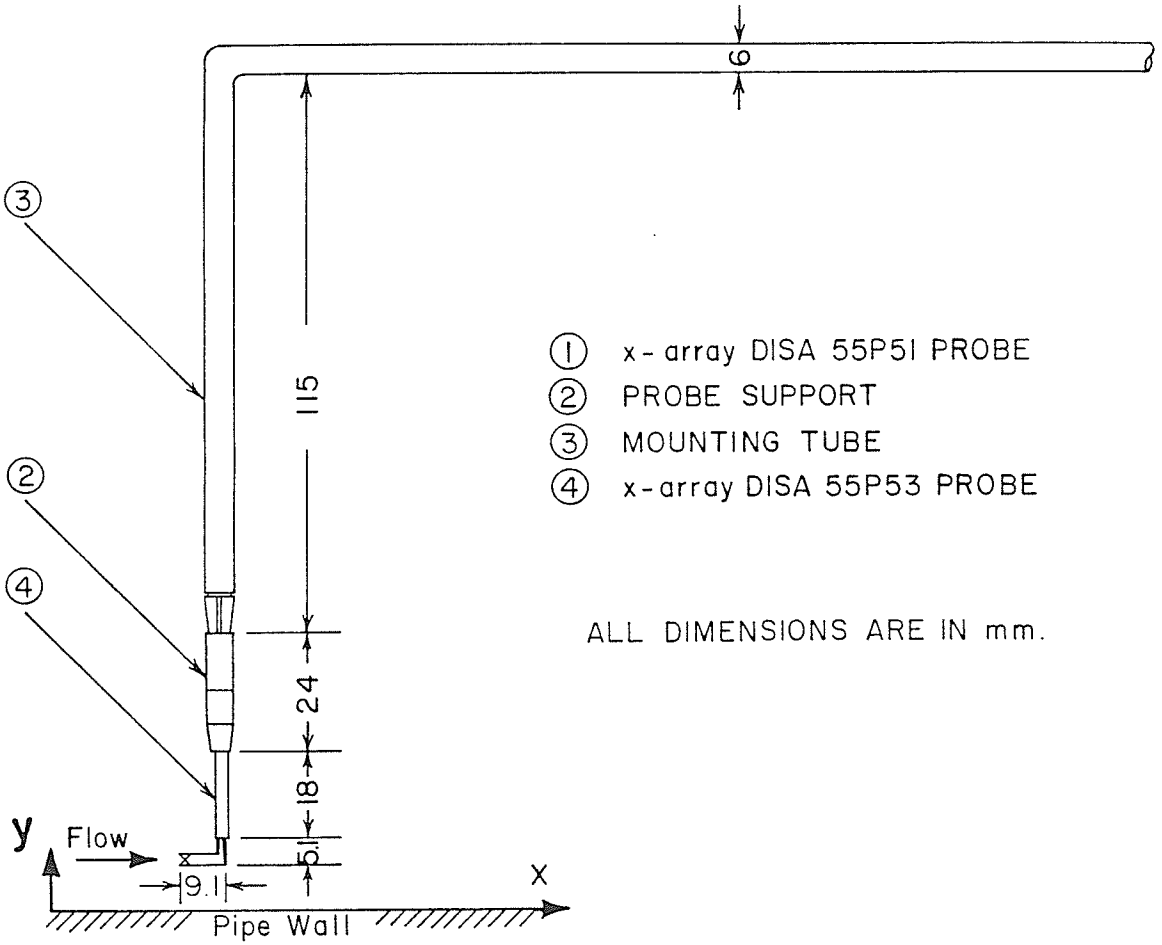

(b) x - array DISA 55P53 TOGETHER WITH ITS SUPPORT AND MOUNTING TUBE

Figure A.1 Geometries of X-array hot-wire probe set-ups used in measurements.

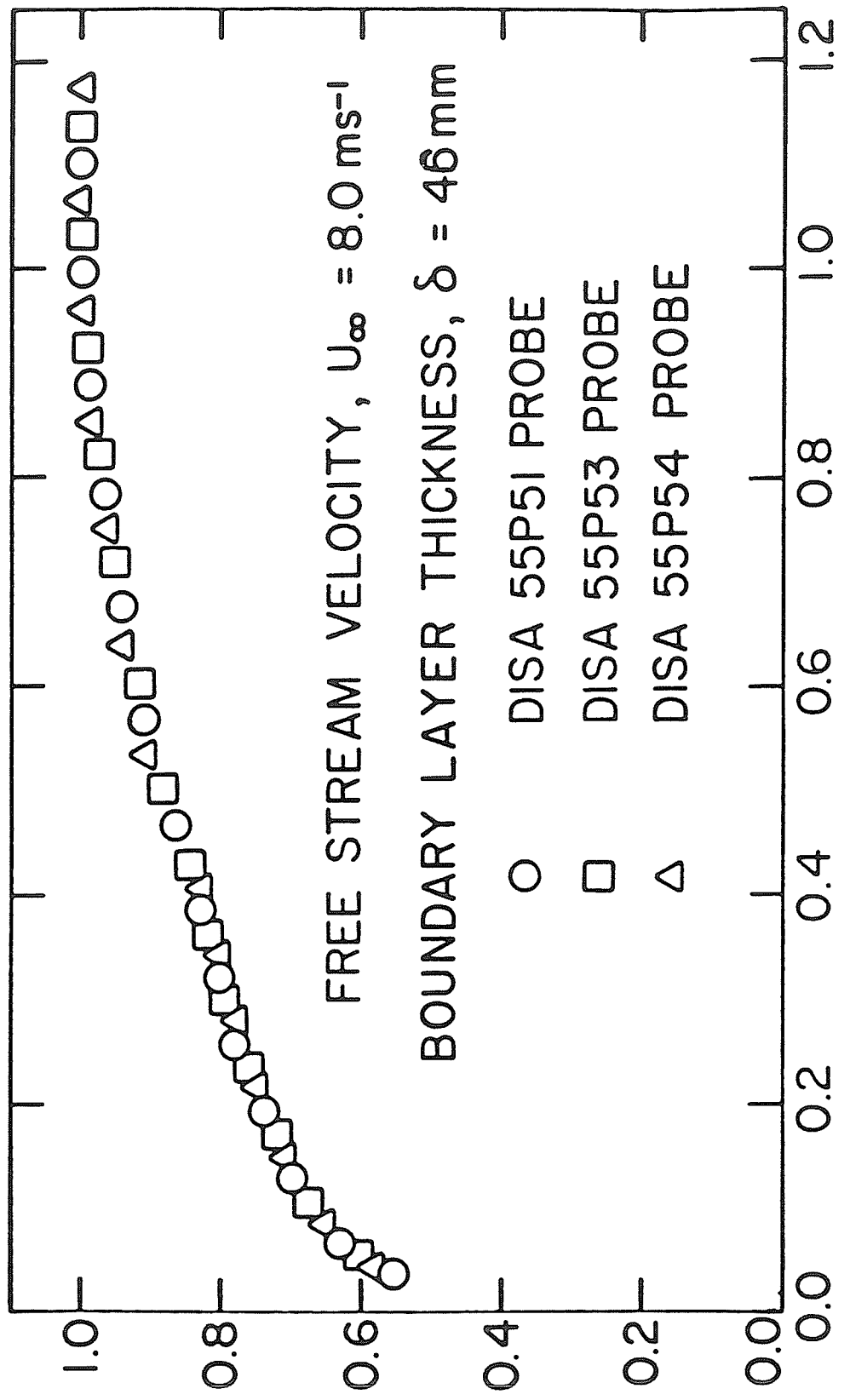

Figure A.2 Mean velocity profile in a boundary layer obtained by three different X-array hot-wire probes.

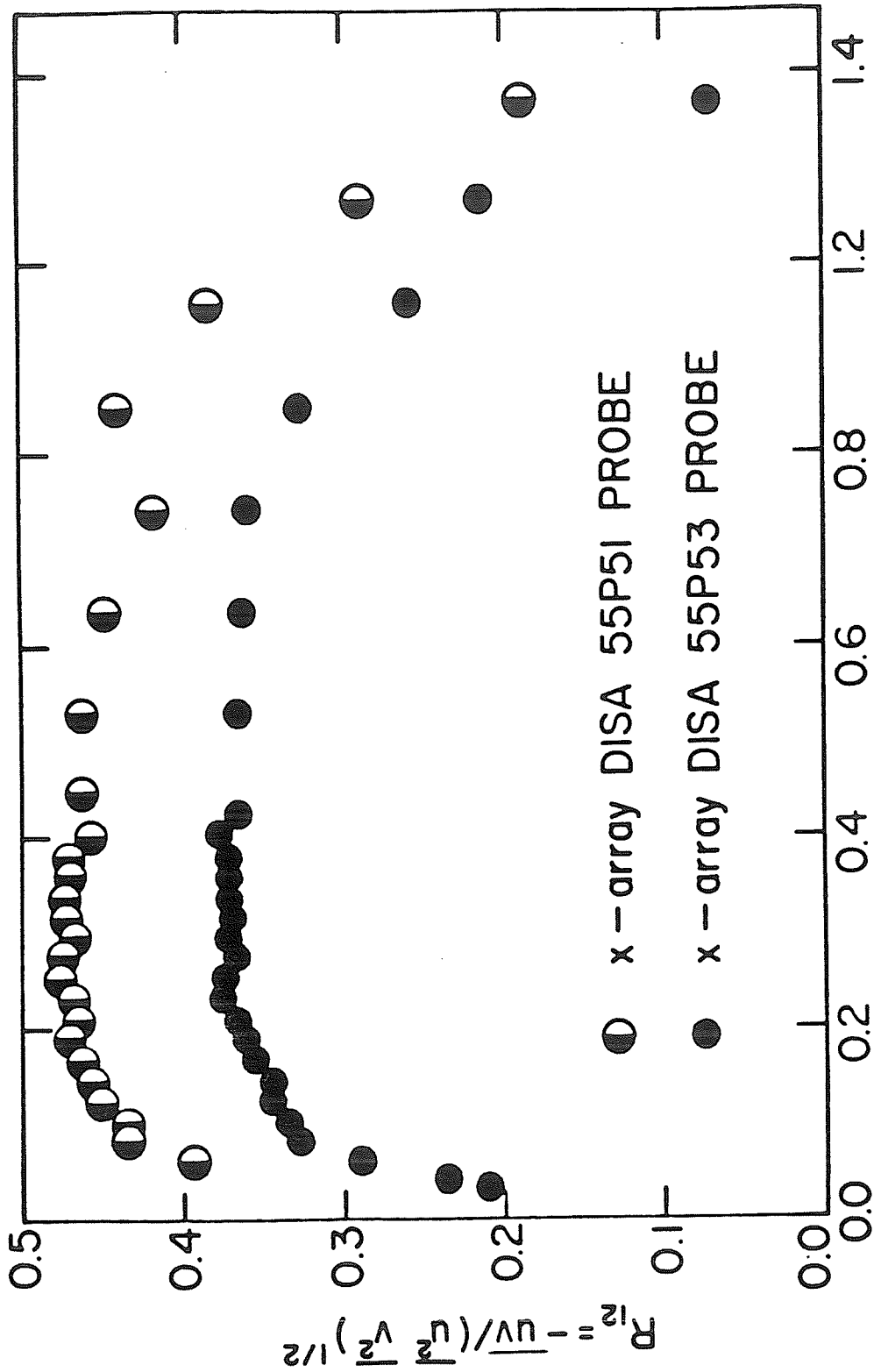

Figure A.3 Distribution of Reynolds stress coefficient, $R_{12} = -\overline{uv}/(\overline{u^2}\overline{v^2})^{1/2}$, in a boundary layer.

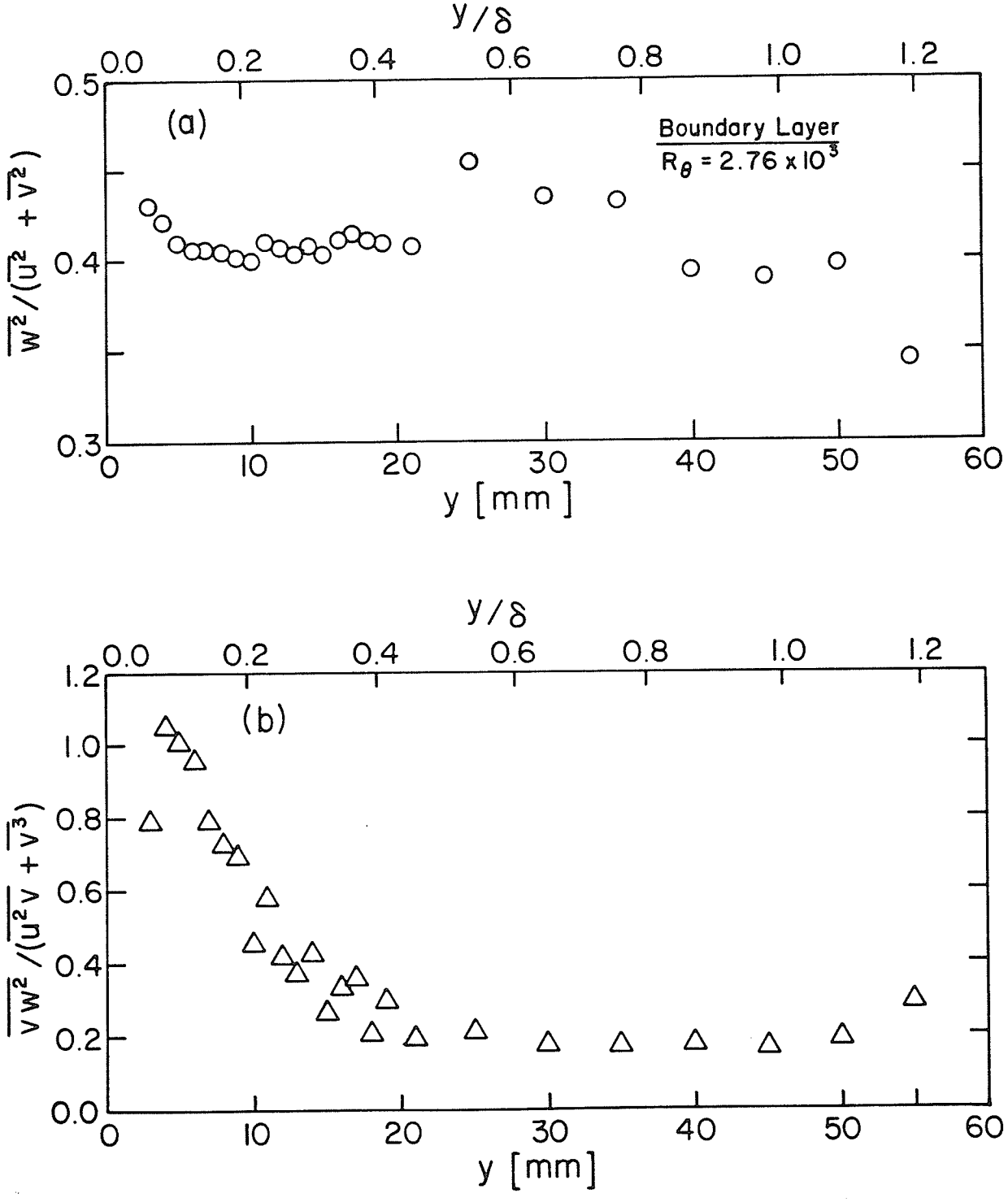

Figure B.1 Moments of turbulent fluctuating velocity in boundary layer
(a) $\overline{w^2}/(\overline{u^2} + \overline{v^2})$
(b) $\overline{vw^2}/(\overline{u^2v} + \overline{v^3})$

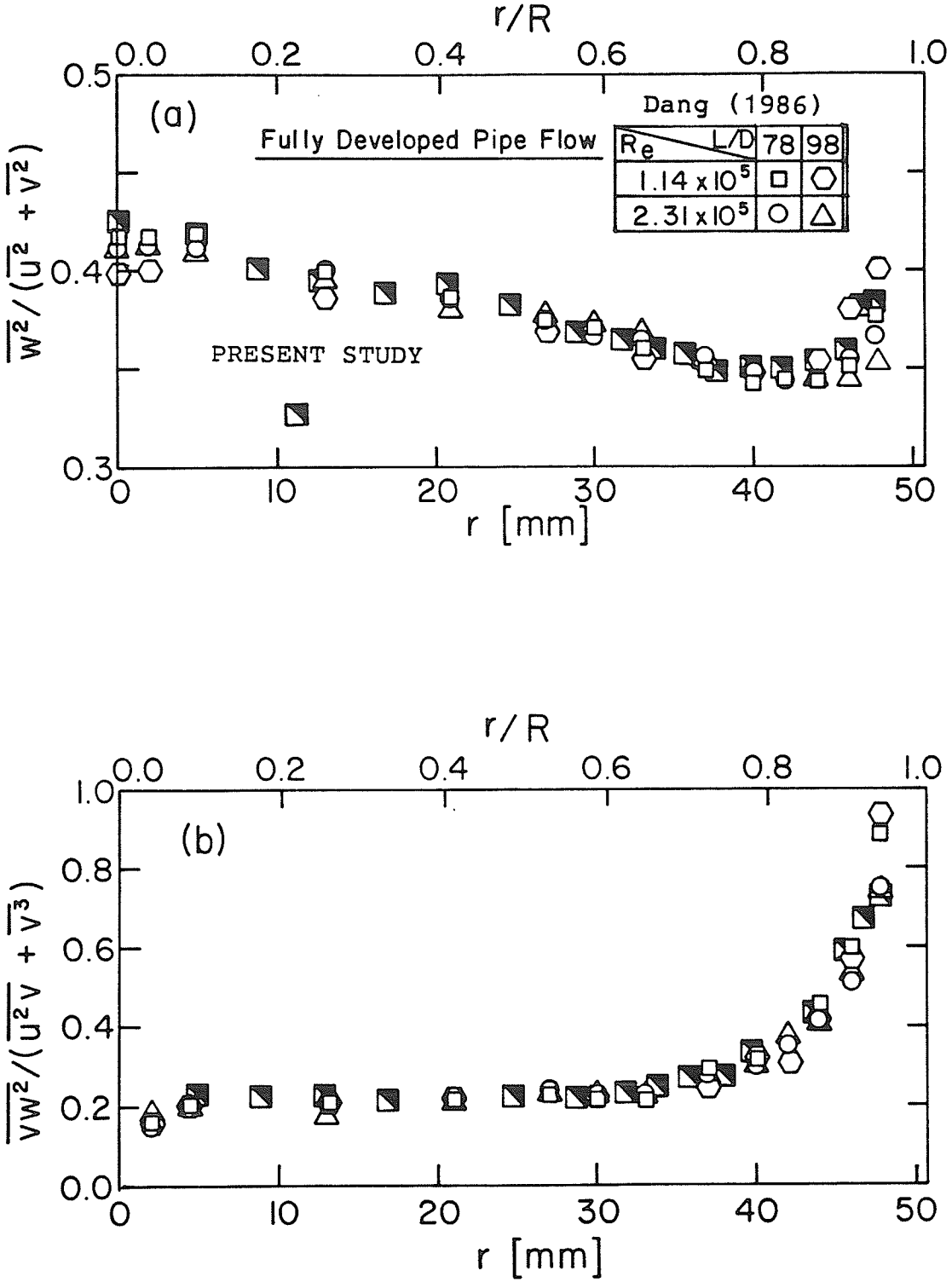

Figure B.2 Moments of turbulent fluctuating velocity in fully developed pipe flow
(a) $\overline{w^2}/(\overline{u^2} + \overline{v^2})$
(b) $\overline{vw^2}/(\overline{u^2v} + \overline{v^3})$

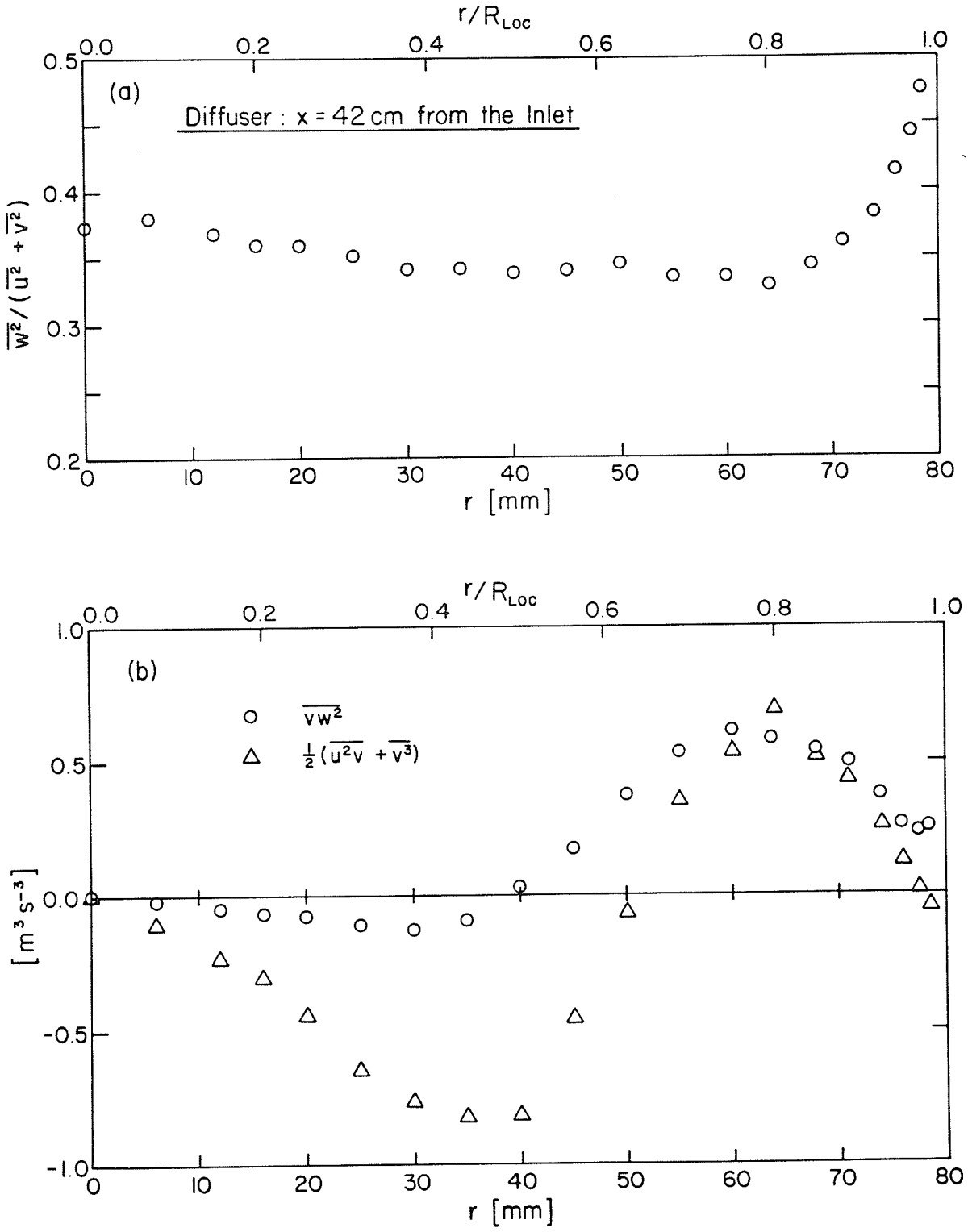

Figure B.3 Moments of turbulent fluctuating velocity in diffuser flow: x= 42 cm from the inlet.
(a) $\overline{w^2}/(\overline{u^2} + \overline{v^2})$
(b) O $\overline{vw^2}$, Δ $0.5(\overline{u^2v} + \overline{v^3})$

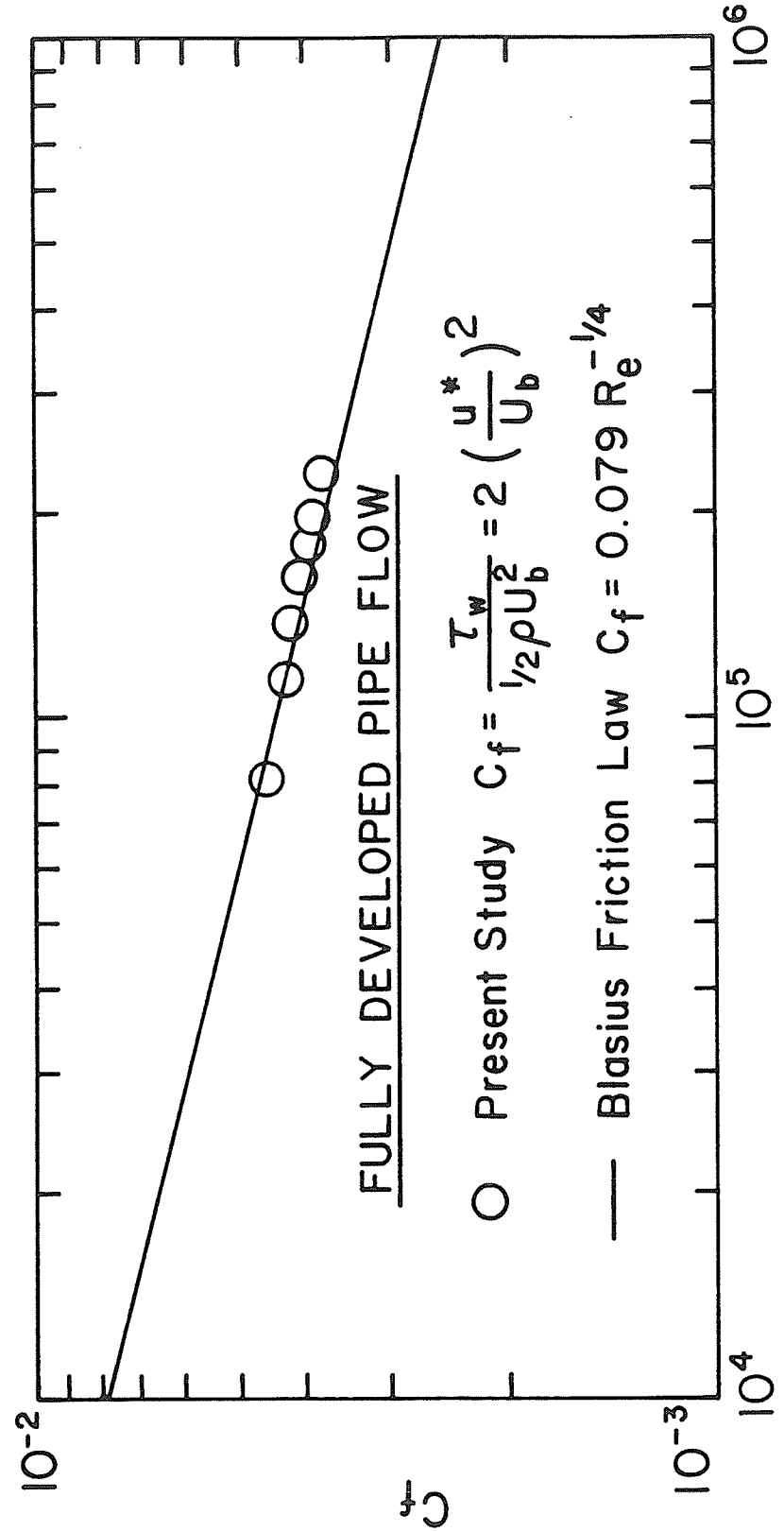

Figure C.1 Skin friction coefficient versus Reynolds number.

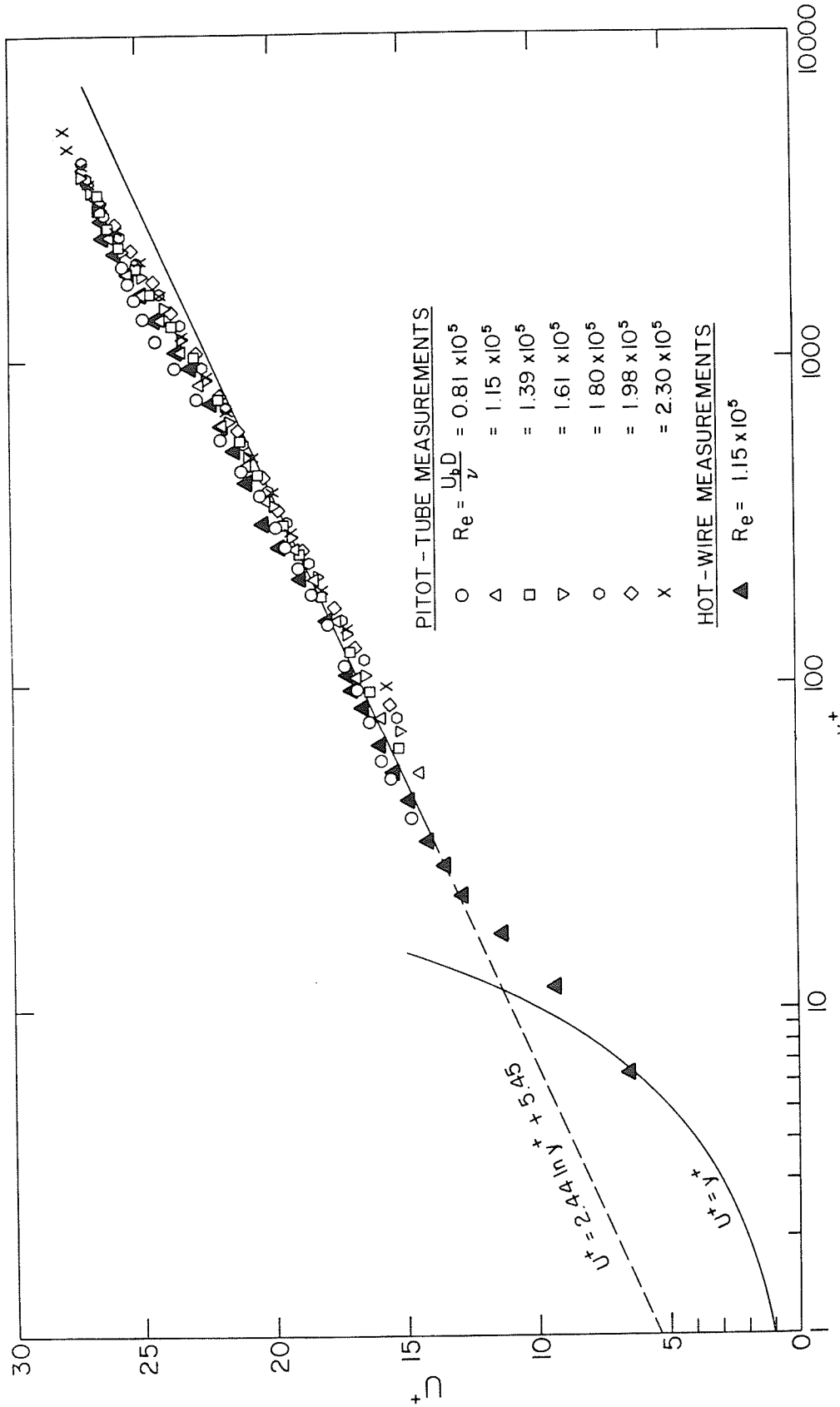

Figure C.2 Distribution of U^+ versus y^+ for different Reynolds numbers.

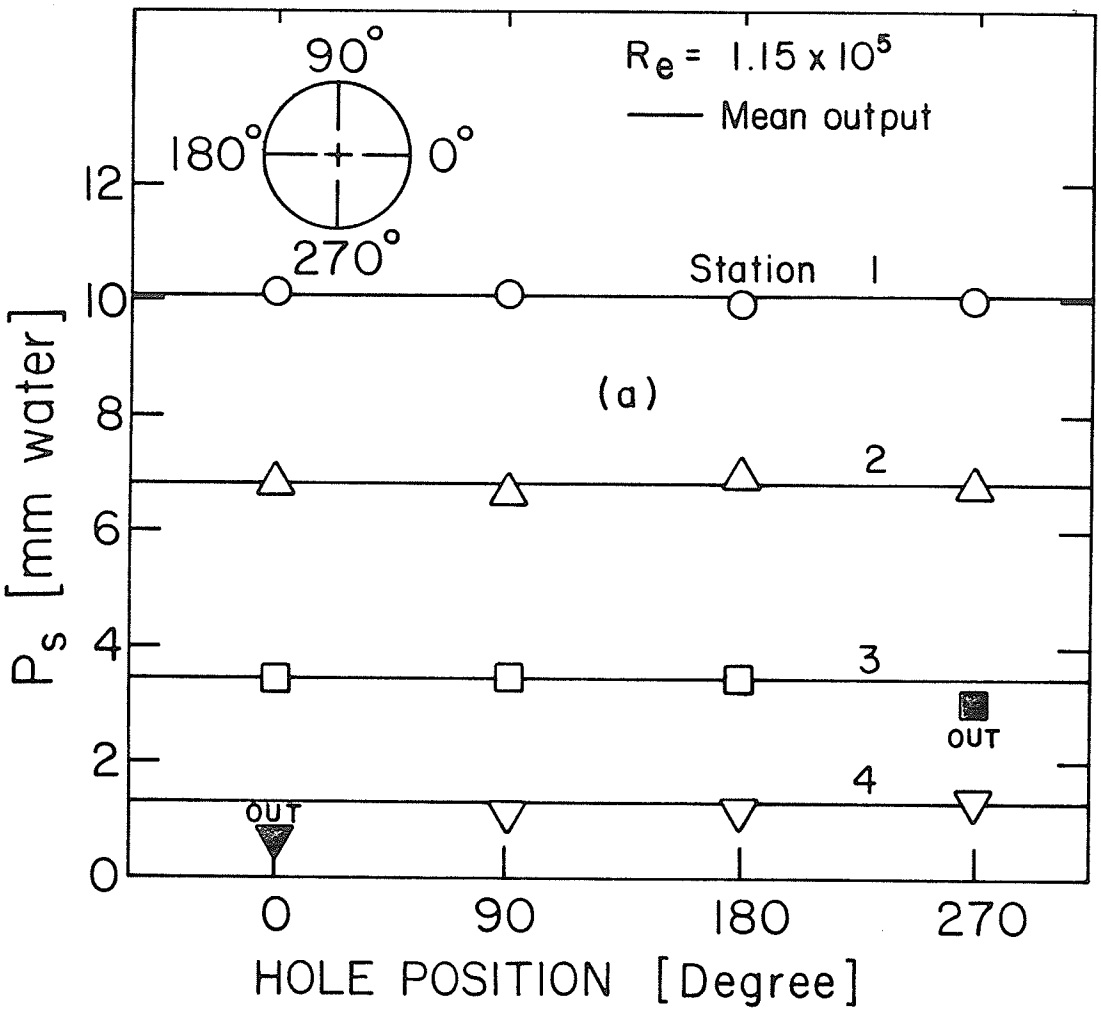

Figure C.3 Wall static pressure measurements.
(a) Circumferential measurements.

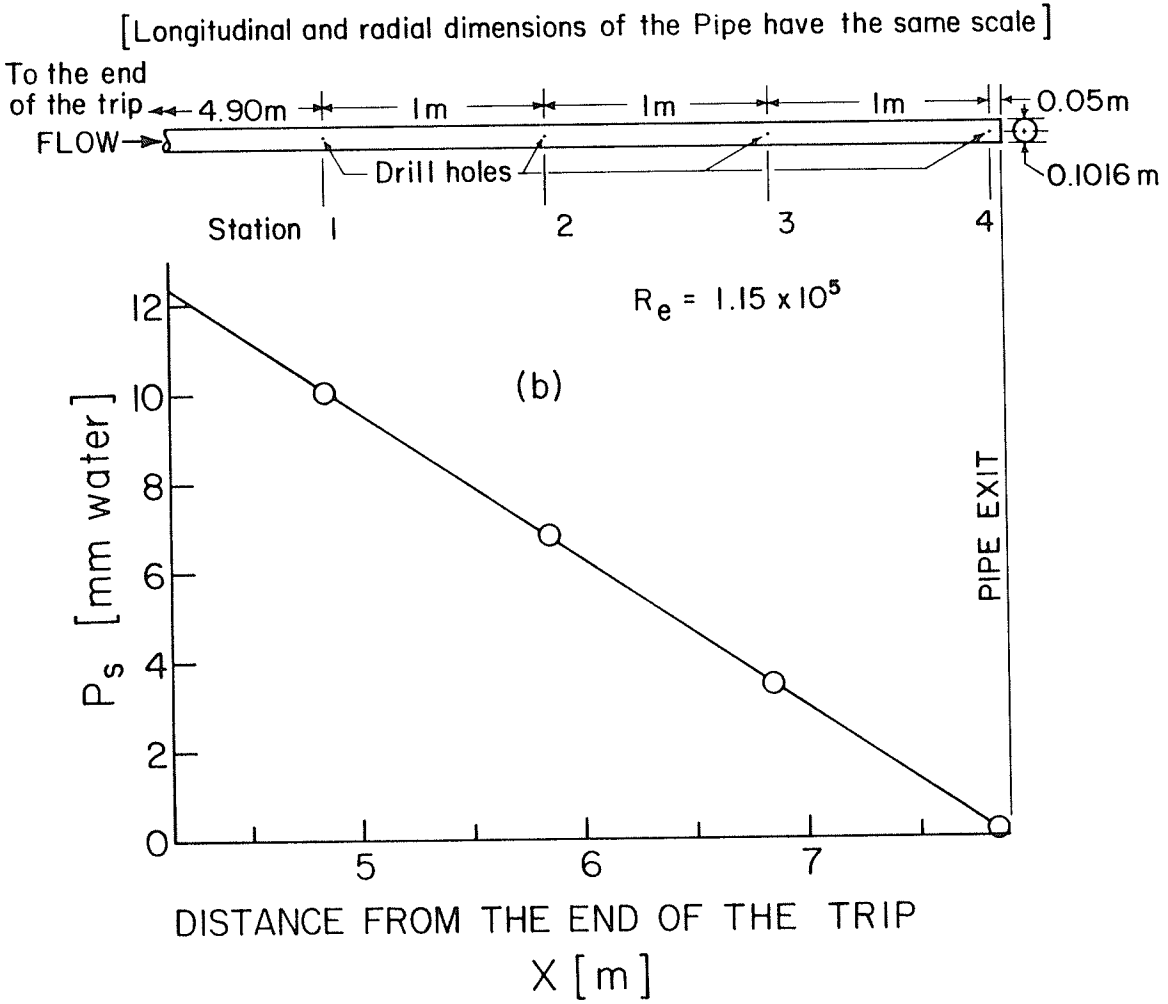

Figure C.3 Wall static pressure measurements.
(b) longitudinal measurements.

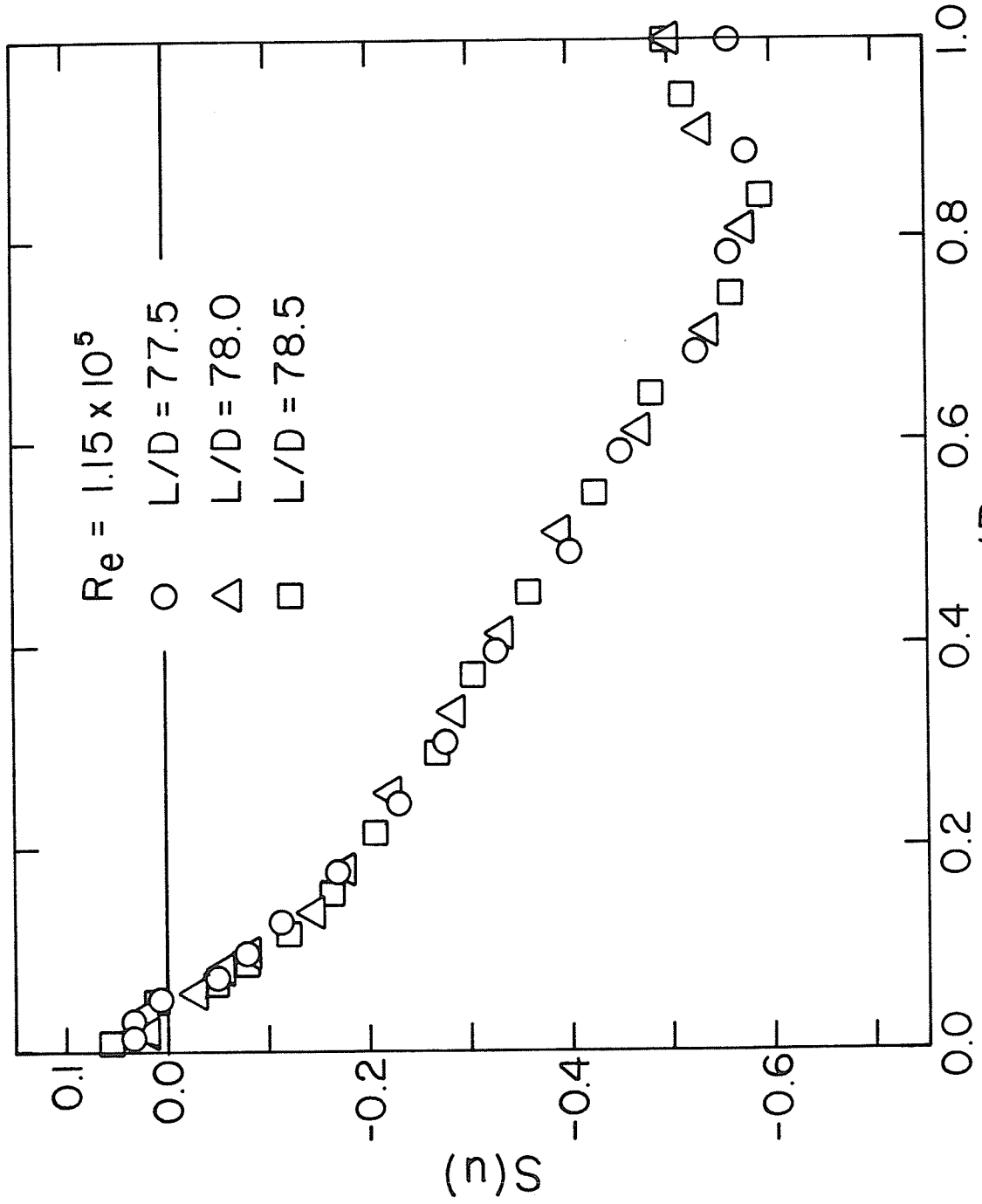

Figure C.4 Distribution of the skewness of u at different stations.

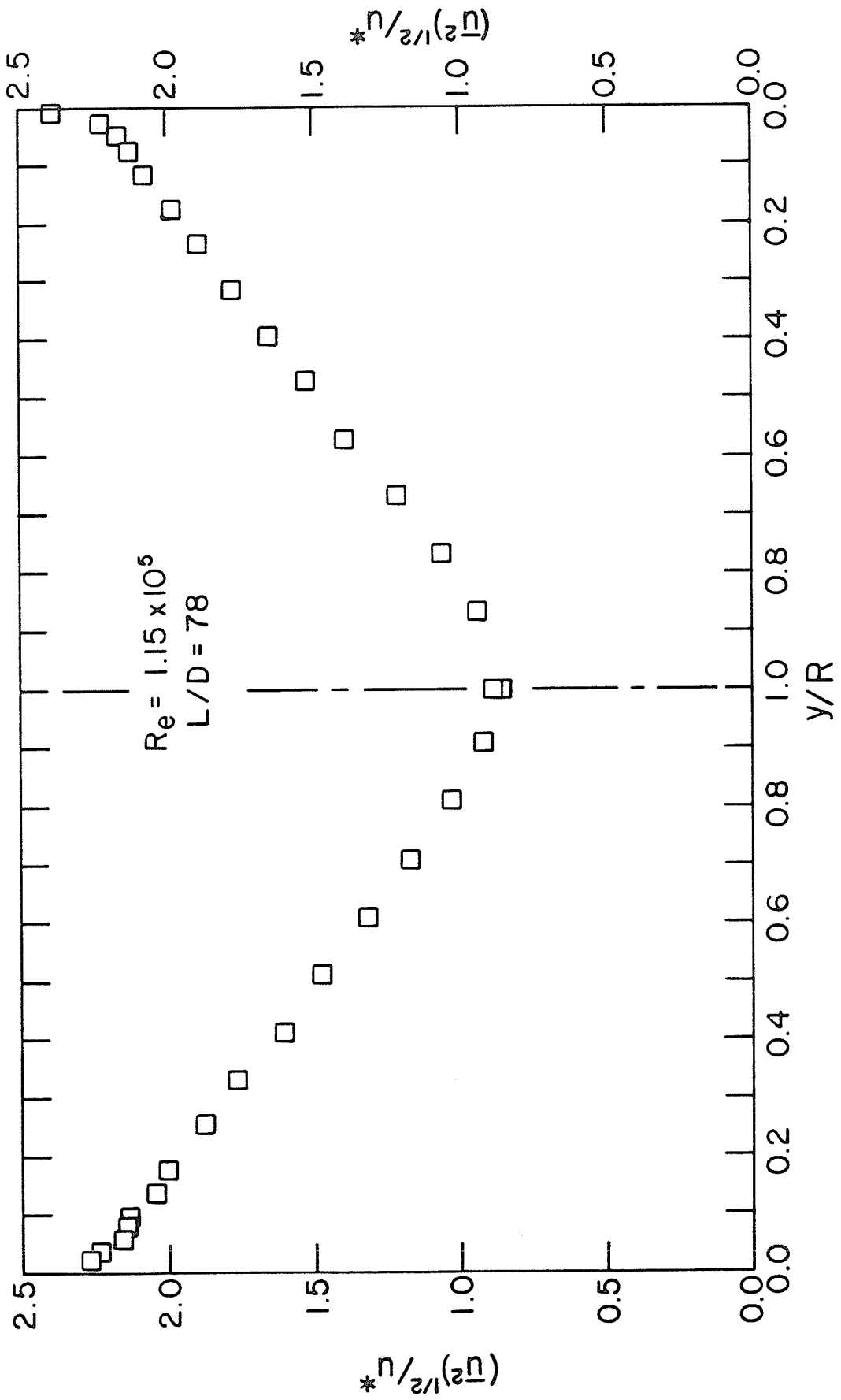

Figure C.5 Longitudinal turbulence intensity across the pipe.

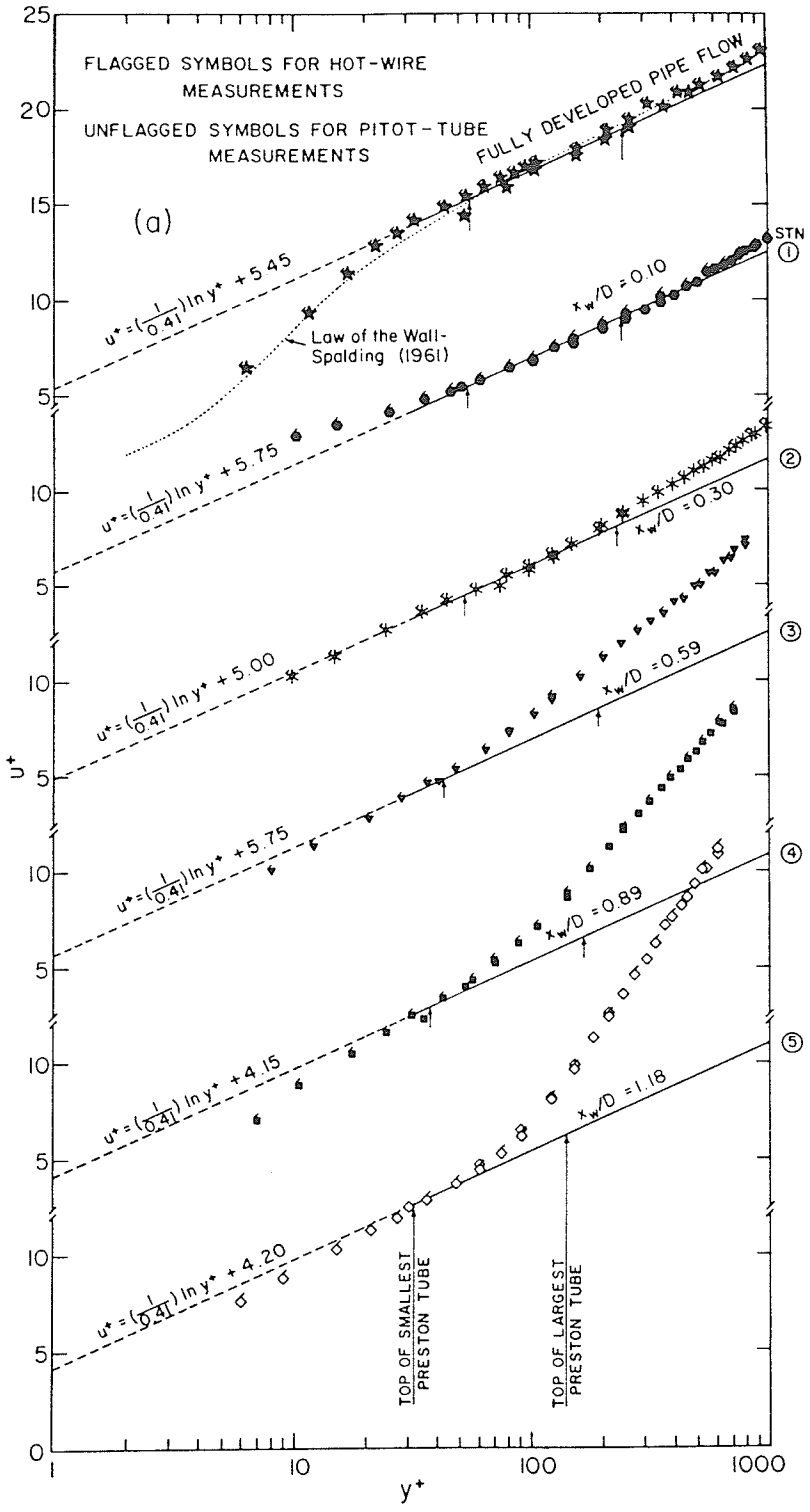

Figure D.1 Dimensionless mean velocity profiles.
(a) Pipe flow and stations 1-5.

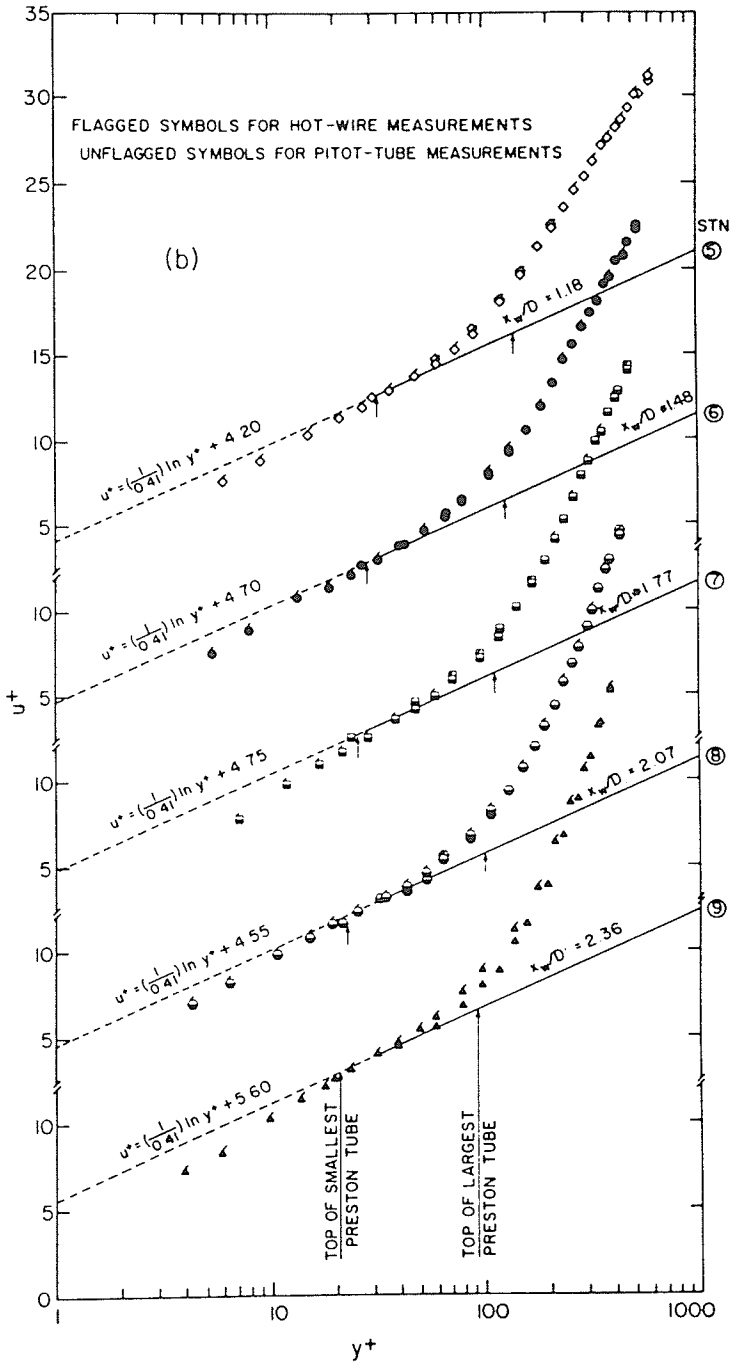

Figure D.1 Dimensionless mean velocity profiles. (b) Stations 5-9.

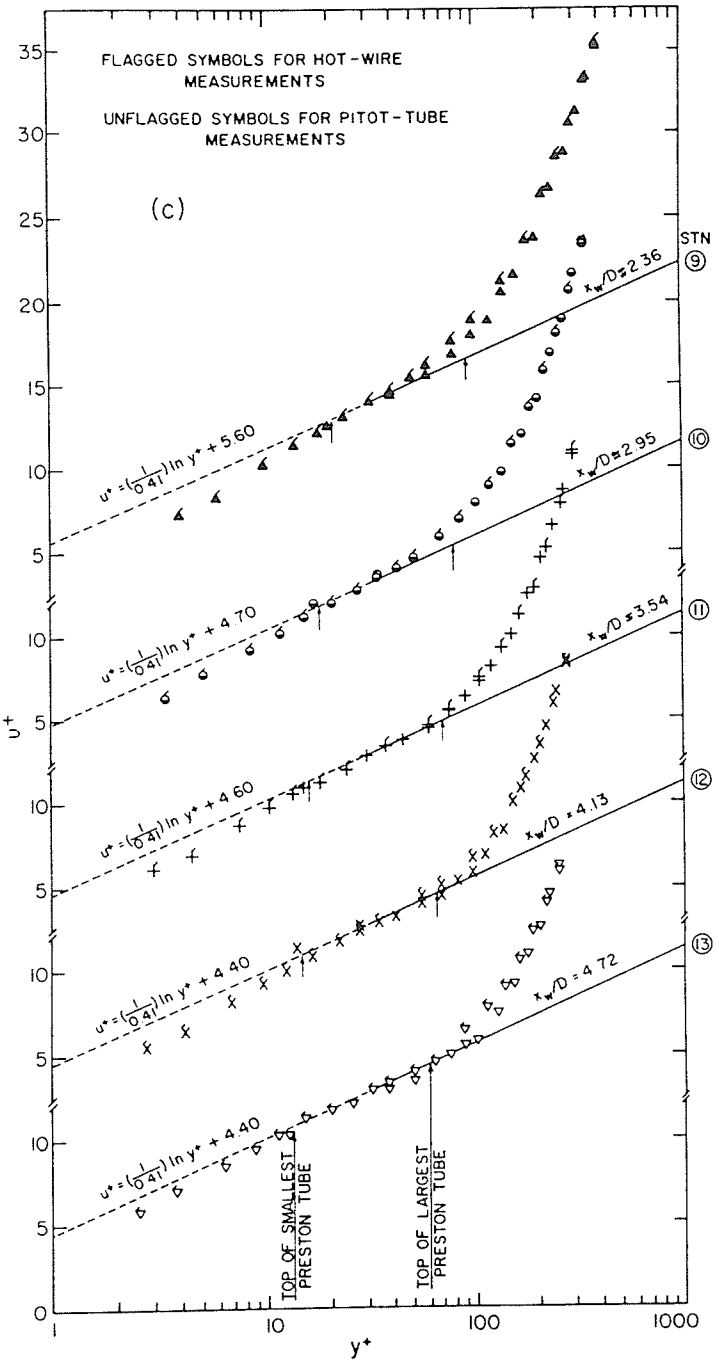

Figure D.1 Dimensionless mean velocity profiles. (c) Stations 9-13.

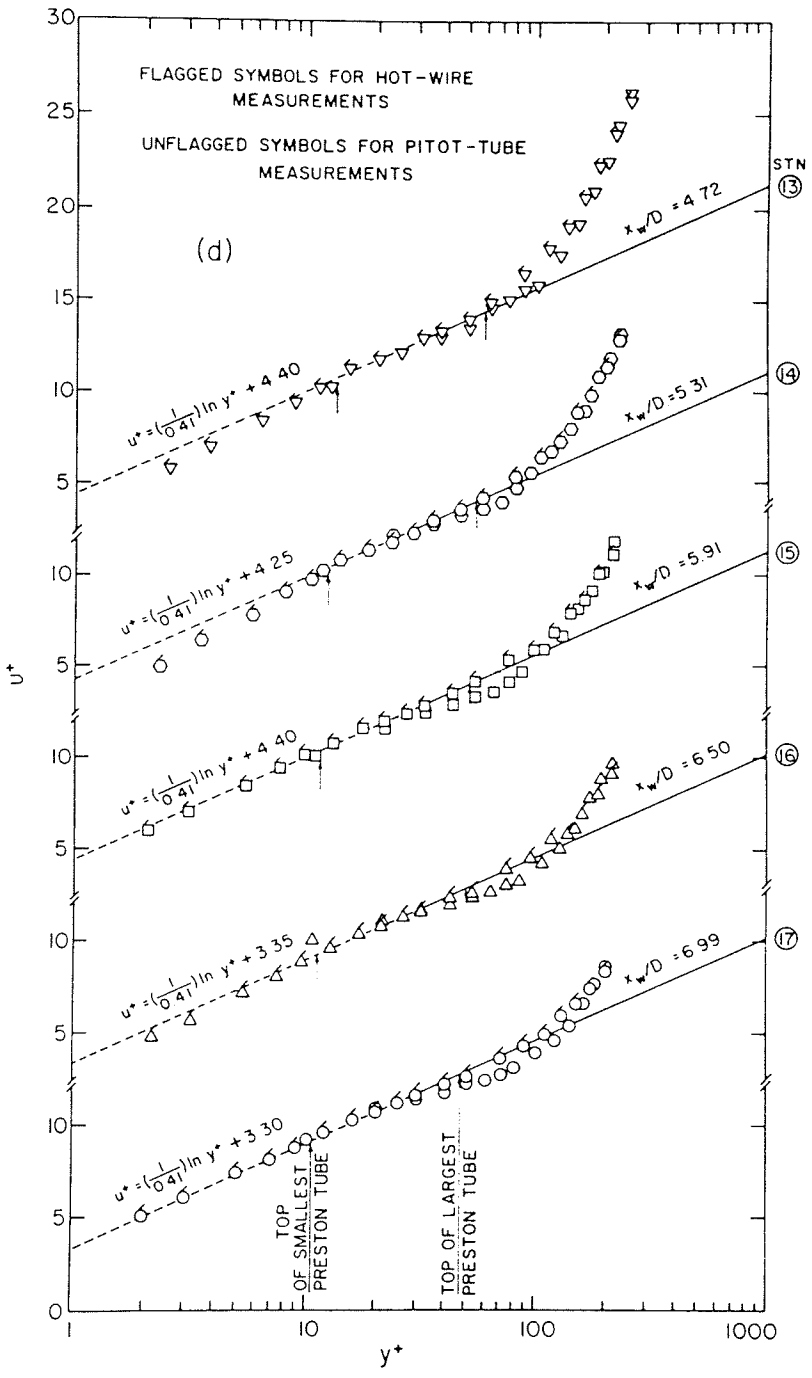

Figure D.1 Dimensionless mean velocity profiles. (d) Stations 13-17.